JAEA-Data/Code
2024-003
DOI:10.11484/jaea-data-code-2024-003

JAEA-Data/Code

Analysis Methodology of the Calculation Code, WRAC-JAEA, for Determining Major Indexes of Corrosive Circumstance in Light Water Reactors

Shunsuke UCHIDA, Kuniki HATA and Satoshi HANAWA

Materials and Structural Integrity Research Division
Nuclear Safety Research Center
Sector of Nuclear Safety Research and Emergency Preparedness

January 2025

Japan Atomic Energy Agency

日本原子力研究開発機構

国立研究開発法人日本原子力研究開発機構　研究開発推進部　科学技術情報課
〒 319-1112　茨城県那珂郡東海村大字村松 4 番地 49
E-mail: ird-support@jaea.go.jp

JAEA-Data/Code 2024-003

Analysis Methodology of the Calculation Code, WRAC-JAEA, for Determining Major Indexes of Corrosive Circumstance in Light Water Reactors

Shunsuke UCHIDA, Kuniki HATA and Satoshi HANAWA[+]

Materials and Structural Integrity Research Division
Nuclear Safety Research Center
Sector of Nuclear Safety Research and Emergency Preparedness
Japan Atomic Energy Agency
Tokai-mura, Naka-gun, Ibaraki-ken

(Received March 11, 2024)

The calculation code for determining corrosive circumstance in light water reactors, WRAC-JAEA, has been developed based on water radiolysis calculation codes for BWR. The code has involved several new calculation functions to apply it for PWR, i.e., (1) high temperature pH (pH_T), (2) pH_T effects on water radiolysis, (3) electrochemical corrosion potential (ECP) based on the mixed potential theory, and (4) ECP based on the water radiolysis calculation results.

Moderation of corrosive conditions in the primary cooling systems is one of the promising procedures to mitigate the loss of reliabilities of major components in the systems, especially in aging plants. However, water chemistry control for corrosive environment mitigation procedures are much different in BWRs and PWRs.

In BWRs, intergranular stress corrosion cracking (IGSCC) of stainless steel is the dominant causes for determining plant reliability. It is difficult to increase pH and injected hydrogen amounts due to direct power cycle operation. So, precise control of hydrogen injection with supported by water radiolysis and ECP analyses has been carried out to keep material reliability.

In PWRs, it is possible to maintain stable control of corrosive circumstances with higher pH and sufficiently large hydrogen concentration. Recently, it was pointed out that one of the major causes of primary water stress corrosion cracking (PWSCC) of nickel alloys was hydrogen. The optimal hydrogen concentration should be evaluated to mitigate ECP without increasing hydrogen concentration. For this, a combined water radiolysis and ECP analysis code is required to determine the suitable hydrogen concentration and ECP.

WRAC-JAEA can contribute not only to evaluation of corrosive conditions each of BWR and PWR, but also to prepare for suitable countermeasures for both BWR and PWR by cross-talking the knowledge and experience with assistance of the code results.

Keywords: Risk, PWR, BWR, Primary Coolant, Corrosive Circumstance, Water Radiolysis, Electrochemical Corrosion Potential, pH, Boiling

---

+Nuclear Emergency Assistance and Training Center

JAEA-Data/Code 2024-003

軽水炉腐食環境主要指標決定のための解析コード
WRAC-JAEA の解析手法

日本原子力研究開発機構 安全研究・防災支援部門 安全研究センター
材料・構造安全研究ディビジョン

内田　俊介、端　邦樹、塙　悟史[+]

（2024 年 3 月 11 日受理）

軽水炉腐食環境評価解析コード WRAC-JAEA は、沸騰水型原子炉（BWR）冷却水を対象に開発された水の放射線分解（ラジオリシス）解析コードをベースに、加圧水型原子炉（PWR）にも適用できる様に開発された。すなわち、(1)高温 pH 算出機能、(2)ラジオリシス計算に及ぼす高温 pH の影響解析機能、(3)混成理論に基づく腐食電位（ECP）解析機能、そして(4)ラジオリシスと ECP の結合解析機能を付加した。

軽水炉 1 次冷却系の腐食環境緩和は、系統を構成する機器、特に経年化原子炉の主要機器の信頼性確保のための有効な手段の一つである。しかし、BWR と PWR では、冷却システムの差異のため 腐食環境緩和のための水化学制御手法は大きく異なる。

BWR では、ステンレス鋼の粒界型応力腐食割れ（IGSCC）の抑制が、機器、配管の信頼性確保のカギを握っているが、直接サイクルを採用するため、pH 制御が難しく、水素添加量が制約される中で、ラジオリシス解析コードと ECP 解析を組合せた緻密な腐食環境の解析と測定を併用しつつ、腐食環境の緩和および構造材の健全性確保が図られてきた。

一方、PWR では、高 pH に維持し、十分な量の水素を添加することにより、水の放射線分解によって生成する酸素、過酸化水素などの腐食性生成種の濃度を、余裕をもって低く抑え、腐食環境を緩和することが可能であった。しかし、ニッケル基合金の 1 次冷却水応力腐食割れ（PWSCC）の発生と進展が水素によって加速される可能性が指摘され、水素添加量と ECP の相関を定量化する必要性が高まってきた。BWR 用に開発されたラジオリシス解析コードは中性水対象であり、高 pH 条件にはそのままでは対応が難しい。ECP 解析も高 pH では異なる。このため、BWR での経験を最大限に生かしつつ、PWR1 次冷却系にも適用可能な腐食環境解析手法の確立が急務となっている。

WRAC-JAEA は、BWR と PWR それぞれの腐食環境評価に資するのみでなく、本コードによる評価を介して、両炉型での主要構造材の知見を相互評価し、構造材に生ずる腐食損傷に係る諸課題への対応に、それぞれの経験、知見を反映する重要な手段を提供することが期待できる。

原子力科学研究所：〒319-1195　茨城県那珂郡東海村大字白方 2-4
＋ 原子力緊急時支援・研修センター

CONTENTS

目　次

LIST OF TABLERS

LIST OF FIGURES

This is a blank page.

1. Introduction

Plant lifetime of light water-cooled reactors (LWRs) is often determined by the structural materials of the primary cooling systems, where the key phenomena to control the lifetime are different in boiling water reactors (BWRs) and pressurized water reactors (PWRs). The major phenomenon to control BWR plant lifetime is intergranular stress corrosion cracking (IGSCC) of stainless steel, while that for PWR is primary water stress corrosion cracking (PWSCC) of nickel-based alloys. Those are much affected by the corrosive circumstances in the primary cooling systems. Then, moderation of corrosive conditions in the primary cooling systems of LWRs, especially in aging plants, is one of the promising procedures to mitigate the loss of reliabilities of major components in the systems, and then, to ensure the plant lifetime [1)].

The procedures of water chemistry control for mitigating corrosive conditions in BWRs and PWRs are much different due to their differences in cooling water conditions. BWRs apply the direct cycle, where the steam generated in the reactor core as a result of nuclear fuel cooling is directly supplied to the turbine for electric generation. PWRs apply the indirect cycle which is divided into two cooling systems; one is the core cooling system and the other is the steam suppling system to the turbine. The former (the primary cooling system) is a closed and pressurized cycle to remove heat from the nuclear fuel without boiling and to transfer the removed heat energy to the steam generator (SG), while the latter (the secondary cooling system) is an open cycle to supply the steam generated at the SG to the turbine for electric generation. Both cycles are divided by steam generators.

Major parameters to determine the corrosive circumstances in the primary cooling systems of LWRs are the concentrations of oxygen, (O_2), hydrogen peroxide (H_2O_2) and hydrogen (H_2), which are generated as a result of water radiolysis in the reactor core region. pH of the cooling water also contributes to the corrosive circumstances. In order to evaluate the corrosion mitigation, one of the macroscopic indexes of the corrosive circumstances, electrochemical corrosion potential (ECP), is applied, especially in BWR primary cooling water [2), 3), 4)].

In order to evaluate IGSCC crack growth rate in the BWR primary system, the relationship between stress intensity factor and crack growth rate for two kinds of austenitic stainless steels, *i. e.*, the normal one and a low carbon containing one, has been proposed as the guideline by the Japan Society of Mechanical Engineers (JSME) as well as the American Society of Mechanical Engineers (ASME) and this guideline has been accepted by the Japanese government [5), 6)]. The relationship has been prepared for two regions of ECP, *i. e.*, normal water chemistry (ECP > -100mV-SHE (standard hydrogen electrode)) and hydrogen water chemistry (ECP < -100mV-SHE) [7)]. In order to suppress ECP in the BWR primary cooling water, hydrogen injection into the feed water is effective, but injected hydrogen easily release from the turbine system to the environment, and then, effective hydrogen contribute to corrosive circumstance suppression is restricted by the barrier of the direct system of BWR. At the same, with increasing concentration of injected hydrogen, oxygen concentration measured at the sampling point decreases rapidly, but at the same time, the main steam line dose rate increases gradually. The dose rate is determined by ^{16}N carried with steam [8)]. The chemical form of ^{16}N is shifted from NO_x form to much volatile NH_4 form due to increased H_2 concentration. The optimal hydrogen injection amount is determined to suppress corrosive circumstance without serious turbine dose rate increase. Determination of hydrogen peroxide concentration is much more difficult. It is not directly measured, and it has been determined theoretically.

Corrosion of structural materials is much affected by the radiolytic species, but it is much difficult to determine their concentration in the cooling water, especially at the location of interest due to their short lifetime in the elevated temperature water. The most influential specie, H_2O_2, is very unstable in high temperature water and changes into O_2 as a result of its decomposition. Direct measurement of pH in the elevated temperature water is possible but it is still difficult to apply the in-situ measurement of the high-temperature pH in the operating plants. ECP is a rare tool to determine the corrosive circumstance in the operation power plants.

The other approach to determine the corrosive circumstance is one based on theoretical procedures. Theoretical evaluation of water radiolysis in the core region can prepare for the concentrations of radiolytic species not only in the reactor core region but also other location in the primary cooling system. Based on the analytical results of the radiolytic specie concentrations, ECP was calculated, which was confirmed with the measured one in the plants.

The effects of water chemistry improvement by hydrogen injection on ECP mitigation can be evaluated by the water radiolysis model and mixed potential models (ECP models), and then, crack growth rate can be calculated by using the formula shown in the Japan Society of Mechanical Engineers (JSME) guideline [5]. Unfortunately, it is impossible to measure corrosive conditions throughout the entire primary cooling system. There is only a restricted location where corrosive conditions can be measured directly. In order to determine ECP at all locations of the primary cooling system, the corrosive conditions should be determined by numerical simulation codes.

For BWRs several calculation codes have been reported to determine the corrosive environments under radiation irradiation conditions in the primary cooling water. Unfortunately, most of them have been unclassified only in the restricted groups which developed their own calculation code. In order to justify the evaluated ECP based on water radiolysis analysis, the standard procedures to determine the concentration of radiolytic species and ECP based on the radiolysis calculation should be authorized. For this, the water radiolysis and their following ECP calculation codes should be opened and sufficient evaluation on the coupled calculation codes should be carried out.

On the other hands, analytical procedures for determining the corrosive conditions of PWR primary coolant have not been developed well, because theoretical evaluation on corrosive circumstances was not required because of sufficient amounts of hydrogen injected to mitigate corrosive circumstances. However, recently PWSCC is not determined by corrosive circumstance (ECP) but also affected strongly by hydrogen concentration, which means that corrosive circumstance should be controlled without excess amount of hydrogen injection [9]. It mean that the optimal hydrogen injection amount is also required for PWR primary cooling system as same as BWR. For this, theoretical approach to evaluate corrosive circumstance in PWR primary cooling system is necessary as same as BWR.

In Japan Atomic Energy Agency (JAEA), the coupled analysis code, i.e., water radiolysis code and ECP analysis code, WRAC-J, has been developed for determining corrosive circumstance in in-pile water loop for IGSCC crack growth rate evaluation [10]. The code could be applied for neutral and non-boiling conditions. Calculation of boiling effects on water radiolysis for BWR plant application and pH calculation based on coupled control of Li and B concentrations for PWR plant application were added on WRAC-J code, and then ECP calculation based on coupled analyses of electrochemistry and oxide layer growth calculations was also added, which resulted in the new corrosive circumstance evaluation code, WRAC-JAEA.

In the document, the details of the necessity of the LWR corrosive circumstance evaluation are shown in Chapter 2, the major parameters to determine corrosive circumstances are introduced in Chapter 3, the latest procedures to determine the BWR corrosive circumstances and major modifications on the proven evaluation procedures to apply them to PWR are summarized in Chapter 4, the details in the numerical analyses for analysing the corrosive circumstances both for BWRs and PWRs are introduced in Chapter 5, the outlines of the developed analysis code are shown in Chapter 6, the examples of major analysis results and their evaluation are shown in Chapter 7, the users' manual of the code is introduced in Chapter 8 and summary and future subjects related to the developed code are listed in Chapter 9.

2. Major Parameters of the Corrosive Circumstances

2.1 Comparison of the Cooling Systems of BWRs and PWRs

Both of PWRs and BWRs use light water (H_2O) as the coolant and the neutron moderator. Furthermore, they both use enriched Uranium as fuel with cylindrical vessel types. The general structure of both reactors are also very similar, as they both consist of the main components of a nuclear reactor: a containment vessel, a reactor vessel, which houses the reactor core, and a steam generating turbine (**Figure 2.1**).

The main difference between the PWR and BWR lies in the process of steam generation. PWRs generate steam indirectly by using two water circuits, a primary one and a secondary one. On the other hand, a BWR produces steam directly using a single water circuit [11), 12)].

In a PWR, heat from the reactor core is used to heat the primary reactor coolant at temperatures over 300°C. This water is kept liquid under high pressure. The heat from the primary water circuit is then transferred to the secondary circuit by way of the pressurized liquid. The secondary circuit then uses this heat to convert liquid water into steam for the turbine. The steam is later condensed and recycled.

In a BWR, steam is directly produced by the boiling the water coolant. The steam is separated from the remaining water in steam separators positioned above the core and passed to the turbines. The steam is later condensed and recycled.

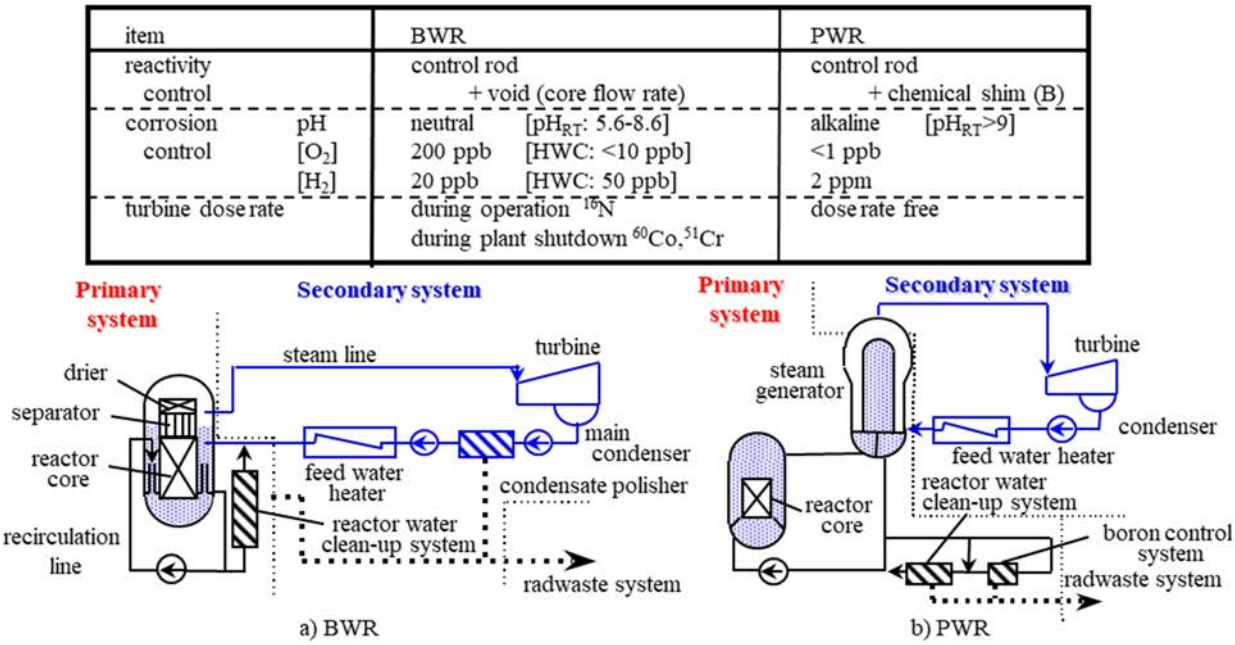

Figure 2.1 Comparison of cooling system of BWRs and PWRs

2.2 Major Component Materials of the Primary Systems of BWRs and PWRs

Major components and their structural materials in the primary systems of PWRs and BWRs are shown in **Figure 2.2**. Major material-related troubles which have ever experienced (flow accelerated corrosion; FAC, IGSCC/PWSCC, Zirconium alloy corrosion of fuel rods, general corrosion of carbon steel) are also shown in the figure [13)].

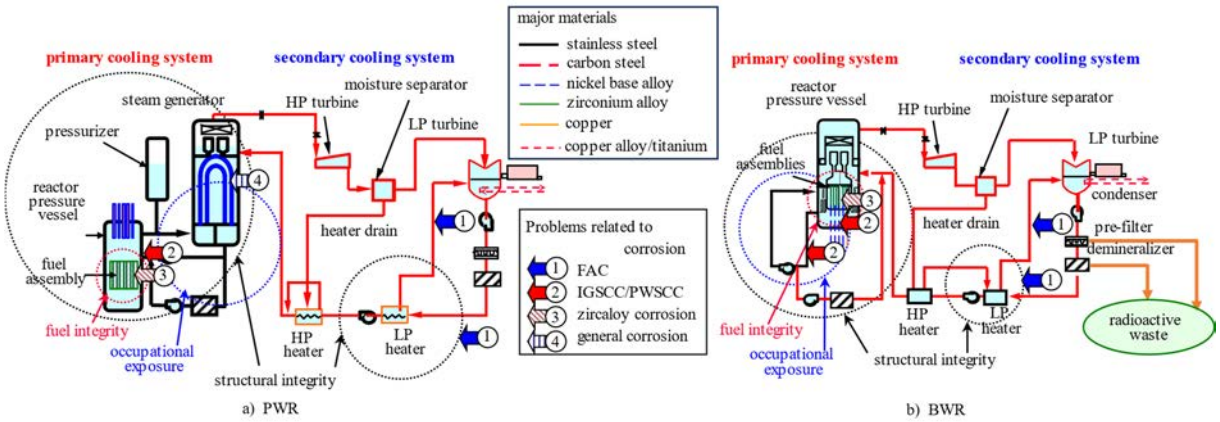

Figure 2.2 Major subjects related to materials in cooling systems of nuclear power plants

In LWRs, the water chemistry of cooling water is carefully monitored and controlled to keep the integrity of structures, *e.g.,* fuel cladding, pressure boundary structures, and core internals, and to reduce occupational exposures of workers due to accumulated radioactive corrosion products. As the demand increases for advanced applications of light water-cooled reactors grows, such as the use of improved fuels, the safe and reliable operation of older plants, and future power rate increases, water chemistry control is expected to play an even bigger role in plant reliability [1)].

Water chemistry affects all materials in contact with the cooling water and at the same time it is affected by the materials themselves. As a result, water chemistry control is necessary to meet the need for better target material integrity and at the same time it is required also being optimal for all materials and systems in the plant. Plant water chemistry is affected by each plant's unique systems, materials used and operational histories, which lead to difficulties in establishing the trio of requirements for water chemistry, *i.e.*, better reliability in reactor structures and fuels, fewer environmental impacts, and fewer radwaste sources, with conventional water chemistry control [14)]. Water chemistry is controlled based on the target values to establish the trio of needs [15)]. Each plant must have its own water chemistry that is tuned for it.

In **Figure 2.3**, the wetted surface ratio of the major structural materials in the primary cooling systems are compared. In PWRs, the ratio of nickel-based alloy is about 70%, which is followed by zirconium alloy for fuel pins, while in BWRs, the ratios of carbon steel, zirconium alloy and stainless steel are almost the same (30%).

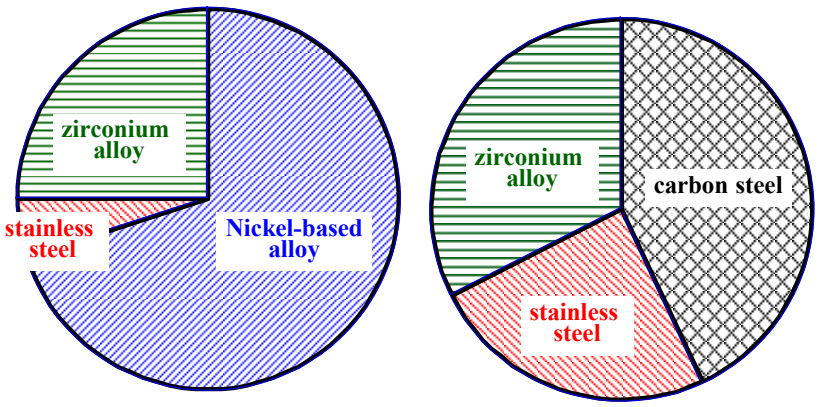

a) PWR (primary system) b) BWR

Figure 2.3 Major materials in primary system - Their wetted surface

In LWRs, the primary roles of the cooling water are (1) heat transfer medium from the fuel to turbine (just coolant) and the moderator for reducing neutron energy. However, as a result of the interaction of water and structural materials several adverse effects are caused, which often develops problem in reliable plant operation. In order to avoid the material-related troubles in the plant, water chemistry should be carefully controlled. The major targets of water chemistry control in the primary coolant and controlled water chemistry parameters are listed in **Table 2.1**.

Table 2.1 Major targets of water chemistry in NPPs and major phenomena related to the targets

1) Major targets	[determining phenomena]
(1) Reactivity control	[thermal hydraulic, water purification & dosage]
(2) Structure integrity	[material-water interaction, thermal hydraulic, water radiolysis]
(3) Fuel integrity	[material-water interaction, thermal hydraulic, water radiolysis, fouling]
(4) Dose rate reduction	[transportation, fouling, thermal hydraulic, water radiolysis]
2) Categories of major phenomenon	[determining major parameters*]
(1) Thermal hydraulic	[temperature (T), pressure (P), flow velocity (v), void fraction, heat flux (q), neutron flux (ϕ)]
(2) Material-water interaction	[**concentration of chemical species ([C])**, **pH**, conductivity, T, v, ϕ]
(3) Transportation	[**concentration and radioactivity of metallic species ([R])**, [C], T, v, q, ϕ]
(4) Fouling	[**pH, conductivity, [C], [R]**, T, v]
(5) Water purification & dosage	[**[C], [R], pH, conductivity**, T]
	*** bolt: chemical parameters**

As a result of careful water chemistry control along with careful plant operation and periodical plant inspection, trouble related to water chemistry have been reduced (**Figure 2.4** [16]). During the early stage of commercial operation of LWRs in Japan, fuel leakages in plant have been often reported. When once fuel defects are detected, the defected fuel should be found out by applying fuel sipping techniques and the defective fuels have been removed from the reactor core. The work for detecting defective fuel need a lot of inspection time, which resulted in decreased plant availability factors. Fortunately, based on enthusiastic efforts of engineers and researchers related to fuel manufacturing, the reliability of fuel cladding was improved drastically, and the ratio of defective fuel decreased. When the trouble related to fuel defects were almost overcome, new troubles were conspicuously increased on pressure boundary materials, i.e., IGSCC of stainless steel in BWRs and SG tube defects in PWRs. Lots of plant side work on inspections and maintenances of the stainless piping and SG tubing resulted in decreasing plant availability and increasing occupational exposures.

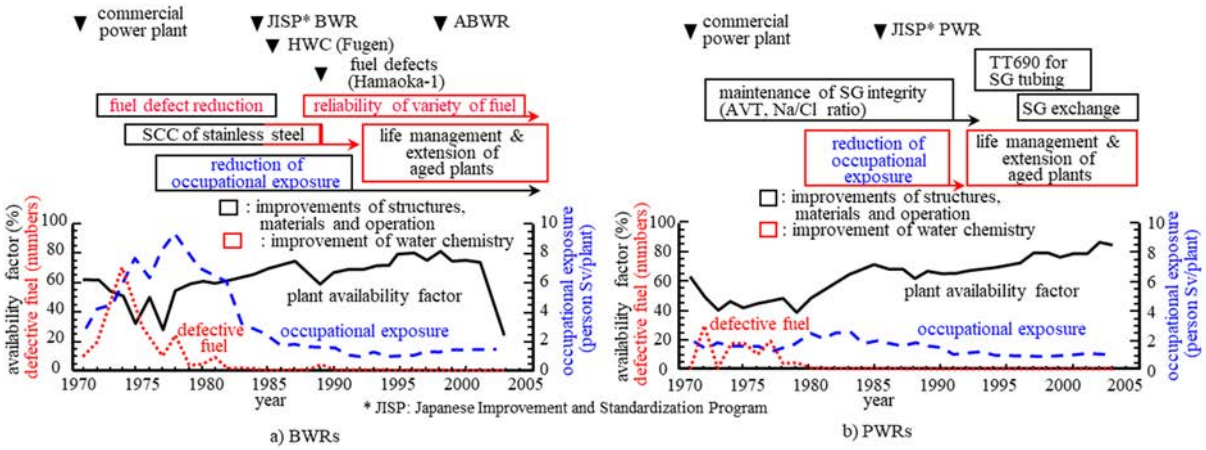

Figure 2.4 Major targets for water chemistry improvement and achievements

In order to satisfy three different targets, increasing fuel reliability, increasing structural integrity and reducing occupational exposure, water chemistry of the primary cooling water should be carefully controlled without any adverse effect (**Figure 2.5**).

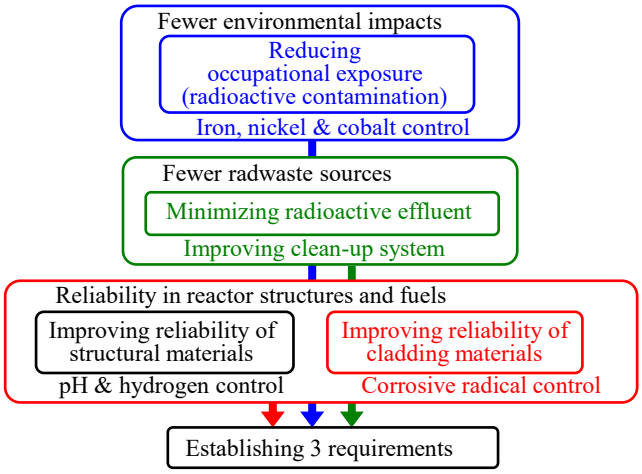

Figure 2.5 Optimal water chemistry control

2.3 Major Parameters to Determine Corrosive Conditions in BWRs and PWRs

In PWR primary cooling systems, water chemistry is kept the oxygen concentration ([O_2]) level as low as possible and pH in alkali, while in BWRs, pH in the cooling water is kept in neutral and some amounts of oxygen from water radiolysis is accepted. Boric acid is injected into the coolant as a result of the use of a chemical shim in the PWR primary cooling system, and its concentration is varied with fuel burn-up (operational time) to compensate for the decrease in reactor core reactivity caused by the fuel burn-up, which results in a change in LiOH concentration to maintain the fixed pH value. The target values for the concentrations of hydrogen and oxygen are listed on the operational safety program, which prohibits their deviation from the target values [15].

The water radiolysis calculation was affected by increasing pH, while the ECP calculation was affected by increasing [Li]. The pH effects on water radiolysis were introduced in the previous paper and the Li effects were shown in the section 5.3. As a result of involving those effect in the couple of calculation procedures, the procedures originally developed for BWRs could be extended to PWRs. In **Table 2.2**, major water chemistry parameters for the primary and secondary cooling systems of BWRs and PWRs. For the three targets, structural integrity, fuel integrity and occupation exposure, along with the reactivity control, water chemistry parameters to be controlled are different. Usually, the control value for each target phenomenon is on the same direction (up/down), but sometime the desired value showed the different direction, which meant the optimal value should be found to meet the optimal control for the different targets.

In order to control the water chemistry parameters to meet the optimal values, determination of water chemistry parameters should be measured in the plant. In **Figure 2.6**, major water chemistry monitoring items related to safe and reliable plant operation are listed, where some parameters, e.g., [H_2] pH, and conductivity, were continuously monitored with in-line monitoring devices. But usually, the data were collected in the cool-down water but not in the real high temperature water. Some of the parameters, e.g., ECP in BWRs could be measured directly under high temperature, even when the installation of the sensors required a lot of task work and maintenance jobs. Radioactive species, e.g., ^{60}Co and ^{58}Co in the water, were collected from the sampled water and determined with semiconductor detectors [17].

Table 2.2 Key of water chemistry parameters

Reastor / Parameter	PWR		BWR	
	primary	secondary	Reactor (primary)	feedwater (secondary)
Temperature (°C)	200-325	20-285	200-285	20-285
Pressure (MPa)	15.5	7.2	7.2	7.2
$pH_{25°C}$ (-)	6.8-7.2* (at T=300 °C)	8.8-9.5	neutral	neutral
(1) Reactivity control	**[B]**	-	**void fraction**	-
(2) Structural integrity	**pH_T**, [B], [Li], $[H_2]$, **conductivity**	**pH**, **$[O_2]$**, $[SO_4^{2-}]$, $[N_2H_4]$, **conductivity**	pH, **$[O_2]$**,**$[H_2O_2]$** conductivity, **ECP**	$[H_2]$, $[Cl^-]$, $[SO_4^{2-}]$
(3) Fuel Integrity	[Li], $[Cl^-]$, [Fe] **pH_T**, $[^{131}I]$	-	pH, $[^{131}I]$, **$[O_2]$**	[Fe], [Cu], $[SO_4^{2-}]$
(4) Activity transport	**pH_T**, [B], [Li], $[^{58}Co]$	-	**$[O_2]$**, **$[^{60}Co]$**	**[Fe]**, [Co], **[Zn]**

Bolt: water chemistry parameters directly influence to material behavior

Some of the water chemistry parameters, e.g., $[O_2]$ and $[H_2O_2]$, were determined by water radiolysis under radiation irradiation conditions in the reactor core region, while others, e.g., [B]. [Li], [Zn], pH, $[H_2]$, were determined by plant operational conditions (Table 2.2). Boron and lithium were injected into the cooling water to control pH, $[H_2]$ was controlled to reduce $[O_2]$ and $[H_2O_2]$. In the other words, some water chemistry parameters are considered as direct control parameters to influence the material behavior, while others are the parameters to influence the direct control parameters.

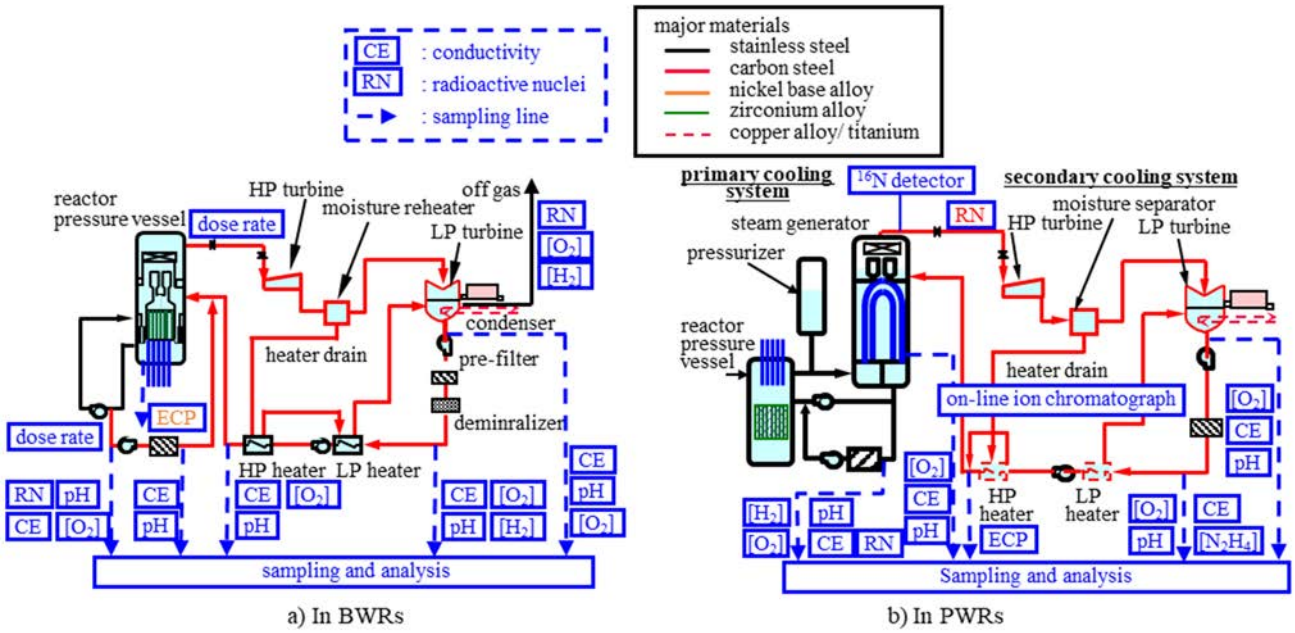

Figure 2.6 Major water chemistry monitoring items related to safe and reliable NPP operation

2.4 Major Problems in the Primary Systems of BWRs and PWRs

IGSCC of stainless steel in BWRs and SG tube cracking in PWRs have been almost overcome by material improvement and water chemistry improvement. However, IGSCC in BWR was still reported in some other

locations but pressure boundary, e.g., reactor core shroud .and jet pump supporting parts. Continuous care for IGSCC is required in BWR primary coolant, where hydrogen injection has been carried out to mitigate corrosive circumstance.

Corrosion of materials is determined by the combined effects of material factors and water chemistry factors. Corrosion of aqueous systems is understood as electrochemistry phenomena. At metal surfaces, metallic ions are released from the base metal and at the same time dissolved metallic ions are oxidized, precipitating as the oxide film on the surface. Metal oxide also developed on the inner surface between the oxide surface and base metal by direct oxidation. Development of the oxide film is one of the consequences of electrochemistry reaction, and its propagation can be controlled the reactions. The properties of the oxide film on the metal surface are much affected by material properties and the effects of complicate corrosion behaviors. In order to understand the problems related to corrosion in NPPs, understanding and analyzing the electrochemical reactions of structural materials and the contribution of oxide film to the reactions are essential.

A schematic diagram for the interaction of structural materials and cooling water are shown in **Figure 2.7**. Oxide film on the surfaces of the materials is a consequence of the interaction and at the same time a reason why the interaction should be controlled.

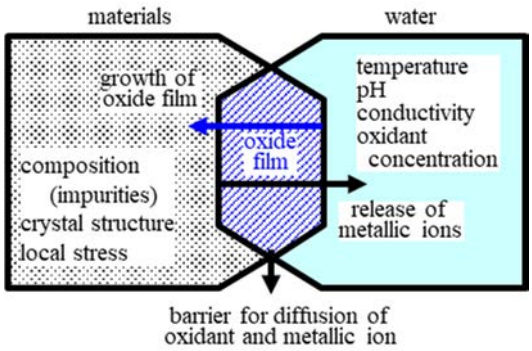

Figure 2.7 Interaction between structural materials and cooling water

IGSCC for stainless steel in the BWR primary cooling system and primary water stress corrosion cracking (PWSCC) for nickel-based alloy of PWR core internals are known to occur as a result of overlapping effects of materials, stress and environmental factors (**Figure 2.8**). IGSCC is known to occur as a result of overlapping effects of materials, stress and environmental factors.

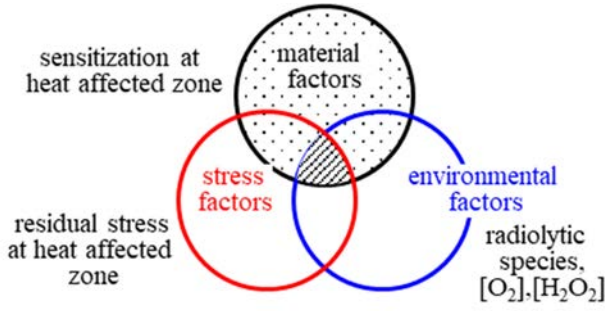

Figure 2.8 Major parameters of IGSCC and PWSCC

In order to mitigate the IGSCC crack growth rate, improvement in materials and water chemistry can control the dissolution rate, while improvement in stress factors can control repeat cycle of oxide film rupture. As the dominant water chemistry factors, the ECP has been applied to evaluate the IGSCC crack growth rate. IGSCC crack growth rates as a function are shown in **Figure 2.9** [6].

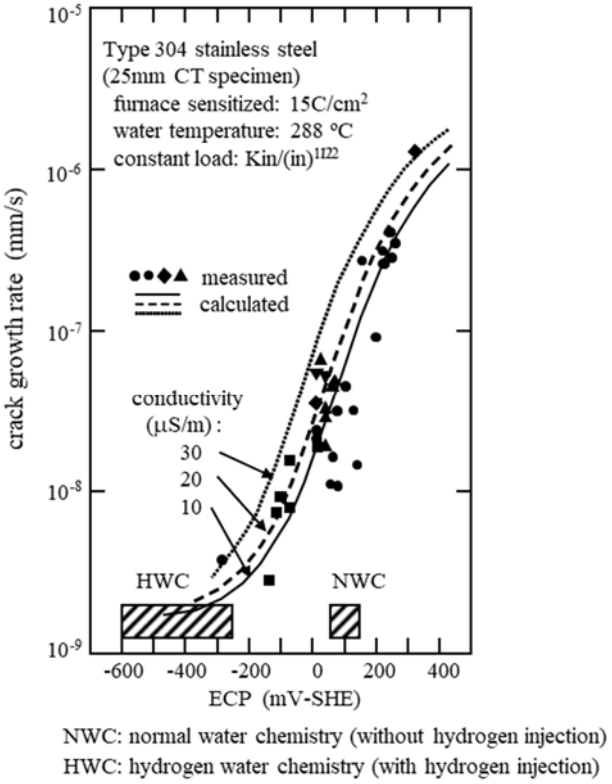

Figure 2.9 Crack growth rate as a function of ECP [6]

It includes major locations for determining corrosive conditions directly with in-line water chemistry sensors or for carrying out analytical procedures of sampled water Corrosive conditions in the BWR primary cooling system are determined mainly by radiolytic species, most of which are unstable in high-temperature water and difficult to determine in sampled water. ECP can be measured directly under high-temperature conditions if ECP sensors can be installed. From the two viewpoints of easy measurement under high-temperature conditions and easy application for the JSME guideline, ECP can be applied as a major parameter for corrosive conditions in the BWR primary cooling system. However, the locations where ECP sensors can be installed are restricted to only the cleanup water lines, vessel drain lines, and some of the in-core monitoring guide tubes. Major portions of the system are outside the direct measurement region, and they represent areas where corrosive conditions should be determined by applying numerical simulation codes. One of the most important purposes for determining corrosive conditions is to predict IGSCC occurrence in stainless steel piping and components. The IGSCC crack growth rate has been described in the guideline of the JSME (**Figure 2.10)**[5].

In order to suppress [O_2] and [H_2O_2] in the primary cooling water of BWRs, hydrogen injection was one of the most hopeful procedures. The procedures were successfully applied in PWRs, which applied the closed cycle and injected hydrogen was closed in the primary system and contribute [O_2] and [H_2O_2] in the coolant. However, in BWRs, the injected hydrogen was easily carried from the reactor core region to the main steam lime with main steam, which resulted in installation of the huge recombiner which recombined hydrogen and oxygen to prevent gaseous effluent into the environment.

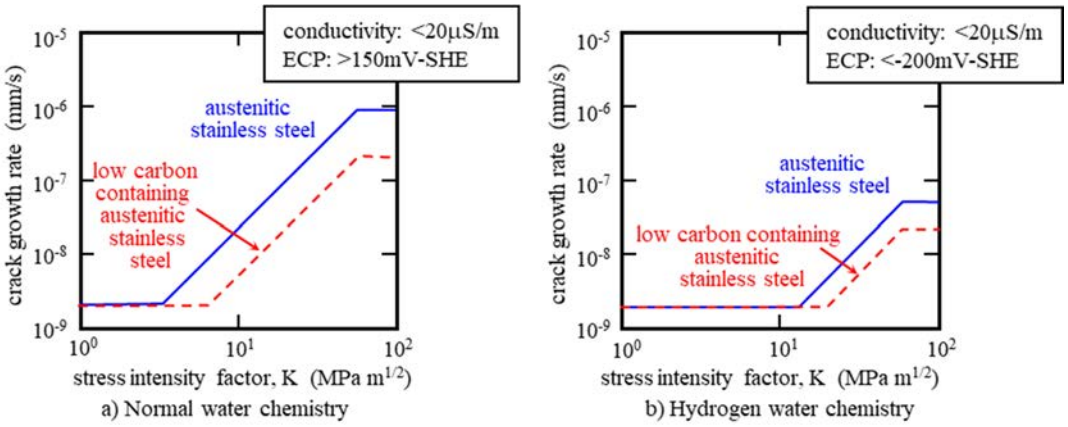

Figure 2.10 JSME guideline for evaluation of crack growth rate

In the middle of 1980s, Swedish vender successfully suppressed [O_2] and [H_2O_2] in the BWR primary cooling systems. They found hydrogen injected into the feed water system played the important roles to recombine [O_2] and [H_2O_2] with [H_2] in the water phase from the feed water inlet through the reactor core region and then it was released to the turbine system with the main steam (**Figure 2.11**).

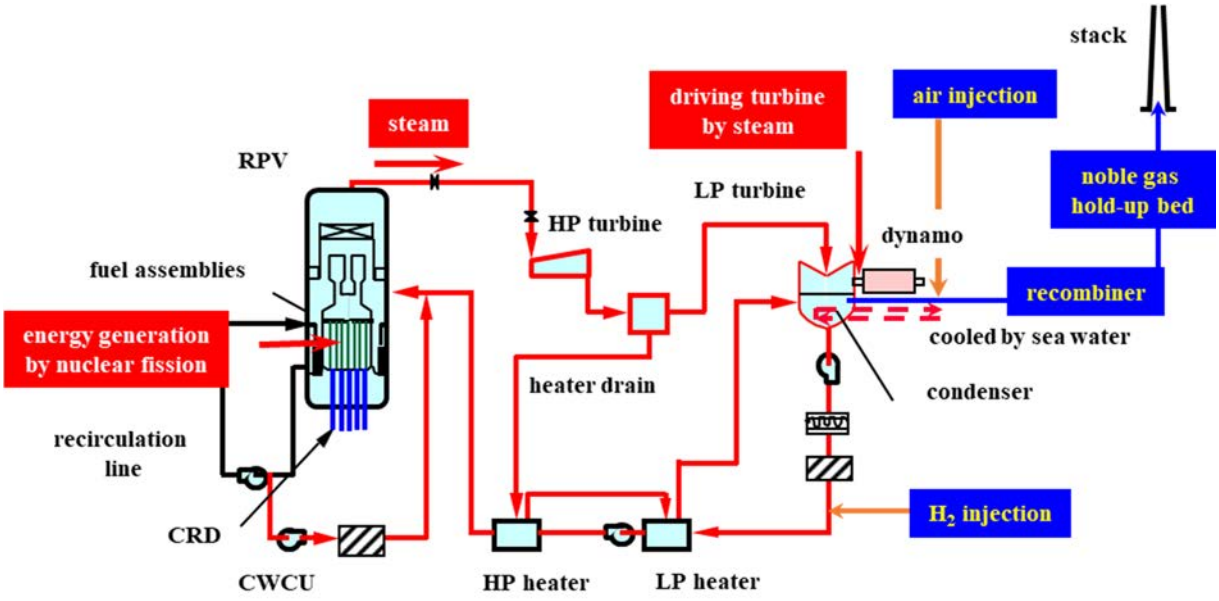

Figure 2.11 Hydrogen injection in operating power plants

The oxidant suppression effects were shown schematically in **Figure 2.12**[18]. Hydrogen injected into the feed water goes into the reactor pressure vessel through feed water sparger nozzles, go down through down-comer and then to the reactor core. In the reactor core, most of the injected hydrogen was transferred to the main steam. Oxidant suppression effects are not much expected as shown in Figure 2.12 A. In the recirculation line, most of the hydrogen injected into the feed water is remained to suppress the oxidant concentrations as shown Figure 2.12 B. Based on the findings, hydrogen injection in BWRs spread rapidly in the world.

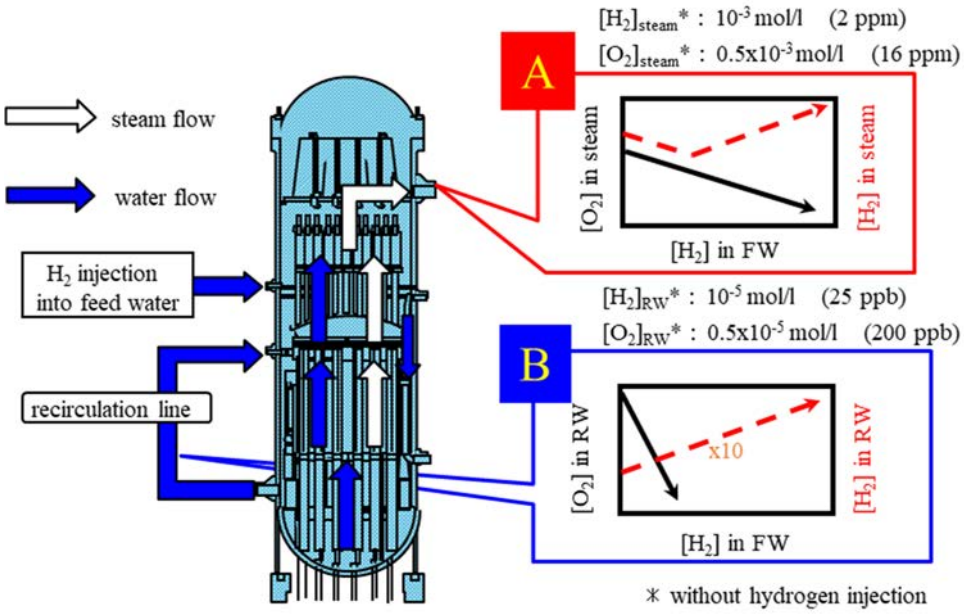

Figure 2.12 Hydrogen water chemistry (HWC)

2.5 Major Analytical Tools to Determine the Corrosive Circumstances

Major radiolytic reactions along the flow path of the BWR primary cooling system are shown in **Figure 2.13** [18]. Generally, numerical simulation codes consist of two kinds of codes, water radiolysis codes and ECP codes.

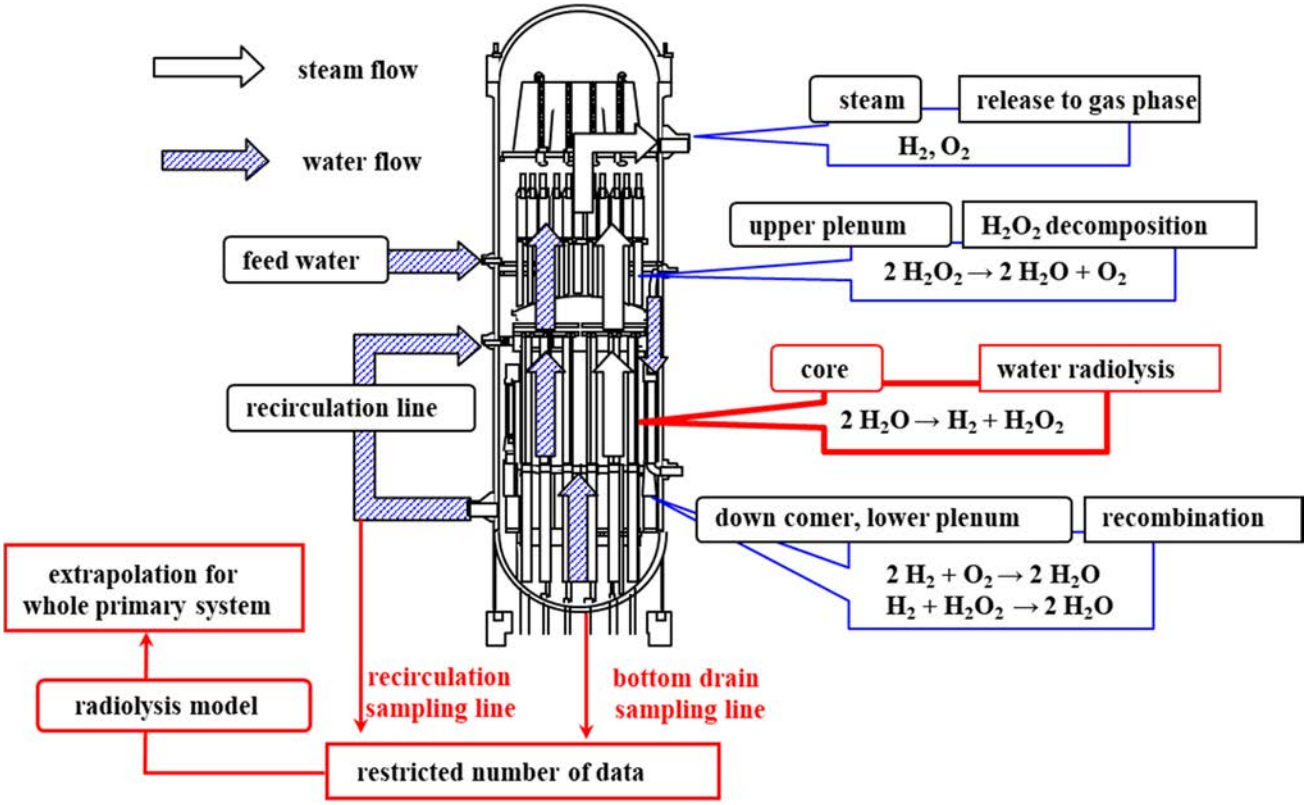

Figure 2.13 Water radiolysis in BWR primary coolant

2.5.1 Water Radiolysis Calculation

The water radiolysis codes have been composed based on nonlinear rate equations for mass balances of radiolytic species in the cooling water, where their generation reactions due to radiation-induced decomposition of H_2O molecules, their reactions for generating other species, and reactions for their disappearance and their transfer between liquid and gaseous phases are expressed (**Figure 2.14** and **Table 2.3**) [18), 19), 20), 21), 22), 23)].

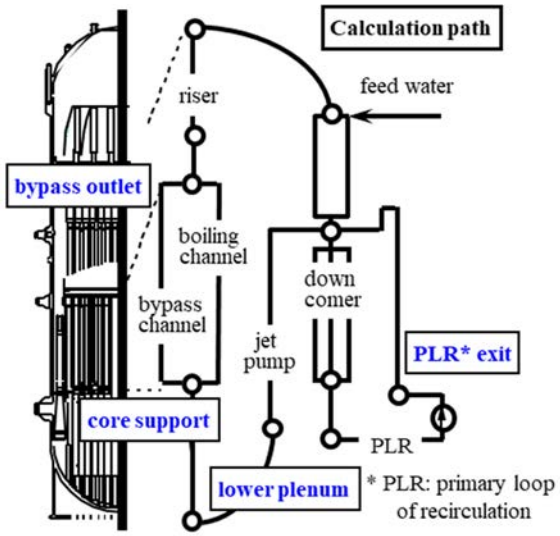

Figure 2.14 Calculation path used for water radiolysis model

Major features of the water radiolysis codes are summarized in **Table 2.4.** In order to calculate the concentrations of radiolytic species, plant parameters, e.g., pipe diameters and lengths, components, flow rate, temperature, spatial distributions of neutrons and gamma-rays, and steam quality in the cooling water, should also be prepared (**Table 2.5**) [24)]. Basic constants for the calculations are generation of major radiolytic species due to radiation-induced decomposition of H_2O molecules (g-values) and reaction rate constants at elevated temperature, which are shown in **Tables 2.6** and **2.7**.

Table 2.3 Basic equation for the radiolysis model

Rate equation along the flow path

$$\partial C_l/\partial t + \nabla(U_m C_l) = D_l \Delta C_l + q_l \quad (1)$$

Rate equation due to generation and annihilation of radiolytic specites

$$q_l = G_i^{\gamma} P^{\gamma} + G_i^{n} P^{n} + \Sigma_{mn} k^{i}_{mn} C_m C_n - C_i \Sigma_s k_{is} C_s + V_f/(1-V_f)(\varepsilon^{*}_l C^{\gamma}_l - \varepsilon_l C_l) \quad (2)$$

(i) (ii) (iii) (iv)

Explanation of each term:

(i) Generation due to radiolytic decomposition of H_2O_2
(ii) Generation due to the reactions of radiolytic species
(iii) Disappearance due to the reactions of radiolytic species
(iv) Transfer between liquid and steam phases

Table 2.4 Major features of water radiolysis code

- Calculated radiolytic species: 11 radiolytic species
  H_2O, O_2 , H_2, H_2O_2 , O_2^- , HO_2^- , H^+, HO^-, e_{aq}^-, H, OH, HO_2
- species generated due to neutron and gamma irradiations (g-values: **Table 2.6**)
- more than 40 reactions (**Table 2.7**)
- transfer of gaseous species to steam (from best fitting for plant data)
- H_2O_2 surface decomposition (experimental data [1])

Reference:

[1] Yeh T.K., Chu F., Electrochemical corrosion potential modeling in the primary heat transport circuit of the Chinshan Boiling Water Reactor under the condition of hydrogen water chemistry with noble metal coating, J. Nucl. Sci. Technol., 39 (12), 2000, pp.1063–1074.

Table 2.5 Major input data for water radiolysis calculation for entire BWR primary cooling system

plant parameters :	
power distribution	[supplied by nuclear design groups]
dose rate (energy absorption distribution)	[supplied by radiation shielding design groups]
flow rate	[supplied by thermal hydraulic design groups]
mixing rate	[do.]
chemical constants :	
g-values at elevated temperature	[radiation chemistry group]
rate constants at elevated temperature	[do.]
others :	
transfer coefficients of gaseous species	[do.]
interaction of radiolytic species and structural surfaces	[do.]

Table 2.6 g-values for BWR conditions (number of species/100eV)

species	gamma rays				neutrons			
	A	B	C	D	A	B	C	D
e^-	3.50	3.61	3.41	3.41	0.60	0.01	0.68	0.68
H	0.90	1.04	0.87	0.87	0.50	0.21	0.52	0.52
H^+	3.50	4.48	3.41	3.41	0.60	0.15	0.68	0.68
H_2	0.60	0.54	0.60	0.60	1.50	1.33	1.52	1.52
H_2O_2	0.55	0.29	0.31	0.31	1.14	0.97	1.22	1.22
HO_2					0.04			
OH	4.50	5.14	4.86	4.86	1.70	0.95	1.80	1.80
OH^-		0.86				0.14		0.00

Blank: not applied in the model

Table 2.7 Comparison of sets of rate constants used BWR conditions

	Forward reactions	Reverse reactions	Reaction constants							
			Forward reactions				Reverse reactions			
			A	B	C	D	A	B	C	D
1	$E^- + H_2O$	$H + OH^-$	2.90E+02	1.71E+02	1.90E+02	1.69E+02				
2	$E^- + H^+$	H	2.60E+11	3.50E+11	2.54E+11	4.11E+11			1.00E+05	
3	$E^- + OH$	OH^-	2.90E+11	2.13E+11	3.17E+11	3.17E+11				
4	$E^- + H_2O_2$	$OH + OH^-$	2.40E+11	1.30E+11	1.38E+11	1.48E+11				
5	H + H	H_2	9.00E+10	8.50E+10	1.06E+11	1.06E+11				
6	$E^- + HO_2$	HO_2^-	3.00E+11	2.13E+11	2.38E+11	2.12E+11				
7	$E^- + O_2$	O_2^-	2.60E+11	2.60E+11	2.01E+11	5.60E+11				
8	$2E^- + 2H_2O$	$H_2 + 2OH^-$	1.75E+06	2.28E+07	1.74E+07	1.73E+07				
9	2OH	H_2O_2	2.50E+10	1.70E+10	4.76E+10	2.00E+10				6.10E-03
10	$OH^- + H$	$E^- + H_2O$	7.00E+08	6.96E+08	6.88E+08	2.12E+08				
11	$E^- + H + H_2O$	$OH^- + H_2$	4.82E+09	5.51E+09	4.76E+09	4.76E+09				
12	$E^- + HO_2^- + H_2O$	$OH + 2OH^-$	5.35E+08	7.71E+08	6.67E+08	6.66E+08				
13	H + OH	H_2O	2.30E+11	5.50E+10	2.12E+11	2.12E+11				
14	$OH + H_2$	$H + H_2O$	1.40E+09	9.56E+08	1.27E+09	1.27E+09		2.46E+02	1.10E+03	
15	$H + O_2$	HO_2	1.50E+11	8.60E+10	2.01E+11	1.07E+11				
16	$H + HO_2$	H_2O_2	3.00E+11	2.13E+11	2.11E+11	2.12E+11				
17	$H + O_2^-$	HO_2^-	3.00E+11	2.13E+11	2.11E+11	2.12E+11				
18	$E^- + O_2^- + H_2O$	$HO_2^- + OH^-$	3.57E+09	9.36E+07	1.13E+08	6.19E+09				
19	$H + H_2O^2$	$OH + H_2O$	2.00E+09	2.06E+09	3.07E+09	1.12E+09				
20	$OH + H_2O_2$	$H_2O + HO_2$	4.20E+08	3.49E+08	3.91E+08	3.91E+08				
21	$OH + HO_2$	$H_2O + O_2$	1.00E+11	8.60E+10	1.27E+11	1.27E+10				
22	$OH^- + H_2O_2$	$HO_2^- + H_2O$	1.00E+10	6.27E+09	1.72E+10	3.44E+09	2.14E+05	4.09E+05	1.08E+05	1.08E+05
23	$2HO_2$	$H_2O_2 + O_2$	5.00E+07	6.29E+07	9.29E+07	3.55E+07				
24	HO_2	$O_2^- + H^+$	3.90E+05	2.74E+05	8.46E+06	6.96E+06	7.70E+11	5.33E+11	5.29E+11	5.29E+11
25	$HO_2 + O_2^-$	$O_2 + HO_2^-$	5.00E+08	5.00E+09	5.16E+08	5.16E+08				
26	$H^+ + OH^-$	H_2O	1.90E+12	1.54E+12	1.48E+12	1.52E+12	1.40E-01	1.57E-01	1.81E-01	1.32E-01
27	$O_2^- + OH$	$OH^- + O_2$	2.90E+11	8.60E+10	1.27E+11	2.72E+11				
28	$2O_2^- + 2H_2O$	$O_2 + H_2O_2 + 2OH^-$	1.27E+05		1.93E+05	1.93E+05				
29	$2H_2O_2$	$2H_2O + O_2$			2.07E-01					
30	H_2O_2	$H^+ + HO_2^-$				3.34E-01				2.12E+11
32	$HO_2^- + OH$	$HO_2 + OH^-$				7.93E+10				

Blank: not applied in the model

As one of examples of the radiolytic calculation, oxidant concentration maps are shown in **Figure 2.15**, where under a NWC condition, oxidant concentrations are kept at higher levels, while under a HWC condition, oxidant concentrations are tremendously.

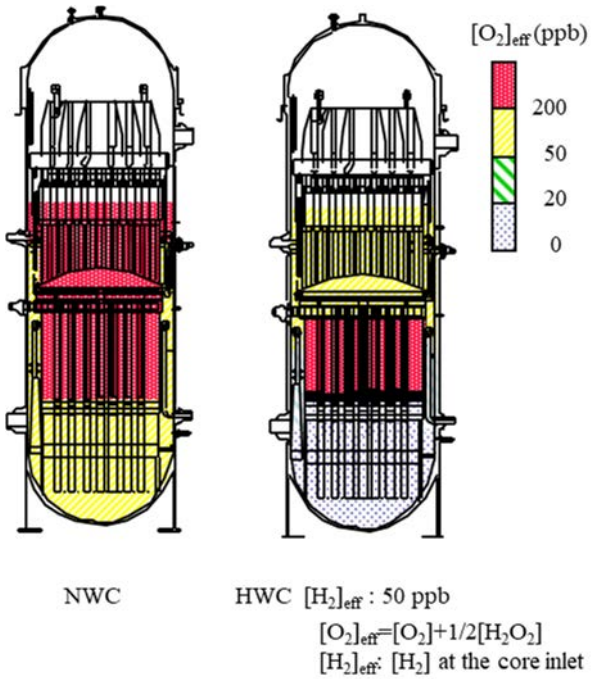

Figure 2.15 Maps of distribution of $[O_2]_{eff}$ in RPV
(Effects of hydrogen injection on suppression of $[O_2]$)

2.5.2 ECP Calculation

The ECP codes were based on a mixed potential theory [25], where the concentrations of major radiolytic species, i.e., O_2, H_2O_2, and H_2, obtained from the water radiolysis codes and anodic polarization properties as functions of potential are applied for determining ECP [26]. ECP is determined as an intersection of the anodic current density curve due to anodic polarization of metal and oxidation of radiolytic species and the cathodic current density curve due to reduction of oxidant species (**Figure 2.16**).

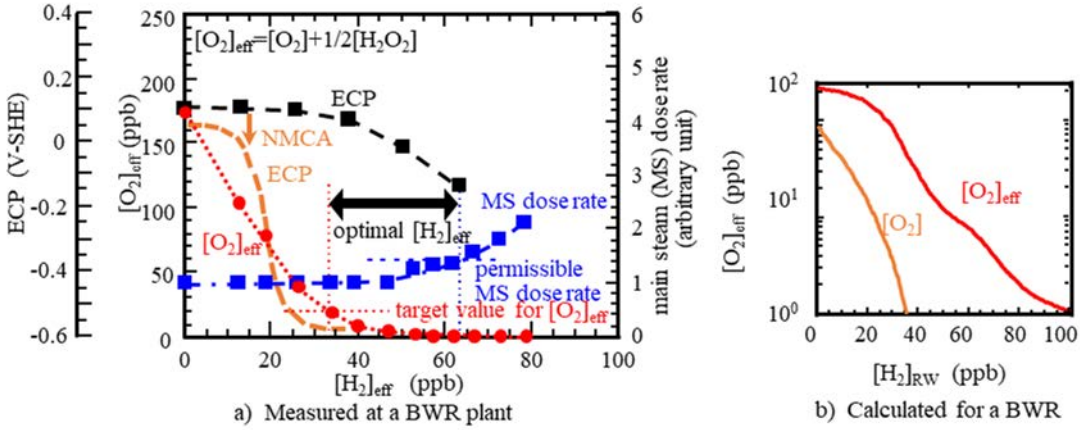

Figure 2.16 Optimal water chemistry control (BWR primary cooling system)

Applied anodic polarization data for each ECP code differ. The major chemical equations to determine ECP are shown in **Table 2.8** and the major equations to determine current densities on the metal surface are shown in **Table 2.9**.

Table 2.8 Major cathodic and anodic reactions

Cathodic reactions:

$H_2O_2 + e^- = OH + OH^-$

$O_2 + e^- = O_2^-$

$O_2 + 2H_2O + 2e^- = 2O_2^- + 2H_2$

$2H^+ + 2e^- = H_2$ (hydrogen generation at low potential)

Anodic reaction:

$M = M^{z+} + ze^-$

Table 2.9 Major equations to determine current densities

Cathodic current densities:

$$I_c = f(\phi)\, C_s \quad (3)$$

$$f(\phi) = z\, F\, k_o \exp(-\alpha z F(\phi-\phi_0)/RT) \quad (4)$$

$$I_c = f(\phi)C^b/(1+ f(\phi)/z/F\ \delta_o D_o)/\{1+ f(\phi)/z/F\ \delta_B/D_B/\ (1+ f(\phi)/z/F\ \delta_o D_o)\} \quad (5)$$

Anodic current densities:

$$I_a = f'(\phi)\,(X_{sat}-X_s) \quad (6)$$

$$f'(\phi) = z'\, F\, k_o' \exp(+\alpha' z' F(\phi-\phi'_0)/RT) \quad (7)$$

$$I_a = f'(\phi)\,[X_{sat}-\{X_b+f'(\phi)X_{sat}/z/F(\delta_o/D_o+\delta_B/D_B)\}/\{1+(f'(\phi)/z/F+\beta)(\delta_o/D_o+\delta_B/D_B)\}] \quad (8)$$

Anodic current densities due to oxidation of H_2O_2:

$$I_a^H = z^*\beta^*F\, k_o\, ^* \exp(+\alpha^* z^* F(\phi-\phi^*_0)/RT)\, C_s^H \quad (9)$$

Major reaction constants for ECP calculations are shown in **Table 2.10**.

Table 2.10 Major parameters for electrochemistry model

	$H_2O_2 + e^- \rightarrow OH + OH^-$	$O_2 + 2H_2O + 2e^- \rightarrow 2O_2^- + 2H_2$	$Fe \rightarrow Fe^{2+} + 2e^-$	Oxidation of H_2O_2
Transfer coefficient, α (-)	0.8	0.3	0.5	0.5
Potential for standard, ϕ_o (V-SHE)	-0.04	-0.04	-0.44	-0.44
Number of electron taken for a reaction, z (-)	1	2	2	2
Electrochemical reaction rate, k (m/s)	5×10^{-5}	2×10^{-7}	10^{-2}	10^{-3}
Oxidation efficient, β^* (-)	-	-	-	0.2

2.6 PWSCC in PWR Primary Cooling System

As a result of full suppression of water radiolysis in the PWR primary system, it has been reported that the major water chemistry factor to determine primary water stress corrosion cracking (PWSCC) is not oxygen but hydrogen [27]. For this, the optimal $[H_2]$ to mitigate PWSCC and at the same time to suppress oxidant concentration [28]. The latest data on PWSCC initiation showed that the crack initiation time decreased monotonously [29]. To mitigate PWSCC initiation and at the same time mitigate crack growth rate, $[H_2]$ should be decreased below the peak value. The water radiolysis model has been developed for PWR conditions to explain ECP for different $[H_2]$ (**Figure 2.17**).

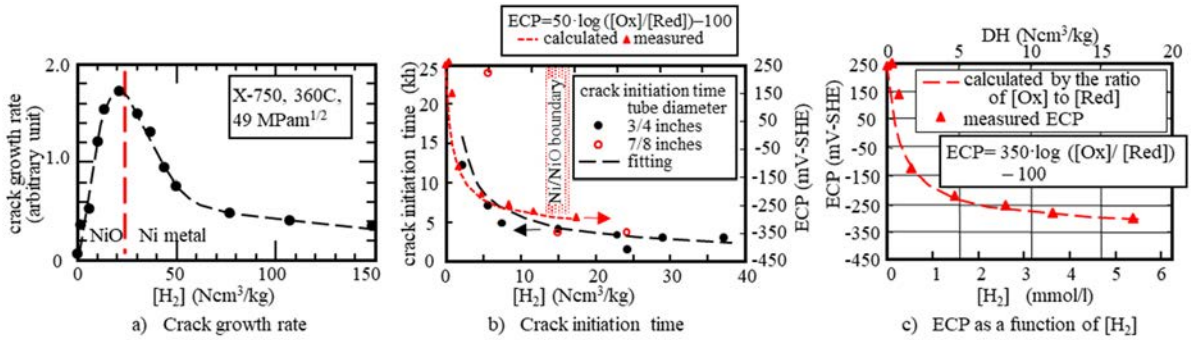

Figure 2.17 Optimal water chemistry control (PWR reactor water)

3. Major Corrosive Parameters to Determine IGSCC and PWSCC

3.1 Corrosive Parameters in BWR and PWR Primary Cooling System

The Outline of the Corrosive parameters in BWR and PWR primary cooling system were shown in the section 2.3. Those for IGSCC of stainless steel in BWRs and PWSCC of nickel alloy in PWRs are summarized in **Table 3.1** [1), 16), 30)].

Table 3.1 Control target value of water chemistry in primary cooling water

Corrosive parameters	(Units)	IGSCC of BWRs	PWSCC of PWRs	Measured in plants
Macroscopic parameters				
pH	(-)	pH_R:	pH_T:	pH_R: possible, pH_T: determined by calculation based on [B] and [Li]
Conductivity	(μS/m)	<10 μs/m	determined by B]/[Li]	measured with in-line monitors
ECP	(V-SHE)	<0.24 V-SHE	not measured in plants	measured by in-situ detector at specified location
Microscopic parameters				
$[H_2O_2]$	(ppb or mol/L)	1-100 ppb	~10 ppb	generally impossible in plants
$[O_2]$		20-200 ppb	< 5 ppb	measured with in-line monitors
$[H_2]$		20-200 ppb	~ 2,000 ppb	
$[C^{L-}]$	(ppm or mol/L)	< 1 ppm	< 1 ppm	
[Li]		-	< 3.5 ppm	
[B]		-	200-2000 ppm	

pH_R: pH at room temperature, pH_T: pH at elevated temperature

3.2 Determination of Corrosive Parameters

The key parameters of water chemistry in nuclear power plants are divided into four kinds, i.e., (1) physical parameters (temperature and pressure), (2) complex chemical parameters that determine corrosive conditions (pH, conductivity), (3) elemental chemical parameters that determine corrosive conditions ($[O_2]$, $[H_2O_2]$, $[H_2]$) and (4) parameters resulting from corrosion (concentrations and radioactivity of corrosion products), as shown in **Figure 3.1** [13)].

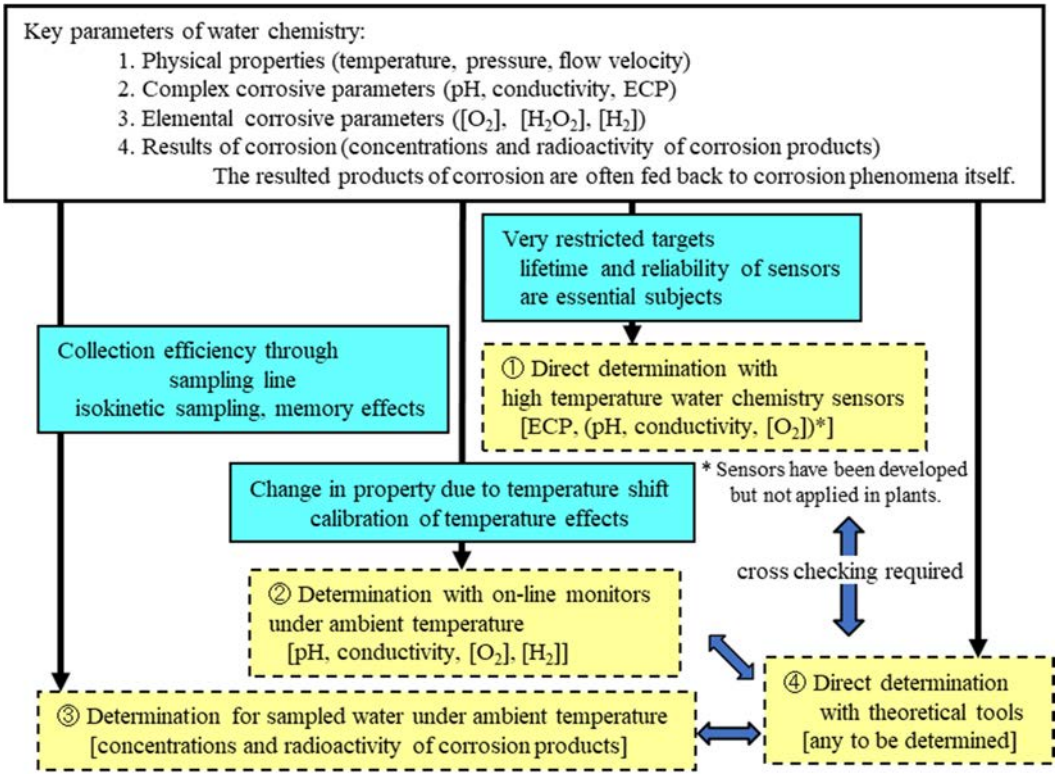

Figure 3.1 Determination of properties of cooling water in NPPs

There are four approaches to determining the key parameters of water chemistry under high temperature, which define four groups of parameters:

(1) Direct determination with high-temperature water chemistry sensors. Electrochemical corrosion potential (ECP) as well as physical parameters, e.g., temperature, pressure and flow velocity, are categorized as parameters of Group (1).

(2) Determination with online monitors at ambient temperature. Conductivity, pH, $[O_2]$, $[H_2]$ and concentrations of some metallic ions and anions are categorized as parameters of Group (2).

(3) Determination from sampled water at ambient temperature. Concentrations and radioactivity of corrosion products are categorized as parameters of Group (3).

(4) Indirect determination with theoretical tools. The distributions of concentrations of radiolytic species and ECP throughout the cooling system are determined by water radiolysis codes and ECP codes. Any to be determined by the theoretical tools are categorized as parameters of Group (4).

Each approach currently has both advantages and disadvantages. Direct determination is restricted to physical properties, e.g., temperature, pressure and flow velocity. An ECP sensor with sufficient lifetime and reliability is still to be developed, while other sensors are still under development for plant application. Determination with online monitors at ambient conditions and from sampled water (Groups (2) and (3)) has problems associated with reducing temperature from the original points of interest to measuring points at lower temperature. The details of the problems and countermeasures are discussed in the section on sampling. Even when the key parameters based on Groups (1) – (3) are determined, there are additional requirements to interpolate or extrapolate the data to locations where the measurements cannot be taken. Also, for application to BWRs in particular, some radiolytic species are so unstable at high temperature that determining their distribution and the resulting ECP throughout the cooling systems can only be achieved with extrapolation based on theoretical tools. There are many such theoretical tools for predicting corrosive conditions, but their reliability is often open to question. On the other hand, several instruments are available to indicate corrosion by measuring the interaction with metal components directly, rather than by quantifying water chemistry parameters. The key parameters to be monitored in water-cooled nuclear plants are compiled in **Table 3.2** [13].

Table 3.2 Key of water chemistry parameters

Reastor / Parameter	PWR		BWR	
	primary	secondary	Reactor (primary)	feedwater (secondary)
Temperature (°C)	200-325	20-285	200-285	20-285
Pressure (MPa)	15.5	7.2	7.2	7.2
$pH_{25°C}$ (-)	6.8-7.2* (at T=300 °C)	8.8-9.5	neutral	neutral
(1) Reactivity control	**[B]**	-	**void fraction**	-
(2) Structural integrity	**pH_T**, [B], [Li], $[H_2]$, **conductivity**	**pH, $[O_2]$**, $[SO_4^{2-}]$, $[N_2H_4]$, **conductivity**	pH, **$[O_2]$,$[H_2O_2]$** conductivity, **ECP**	$[H_2]$, **$[Cl^-]$**, $[SO_4^{2-}]$
(3) Fuel Integrity	[Li], $[Cl^-]$, [Fe] **pH_T**, $[^{131}I]$	-	pH, $[^{131}I]$, **$[O_2]$**	[Fe], **[Cu]**, $[SO_4^{2-}]$
(4) Activity transport	**pH_T**, [B], [Li], **$[^{58}Co]$**, **$[^{58}Co]$**	-	**$[O_2]$**, **$[^{60}Co]$**	**[Fe]**, **[Co]**, **[Zn]**

Bolt: water chemistry parameters directly influence to material behavior

3.3 Instruments for Determining the Key Parameters of Water Chemistry

3.3.1 Proven Instruments

The reactor control items and the key parameters to be monitored are listed in Table 3.2. Determination of physical parameters and macroscopic parameters is based on traditional instruments. The reliability of the reference electrode is the key issue in ECP measurement. The determination of macroscopic parameters is based on traditional polarography instruments, while that of H_2O_2 concentration is based on newly developed luminol luminescence spectroscopy [31]. Boron concentration is determined by neutralization titration and Li concentration is determined by atomic absorption spectroscopy (AAS) [32), 33), 34)]. Metallic ion concentration is measured with AAS or inductively coupled plasma - atomic emission spectrometry (ICP-AES or, with mass spectrometric analysis, ICP-MS), while in Japan X-ray fluorescence spectroscopy (XFS) has been applied to samples collected on membrane filters. Stripping polarography has been used at some plants in the US. Membrane filters can also be used to determine radioactive nuclides with Ge (Li) or high-purity Ge semiconductor detectors [35), 36), 37)].

3.3.2 High-temperature Sensors

High-temperature water chemistry sensors are divided into those determining water chemistry directly and those determining corrosive conditions indirectly by analyzing the interaction between water and materials [12)]. Major high-temperature water chemistry sensors are listed in **Table 3.3**.

Table 3.3 High temperature water chemistry sensors

Measured items		Detector	Principle	Applied	Ref.
1) Water chemistry	a) [O_2]	pressure balance type	membrane + polarography	LAB	[1]
		ECP detector	ECP-[O_2] relationship	LAB	[1,2]
	b) [H_2]	pressure balance type	membrane + polarography	LAB	[3]
		Pd wire type H_2 detector	H_2 absorption + ER	LAB	[4]
	c) [H_2O_2]	Sensor array	a couple of ECP and FDCI	LAB	[5]
	d) Conductivity	coupled/triple electrodes	complex impedance	LAB	[6]
	e) pH	ZrO_2 type pH sensor	ion electrode	LAB	[7]
		TiO_2 type pH sensor	flat band potential	LAB	[8]
2) interaction between water and materials	a) ECP	external (Ag/AgCl)	ion electrode	NPP	[2]
		internal (Pt)	ion electrode	NPP	[9]
		internal (Ag/AgCl)*	ion electrode	NPP	[10]-[12]
	b) Corrosion rate	DC current measurement	ER change due to thinning	LAB	[3]
		DC corrosion detector	Tafel plot	LAB	[3]
		AC corrosion detector	Board diagram	LAB	[3]
		HEPro	H_2 effusion	NPP	[13]
		FOLTM	Ultrasonic gauging	NPP	[14]
	c) Oxide film properties	CDE-arrangement detector	contact electric resistance measurement	LAB	[15], [16]
		FDCI sensor	complex impedance	LAB	[17]
	d) Crack initiation	ECP detector	potential noise analysis	LAB	[18], [19]
	e) Crack growth	CT specimen	potential drop measurement	NPP	[20]
		DCB type	potential drop measurement	NPP	[21]

*: Many electrodes, e.g., Ag/AgCl, F/Fe_2O_3, Ni/NiO are applied.

Lab: used only in laboratory experiments NPP: applied in operating nuclear power plants ER: electric resistance

CT: compact tension DCB: double cantilever beam CDE: controlled distance electrochemistry FDCI: frequency dependent complex impedance

FOLTM: feeder online thickness measurement HEPro: measures FAC via atomic hydrogen generated

References:

[1] Uchida S, et al., An electrochemical sensor array for in-situ measurements of oxide film electric resistance in high temperature water. ECS Trans. 2007;2(25):39–50.

[2] Uchida S, Katsumura Y. Water chemistry technology – one of the key technologies for safe and reliable nuclear power plant operation. J Nucl Sci Technol. 2013;50:346–362.

[3] Vajda N, et al., Analysis of actinides in the primary coolant of a WWER-440 type reactor. J Radioanal Nucl Chem. 2005;170(2):399–409.

[4] Asakura Y, et al., Inline monitor for electrical conductivity of high tem perature aqueous environments. J Electrochem Soc. 1989;136:3309–3313.

[5] Tachibana K. Pressure-balance pH sensing system for high temperature and high pressure water. Materia Japan. 1995;34:1227–1232. Japanese.

[6] Hara N, Sugimoto K. A Nb-doped TiO_2 semiconductor pH sensor for use in high temperature aqueous solutions. J Electrochem Soc. 1990;137(8):2517–2523.

[7] Nagata N. In core measurement of electrochemical corrosion potential in Tsuruga-2. Paper presented at: International Workshop on Optimization of Dissolved Hydrogen Content in PWR Primary Coolant; 2007 Jul 18– 19; Sendai: Tohoku University. (Paper 16).

[8] Ashida S, et al., First experience of hydrogen water chemistry at Japanese BWRs. Paper presented at: International Conference on Water Chemistry of Nuclear Reactor Systems 6; 1992 Oct 12–15; Bournemouth: British Nuclear Energy Society.

[9] Takiguchi H, et al., Evaluation of effectiveness of hydrogen water chemistry for different types of boiling water reactors. J Nucl Sci Technol. 1999;36(2):179– 188.

[10] Bosch RW, et al., LIRES; European sponsored research project to develop light water reactor reference electrode. Paper presented at: EUROCORR2003; 2003 Sep 26 to Oct 2; Budapest: European Federation of Corrosion.

[11] McKeen K, et al., Hydrogen effusion probe development and installation at the Point Lepreau Generating Station. Paper presented at: 28th Annual Conference of the Canadian Nuclear Society; 2007 Jun 3–6; St. John: Canadian Nuclear Society.

[12] Aiken J., New Brunswick innovation to assist energy challenges. RPC Tech. release; 2007 Nov 27. Fredericton: Research and Productivity Council, Fredericton, New Brunswick, Canada.

[13] McKeen K, Lalonde M, Scott A, Ross J., Hydrogen effusion probe development and installation at the Point Lepreau Generating Station. Paper presented at: 28th Annual Conference of the Canadian Nuclear Society; 2007 Jun 3–6; St. John: Canadian Nuclear Society.

[14] Aiken J. New Brunswick innovation to assist energy challenges. RPC Tech. release; 2007 Nov 27. Fredericton: Research and Productivity Council, Fredericton, New Brunswick, Canada.

[15] Bojinov M. Development of electrochemical techniques to study oxide films on construction materials in high temperature water. Paper presented at: JAIF International Conference on Water Chemistry in Nuclear Power Plants; 1998 Oct 13–16; Kashiwazaki: Japan Atomic Industrial Forum.

[16] Bojinov M, et al., A conduction mechanism of the passive film on iron based on contact electric impedance and resistance measurement. J Electrochem Soc. 2001;148:B243–B250.

[17] Tachibana K. Pressure-balance pH sensing system for high temperature and high pressure water. Materia Japan. 1995;34:1227–1232. Japanese.

[18] Hickling J, et al., Use of electrochemical noise to detect stress corrosion crack initiation in simulated BWR environments. Mater Corrosion. 1998;49:651–658.

[19] Liu C, et al., Probing corrosion activity in high subcritical and supercritical water through electrochemical noise analysis. Corrosion. 1994;50:687–694.

[20] Catlin WR, et al., Coffin LF. The reversing D-C electric potential method. In: Cullen WH, Landgraf RW, Kais and LR, Underwood JH, editors. Automated test methods for fracture and fatigue crack growth, ASTM STP, 887, 67. Philadelphia (PA): American Society for Testing and Materials; 1985.

[21] Weinstein D. Real time in reactor monitoring of double cantilever beam crack growth sensors. Paper presented at: 6th International Symposium on Environmental Degradation of Materials in Nuclear Power Systems – Water Reactors; 1993 Aug 1–6; San Diego (CA): American Nuclear Society; 645–650.

The purposes of high-temperature water chemistry sensors are divided into three categories:

Category 1: Direct determination of water chemistry parameters at elevated temperature instead of theoretical extrapolation from data obtained at room temperature. Changes in data at room temperature and elevated temperature are estimated but the extrapolation procedures may contain uncertainties (e.g., relating to pH and conductivity).

Category 2: Indirect determination of water chemistry parameters when the water chemistry index cannot be determined at room temperature. Some chemical species disappear due to thermal decomposition during the

cooling-down process ([H_2O_2] in BWR reactor water) and chemical reactions in the sampling line ([O_2] in PWR feedwater).

Category 3: Direct measurement of interaction of water and materials at elevated temperature (ECP, corrosion rate, crack growth).

An international collaborative programme on high temperature water chemistry sensors has been carried out by the International Atomic Energy Agency, IAEA (WACOLIN (1986–1991) [38]: WACOL (1992–2000) [39]: and DAWAC (2001–2005) [40]). As a result of compiling the literature survey and internationally exchanging information and experience on high-temperature sensors, it was concluded that many instruments had been developed for direct measurement of water quality, and some of them had been successfully applied in laboratory tests, but only a few had been applied to operating power plants [41]. The instruments reviewed appear in Table 3.2.

The requirements for applying high-temperature sensors in operating plants are as follows:

(1) High accuracy: application without cooling to determine water chemistry index directly;

(2) Quick response: direct connection between sensor and data acquisition system; and

(3) High reliability and safety: easy calibration, maintenance-free at least for a light-water reactor (LWR) operation period (1–1.5 years).

Of great importance as a transient species in BWR reactors, H_2O_2 unfortunately is unstable in high temperature water so determining its concentration by sampling is difficult. Almost all of the H_2O_2 disappears during the sampling process. The procedures to determine [H_2O_2] are the application of theoretical radiolysis models or the direct or indirect measurement at elevated temperature [42].

One measurement technique for [H_2O_2] employed in the laboratory is frequency-dependent complex impedance (FDCI), which records the impedance of an interface as a sinusoidal potential difference is applied. To measure [H_2O_2], the semicircles of Cole-Cole (Nyquist) plots of the real part of the impedance against the imaginary part have been correlated with the concentration. As [H_2O_2] was reduced from 100 to 5 ppb in a BWR environment with stainless steel electrodes, the radii of the low-frequency semicircles on the Cole-Cole plots increased continuously, while the ECP remained constant at concentrations down to 10 ppb and then decreased a little to 5 ppb [35]. The increasing radii meant an increasing resistance from formation of oxide on the electrode. Both dependences of ECP and FDCI semicircle radii on [H_2O_2] were not affected by co-existent [O_2] with the same level of oxidant concentration.

As a result of water radiolysis evaluation for BWR reactor water, it was concluded that 100 ppb H_2O_2 co-existed with 200 ppb O_2 under normal water chemistry (NWC), while 10 ppb H_2O_2 existed without measurable concentrations of O_2 under hydrogen water chemistry (HWC). Coupled with the FDCI measurements, this meant that corrosive conditions of HWC were the same as those of NWC from the viewpoint of ECP, even as [H_2O_2] was varied over a wide range. The corrosion of structural materials could be affected. By contrast, in situ experiments of the general corrosion of AISI 316L stainless steel under BWR conditions with varying concentrations of H_2O_2 and H_2 with no added O_2 indicated that as NWC was switched to HWC so that the ECP fell from + 0.15 V (vs. saturated hydrogen electrode, SHE) to −0.56 V, the corrosion rate increased sharply, but when the fall was from + 0.15 to −0.42 V there was no change in corrosion rate. It was pointed out that the equilibrium potential for the transition between α-Fe_2O_3 and Fe_3O_4 is −0.47 V, so the difference in behavior between the two experiments was described to changes in the structure of the oxide film at the lowest potential [43]. We note that inferring high-temperature ECP, corrosion rate and crack growth rate by extrapolation from the data obtained at room temperature causes a large uncertainty due to insufficient

data bases to support the extrapolation.

High-temperature sensors applied at operating plants are listed in Table 3.3. Most of them are sensors for structural material integrity. High-temperature reference electrodes for ECP measurements and in situ potential drop detectors for crack propagation measurements on compact tension test specimens have been applied during the benchmark tests of HWC in operating BWRs. Flow-accelerated corrosion (FAC) of the feeders in CANDU primary coolants has been monitored with FOLTMs and HEPros, and the latter have been applied to feedwater piping in CANDUs and thermal plants and to water-wall tubing in thermal plants. In order to ensure a reductive environment and thus mitigate secondary side corrosion of SG tubing, the optimum hydrazine content in the secondary system of dual-cycle reactors can be assessed from ECP measurements. However, ECP measurements are carried out only in a very few units where, once the optimum hydrazine condition is defined, the plant staff need only monitor hydrazine routinely and ECP measurements can then be discontinued. Instead of direct ECP measurements, a combined approach of concentration measurements of anions and cations by ion chromatography and empirical calculations based on crevice concentration factors and pH evaluation may be successfully applied to determine the corrosive conditions at the tubing and in the crevice between the tubing and the tube support plates. The value of ECP control for secondary coolant systems has been demonstrated by Turner and Guzonas [44], who presented the safe operating zones for common SG tube materials in terms of the ECP versus high-temperature pH in the SG crevices [45].

High-temperature sensors for water chemistry, namely pH, conductivity and [O_2], have provided valuable data in laboratory tests. However, their application in operating plants is still at the final stage of being accepted. In order to facilitate their application, the following steps should be taken.

(1) Clear presentation of their necessity and benefits.

(2) Improvement of their reliability during operation: sufficient integrity of sensors themselves with straightforward calibration procedures at suitable intervals.

(3) Ensuring protection against their failure during application: suitable procedures for avoiding release of loose parts and chemical contamination.

(4) Provision of information from case studies involving plant diagnoses of systems based on high-temperature sensors.

Much experience with developing high-temperature sensors in laboratory tests and then improving their reliability and ease of handling suggests opportunities for their application not only in nuclear plants but also in thermal power plants. However, significant barriers to their installation in primary coolants in nuclear plants are the existence of unstable and often aggressive radiolytic species which degrade the sensor materials, as well as the irradiation damage of the sensors themselves, and in thermal plants the barriers are the higher temperatures and chemical treatments which again degrade the sensor materials.

3.4 The Gaps between the Desired Information and the Measured Data

Major gaps between the information needed to understand the phenomena and the measured water chemistry data are shown in **Table 3.4**, along with measures to bridge the gaps [4]. Some mismatching between the information desired to understand plant conditions at elevated temperature and the water chemistry data measured at room temperature has been reported [1]. From the viewpoint of water chemists, procedures for bridging the gaps as well as provision of quality assurance for acquiring water chemistry data are essential for optimum operation of the plant. The major measures to bridge the gaps are twofold: the theoretical approach and the direct determination by applying high-temperature water chemistry sensors.

Table 3.4 Gaps between desired information and measured data

Desired information to understand phenomena	Measured WC data in plants	Major measures to bridge the gaps
Corrosive conditions [H_2O_2, O_2, H_2]	• Measured [O_2, H_2]	• Theoretical models for water radiolysis • *High temperature O_2 sensors* • ECP sensors
Crack propagation rate	• Crack growth rate under simulated conditions	• *High temperature crack growth rate sensors* • Theoretical & empirical models for crack propagation rate
High temperature pH	• pH at cooled water	• Theoretical evaluation • *High temperature pH sensors*
Properties of oxide film on sampled specimens	• Characterization of oxide film	• Theoretical oxidation models • *High temperature impedance sensors*

Italic: high temperature sensors

4. An Approach Toward Determining Corrosive Parameters

4.1 Water Radiolysis

However, procedures for determining corrosive conditions have not been authorized by any institute yet. There are several sets of calculation codes for determining corrosive conditions which basically depend on the same theoretical basis, but their numerical treatments and major calculation constants and input data taken from plant operational features are not the same [18), 19), 20), 21), 22), 23)]. A trio of authorized procedures for crack growth rates, corrosive conditions and stress intensity factors should be set and then the entire procedures for evaluation of reliabilities of major components could be accepted by the government and the public.

4.1.1 Basic Equations

The concentration of radiolytic species is calculated along the flow path shown in **Figure 4.1**. The figure shows the flow path of a BWR. That for a PWR is almost the same as BWR. For PWRs, flow line for the SG is added and transfer of the radiolytic species from liquid phase to gas phase can be neglected.

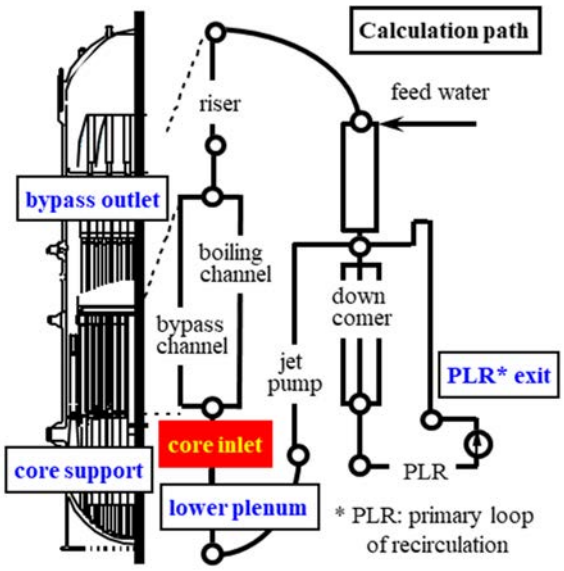

Figure 4.1 Calculation path used for water radiolysis model

Mass balance calculation in each cell is divided into two processes; one is the fast process (radiolytic reaction) based on direct generation of radiolytic species due to radiation-induced water decomposition and the secondary generation and disappearance by their cross-interaction reactions, and the other is rather slow process. The slow process is based on flow-in and flow-out of water containing the radiolytic species and their cross interactions between the liquid and steam phases.

1) Fast reaction in each cell

$$dC_i/dt = \{G^{\gamma}{}_i E^{\gamma}{}_r + G^{n}{}_i E^{n}{}_r + G^{\alpha}{}_i E^{\alpha}{}_r \} + \Sigma \{k_{mn} C_m C_n\} - C_i \Sigma \{k_{is} C_s\} \quad (i = 1,J) \quad (4\text{-}1)$$

$$G_i = g_i F \quad (4\text{-}2)$$

,where g_i: microscopic g-value (numbers of species/100eV) [subscript: i; i-th radiolytic specie],
[superscript: γ; gamma-rays, n; neutrons, α; alpha-rays]
k_{mn}: rate constant $((mol/m^3)^{-1}\ s^{-1})$ [subscript: m and n; m-th and n-th radiolytic species]
C_i: concentration of i-th specie $(mol/\ m^3)$
G_i: macroscopic g-vale of i-th specie (mol/J)
F: conversion factor ((mol/J)/(atom/100eV))

$$[1/10^2/(1.602\times10^{-19}\times6.023\times10^{23})] = [1.04\times10^{-7}]$$

E_r: energy deposition rate (J/ m^3/s)

2) Reactions on the surface of each cell (Fast reaction)

$$dC^w_i/dt = + \Sigma \{k^w_{mn}C^w_mC^w_n\} - C^w_i \Sigma \{k^w_{is}C^w_s\} \quad (4\text{-}3)$$

,where k^w_{mn}: rate constant at the surface $((mol/m^3)^{-1}\ s^{-1})$
[subscripts: m and n; m-th and n-th radiolytic species]
C^w_i: concentration of i-th specie at the surface (mol/ m^3)

3) Mass transfer due to mixing between the cell and surface

$$dC_i/dt = dC_i/dt + \delta\ (dC^w_i/dt - dC_i/dt) \quad (4\text{-}4)$$

4) Mass transfer due to the flow [one dimensional steady]

$$[dC_i/dt] = \partial\ C_i/\partial\ t + v\ \partial\ C_i/\partial\ x \quad (4\text{-}5)$$

$$\partial\ C_i/\partial\ t = dC_i/dt \quad (4\text{-}6)$$

$$v\ \partial\ C_i/\partial\ x = v^{l-1}S^{l-1}C_i^{l-1} - v^lS^lC_i^l \quad (4\text{-}7)$$

,where v^l: velocity (m/s) [superscript: l; l-th cell]
S^l: cross section area (m^2) [superscript: l; l-th cell]

5) Mass transfer between the liquid and steam phases

$$dC_i/dt = \varepsilon\ F_vC_i + \varepsilon^*F_vC^g_i \quad (4\text{-}8)$$

,where C_i: concentrations of i-th species (mol/L) [superscript: g; gas phase]
ε : gas release rate (1/s)
ε^*: gas absorption rate (1/s)
F_v: factors (-)

6) Concentration of gaseous species in the end cell

$$Cg = R^l/(U^gS^g) = \int_0^t(\varepsilon\ V_fC_i + \varepsilon^*V_fC^g_i)S^oU^l dt/(U^gS^g) \quad (4\text{-}9)$$

,where C_i: concentrations of i-th species (mol/L) [superscript: g; gas phase]
R^l: flow rate of i-th specie in gas phase (mol/s)
U: flow velocities of water and gas (m/s) [superscript: l; liquid phase, g; gas phase]
S: channel cross section (m^2) [superscript: l; liquid phase, g; gas phase, o; total]
V_f: void fraction (-)

The equations (4.1) - (4.9) were integrated along the flow path and the concentrations of the species were obtained based on the initial guess at the flow entrance (**Figure 4.1**).

4.1.2 Previous Calculation Codes

Water radiation calculation codes based on numerical integration of multi-differential equations have been developed [46), 47), 48)]. The results of the calculation codes, i.e., $[H_2O_2]$ and $[O_2]$, could be applied to bridge the gap between the measured ECP and measured $[O_2]$. Those code could successfully applied to explain the contribution of H_2O_2 to ECP especially at high H_2 injection rate The $[H_2O_2]$ and $[O_2]$ have been calculated and for both normal water chemistry (NWC: without H_2 injection) and hydrogen water chemistry (HWC: with H_2) conditions, $[H_2O_2]$ alone was high enough to determine ECP From the viewpoint of structural integrity of BWRs, monitoring and control of $[O_2]$, $[H_2]$, ECP and main steam dose rate are important. To

explain the gap quantitatively and to extrapolate the measured values to any location of interest, water radiolysis models have been applied. The models were extended to understand ^{16}N behaviors in the reactor water and main steam line [8].

Water radiolysis calculation has been applied only for BWR conditions, where suitable amounts of hydrogen has been added to suppress [H_2O_2] and [O_2] to mitigate IGSCC occurrence and its propagation in the primary cooling system. The excess amounts of injected hydrogen resulted in increasing ^{16}N transfer from the reactor to turbine systems and increased turbine dose during the plant operation. On the other hands, insufficient amounts of hydrogen could not suppress [H_2O_2] and [O_2] for mitigation of IGSCC. In PWR, Sufficient amounts of hydrogen was injected into the primary coolant to suppress oxidant concentrations. They used not to control hydrogen concentration precisely. However, it was reported that one of the parameters to determine PWSCC was hydrogen itself, and then, oxidant concentration should be suppressed with minimum charge of hydrogen. For obtaining the suitable amounts of hydrogen and oxidants, in PWRs water radiolysis calculation is going to be required to suitable hydrogen amounts and oxidant concentrations.

This is the reason why the water radiolysis analysis is required not only for BWR primary system but also for PWR primary cooling systems. However, in order to apply the water radiolysis calculation code to the PWR primary cooling system, several functions, e.g., calculation of pH_T effects on radiolysis, should be added to the original one developed for BWR primary cooling system. Additionally, ECP calculation for different water chemistry conditions of PWR primary cooling system should follow the water radiolysis calculation.

4.1.3 Subjects to Improve the Previous Water Radiolysis Models

Major functions to be added to the water radiolysis calculation code developed for application to BWR primary cooling system are as follows.

(1) pH_T calculations: Water radiolysis is much affected by pH_T. For Evaluation of BWR primary cooling system, pH_T was determined only by the dissociation of H_2O, which could be calculated by applying Marshall-Frank formula [49], while for PWR primary cooling system, the complex relationship of combined control of boric acid and lithium hydroxide. The pH_T is determined by applying the multi-step dissociation constants of boric acid proposed by Mesmar [50]. The pH_T calculation have to be calculated in priory to water radiolysis calculation.

(2) pH_T effect: Water radiolysis calculation, especially calculation of [H_2O_2] are much affected by H radical concentration, which determined by [H^+], i.e.,pH_T [3]

(3) Void effects: Only subcooled boiling is considered in the PWR primary cooling system. However, the effects of boiling in the coolant have to be considered for water radiolysis calculation. Original void effects have been developed by E. Ibe [51].

(4) Oxide layer effects: As a result of exposure time, thick oxide layers developed on the structure surface, which effect on the electric resistance of ferrous ions from the metal and then anodic polarization currents. A coupled model of oxide layer growth and electrochemistry has been developed to evaluate the anodic current densities due to oxide layer growth [52].

(5) Coupled calculation of water radiolysis and ECP: ECP calculation was used to be carried out by following the water radiolysis calculation based on the radiolysis calculation results. However, to have traceability of the calculation procedures, computer code complex containing water radiolysis and ECP calculations are required [24].

The details of subjects in (1) through (3) are shown as follows, while those in (4) and (5) are shown in the next section.

4.1.4 pH_T Calculations

1) Dissociation of H_2O

Temperature dependent dissociation constant of water is expressed with Marshall-Franck's equation (Eqs. (4-10) and (4-11)) [42].

$$H_2O \rightarrow H^+ + OH^-$$

$$k_W = [H^+][OH^-]/[H_2O]$$

$$\log(k_W) = -4.093 - 3245/T + 2.236\times10^5/T^2 - 3.985\times10^7/T^3 + (13.96 - 12626/T + 8.5646\times10^5/T^2)\log(\rho_w) \quad (4\text{-}10)$$

$$\rho_w = \{1.0 + 0.1341(374.11 - t)^{1/3} - 3.946\times10^{-3}(374.11 - t)\}/\{3.198 - 0.3152(374.11 - t)^{1/3} - 1.203\times10^{-3}(374.11 - t) + 7.489\times10^{-13}(374.11 - t)^4\} \quad (4\text{-}11)$$

, where T: temperature (K)

t: temperature (ºC)

$$\kappa = Z_{H+}F[H^+]\lambda_{H+} + Z_{OH-}[OH^-]\lambda_{OH-}$$

, where κ: conductivity (μS/m)

$[H^+]$, $[OH^-]$: concentration of H^+/OH^- (mol/L)

Z: charge number (-)

F: Faraday constant (96,485.3321 coulomb/mol)

λ: ion mobility ($m^2/s/V$)

pH_T for neutral conditions can be determined by Marshall-Franck's equation. The temperature dependent pH_T for neutral conditions is shown in **Figure 4.2**.

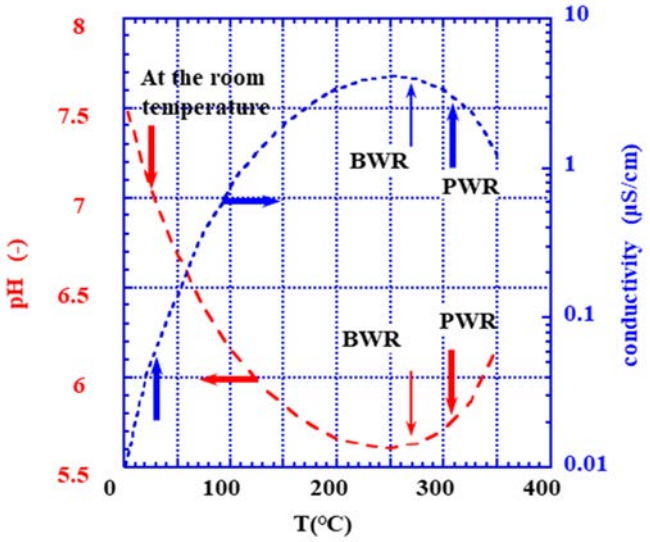

Figure 4.2 Temperature dependent pH_T and conductivity

Temperature dependent pH under combined control of boric acid and lithium hydroxide should be calculated based on Mesmer's multi-stem dissociation constant of boric acid (Eqs.(4-12)-(4-16)) [50].

$B(OH)_3+OH^- \rightarrow B(OH)_4^-$

$Q_{11}= [B(OH)_4^-]/\{[B(OH)_3][OH^-]\}$

$Log10(Q_{11})=1573.21/T+28.6059+0.012078T-13.2258logT+f(I)$ (4-12)

$2B(OH)_3 +OH^- \rightarrow B_2(OH)_7^-$

$Q_{21}= [B_2(OH)_7^-]/\{[B(OH)_3]^2[OH^-]\}$

$Log10(Q_{21})=2756.1/T-18.7322-0.00033T+5.835logT-f(I)$ (4-13)

$3B(OH)_3 +OH^- \rightarrow B_3(OH)_{10}^-$

$Q_{31}= [B_3(OH)_{10}^-]/\{[B(OH)_3]^3[OH^-]\}$

$Log10(Q_{31})=3339.5/T-7.850-0.00033T+1.497logT-f(I)$ (4-14)

$4B(OH)_3 +2OH^- \rightarrow B_4(OH)_{14}^{2-}$

$Q_{41}= [B_4(OH)_{14}^{2-}]/\{[B(OH)_3]^4[OH^-]^2\}$

$Log10(Q_{41})=12820/T-134.33-0.00033T+42.105logT-f(I)$ (4-15)

Calibration constant $f(I)=(0.3250-0.00033T)I-0.0912I^{3/2}$ (4-16)

$I=1/2\Sigma_i(C_iZ_i^2)$ (4-17)

, where I: molar intensity of ions

C_i: ion (mol/L)

$Z_{i:}$ valence number of ions (-)

The dissociation reactions between

$B(OH)_4H \rightarrow B(OH)_4^- + H^+$ (perfect dissociation) k=1

$B_2(OH)_7H \rightarrow B_2(OH)_7^- + H^+$

$B_3(OH)_{10}H \rightarrow B_3(OH)_{10}^- + H^+$

$B_4(OH)_{14}H_2 \rightarrow B_4(OH)_{14}^{2-} + 2H^+$

$B(OH)_4Li \rightarrow B(OH)_4^- + Li^+$

$B_2(OH)_7Li \rightarrow B_2(OH)_7^- + Li^+$

$B_3(OH)_{10}Li \rightarrow B_3(OH)_{10}^- + Li^+$

$B_4(OH)_{14}Li_2 \rightarrow B_4(OH)_{14}^{2-} + 2Li^+$

$LiOH \rightarrow Li^+ + OH^-$ (perfect dissociation) $k_{Li}==[Li^+][OH^-]/[LiOH]=1$

Those dissociations were calculated along with the radiolysis calculation. It was known that pH_T had large influence on water radiolysis calculation, but water radiolysis had not shown any effects on pH_T calculation.

4.1.5 pH_T Effects

pH_T was obtained based on the water radiolysis calculation, where pH_T played important contribution to determine the concentrations of radiolytic species except $[H^+]$.

4.1.6 Void Effects

In the BWR primary cooling system, water is heated along the fuel channels and some portion of the cooling water changes to steam, which involves some radiolytic species. In the steam with much lower density than water, the generation of radiolytic species and secondary reactions of species can be neglected. Only their transfer between water and steam phases should be considered as shown in Eq. (4-8). In PWR primary cooling system, small amounts of subcooled boiling has been reported, where the effects of boiling on water radiolysis might be negligibly small.

In order to evaluate the effects of steam void on the water radiolysis calculation, void distribution along the flow path first. But to determine the void fraction along the flow path, thermal hydraulic analysis along the fuel channel for every power plant, every fuel assembly and every fuel cycle is required. In **Figure 4.3**, an example of calculated two-phase flow profiles in boing channel [19]. As one of the typical examples of two-phase flow profiles, Figure 4.3 and their best fitting curves can be applicable for BWR water radiolysis analysis.

Relationship among void fraction, V_f, steam velocity, V_s and liquid velocity, V_l, shown in Figure 4.3 can be fitted as shown in Est. (4-18) through (4-21).

Void fraction: $V_f=0.67(1-\exp(-0.012(x-60)))$ (4-18)

Steam quality: $Qs=0.19(1-\exp(-0.005(x-60)))$ (4-19)

Steam velocity: $Vs=7(1-\exp(-0.005(x-60)))+1.5$ (4-20)

Liquid velocity: $V_l=2.4(1-\exp(-0.005(x-60)))+1.5$ (4-21)

, where x: distance from the void initiation point (m)

V_f: void fraction (-)

V_s: steam velocity (-)

V_l: liquid velocity (m/s)

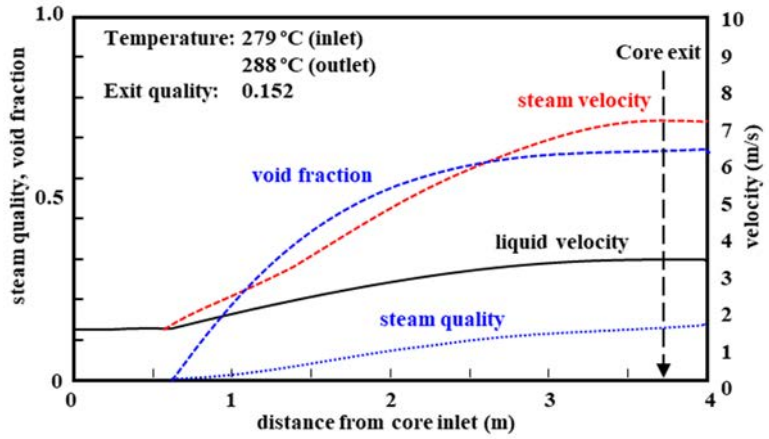

Figure 4.3 Example of calculated two-phase flow profiles in boing channel

4.2 Electrochemical Corrosion Potential

4.2.1 Mixed Potential Model

The outline of the mixed potential model was introduced in Paragraph 2 of Section 2.5 (Tables 2.8 and 2.9).

4.2.2 Major Constants

The major constants of the mixed potential model were also introduced in Paragraph 2 of Section 2.2 (Table 2.10).

4.2.3 Subjects to Improve the Previous ECP Models

1) Anodic polarization curves for the specific oxidant: In the previous models, for cathodic polarization current densities, reduction current of oxygen and hydrogen peroxide were applied, while for anodic polarization current densities oxidation of hydrogen peroxide were applied. As cathodic current density reduction current density of lithium and others were added, while for anodic current density, oxidation current density hydrogen and others were added [4].

2) Oxide layer effects: As a result of exposure time, thick oxide layers developed on the structure surface, which effect on the electric resistance of ferrous ions from the metal and then anodic polarization currents. A coupled model of oxide layer growth and electrochemistry has been developed to evaluate the anodic current densities due to oxide layer growth [53].

3) Coupled calculation of water radiolysis and ECP: ECP calculation was used to be carried out by following water radiolysis calculation based on the radiolysis calculation results. However, to have traceability of the calculation procedures, computer code complex containing both of water radiolysis and ECP calculations are required [24].

4.2.4 Anodic Polarization Curves

Anodic polarization curves for oxygen and hydrogen peroxide might be different. However, when the effects of oxidation current of hydrogen peroxide on the anodic current was considered to apply the same anodic polarization current density both for oxygen and hydrogen peroxide. At the same time, the oxide layers developed on the steel surface should be also considered to determine anodic current density.

A schematic diagram of charge balances at the surface based on cathodic and anodic reactions (Evans diagram) is shown in **Figure 4.4** [54]. Oxygen takes electrons from the metal surface to maintain the cathodic reaction.

[cathodic reactions]

$O_2 + 2H^+ + 2e^- \rightarrow H_2O_2$

$H_2O_2 + 2H^+ + 2e^- \rightarrow 2H_2O$

$H_2O_2 + 2Li^+ + 2e^- \rightarrow 2Li_2OH$

$2H^+ + 2e^- = H_2$ (hydrogen generation at low potential)

[anodic reactions]

$H_2O_2 \rightarrow O_2 + 2H^+ + 2e^-$

$Fe \rightarrow Fe^{2+} + 2e^-$ (Metal dissolution)

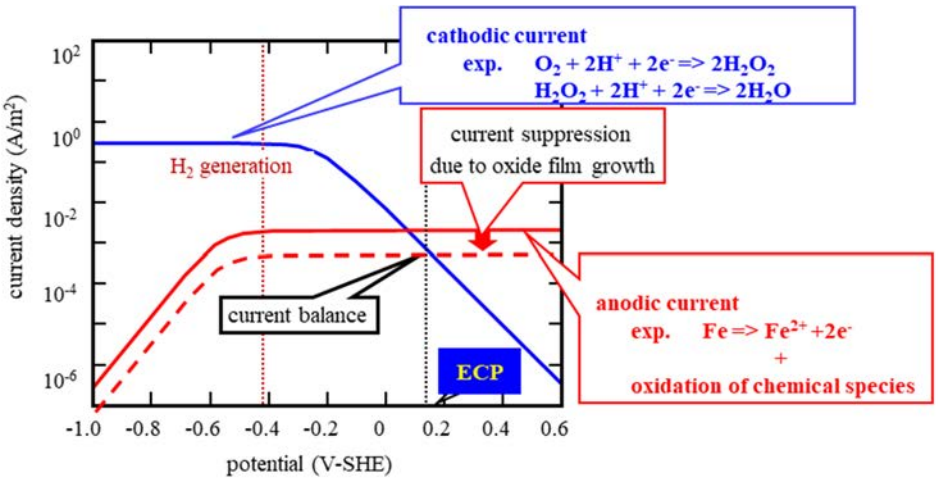

Figure 4.4 Electrochemical model
(Balance of anodic and cathodic current densities at the surface)

Current density due to the cathodic reaction is expressed by Eqs. (4-22) and (4-23) [55].

$$I_c = f_c(\varphi)\, C_s \quad (4\text{-}22)$$

$$f_c(\varphi) = z\, F\, k_o \exp(-\alpha z F(\varphi-\varphi_0)/RT) \quad (4\text{-}23)$$

The oxidant concentration at the metal surface is determined by its diffusion from bulk to surface through the surface boundary and oxide layers. Diffusion processes of oxygen through the surface boundary layer from the bulk water are expressed by Eq. (4-24).

$$D_B(C_b-C_s)/\delta_B = I_c/z/F \quad (4\text{-}24)$$

The current density due to the cathodic reaction is expressed by Eq. (4-25) by determining C_s from Eq. (4-24).

$$I_c = f_c(\varphi)\, C_b /\{1+f_c(\varphi)\delta_B/D_B/z/F\} \quad (4\text{-}25)$$

Total cathodic current densities is shown in Eq. (4-26)

$$I_{ctotal}=\Sigma_l{}^k\{ I_c{}^j\} = \Sigma_l{}^k[f_c{}^j(\varphi)\, C_b{}^j /\{1+f_c{}^j(\varphi)\delta_B/D_B/z^j/F\}] \quad (4\text{-}26)$$

Ferrous ion and electrons are released into the water from the metal surface.

$$M = M^{z+} + ze^-$$

Current density due to the metal release is expressed by Eq. (4-27) [56]

$$I_a = f'(\varphi)\,(X_s) \quad (4\text{-}27)$$

$$f'(\varphi) = z'\, F\, k_o' \exp(+\alpha' z' F(\varphi-\varphi'_0)/RT) \quad (4\text{-}28)$$

, where I_c: cathodic current density (A/cm^2)

C_s: oxidant concentration at the metal surface (mol/m^3) (superscript: s, metal surface; B, boundary layer;b, bulk water)

F: Faraday's constant (96,485C/mol)

k_o: electrochemical reaction constant (m/s)

R: gas constant (J/mol/K) [8.31J/mol/K]

T: temperature (K)

z: number of electrons taken for a reaction (-)

α: transfer coefficient (0.5)

ϕ: potential (V-SHE)

ϕ_0: potential for standard (V-SHE)

The anion concentration at the metal surface is determined by its diffusion from the metal surface to the oxide layer surface through the oxide layers.

$$D_o(X_{sat} - X_s)/\delta_o = I_a/z/F \quad (4\text{-}29)$$

, where D: diffusion coefficient (m^2/s)

(subscript: B, boundary layer; o, oxide layer; Fe, ferrous ion),

(superscript: a, anion; c, cation)

δ: thickness (m) (subscript: B, boundary layer; o, oxide layer)

The current density due to the anodic reaction is expressed by Eq. (4-30) by determining X_s from Eq. (4-29).

$$I_a = f'(\varphi)\, X_{sat}/[1 + f'(\varphi)\, \delta_o/D_o\, z/F] \quad (4\text{-}30)$$

, where I_a: anodic current density (A/cm^2)

X: oxidant concentration (mol/cm^3)

(superscript: s, metal surface; B, boundary layer; b, bulk water)

The oxidation reaction of hydrogen peroxide on the metal surface, whose current density overlaps that due to ferrous ion release, is expressed as Eq. (4-30) [57)]

$$I_{atotal} = f'(\varphi)\, X_{sat}/[1 + f'(\varphi)\, \delta_o/D_o\, z/F] + f_{hpo}(\varphi)\, C_{hpo}/\{1 + f_{hpo}(\varphi)\delta_B/D_B/z_{hpo}/F\} \quad (4\text{-}31)$$

Cathodic current density is positive, while the anodic one is negative at the surface. Both current densities are balanced at the surface in the equilibrium state, where the potential is the electrochemical corrosion potential without net current density at the surface.

The electrochemical corrosion potential, ECP, can be obtained from the intersection potent of the absolute values of the total anodic and cathodic current densities (Figure 4.4). The minimum potential is determined by the hydrogen generation potential, which was determined by pH and temperature in water [53)].

4.2.5 Coupled Calculations of Electrochemistry and Oxide Layer Growth

ECP has been calculated with the coupled models of the static electrochemistry model and dynamic oxide layer growth model (**Table 4.1**) [53), 54), 58)]. Anodic and cathodic current densities and ECP are calculated with the static electrochemistry model and metallic ions release rate determined by the anodic current density is applied as input for the dynamic oxide layer growth model. The thicknesses of oxide layers developed on the surface can be calculated according to the mass balance on oxidation of metallic ions that were dissolved and formed the oxide layers (**Figure 4.5**)[53)]

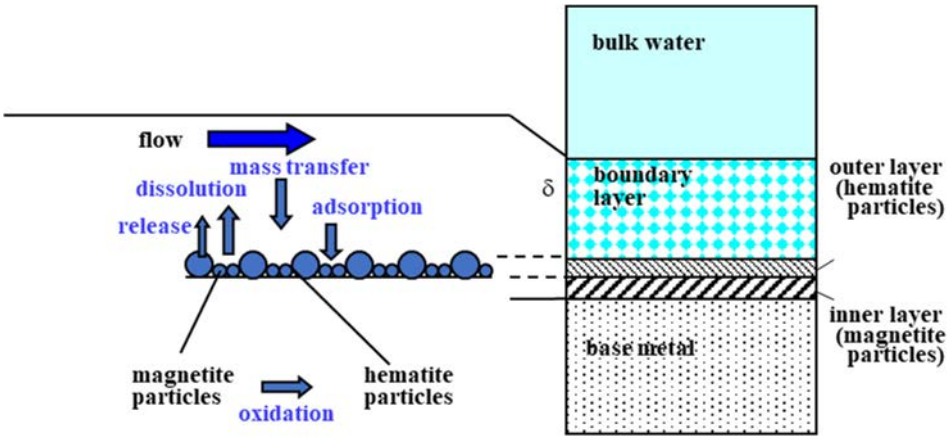

Figure 4.5 Oxide layer growth model

Thickness of oxide film (oxide layer) and its characteristics are applied for the electrochemistry model to determine the resistance of the cathodic current from the bulk to the surface and anodic current from the surface to bulk.

Table 4.1 Coupled calculation of electrochemistry model and oxide layer growth model

Sub-model	electrochemistry model (static model)	oxide layer growth model (dynamic model)
Input	temperature, $[O_2]$, pH, k_m, mass transfer coefficient (h_m) oxide film thickness, oxide properties	temperature anodic/cathodic current densities ECP
	coupling calculation	
Output	anodic/cathodic current densities ECP	oxide film thickness properties (Fe_2O_3/Fe_3O_4 ratio)

4.2.6 Anodic Polarization Curves

As a result of applying the coupled electrochemistry and ECP models, only preparation of metal dissolution properties for basic anodic current densities resulted in increasing thickness of oxide layer developing on the metal surface, and then the reduction of current densities due to increasing electric resistance of the oxide layers, which prepared for exposure time dependent anodic current densities. At the same time, increase in oxidation current of hydrogen peroxide could prepared for level-off phenomena of ECP under the elevated hydrogen peroxide concentrations.

In **Figure 4.6**, the empirical anodic polarization curves prepared for ECP calculation and those calculated with the coupled electrochemistry and ECP calculation models [54), 59), 60)].

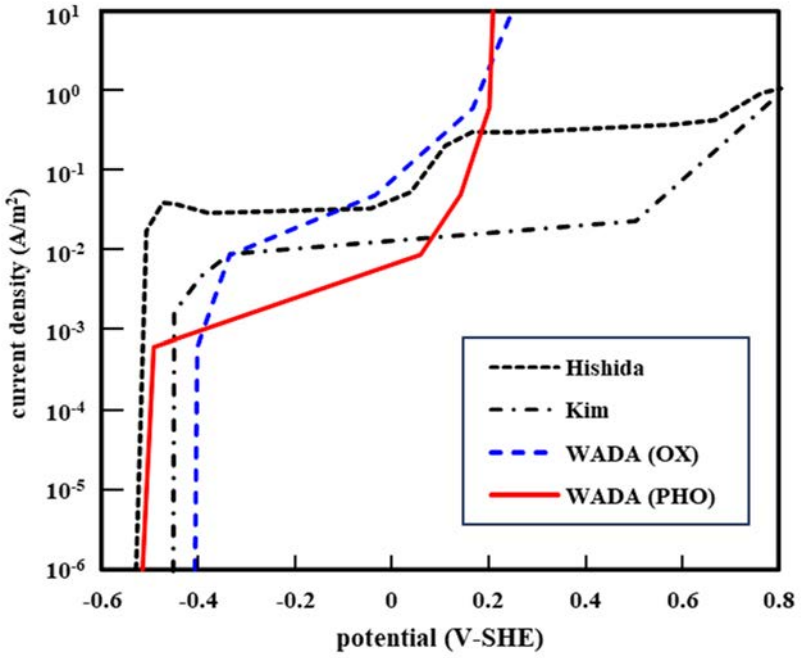

Figure 4.6 Measured and empirical anodic curves (Comparison of previous polarization curves and those calculated with the coupled model)

For oxygen, anodic current densities calculated based on ferrous ion solubility from stainless steel varied with exposure time. As increasing exposure time, thickness and properties of oxide layers (thickness and properties, e.g., magnetite/hematite ratio) changed. The anodic polarization curves were affected by oxide layers and then the exposure time. In Figure 4.6. There were several empirical anodic polarization curves shown with measured for different exposure conditions. The anodic polarization curve for hydrogen peroxide are also shown. The oxide layer thickness and their properties might be different for the specimens exposed under oxygen and hydrogen peroxide containing water. Hydrogen peroxide contribute not only to cathodic polarization current densities but also to anodic polarization current densities.

In **Figure 4.7**, the anodic polarization curves determined based on ferrous ion solubility were calculated for two different oxide layers.

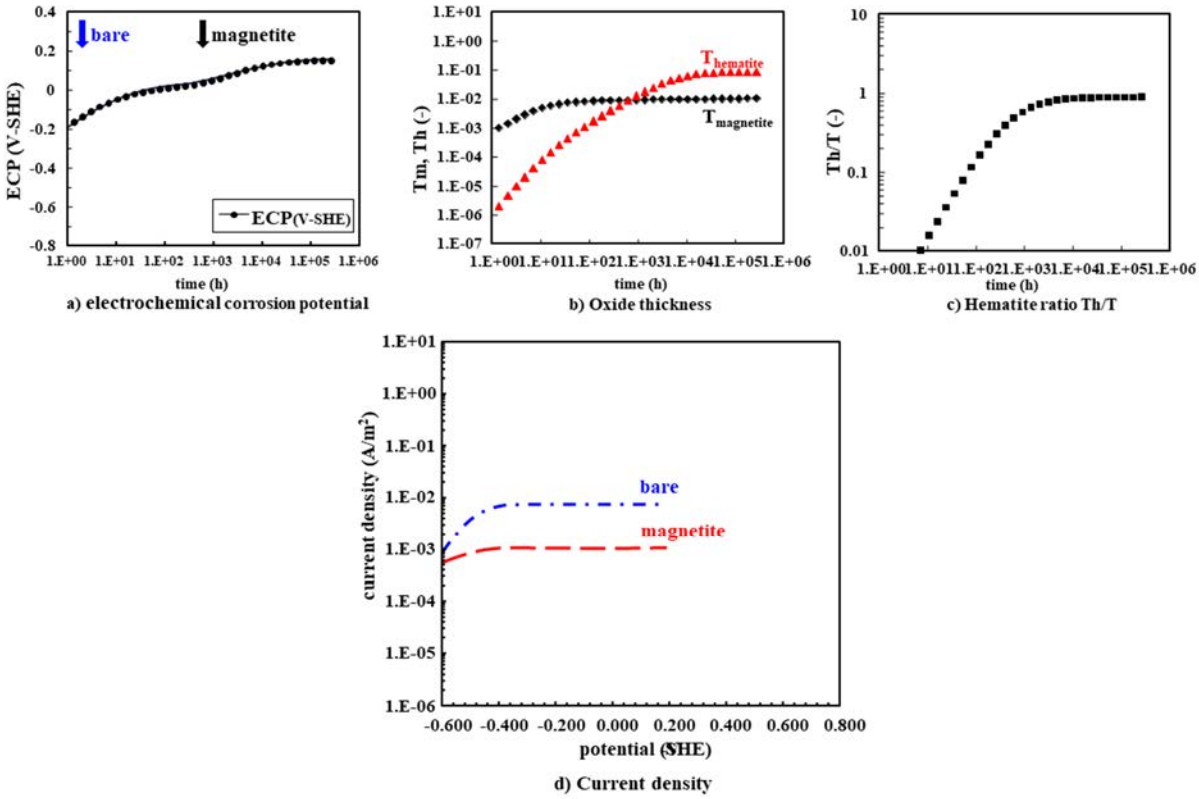

Figure 4.7 Anodic polarization curves calculated

with the coupled electrochemistry and oxide layer growth models under O_2 water

The anodic polarization curves for hydrogen peroxide contained water might be the same as those for oxide contained water. But as a result of the effects of oxidation of hydrogen peroxide, the apparent anodic polarization curves containing oxidation current of hydrogen peroxide could be calculated, which are shown in **Figure 4.8,** with the empirical one [61].

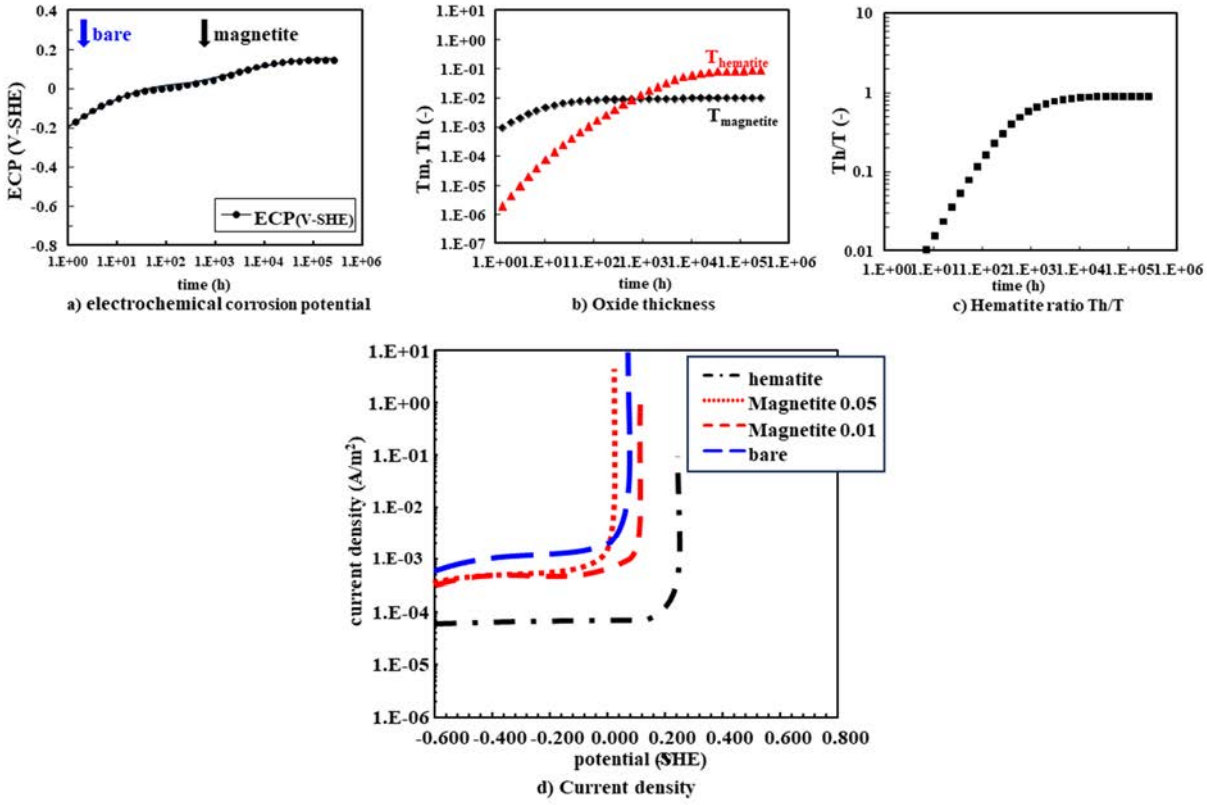

Figure 4.8 Anodic polarization curves calculated

with the coupled electrochemistry and oxide layer growth models under H_2O_2 water

When the empirical anodic polarization curves were applied for oxygen and hydrogen peroxide mixed conditions, it was proposed that the anodic polarization curve was obtained as a cathodic current density-weighted average of both anodic polarization curves (Eqs. (4-32) and (4-33), **Figure 4.9**).

$$I_a = I_a^{ox} W_{ox} + I_a^{hpo} W_{hpo} \quad (4\text{-}32)$$

$$W_{ox} = I_c^{ox} / (I_c^{ox} + I_c^{hpo}) \ , \ W_{hpo} = I_c^{hpo} / (I_c^{ox} + I_c^{hpo}) \quad (4\text{-}33)$$

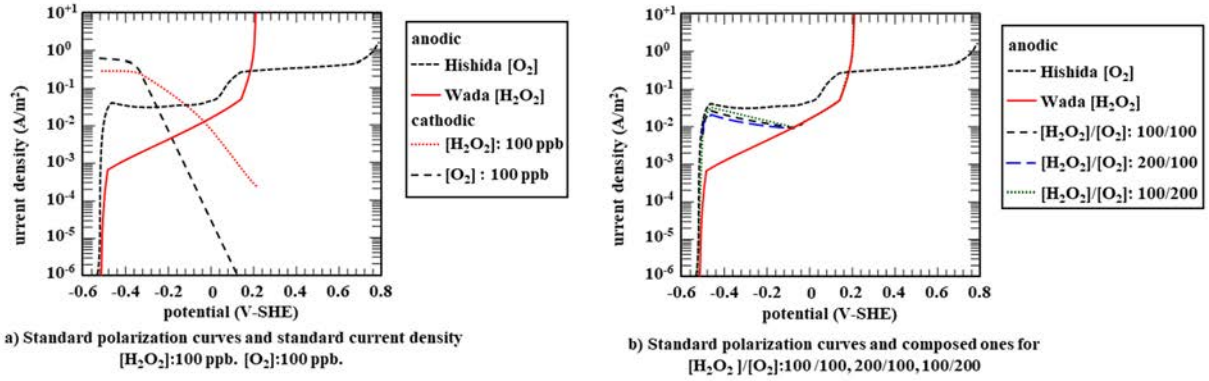

Figure 4.9 Composed anodic polarization curves based on those for O_2 and H_2O_2

Unfortunately, empirical anodic polarization curves have been reported only for neutral water conditions but not for higher pH conditions. So, the apparent anodic polarization curves are not suitable for evaluation of ECP under elevated pH conditions. The pH-dependent anodic polarization curve should be applied along with oxidation current density of hydrogen peroxide.

One of the important terms to determine the anodic polarization curves is pH-dependent ferrous ion dissolution form steel, which are supported by oxide layer effects and oxidation reaction of hydrogen peroxide at the surface.

4.2.7 Ferrous Ion Solubility

Solubility of metallic ions are much affected by pH and temperature [62]. The anodic current densities of stainless steel can be calculated by applying the data base of pH and temperature dependent solubility of ferrous ion. For ECP calculation, the solubility data were shown as fitting functions as shown in **Table 4.2** and compared with the original data in **Figure 4.10**.

Solubility of ferrous ions have been systematically evaluated. But the data for nickel ions were very restricted [63]. For determining anodic polarization curves for nickel-based alloys, solubility data base for nickel ions are strongly required.

Table 4.2 Fitting curves for ferrous ion solubility

$\log([Fe^{2+}])=a(pH_r-b)c+d$

Temperature	Parameter	Zone			Standard deviation	
		pHr>8.5	0.65<pHr<8.5	pHr<6.5	σ_{total}	$\sigma_{pH>8.5}$
573K	a	0.19	0.25	-0.1	0.7%	0.7%
	b	-10.4	-7	-6.9		
	c	2	2	2		
	d	-7.8	-7	-6.9		
523K	a	0.29	0.2	-0.22	0.4%	0.6%
	b	-10.45	-7	-6.9		
	c	2	2	2		
	d	-8.05	-6.5	-6.35		
473K	a	0.3	0.18	-0.1	0.4%	0.6%
	b	-11	-7	-6.9		
	c	2	2	2		
	d	-8.22	-6	-5.9		
423K	a	0.35	0.18	-0.1	0.6%	0.6%
	b	-11.3	-6.7	-7		
	c	2	2	2		
	d	-8.6	-5.7	-5.7		
373K	a	0.45	0.18	-0.1	0.7%	0.8%
	b	-11.4	-6.7	-7		
	c	2	2	2		
	d	-8.9	-5.7	-5.7		

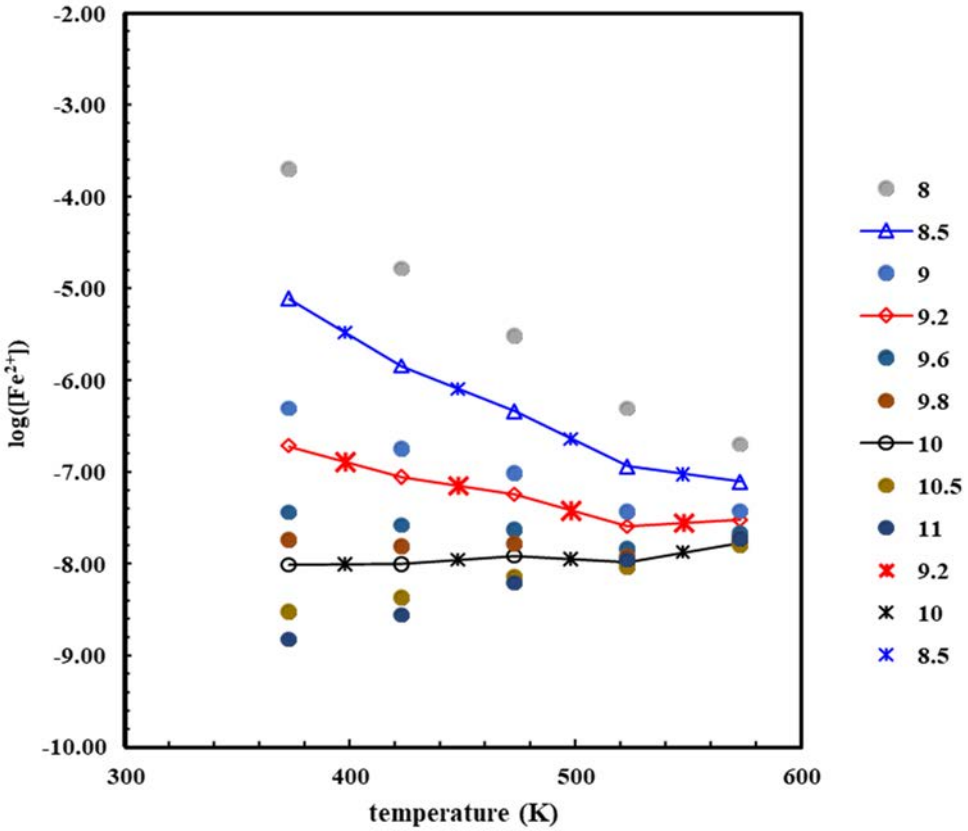

Figure 4.10 Temperature and pH dependent ferrous ion solubility

4.2.8 Other Constants for ECP Calculation

Several electrochemistry reactions were considered for cathodic and anodic polarization curves. Major rate constants, transfer coefficients, and standard electrode potentials for the reactions are listed in **Table 4.3**. The potential for each electrochemical reaction calculation was calculated based on the concentrations of species of the reaction [64), 65)].

The major parameters to determine ECP in the wide pH_T region from 5.6 to 7.1 are listed in **Table 4.4** [24)], where a mechanistic relationship between the parameters and ECP is shown. H_2O_2 served as an oxidant as well as a reductant, while H_2 served as a reductant. The pH of ECP is influenced by the pH-dependent solubility of ferrous ion. Through oxide film thickness, flow velocity had a vital influence.

Table 4.3 Rate constants for the ECP model

Electrochemical reactions	Transfer coefficients α (-)	Standard electrode potential F (V-SHE)	Rate constants k	
			Forward reactions (Cathodic reaction)	Backward reactions (Anodic reaction)
① $H_2O_2+2H^++2e^-=>2H_2O$	0.5	1.58	5.0×10^{-6} $(mol/L)^{-2}/s$	-
② $H_2O_2+2Li^++2e^-=>2LiOH$ *	0.5	0.885	1.0×10^{-4} $(mol/L)^{-2}/s$	-
③ $O_2+2H^++2e^-<=>H_2O_2$	0.7	0.48	2.0×10^{-4} $(mol/L)^{-2}/s$	1.0×10^{-10} s^{-1}
④ $O_2+4Li^++4e^-=>2Li_2O$ *	0.5	-0.132	1.0×10^{-9} $(mol/L)^{-4}/s$	-
⑤ $2H^++2e^-<=>H_2$	0.5	0.0	5.0×10^{-4} $(mol/L)^{-1}/s$	1.0×10^{-10} s^{-1}
⑥ $Fe^{2+}+2e^-<=Fe$	0.5	-0.44	-	1.0×10^{-3} $m\ s^{-1}$

* Newly defined.

Table 4.4 Major parameters to determine ECP

Parameters		Mechanism s to control ECP
Oxidant	Hydrogen peroxide	To determine cathodic current densities
	Oxygen	Ditto
Reductant	Hydrogen peroxide	To determine anodic current densities
	Hydrogen	Ditto
Temperature		Solubility, Temperature dependent reaction constants
pH		Solubility, Oxide film
Solubility (Ferrous ion concentration)		To determine anodic current densities
Oxide film	Chemical form	To determine anodic current densities due to electric resistance
	Density (porosity)	Ditto
	Thickness	Ditto
Flow velocity		To determine cathodic and anodic current densities due to the thickness of the surface boundary layers

4.2.9 Oxide Layer Effects

Oxide layers developed on the metal surface also played important role in anodic current densities. In order to evaluate exposure time dependent anodic and cathodic current densities, coupled analysis of electrochemistry and oxide layer growth models has been developed [57].

The electrochemistry model shows the static balance of charge at the oxide surface with a given oxide film thickness, while the oxide layer growth model shows the dynamic balance of oxide film and film thickness is calculated as a result of accumulated mass balance of metal released from the base metal. The oxide film growth model was previously shown in Figure 4.5. In the model, ferrous ions were released from base metal through the oxide layers, which consist of magnetite inner and hematite outer layers [66), 67)].

Ferrous ion release rate from base metal is determined as a result of the electrochemistry model (Eq. (4-34)).

$$dM/dt= -I_a/z/F \quad (4\text{-}34)$$

, where M: thickness of base metal (mol/m^2)

Some of the ferrous ions released into the surface boundary layer are removed to the bulk water and others are absorbed on the surface of the magnetite and hematite particles depositing on the metal surface, while the major portion over the super-saturation concentration in the boundary layer precipitate as oxide particles, which deposit on the surface to become an oxide layer (magnetite particles). Magnetite particles are oxidized as hematite on the metal surface. The conversion factor from magnetite to hematite is expressed as a function of ECP. Ferrous ions and ferric ions are released from oxide particles on the metal surface into the boundary layer. Mass balance equations of ferrous ion and magnetite particle in the boundary layer are expressed by Eqs. (4-35) and (4-36).

$$dC/dt\ \tau_b=I_a/z/F-\delta_m CS_m C_m\tau_b^2-\delta_h CS_h C_h\tau_b^2-k_g C/C_{sat}f_b(C)\tau_b-k_m(C-C_b)\tau_b+\zeta_m T_m+\zeta_h T_h \quad (4\text{-}35)$$

, where C, C_p: concentrations of ferrous ions and oxide particles (mol/m^3) [subscript: b; bulk water]

C_m, C_h: number densities of magnetite and hematite particles on the surface ($1/m^2$)

[subscript: m; magnetite h; hematite]

C_{sat}: saturated concentration of ferrous ion (mol/m^3)

$f_b(C)$: a function for education rate

$$f_b(C)= \exp[-\beta\{(C_{sat}-C)^2+\{(C_{sat}-C)^2\}_{1/2}(C_{sat}-C)\}]$$

$$f_m=4\pi\{3\xi/(4\pi\rho_h\tau_b)\}^{2/3},\ f_h=4\pi\{3\xi/(4\pi\rho_h\tau_b)\}^{2/3}$$

F: Faraday's constant (96,485C/mol)

I_a: anodic current density (A/cm^2)

k_m, k_h: mass transfer rates of magnetite and hematite particles through boundary (1/s)

k_g: generation rate coefficient of oxide particles (1/s)

S_m, S_h: surface area of oxide particle (m^2) [superscript: m; magnetite, h; hematite]

T_m, T_h: total thicknesses of magnetite and hematite layers (mol/m^2)

[superscript: m; magnetite, h; hematite]

z: number of electrons taken for a reaction (-)

δ_m, δ_h: absorption coefficients of ferrous ion on oxide particles ($s^{-1}m^{-2}$)

[subscript: m; magnetite h; hematite]

τ_b: thickness of boundary layer (m)

[subscript: b; boundary layer, o; oxide layer, Fe; ferrous ion]

ζ_m, ζ_h: release rates of oxide layers (s^{-1})

$$dC_p/dt\ \tau_b = k_g C/C_{sat}f_b(C)/W_m\ \tau_b -k_d C_p-k(C_p-C_{pb})\ \tau_b \quad (4\text{-}36)$$

, where W_m: weight of magnetite particles just after generation (mol)

k_d: particle deposition rate (m/s)

The first term on the right side of the Eq. (4-35) presents release from the base metal, The second and the third terms are absorption on oxide particles, the fifth term shows condensation of ferrous ion as magnetite particles, the sixth term is the most important mass transfer term from the boundary layer to the bulk water and the seventh and eighth terms are release from oxide particles.

The inner layer is formed by direct oxidation. The maximum thickness of the inner layer is designated as T^b_{m*}. The thickness of the inner oxide layer is expressed as Eqs. (4-37) and (4-38)

$$dT^b_m/dt = \Phi - \zeta_m T^b_m \quad \text{for } T^b_m < T^b_{m*} \tag{4-37}$$

$$= 0 \quad \text{for } T^b_m > T^b_{m*} \tag{4-38}$$

$$\Phi = \Phi_{OX}(ECP) + \Phi_{HPO}([H_2O_2]) + \Phi_H \tag{4-39}$$

$$\Phi_{OX}(ECP) = \Phi_{OX*}(ECP-ECP_B)^{1/2}/\ T^b_m \quad \text{for ECP} > ECP_B \tag{4-40}$$

$$= 0 \quad \text{for ECP} < ECP_B \tag{4-41}$$

$$\Phi_{HPO}([H_2O_2]) = \Phi_{HPO*}([H_2O_2])/\ T^b_m \tag{4-42}$$

$$\Phi_H = \Phi_{H*}/\ T^b_m \tag{4-43}$$

, where Φ: direct oxidation of base metal (mol/m^2/s)

Φ_{ECP}, Φ_{HPO}, Φ_H: contributions of ECP and hydrogen peroxide and base oxidation

[subscript: B; boundary layer, o; oxide layer]

ECP: ECP at the surface (V-SHE)

ECP_B: hydrogen generation potential as a function of temperature and pH (V-SHE)

The outer layer is formed by precipitated magnetite particles. Number density of the magnetite particles and the effective thickness of the outer oxide layer are expressed as Eqs. (4-44) through (4-46).

$$dC_m/dt\ \tau_b = k_d C_p \tau b - (\chi + k_m) C_m\ \tau_b \tag{4-44}$$

$$dT_m/d_t = \delta_m C S_m C_m \tau_b^2 + k_d C_p W_m \tau_b - (\zeta_m + \chi + k_m) T_m \quad \text{for } T^b_m > T^b_{m*} \tag{4-45}$$

$$dT_m/d_t = \delta_m C S_m C_m \tau_b^2 + k_d C_p W_m \tau_b - (\zeta_m + \chi + k_m) T_m + \Phi \quad \text{for } T^b_m < T^b_{m*} \tag{4-46}$$

The transfer ration from magnetite to hematite is expressed as Eqs. (4-47) and (4-50).

$$\chi = \chi_{OX} + \chi_{HPO} \tag{4-47}$$

$$\chi_{OX} = \chi_{OX*}\ (ECP-ECP_B)^{1/2} \quad \text{for ECP} > ECP_B \tag{4-48}$$

$$= 0 \quad \text{for ECP} < ECP_B \tag{4-49}$$

$$\chi_{HPO} = \chi_{HPO*}([H_2O_2]) \tag{4-50}$$

, where χ: transfer coefficient from magnetite to hematite (s^{-1})

χ_{ECP}, χ_{HPO}: contributions of ECP and hydrogen peroxide δ: thickness (m)

The hematite part of outer layer is formed by precipitated hematite particles. Number density of the hematite particles and the effective thickness of the outer oxide layer are expressed as Eqs. (4-51) and (4-52).

$$dC_h/dt\ \tau_b = \chi C_m\ \tau_b - k_h C_h \tau_b \tag{4-51}$$

$$dT_h/dt = \chi T_m + \delta_h C S_h Ch\ \tau_b^2 - (\zeta_h + k_h) T_h \tag{4-52}$$

4.3 Coupled Calculation of Water Radiolysis and ECP

Theoretical approaches to determine the corrosive conditions in the cooling water of BWRs and PWRs are illustrated in **Figure 4.11**. At the first step of the evaluation procedures of corrosive conditions, non-linear rate equations were calculated to obtain the concentration distributions of corrosive radiolytic species, *e.g.,* [O_2] and [H_2O_2], throughout the primary coolant [**water radiolysis code**], which was followed by the evaluation procedures of ECP [**ECP analysis code**]. In the earlier paper [54], the specifics of the water radiolysis computation were shown. The ECP was calculated using a mixed potential model, with the concentrations of the radiolytic species as a result of the water radiolysis calculation as input data.

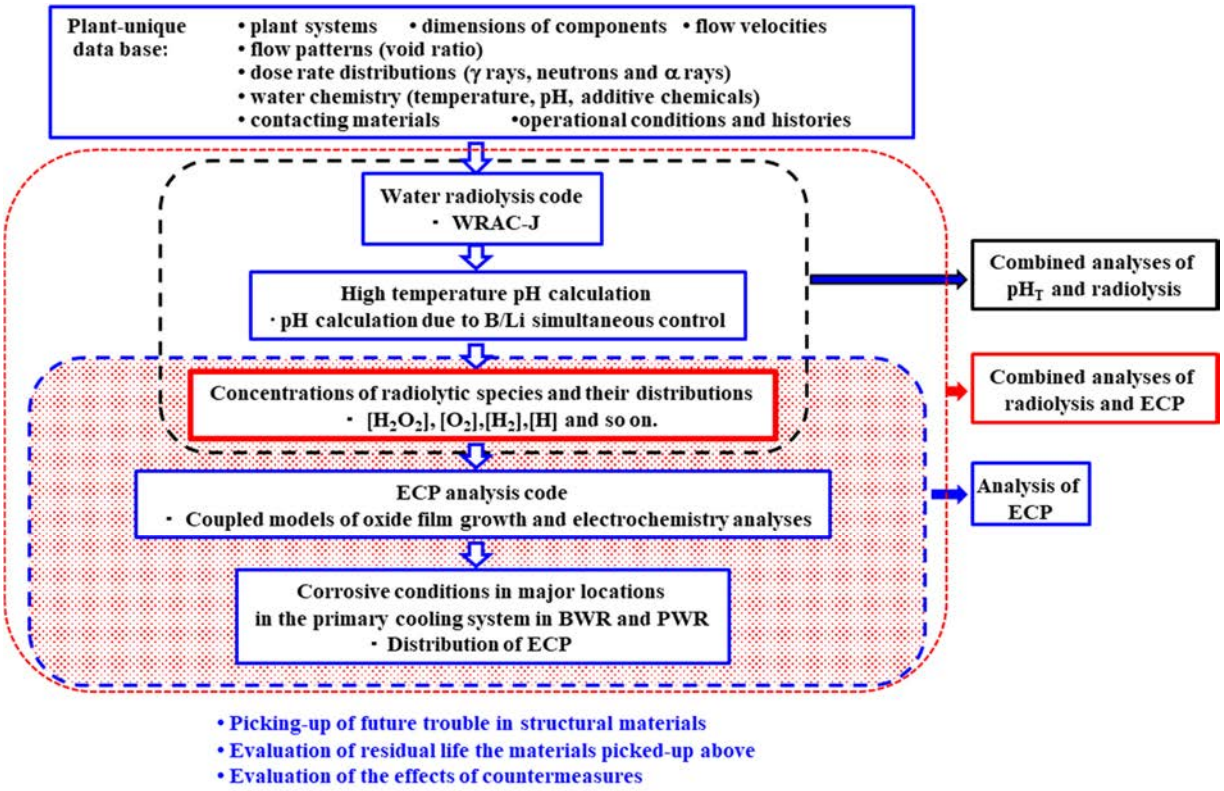

Figure 4.11 A coupled evaluation procedures of corrosive conditions

(Water radiolysis calculation and ECP calculation)

The concentrations of oxidants ($[O_2]$ and $[H_2O_2]$) change along the recirculation flow path and differ in BWRs and PWRs mainly based on their water chemistry, *e.g.,* temperature, pH, energy depositions, and radiation qualities. So, the corrosive conditions differ between BWRs and PWRs [3].

The only point in the recirculation line where oxidant concentrations can be determined is at the end of the sampling line, where water is cooled and depressurized for measurement by a probe-type oxygen detector, and the contributions of H_2O_2 to the corrosive conditions cannot be confirmed from the measured results. ECP measurement with an ECP detector in high-temperature water is the only approach to measure H_2O_2 contributions to corrosive conditions.

5. Calculation Procedures

5.1 Water Radiolysis

5.1.1 Basic Equations for Water Radiolysis and Dissociation of Water

(1) Fast reactions

$$dC_i/dt = \{G^{\gamma}_i E^{\gamma}_r + G^{n}_i E^{n}_r + G^{\alpha}_i E^{\alpha}_r\} + \Sigma\{k_{mn} C_m C_n\} - C_i \Sigma\{k_{is} C_s\} \quad (i = 1,J) \qquad (4\text{-}1)$$

$$dC^{w}_i/dt = + \Sigma\{k^{w}_{mn} C^{w}_m C^{w}_n\} - C^{w}_i \Sigma\{k^{w}_{is} C^{w}_s\} \qquad (4\text{-}3)$$

$$dC_i/dt = dC_i/dt + \delta\,(dC^{w}_i/dt - dC_i/dt) \qquad (4\text{-}4)$$

(2) Slow reactions

$$v\,\partial C_i/\partial x = v^{l-1} S^{l-1} C_i^{l-1} - v^{l} S^{l} C_i^{l} \qquad (4\text{-}7)$$

$$dC_i/dt = \varepsilon F_v C_i + \varepsilon^{*} F_v C^{g}_i \qquad (4\text{-}8)$$

In a unit cell along the flow the fast reactions should be calculated based on the calculated concentration in the flow-in cell. The numerical calculation to determine the concentration of radiolytic species were based on Newton method [68]. The rate constants of the radiolysis reactions are so large to cause possible unstable numerical results. The multi-order, multi-dimensional simultaneous equations with larger rate constants were designated as so-called stiff equations, which were required to prepare for suitable initial values for numerical calculation. For the stiff equation, the backward differential formula developed by Gear [69] were applied.

5.1.2 Dissociation of Water to Determine High Temperature pH

Temperature dependent dissociation constant of water is expressed with Marshall-Franck's equation [51].

Temperature dependent pH under combined control of boric acid and lithium hydroxide should be calculated based on Mesmer's multi-stem dissociation constant of boric acid [50].

5.1.3 Numerical Solution

The solutions of the fast equations (4-1), (4-3) and (4-4) were solved by applying Newton method. The equation was generalized as follows.

$$dY/dt = f(Y) \qquad (5\text{-}1)$$

where, Y: a set of concentrations of species C_1, C_2, C_i, C_m)

f(Y): the functions for equations (4-1), (4-3) and (4-4)

(1) Solution of differential equations

Newton iteration:

It was difficult to apply the simple newton method to obtain the stable results.

In a small time mesh ($<10^{-9}$ s) the differential equations were solved with the simple Newton method. But as a result of larger rate constants, the results were calculated based on Backward Differential Formula (BDF) [69] method for time mesh $>10^{-6}$ s.

Initial guess $\quad \boldsymbol{Y}_n^{(0)} = \Sigma_1^6 \alpha_i \boldsymbol{Y}_{n-i} + h \Sigma_1^6 \beta_i \boldsymbol{f}_{n-i} \qquad (5\text{-}2)$

Iteration results $\quad \boldsymbol{Y}_n^{(m+1)} = \Sigma_1^6 \alpha_i \boldsymbol{Y}_{n-i} + h\,\beta_0 \boldsymbol{f}_n^{(m)} \qquad (5\text{-}3)$

Complete solution $\quad \boldsymbol{Y}_n = h\,\beta_0 \boldsymbol{f}_n + \Sigma_1^6 \alpha_i \boldsymbol{Y}_{n-1} \qquad (5\text{-}4)$

Where, α and β were determined by Gear.

$\alpha_1 = 360/147$

$\alpha_2 = -450/147$

α_3=400/147

α_4=-225147

α_5=72/147

α_6=-10/147

$\beta = \beta_0\ \alpha$

β_0=60/147

Application of Newton iteration to obtain stable solution of Eq.(5-4)

$$\boldsymbol{F}(\boldsymbol{Y}_n) = \boldsymbol{Y}_n - \beta\, h\, \boldsymbol{f}_n(\boldsymbol{Y}_n) - \Sigma_1^6 \alpha_i \boldsymbol{Y}_{n-i} \tag{5-5}$$

$\boldsymbol{Y}_n$ should be obtained

(2) Newton method

$$\boldsymbol{F}(\boldsymbol{Y}_n^m + \boldsymbol{\Delta}\boldsymbol{Y}_n^m) = \boldsymbol{F}(\boldsymbol{Y}_n^m) + \partial\, \boldsymbol{F}(\boldsymbol{Y}_n^m)/\partial\, \boldsymbol{Y}_n^m\ \boldsymbol{\Delta}\mathbf{Y}_n^m = 0 \tag{5-6}$$

$$\partial\, F_n(Y)/\partial\, Y_n = \mathbf{1} - \beta\, h\ \partial\, f_n(Y)/\ \partial\, Y_n \tag{5-7}$$

$$\partial\, F_n(Y)/\partial\, Y_s = -\beta\, h\ \partial\, f_n(Y)/\ \partial\, Y_n \tag{5-8}$$

$$\boldsymbol{X}_n^{(m+1)} = \boldsymbol{Y}_n^{(m+1)}/\boldsymbol{Y}_{n-1} \tag{5-9}$$

$$d\boldsymbol{X}_n^{(m+1)} = d\boldsymbol{Y}_n^{(m+1)}/\boldsymbol{Y}_{n-1} \tag{5-10}$$

$$\boldsymbol{Y}_n^{m+1} = \boldsymbol{Y}_n^m + \boldsymbol{Y}_{n-1}\, \boldsymbol{\Delta}\mathbf{X}_n^m \tag{5-11}$$

$$\boldsymbol{F}(\boldsymbol{X}_n^m + \boldsymbol{\Delta}\boldsymbol{X}_n^m) = \boldsymbol{F}(\boldsymbol{X}_n^m) + \partial\, \boldsymbol{F}(\boldsymbol{Y}_n^m)/\partial\, \boldsymbol{Y}_n^m\ d\boldsymbol{Y}_n^m / d\boldsymbol{X}_n^m\ \boldsymbol{\Delta}\mathbf{X}_n^m = 0 \tag{5-12}$$

$$\boldsymbol{F}(\boldsymbol{X}_n^m + \boldsymbol{\Delta}\boldsymbol{X}_n^m) = \boldsymbol{F}(\boldsymbol{X}_n^m) + \partial\, \boldsymbol{F}(\boldsymbol{Y}_n^m)/\partial\, \boldsymbol{Y}_n^m\ \boldsymbol{Y}_{n-1}\, \boldsymbol{\Delta}\mathbf{X}_n^m = 0 \tag{5-13}$$

$$f_n(Y_n) = g_n + \Sigma\, k^n_{ij} Y_i Y_j - Y_n \Sigma\, k_{ns} Y_{ns} - \delta\, Y_n + \zeta\, Y^w_n \tag{5-14}$$

$$f_n(Y^w_n) = + \Sigma\, k^n_{ij} Y^w_i Y^w_j - Y^w_n \Sigma\, k_{ns} Y^w_{ns} - \delta\, Y_n + \zeta\, Y^w_n \tag{5-14}*$$

****

$$\partial\, f_n(Y_n)/\partial\, Y_n = -\Sigma\, k_{ns} Y_s - \delta \tag{5-15}$$

$$\partial\, f_n(Y_n)/\partial\, Y_s = \Sigma\, k^n_{is} Y_i - Y_n k_{ns} \tag{5-15}*$$

$$\partial\, f_n(Y_n)/\partial\, Y^w_n = +\zeta\ T/(V/S) \tag{5-15}**$$

$$\partial\, f_n(Y_n)/\partial\, Y^w_s = 0 \tag{5-15}***$$

$$\partial\, f_n(Y^w_n)/\partial\, Y^w_n = -\Sigma\, k_{ns} Y^w_s - \delta\ (V/S)/T \tag{5-16}$$

$$\partial\, f_n(Y^w_n)/\partial\, Y^w_s = \Sigma\, k^n_{is} Y^w_i - Y^w_n k_{ns} \tag{5-16}*$$

$$\partial\, f_n(Y_n)/\partial\, Y^w_n = +\zeta \tag{5-16}**$$

$$\partial\, f_n(Y_n)/\partial\, Y^w_s = 0 \tag{5-16}***$$

****

$$a_i = \partial\, F_i(\mathbf{Y})/\partial\, Y_1 Y_{1n-1},\ b_i = \partial\, F_i(\mathbf{Y})/\partial\, Y_2\, Y_{2n-1} \quad q_i = \partial\, F_i(\mathbf{Y})/\partial\, Y_q\, Y_{qn-1} \tag{5-17}$$

$$x_k = \Delta\, X_k \tag{5-18}$$

$$a_i x_1 + b_i x_2 + q_i x_q = -f_i(\mathbf{Y}) \quad (I=1,q) \tag{5-19}$$

Based on $\mathbf{Y}_{n-1}$~$\mathbf{Y}_{n-6}$, $\mathbf{Y}_n$ was calculated, and then Newton calculation had to be repeater until $\mathbf{Y}_n$ converged.

5.1.4 Major Constants

(1) G-values

For BWR G-values for only neutron and gamma-rays should be applied, while for PWR those for alpha-rays should be added to evaluate alpha-rays from $^{10}B(n,\alpha)^7Li$ reaction.

(2) Rate constants

In addition to rate constants for the radiolytic species dissociation constants of water and boric acid and lithium hydroxide should be applied.

(3) Geometry and flow constants

Flow loops composing the cooling system, volume of the flow cells, water temperature of the cells, energy deposition rate to determine the source of radiolytic species were required for calculations. The details are shown in the code manual in Chapter 6.

5.2 Electrochemical Corrosion Potential

5.2.1 Mixed Potential Model

$$I_{ctotal}=\Sigma_l^k\{ I_c^j\}= \Sigma_l^k[f_c^j (\varphi) C_b^j /\{1+f_c^j (\varphi)\delta_B/D_B/z^j/F\}] \quad (4\text{-}26)$$

$$I_{atotal}= f'(\varphi) X_{sat}/[1+ f_a'(\varphi) \delta_o/D_o z/F]+ f_{hpo}(\varphi) C_{hpo} /\{1+f_{hpo}(\varphi)\delta_B/D_B/z_{hpo}/F\} \quad (4\text{-}31)$$

The electrochemical corrosion potential, ECP, could be obtained from the intersection potent of the absolute values of the total anodic and cathodic current densities (Eqs. (4-26) and (4-31), Figure 4.4).

5.2.2 The Effects of Boundary Layers and Oxide Layers on Current Densities

The effects of oxide layers on current densities could be calculated with the electrochemistry and oxide layer growth model. Those of surface flow are also determined by thermal hydraulic analysis. The details were shown in Section 4.2. The current resistance determined by the boundary layers and oxide layers (Eqs. (5-19) and (5-20)) were evaluated the electrochemistry and oxide layer growth model and then the results was applied as electric resistances in the mixed potential model.

$$h_{BL}=D_{BL}/\delta_{BL} \quad (5\text{-}20)$$

$$h_{ox}=D_{ox}/\delta_{ox} \quad (5\text{-}21)$$

5.3 Coupled Model of Water Radiolysis and ECP Analysis

The water radiolysis model was carried out first and then the mixed potential model (ECP model) followed based on the calculated concentration of radiolytic species. Those calculations used to be carried out independently, and the calculated results of the water radiolysis models were applied as the input data of the ECP models. The separate processes for obtaining the ECP results might result in misconnection of the input data and at the same time the procedures caused some difficulties on the future confirmation of the calculation processes. There were some problems in the traceability of the calculation processes. As a result of combining both models, calculation processes for both water radiolysis and ECP were recorded in only one process and total input data might be kept in a single record, which might prepare for much easier traceability of the processes.

When the users of computer program packages, e.g., WRAC-JAEA, apply them for plant analysis, they required to have sufficient reliability on the packages. Recently, every computer code was required to be authorized based on verification and validation (V&V) procedures. In the document, a part of the V&V procedures on WARC-JAEA are introduced. The major procedures on the calculation codes for determining corrosion conditions in the BWR primary cooling system were introduced in the previous article [24].

Some examples of V&V procedures on WRAC-JAEA are shown in **Chapter 7**.

6. Calculation Code, WRAC-JAEA

6.1 PAD of the Calculation Code

6.1.1 Main Calculation Routine

A coupled calculation code of water radiolysis and ECP models consisted of three sub-codes,

INPUT (to read and prepare input data),

WRAC (water radiolysis calculation) and

ECPCAL (ECP calculation).

The INPUT subcode consisted of 4 support codes,

SPECIES (arrange of radiolysis data set),

INITCONC (initial guess for radiolysis calculation),

GVALUE (arrange of G-value data set) and

Init_gas_liquid (initial guess for gaseous specie calculation).

The WRAC sub-code was the major sub code to determine the concentrations of radiolytic species, which consisted of 3 support codes,

INITCALC (setting initial values for mass balance calculation),

EULER (preparation of differential calculations) and

BDFNEWTON (control of Newton calculation).

The ECPCAL sub-code consisted of 2 support codes,

SOLUBILITY (calculating T and pH_T dependent ferrous ion solubility) and

CURRENTDNS (calculating the inter section of anodic and cathodic current densities).

Two support codes, INITCALC and BDFNEWTON were also supported by multi-step subroutines.

A program analysis diagram (PAD) of WRAC-JAEA is shown in **Table 6.1**.

The source code was written in MS-Word, which was converted into FORTRAN for calculation. The source code is shown in Appendix C and the execution version is attached in the CD-ROM.

Table 6.1 Program diagram for main routine (1/5)

```
Main
    Dimension
    File setting    open (13,FILE='TITLE-INPUT.txt')
                    open (7,FILE='REACTIONk-A.txt')
                    open (10,FILE='GVALUE.txt')
                    open (12,FILE='RT-INPUT.txt')
                    open (14,FILE='NodeConnect-k2.txt')
                    open (560,FILE=' OUTPUTF.DAT')  Summary of input and output data
                    open (550,FILE='REGALL1.DAT')   Eine results for the mesh points
                    open (580,FILE='REGALL2.DAT')   Results for the regions
                    open (570,FILE='REGALL3.DAT')   Results related to ECP calculation
        Read input data 1 Calculation condition (TITLE-INPUT), case number (ICASEN), iiterm (Max of iteration No),
                          [B]. [Li], [O2], [H2], [H2O2], [H2]inject

145     Do 108 k10=1,ICASEN

461*        <=  154**
    INPUT(Q,Q3,QN,QN3,QA,QA3,HWC, &
    &RN,F1,F2,F3,R1,R2,R3,FN1,FN2,FN3,RN1,RN2,RN3,FK0, &
    &RK0,WFK0,WRK0,FK,RK,WFK,WRK,FAE,RAE,REG,ID,C,CAQ2,N, &
    &GG,GN,GA, HN,ON,CH,TEM0,TEM,DIO,O2C,O2C2,RT, &
    & G2,WDE,NCN,PNDN,NDN,RMIX, RRMIX,LNDN,GNDN, H2O2C, &
    & H2O2C2,IDH2,H2INJ,H2INJ2,VAL,IECPS,IDECPS,IECPE,IECPN, &
    & IPWRR1,IPWRR2, IPWRP1,IPWRP2,IECPR1,IECPR2, BoronC,LiOHC,&
    & IECPP1,IECPP2,IECPV1, RECPV1,RECPV2,RECPV3, CECPC, ECPV, AAH0, &
    & ISOLP,SOLPHH,SOLPHL,TISOL,FSOLF,TEM1,TEM2, KW01,KW02,KW, &
    & HHOXD1,HHBND1,BoronC2,LiOHC2,IDH,ICASEN,IPRINTN,IPREGN, &
    & AITIC, iiter,iitermax,TITLE,k10)
    Dimension                                   VAL(7-10.i01) : unit cm => m where
        Read input data 2. Input data of node conditions (RT-INT.txt) Node number:REG
                        3. Input data of node connections (NodeConnect-k2.txt), Connection number: NCN
                        4. Input of rate constants (REACTIONk-A.txt) Reaction number: RN
                        5. Input G-values (GVALUE.txt), G-value number: GVN
                        6. Input data are stored in FILE='OUTPUTF.DAT'

2749    <=  822-827
    SPECIES(F1,FS,NUL,RN,FSN,FHN,FON,FCH,FHN1,FON1,FCH1)
    SPECIES(F2,FS,NUL,RN,FSN,FHN,FON,FCH,FHN1,FON1,FCH1)
    SPECIES(F3,FS,NUL,RN,FSN,FHN,FON,FCH,FHN1,FON1,FCH1)
    SPECIES(R1,FS,NUL,RN,FSN,FHN,FON,FCH,FHN1,FON1,FCH1)
    SPECIES(R2,FS,NUL,RN,FSN,FHN,FON,FCH,FHN1,FON1,FCH1)
    SPECIES(R3,FS,NUL,RN,FSN,FHN,FON,FCH,FHN1,FON1,FCH1)
            Data rearranging of rate constants from the order of INPUT table to specie order

    I01=1
2527    <=  834
    INTCONC(N,ID,IC,FS,FSN,RS,RSN,1,CAQ,FHN,FON,FCH,
        RHN,RON,RCH,HN,ON,CH,1,O2C2,IDH2,H2O2C2)
            Setting initial values for calculation matrix (Region#=1)

    I01>1
2527    <=  840
    INTCONC(N,ID,IC,FS,FSN,RS,RSN,1,CAQ,FHN,FON,FCH,
        RHN,RON,RCH,HN,ON,CH,1,O2C2,IDH2,H2O2C2)
            Setting initial values for calculation matrix (Region#>2)

2387    <=  855
    GVALUE(N,ID,GID,GVN,GG,GN,GA,data1,data2,data3)
            Calculation of energy deposition rate based on G-value and energy absorption
```

Table 6.1 Program diagram for main routine (2/5)

Table 6.1 Program diagram for main routine (3/5)

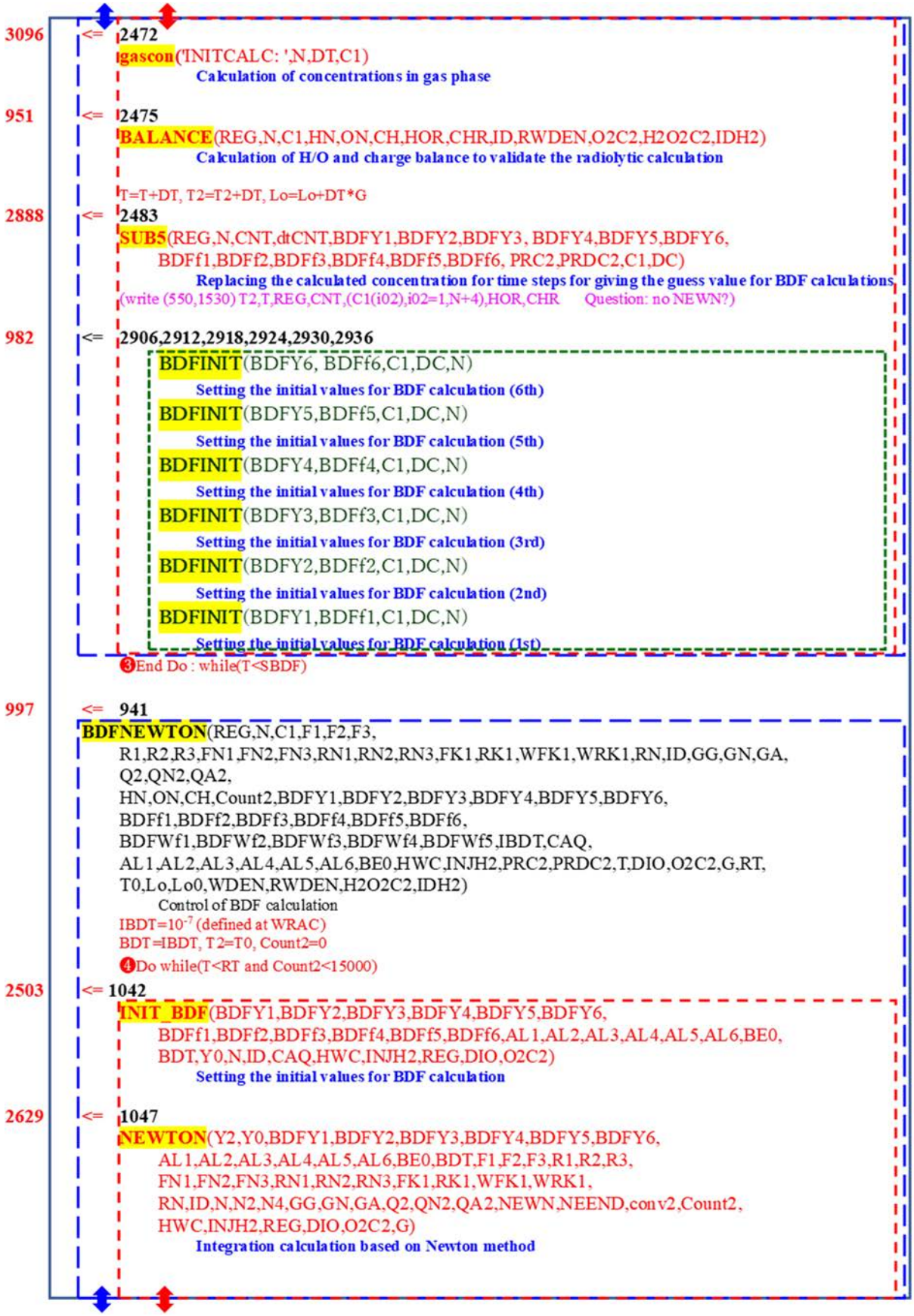

Table 6.1 Program diagram for main routine (4/5)

Table 6.1 Program diagram for main routine (5/5)

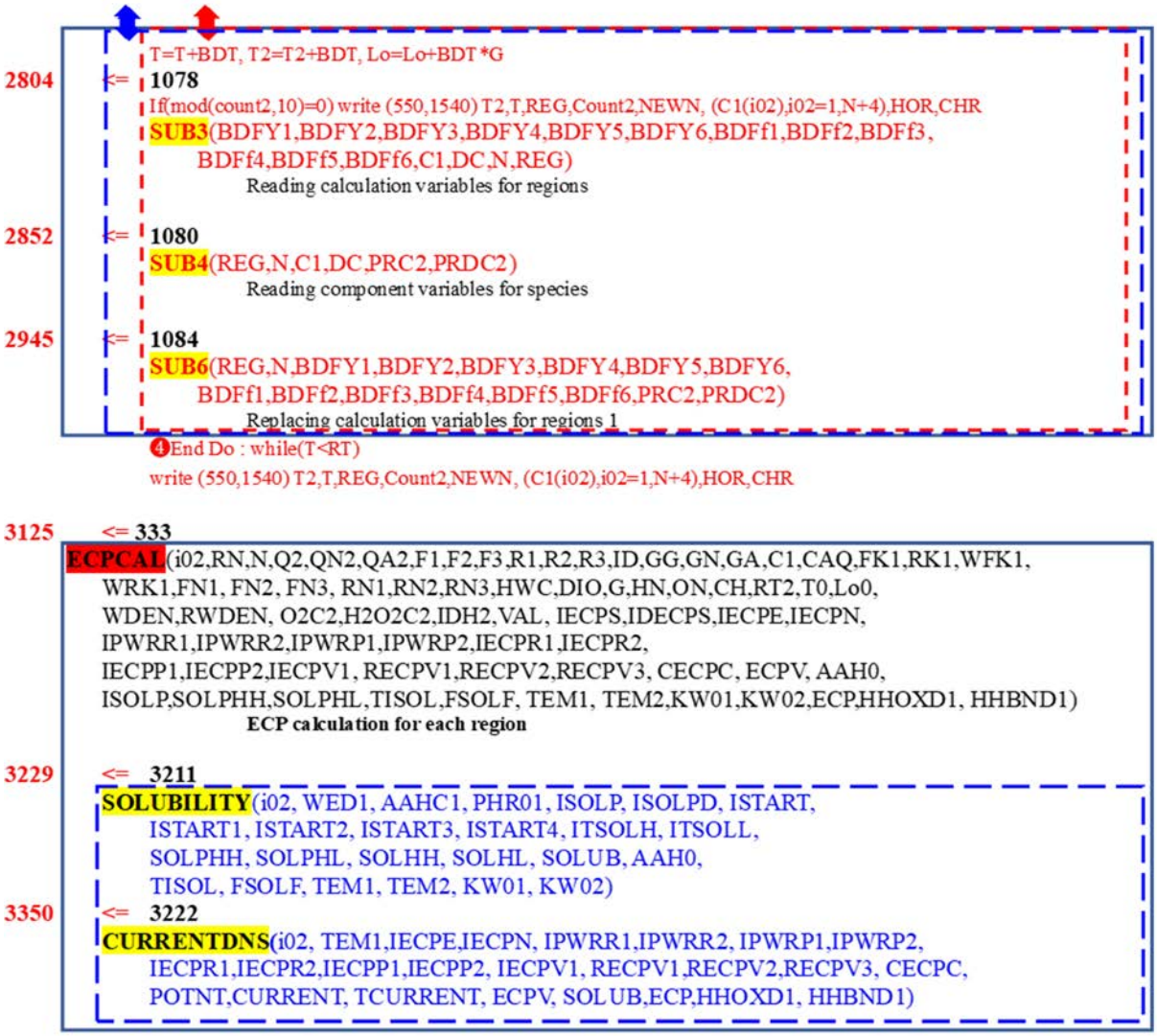

write (560,1560) comint(1),comrel(1),comint(2),comint(3),(C1(i01),i01=1,N+4),comrel(2),comrel(3),ECP

383 ❷end do

384 LON=LON+1

Iteration check with {[O_2],[H_2O_2].[H_2]] at the entrance of Reg 1. If not convergence, go to ❶

if(iiter.ge.iitermax) then go to 999

iiter=iiter+1

385 ❶end do

455 **go to 110**

456 **999 continue**

457 **108 continue**

end

***Line number of the head of the subroutine or the actions**

****Line number of the location where the subroutine was called.**

6.1.2 Major Subroutines for Water Radiolysis (WRAC)

The details and sub-PAD of WRAC are shown in Appendix A.

6.1.3 Major Subroutines for ECP Calculations (ECPCAL)

The details and sub-PAD of ECPCAL are shown in Appendix B.

6.2 Computer Code Complex

6.2.1 Source Code

The source code is attached to Appendix C

6.2.2 Fortran for Calculation

The source code was originally written in MS-Word, which was easily translated into FORTRAN. How to use the FORTRAN, how to arrange the input data and how to read the output are show in Chapter 8 CALCULATION CODE MANUAL OF WRAC-JAEA.

7. Calculation Results and Evaluation of the Results

7.1 Water Radiolysis

7.1.1 High Temperature pH Calculation

In the previous model, pH_T was given as input data for the water radiolysis calculation, while in the latest version of the water radiolysis calculation code, coupled concentrations of B and Li were given as input data for the radiolysis code and then pH_T was calculated in the code along with calculating the concentrations of the radiolytic species. Then, two codes, water radiolysis calculation code and ECP calculation code, were coupled as the integrated code to calculate the ECP based on the radiolytic specie concentrations in the single code. Major reactions and their reaction constants are listed in **Table 7.1** [49), 50)].

Table 7.1 Major dissociation reactions and their constants

Dissociation reaction of water (Marshall-Franck's formula) [1)]

$H_2O \rightarrow H^+ + OH^-$ $\quad k_W = [H^+][OH^-]/[H_2O]$

$\log(k_W) = -4.093 - 3245/T + 2.236\times10^5/T^2 - 3.985\times10^7/T^3 + (13.96 - 12626/T + 8.5646\times10^5/T^2)\ \log(\rho_w)$

$\rho_w = \{1.0 + 0.1341\ (374.11-t)^{1/3} - 3.946\times10^{-3}(374.11-t)\}/\{3.198 - 0.3152(374.11-t)^{1/3} - 1.203\times10^{-3}\ (374.11-t) + 7.489\times10^{-13}(374.11-t)^4\}$

$LiOH \rightarrow Li^+ + OH^-$ assumed as complete dissociation

$k_{Li} = [Li^+][OH^-]/[LiOH] = 10$ (mol/L)

Dissociation of boric acid (Mesmer's formula) [2)]

$B(OH)_3 + OH^- \rightarrow B(OH)_4^-$ $\quad Q_{11} = [B(OH)_4^-]/\{[B(OH)_3][OH^-]\}$

$\mathrm{Log10}(Q_{11}) = 1573.21/T + 28.6059 + 0.012078T - 13.2258\log(T) + f(I)$

$2B(OH)_3 + OH^- \rightarrow B_2(OH)_7^-$ $\quad Q_{21} = [B_2(OH)_7^-]/\{[B(OH)_3]^2[[OH^-]\}$

$\mathrm{Log10}(Q_{21}) = 2756.1/T - 18.7322 - 0.00033T + 5.835\log(T) - f(I)$

$3B(OH)_3 + OH^- \rightarrow B_3(OH)_{10}^-$ $\quad Q_{31} = [B_3(OH)_{10}^-]/\{[B(OH)_3]^3[[OH^-]\}$

$\mathrm{Log10}(Q_{31}) = 3339.5/T - 7.850 - 0.00033T + 1.497\log(T) - f(I)$

$4B(OH)_3 + 2OH^- \rightarrow B_4(OH)_{14}^{2-}$ $\quad Q_{41} = [B_4(OH)_{14}^{2-}]/\{[B(OH)_3]^4[[OH^-]^2\}$

$\mathrm{Log10}(Q_{41}) = 12820/T - 134.33 - 0.00033T + 42.105\log(T) - f(I)$

Reactions of daughters of boric acid

$B(OH)_4H$	$\rightarrow B(OH)_4^-$	$+H^+$	reaction constants for all reactions were assume as 10 for the forward reactions and 100 for the backward reactions.
$B_2(OH)_7H$	$\rightarrow B_2(OH)_7^-$	$+H^+$	
$B_3(OH)_{10}H$	$\rightarrow B_3(OH)_{10}^-$	$+H^+$	
$B_4(OH)_{14}H_2$	$\rightarrow B_4(OH)_{14}^{2-}$	$+2H^+$	
$B(OH)_4Li$	$\rightarrow B(OH)_4^-$	$+Li^+$	
$B_2(OH)_7Li$	$\rightarrow B_2(OH)_7^-$	$+Li^+$	
$B_3(OH)_{10}Li$	$\rightarrow B_3(OH)_{10}^-$	$+Li^+$	
$B_4(OH)_{14}Li_2$	$\rightarrow B_4(OH)_{14}^{2-}$	$+2Li^+$	

1) Marshall WL, Franck EU, Ion product of water Substance, 0-1,000ºC, 1-10,000 Bars, New international formulation and its background, J. Phys, Chem, Ref Data, 10 (2) 295-304 (1981).

2) EPRI, PWR Advanced All-Volatile Treatment Additives, By-Products, and Boric Acid, EPRI TR100755 (1992).

The rate constants related to boron and lithium are shown in the rate constant table (**Table 7.2**).

Table 7.2 Reaction constants for radiolysis calculation

Reactants	Products	Reaction constants*		Activation energy	
		Forward	Backward	Forward	Backward
$H^+ + OH^-$	$\rightarrow H_2O$	Determined based on Marshall-Franck's formula			
H_2O_2	$\rightarrow 2HO$	0.00E+00	5.5E+09	0.00E+04	7.90E+03
$B(OH)_3 + OH^-$	$\rightarrow B(OH)_4^-$	Determined based on Mesmar's formula			
$2B(OH)_3 + OH^-$	$\rightarrow B_2(OH)_7^-$	do		Rate constant for Boric acid and lithiuhydroxide	
$3B(OH)_3 + OH^-$	$\rightarrow B_3(OH)_{10}^-$	do			
$4B(OH)_3 + OH^-$	$\rightarrow B_4(OH)_{14}^{2-}$	do			
LiOH	$\rightarrow Li^+ + OH^-$	1.00E+01	1.00E+02	Temperature	
$B(OH)_4H$	$\rightarrow B(OH)_4^- + H^+$	1.00E+01	1.00E+02	independent constants	
$B_2(OH)_7H$	$\rightarrow B_2(OH)_7^- + H^+$	1.00E+01	1.00E+02	were assumed	
$B_3(OH)_{10}H$	$\rightarrow B_3(OH)_{10}^- + H^+$	1.00E+01	1.00E+02		
$B_4(OH)_{14}H_2$	$\rightarrow B_4(OH)_{14}^{2-} + 2H^+$	1.00E+01	1.00E+02		
$B(OH)_4Li$	$\rightarrow B(OH)_4^- + Li^+$	1.00E+01	1.00E+02		
$B_2(OH)_7Li$	$\rightarrow B_2(OH)_7^- + Li^+$	1.00E+01	1.00E+02		
$B_3(OH)_{10}Li$	$\rightarrow B_3(OH)_{10}^- + Li^+$	1.00E+01	1.00E+02		
$B_4(OH)_{14}Li_2$	$\rightarrow B_4(OH)_{14}^{2-} + 2Li^+$	1.00E+01	1.00E+02		
$H + H$	$\rightarrow H_2$	9.00E+10	0.00E+00	1.26E+04	0.00E+00
$E^- + HO_2$	$\rightarrow HO_2^-$	3.00E+11	0.00E+00	1.26E+04	0.00E+00
$E^- + O_2$	$\rightarrow O_2^-$	2.60E+11	0.00E+00	1.26E+04	0.00E+00
$2E^- + 2H_2O$	$\rightarrow H_2 + OH^-$	1.75E+06	0.00E+00	1.26E+04	0.00E+00
$2OH$	$\rightarrow H_2O_2$	2.50E+10	0.00E+00	8.40E+03	0.00E+00
$OH^- + H$	$\rightarrow E^- + H_2O$	7.00E+08	0.00E+00	1.26E+04	0.00E+00
$E^- + H + H_2O$	$\rightarrow OH^- + H_2$	4.82E+09	0.00E+00	1.26E+04	0.00E+00
$E^- + HO_2^- + H_2O$	$\rightarrow OH + 2OH^-$	5.35E+08	0.00E+00	1.26E+04	0.00E+00
$H + OH$	$\rightarrow H_2O$	2.30E+11	0.00E+00	1.26E+04	0.00E+00
$OH + H_2$	$\rightarrow H + H_2O$	1.40E+09	0.00E+00***	1.93E+04	0.00E+00
$H + O_2$	$\rightarrow HO_2$	1.50E+11	0.00E+00	1.26E+04	0.00E+00
$H + HO_2$	$\rightarrow H_2O_2$	3.00E+11	0.00E+00	1.26E+04	0.00E+00
$H + O_2^-$	$\rightarrow HO_2^-$	3.00E+11	0.00E+00	1.26E+04	0.00E+00
$E^- + O_2^- + H_2O$	$\rightarrow HO_2 + 2OH^-$	3.57E+09	0.00E+00	1.26E+04	0.00E+00
$H + H_2O_2$	$\rightarrow OH + H_2O$	2.00E+09	0.00E+00	1.89E+04	0.00E+00
$OH + H_2O_2$	$\rightarrow H_2O + HO_2$	4.20E+08	0.00E+00	1.43E+04	0.00E+00
$OH + HO_2$	$\rightarrow H_2O + O_2$	1.00E+11	0.00E+00	1.26E+04	0.00E+00
$2HO_2$	$\rightarrow H_2O_2 + O_2$	5.00E+07	0.00E+00	1.89E+04	0.00E+00
HO_2	$\rightarrow O2 + H+$	3.90E+05	7.70E+11	1.26E+04	1.26E+04
$HO_2 + O_2^-$	$\rightarrow O_2 + HO_2^-$	5.00E+08	0.00E+00	1.89E+04	0.00E+00
$O_2^- + OH$	$\rightarrow OH- + O_2$	2.90E+11	0.00E+00	1.26E+04	0.00E+00
$2O_2^- + 2H_2O$	$\rightarrow O_2 + H_2O_2 + 2OH^-$	1.27E+05	0.00E+00	1.89E+04	0.00E+00
$H_2O_2 + OH^-$	$\rightarrow HO_2^- + H_2O$	1.00E+10	2.14E+05	1.26E+04	1.26E+04
H_2O_2	$\rightarrow O_2 + H_2O$	1.40E-02	0.00E+00	6.00E+04	0.00E+00

* unit: $1/(mol/m^3)/s$ for two bodies reactions, and $1/(mol/m^3)^2/s$ for three bodies reactions

** unit: kJ/mol/K

***The value were changed from 0 to 1.6E4 $dm^3/mol/s$. Hata, K. et al., Optimization of dissolved hydrogen concentration for mitigating corrosive conditions of pressurized water reactor primary coolant under irradiation (1) Evaluation of water radiolysis, J. Nucl. Sci. Technol., 61(4), 2024, pp. 448-458.

In the present code, the reactions of Li and boric acid compounds were restricted only with H^+ and OH^- and no reaction with other radiolytic species. So, in the code boron and lithium could determine pH_T and then contribute to the concentrations of the radiolytic species but H^+ and OH^- through the changes in $[H^+]$ and $[OH^-]$. The calculated pH_T as functions of [B] and [Li] are shown in **Figure 7.1** with those with EPRI data [50].

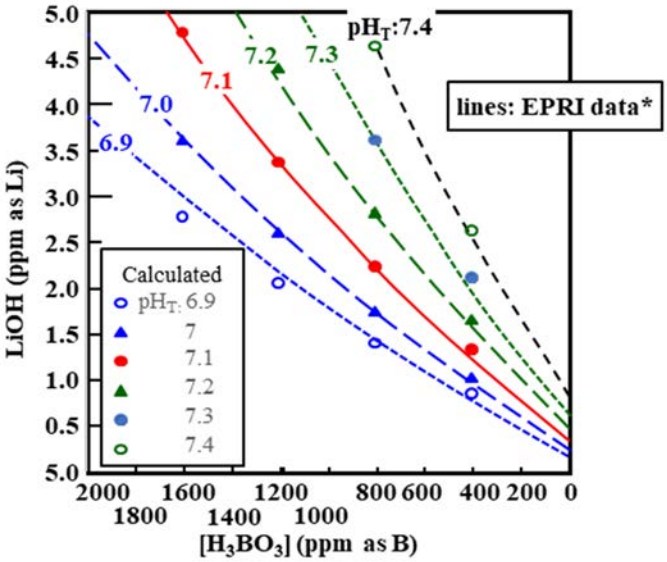

Figure 7.1 Relationship of [Li], [B] and pH_T (300 ºC)

* EPRI, PWR Advanced All-Volatile Treatment Additives, By-Products, and Boric Acid, EPRI TR-100755 (1992).

7.1.2 INCA In-pile Loop

There were not so many data on radiolytic species and ECP under irradiation especially PWR water chemistry conditions. As the comparison targets, ECP measured data in Studsvik in-pile loop (INCA) were selected [70].

The schematic diagram of the INCA in-pile loop is shown in **Figure 7.2**.

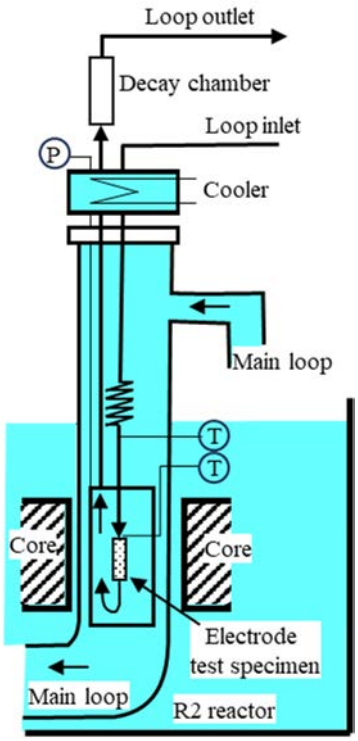

Figure 7.2 Schematic diagram of the INCA in-pile loop (Studsvik R2 reactor)

To understand the difference between INCA loop and a primary coolant system in PWR, major characters of INCA loop are shown in **Table 7.3** with comparing those of Tsuruga-2 PWR. The water temperature and water flow rate for the ECP measurement are introduced with the estimated dose rate at the irradiation segment of the INCA loop.

Table 7.3 Major characteristics of the in-pile INCA loop and in-pile region of Tsuruga-2

Parameters	Unit	INCA loop	Tsuruga-2
Temperature	(K)	563.2	578.2
	(°C)	290	305
Flow rate	(kg/s)	0.139	-
Dose rate	(Gy/s)		
Gamma rays		4000	1500
Neutrons		4300	5000
Alpha rays	normal α*1	2470	-
	low α*2	674	-
Thermal neutrons	(n/m^2/s)	1.7×10^{18}	4.2×10^{17}

*1 calculated based on the thermal neutron flux at the irradiated segment of the INCA loop
*2 those at the irradiated segment of the Tsuruga-2 PWR

The dose rate of fast neutron in the INCA loop was comparable to those of Tsuruga-2 NPP though the dose rates of gamma-ray and alpha particles in the INCA loop were relatively higher than those in Tsuruga-2. The dose rate of alpha-ray was not directly measured; it was estimated from the thermal neutron flux and its reaction cross-section against boron added in the loop. The effect of alpha-ray on the dose rate in the Tsuruga-2 primary coolant is one order of magnitude less than that in the INCA loop. To understand the effect of alpha-rays, we conducted calculations using two levels of alpha-ray dose rate. One is estimated from the conditions of the INCA loop, whereas the other is estimated from the Tsuruga-2 primary coolant.

Irradiation conditions of INCA were detailly introduced in the previous paper [70]. The injection hydrogen dependence of the radiolytic specie concentrations were calculated for the coupled concentration of boron (1600 ppm) and Li (2 ppm). pH_T was constant as a function $[H_2]_{injected}$. $[O_2]$ decreased rapidly, while $[H_2O_2]$ decreased slowly and reached the constant value. $[H_2]$ was a little high around low $[H_2]$injected but as a result of radiolysis suppression due to $[H_2]$injected it was reduced once and then $[H_2]_{injected}$ contributed to increase it.

Major parameters for water radiolysis calculation are listed in **Table 7.4**. Major parameters shown in table are discussed in the following columns.

Table 7.4 Major parameters to determine water radiolysis

Parameters	Mechanisms to control water chemistry
Radiation	g-values and rate constants of the mass balance equations for water radiolysis
Gamma rays	
Neutrons	
Alpha rays	
Temperature	Temperature dependent g-values and rate constants
Hydrogen	H_2/O_2 and H_2/H_2O_2 reaction based on OH radicals
pH	$[OH^-]$ affects $[e_{aq}^-]$ which affects $[H_2O_2]$

Table 7.5 shows the G-values used in this study [71]. In the radiolysis calculations, the effects of alpha-rays are considered as well as the effects of gamma-rays and neutron. In general, G-values of radical species are decreased and G-values of molecular species, such as H_2 and H_2O_2, are increased when the irradiated particle becomes heavier because chemical species are densely generated and react quickly with each other in the heterogeneous regions generated through the tracking of radiation at an early water radiolysis stage [72].

Table 7.5 G-values implemented into WRAC-J radiolysis code for calculation of PWR primary coolant conditions

Species	Gamma-rays	Neutrons	Alpha-rays
e_{aq}^-	3.50	0.60	0.13
$H^\bullet$	0.90	0.50	0.12
H^+	3.50	0.60	0.13
H_2	0.60	1.50	1.65
H_2O_2	0.55	1.14	1.55
$HO_2^\bullet$	0.0	0.04	0.0
$^\bullet OH$	0.45	1.7	0.45

Unit: number of species/100 eV-energy absorption

7.1.3 Radiation Quality Dependence of Calculated Hydrogen Peroxide Concentrations

The effects of pH, temperature, and radiation qualities on H_2O_2 generation were discussed before evaluating the optimal H_2 concentration in the PWR primary coolant. **Figures 7.3-7.5** show the $[H_2]_{inlet}$ dependences of H_2O_2 equilibrium concentration obtained by the INCA loop's radiolysis analysis [73]. In all cases, the H_2O_2 generation was sufficiently suppressed when the $[H_2]$inlet increased by at least 100ppb ($\cong 5.0 \times 10^{-5}$ mol/dm^3).

Figure 7.3 describes the effects of each radiation on the H_2O_2 concentration. The INCA loop's gamma-ray and neutron dose rates were used for this calculation. Alternatively, two dose rate levels were used to evaluate the effect of alpha-ray. One is estimated in the INCA loop (2,470 W/kg of thermal neutron, described as 'normal α' in the figure), and the other is estimated in the Tsuruga-2 primary coolant (674 W/kg of thermal neutron, described as 'low α' in the figure). The dose rates were calculated using the thermal neutron flux and the thermal neutron absorption cross-section of boron. The H_2O_2 concentration was increased in the order of alpha-ray ≥ neutron > gamma-ray, which would be relevant to the G-values of H_2O_2. The total H_2O_2 concentration was not obtained as a sum of the H_2O_2 concentrations generated by each radiation. This is due to the effects of radicals, which are produced in large quantities by gamma-ray irradiation and prefer to scavenge molecular products such as H_2O_2. A significant difference was observed between H_2O_2 concentrations generated by alpha-ray irradiation with higher and lower dose rates. However, this difference did not affect the total H_2O_2 concentration.

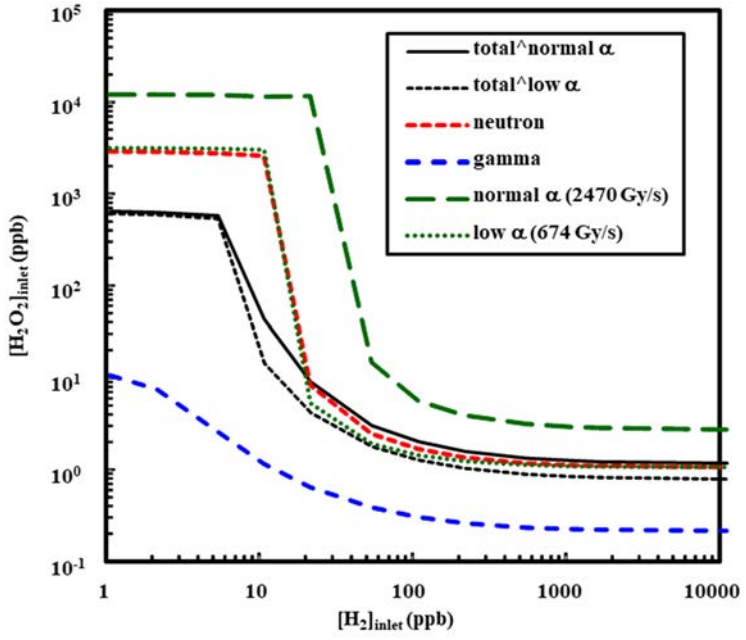

Figure 7.3 The Radiation quality dependence on H_2O_2 generation

7.1.4 Temperature Dependence of Calculated Hydrogen Peroxide Concentrations

Figure 7.4 describes the effects of each radiation on the H_2O_2 concentration. The INCA loop's gamma-ray and neutron dose rates were used for this calculation. Alternatively, two dose rate levels were used to evaluate the effect of alpha-ray. One is estimated in the INCA loop (2,470 W/kg of thermal neutron, described as 'normal α' in the figure), and the other is estimated in the Tsuruga-2 primary coolant (674 W/kg of thermal neutron, described as 'low α' in the figure). The dose rates were calculated using the thermal neutron flux and the thermal neutron absorption cross-section of boron. The H_2O_2 concentration was increased in the order of alpha-ray ≥ neutron > gamma-ray, which would be relevant to the G-values of H_2O_2. The total H_2O_2 concentration was not obtained as a sum of the H_2O_2 concentrations generated by each radiation. This is due to the effects of radicals, which are produced in large quantities by gamma-ray irradiation and prefer to scavenge molecular products such as H_2O_2. A significant difference was observed between H_2O_2 concentrations generated by alpha-ray irradiation with higher and lower dose rates.

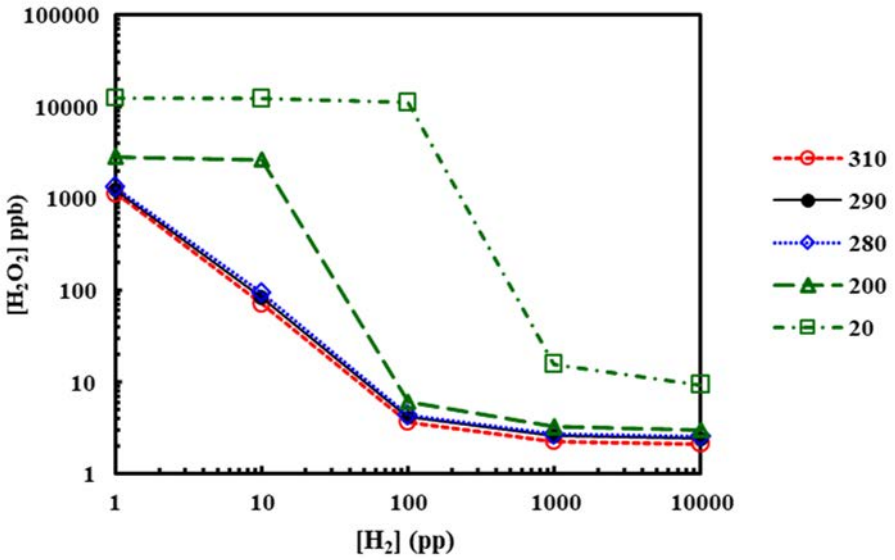

Figure 7.4 The temperature dependence on H_2O_2 generation at pH_T: 7.1

7.1.5 High Temperature pH Dependence of Calculated Hydrogen Peroxide Concentrations

However, this difference did not affect the total H_2O_2 concentration. **Figure 7.5** shows the temperature effect on H_2O_2 generation. H_2O_2 generation was slightly decreased at higher temperatures; however, the difference was neglected in the temperature range expected in the PWR primary coolant. The effect of pH at 290°C (pH_T) on the H_2O_2 concentration was also investigated (Figure 7.5). At 290°C, the neutral pH was 5.6 due to the change in the dissociation constant of water [11]. The H_2O_2 concentration was affected by pH_T. The effect of the $[H_2]_{inlet}$ on the H_2O_2 concentration was greater in alkaline conditions.

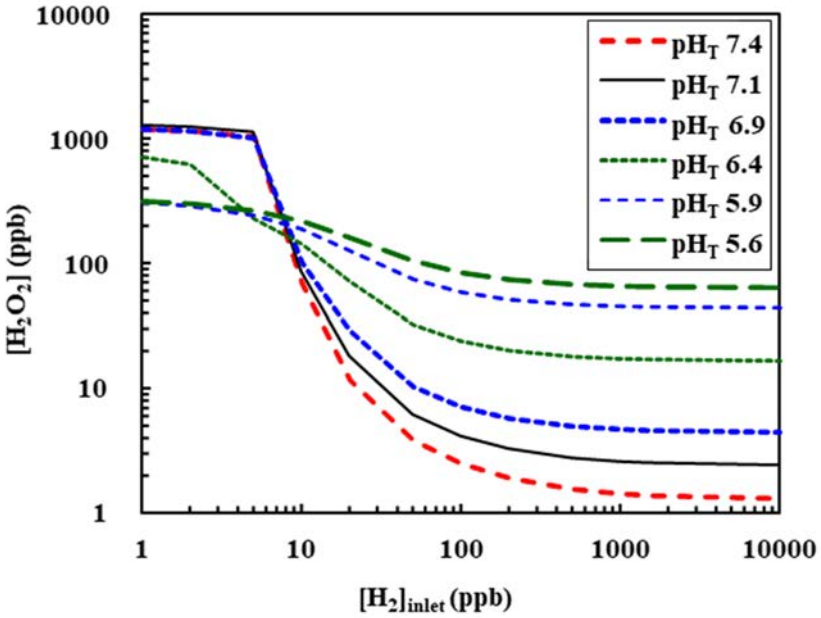

Figure 7.5 The pH_T dependence on H_2O_2 generation at 290ºC

7.1.6 H_2O_2 Suppression by H_2 and OH^- in Alkaline Solutions

The radiolysis calculation in the PWR primary coolant conditions revealed that increasing the concentrations of both H_2 and OH^- (high pH) successfully inhibited H_2O_2 formation (see Figure 7.5). The mechanism of the pH effect is discussed. Four second order reactions that directly decompose H_2O_2 can be found in the reaction data set (Table 7.2).

$$e_{aq}^- + H_2O_2 \rightarrow {}^{\bullet}OH + OH^- \quad (7\text{-}1)$$

$$H^{\bullet} + H_2O_2 \rightarrow {}^{\bullet}OH + H_2O \quad (7\text{-}2)$$

$$^{\bullet}OH + H_2O_2 \rightarrow HO_2^{\bullet} + H_2O \quad (7\text{-}3)$$

$$OH^- + H_2O_2 \rightarrow HO_2^- + H2O \quad (7\text{-}4)$$

A first-order reaction of H_2O_2 decomposition is also present in the data set. However, this reaction was not considered for the following discussion because the first-order reaction is unaffected by the other additives or pH.

Reaction No.5 is a possible candidate for direct suppression of H_2O_2 at alkaline pH. On the other hand, a direct pH effect is not obvious for the other three reactions. **Figure 7.6** shows the equilibrium H_2O_2 concentration estimated by radiolysis calculations, with the rate constant of Reaction No.5 varied by a factor of 10 and 0.1. Although the H_2O_2 concentration was slightly affected at the lower $[H_2]_{inlet}$, the result did not reveal the effect of this reaction on the drastic change of H_2O_2 concentration at the higher $[H_2]_{inlet}$.

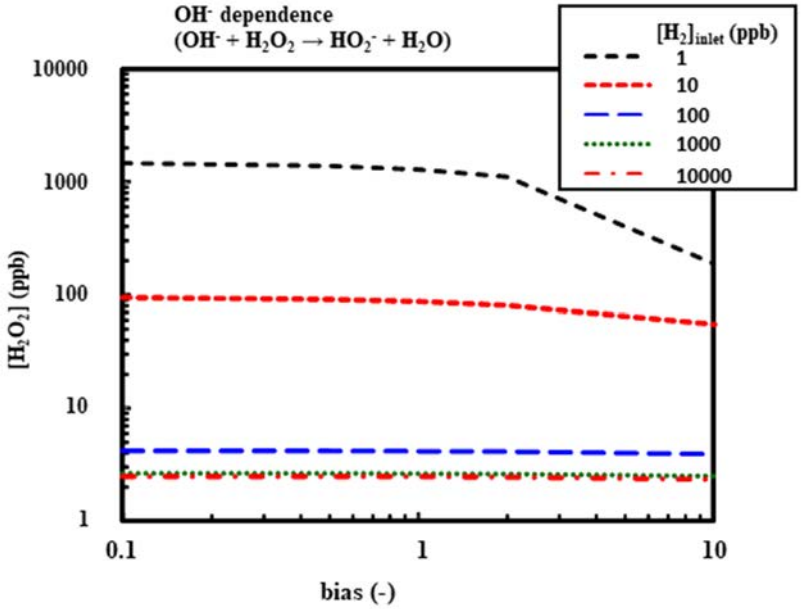

Figure 7.6 Dependence of the rate constant of Reaction No.5 ($OH^- + H_2O_2 \rightarrow HO_2^- + H_2O$)

Figure 7.7 shows the equilibrium concentrations of chemical species estimated by the radiolysis calculation in the PWR primary coolant. At high pH_T, the H_2O_2 concentration is decreased and the hydrated electron, e_{aq}^-, is increased by one order of magnitude greater than at neutral pH_T. The concentrations of other species are not affected by pH_T change. This result indicates that the effect of e_{aq}^- (Reaction No.2) is crucial in the suppression of H_2O_2 in the PWR primary coolant conditions.

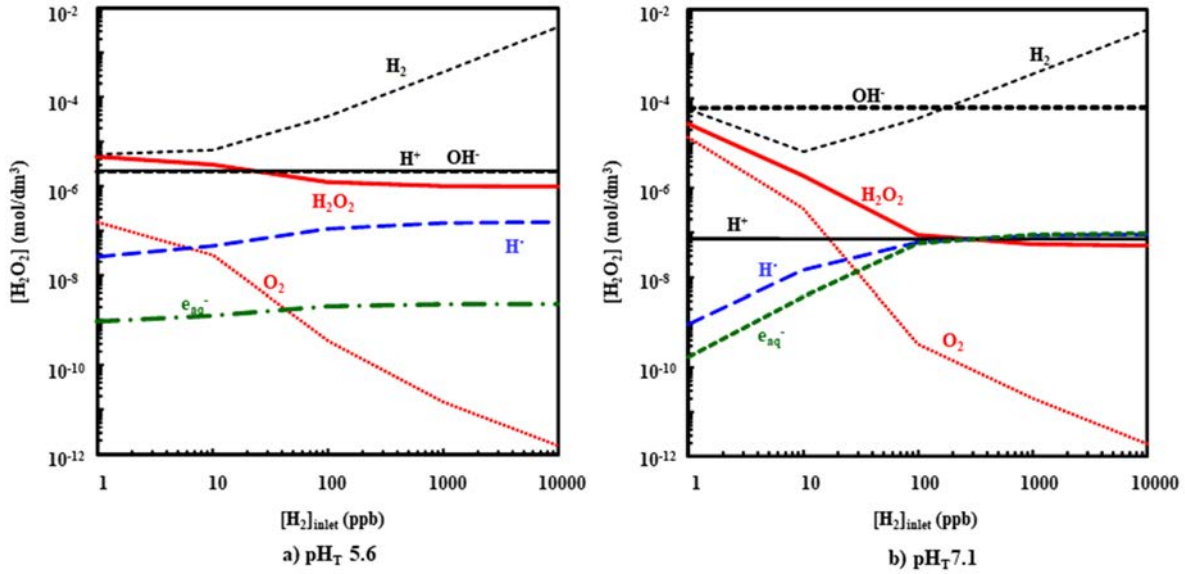

Figure 7.7 The equilibrium concentrations of chemical species estimated by the radiolysis calculation in the PWR primary coolant at neutral pH_T (left) and an alkaline pH_T (right) at 290ºC

The effect of Reaction No.2 was investigated by performing a radiolysis calculation, in which the rate constant of this reaction was varied by a factor of 10 and 0.1 (**Figure 7.8**).

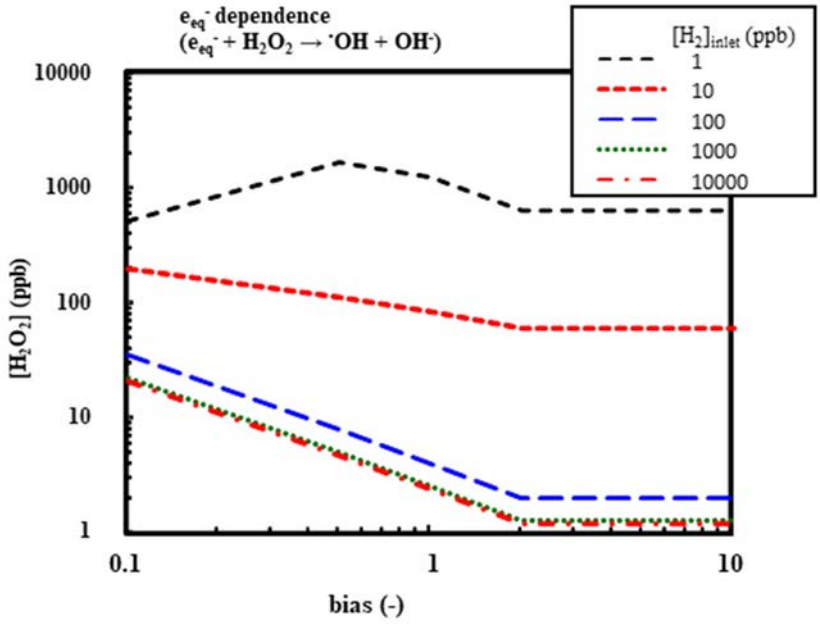

Figure 7.8 Dependence of the rate constant of Reaction No.2 ($e_{aq}^- + H_2O_2 \rightarrow {}^{\cdot}OH + OH^-$) on H_2O_2 generation

The H_2O_2 concentration changed based on the rate constant, and the effect was significantly larger in the high $[H_2]_{inlet}$ conditions. Further, the reason for the increase in e_{aq}^- at both high pH_T and high $[H_2]_{inlet}$ should be considered. According to the reaction below, hydrogen is mainly scavenged by the OH radical in water radiolysis.

$$*OH + H_2 \rightarrow H^* + H_2O \quad (7\text{-}5)$$

The production of this reaction, $H^{\cdot}$, can change into e_{aq}^- at high pH [79].

$$OH^- + H^* \rightarrow e_{aq}^- + H_2O \quad (7\text{-}6)$$

Figure 7.9 shows the result of the sensitivity analysis for Reaction No.7. H_2O_2 generation was inhibited in the high $[H_2]_{inlet}$ conditions. Thus, the three-step reactions shown in **Figure 7.10** are considered to be the main paths for H_2O_2 inhibition in the PWR primary coolant. These three reactions are also taken into account in the other reaction data sets [25), 75)]. This synergetic effects of H_2 and OH^- on the suppression of the H_2O_2 generation would be expected in the other radiolysis codes.

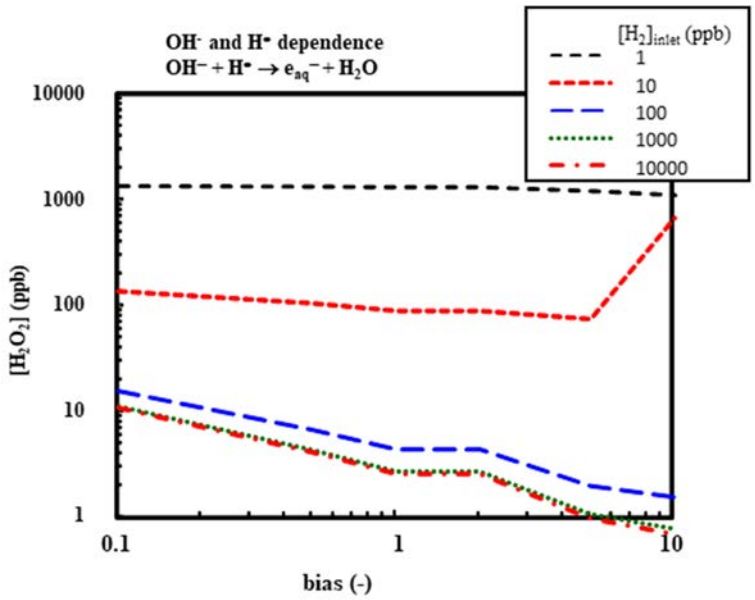

Figure 7.9 Dependence of the rate constant of Reaction No.7 ($OH^- + H^\bullet \rightarrow e_{aq}^- + H_2O$) on H_2O_2 generation

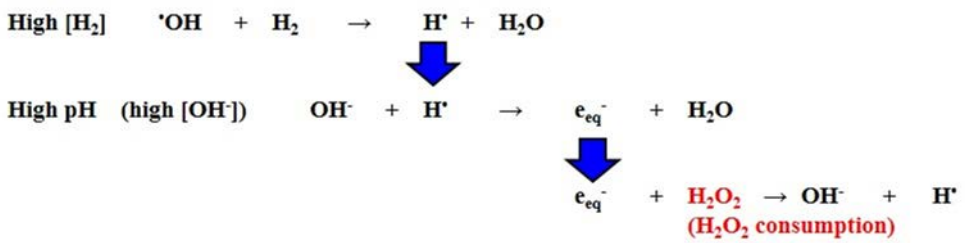

Figure 7.10 A possible reaction scheme for H_2O_2 suppression in PWR primary conditions

7.1.7 Evaluation of Major Rate Constants on Radiolysis Calculation

The water radiolysis code, WRAC-JAEA, was supported by 30 chemical reactions [10]. Recently it was reported that the backward reaction of 'OH + H_2 => $H^\cdot$ + H_2O' had large effects on radiolysis calculation and several backward reaction constants were proposed [74), 75), 76)]. Major backward reaction rates are shown in **Table 7.6.** Unfortunately, the effects of the backward reaction on calculation results of water radiolysis in BWR primary coolant were not reported yet, though the rate constant, 5,000 dm^3/mol/s, was recommended in the BWR standard set [75)]. In this section, the effects of the backward reaction rates on water radiolysis calculation results in the INCA in-pile-evaluated. The concentrations of H_2O_2, H_2, and O_2 both in the irradiated segment in the INCA in-pile-loop were calculated with WRAC-JAEA code as a function of the concentration of the injected H_2 in the loop, which was shown in **Figure 7.11**. The [H_2O_2] in the irradiated segment was decreased with [H_2], and it reached almost the same value as a result of the balance of its generation and disappearance by their secondary reactions. But the decrease trends depended on the backward reaction constants. The decrease rates were mitigated with backward rate constant. At the current calculation condition, the backward reaction rate reported by Elliot and Bartels gave the reasonable ECP s measured at the INCA loop [4)]. However, much more discussions on suitable combination of the rate constants of the water radiolysis should be required for water radiolysis analysis for BWR primary coolant conditions, which were covered by a plenty of measured ECP data, and then, for PWR primary coolant conditions.

Table 7.6 Major rate constants for the reaction, "$H^{\cdot} + H_2O \rightarrow {}^{\cdot}OH + H_2$" at 290ºC

Reference	Rate constant (dm^2/mol/s)
Previous BWR sets[10)]	0
Elliot and Bartels[74)]	1,330
The latest BWR standard sets[75)]	5,000
Moriya et. al.[76)]	16,000

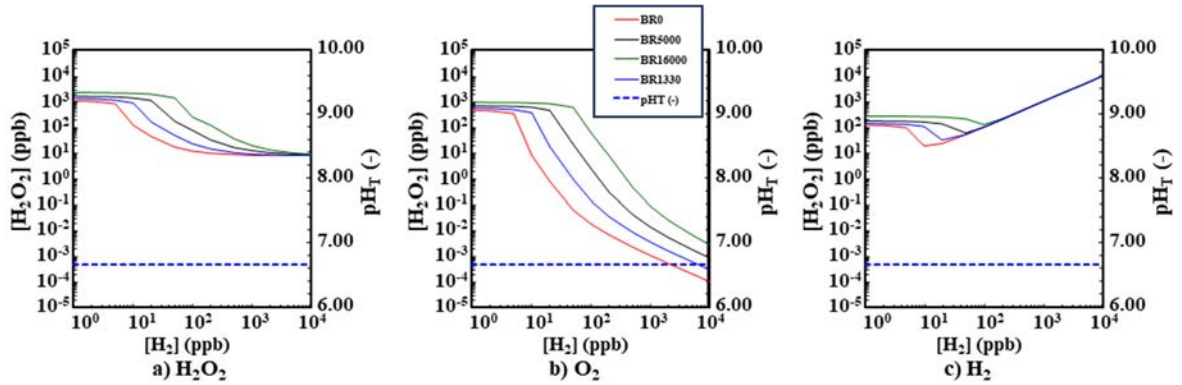

Figure 7.11 Dependence of backward reaction rate on H_2O_2 concentrations

7.1.8 Evaluation of Boiling Effects on Radiolysis Calculation

The previous type of WRAC-JAEA has been developed for evaluation of water radiolysis under irradiation in in-pile loop experiments, where no boiling has not been considered on water radiolysis. For PWR application of WRAC-JAEA boiling effects had less importance on radiolysis calculation. But, in order to apply WRAC-JAEA code for BWRs as well as PWRs, the effects of boiling on radiolysis calculation were one of key issues.

In **Table 7.7**, boiling effects of three type reactors, i.e., PWR, CANDU and BWR, are compared. In PWR only subcooled boiling is accepted in the core region, where it has not had only small effects on water radiolysis. For CANDU boiling effects on water radiolysis should be considered along with pH effects. For BWR lots of reports were published on boiling effects on water radiolysis. In order to apply the WRAC-JAEA for water radiolysis evaluation of three type reactors, the ability to calculate the boiling effects on water radiolysis might be one of the necessary items.

Table 7.7 Major parameters for plant radiolysis calculation

Parameters		PWR	CANDU	BWR	WRAC-JAEA
Temperature (ºC)		~310		~285	○
pH control: pH_T(-)		[B]/[Li] control: ~7.0		neutral: ~5.6	○
Energy deposition e rate (Gy/s)	neutrons	~5,000		~1,500	○
	γ rays	~1,500		~1,500	○
	α rays	~600		-	○
Boiling rate (void rate)		subcooled boiling (<5 %)	boiling (10%)	boiling (15%)	◎

The calculation procedures for boiling effects on water radiolysis processes were introduced in Chapter 5. In this Chapter, the calculated results were introduced.

A schematic flow diagram of the primary loop of BWRs is illustrated in **Figure 7.12**. The core regions are shown as regions 1 through 3 and the region 4 is the main steam line. The recirculation line were divided into two lines, one of which showed the downcomer region where gamma irradiation was assumed (dose rate was

about a tenth of that in the core region).

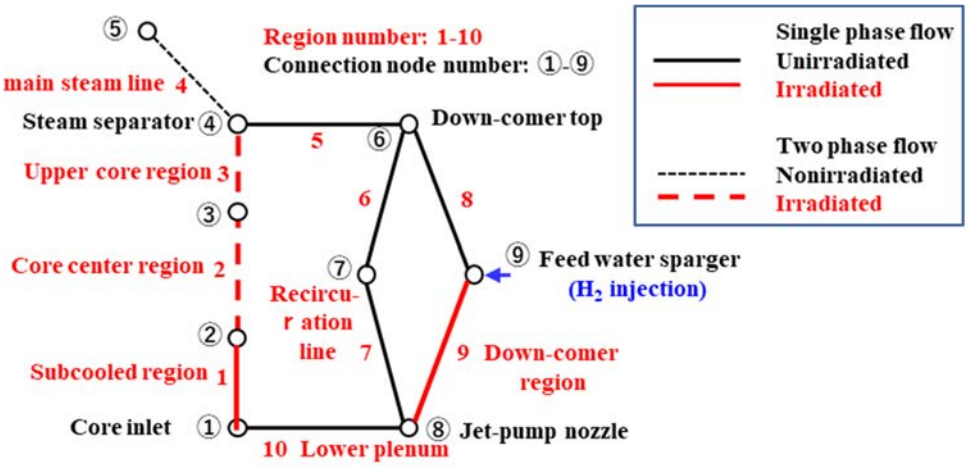

Figure 7.12 Flow lines of a hypothetical BWR primary cooling system

An example of the calculated results is shown in **Figure 7.13**. In core region, as a result of boiling some no gaseous species, O_2 and H_2, were transferred from water phase to the steam phase. As a result of hydrogen injection at the entrance of region 9, oxidant concentration decreased and then their concentrations increased due to mixing with the flow through non-injected region.

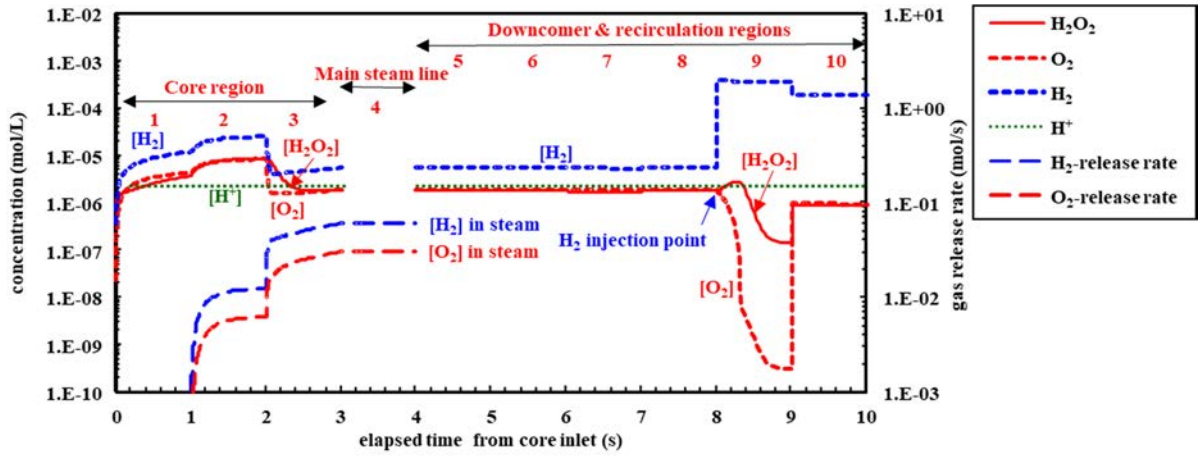

Figure 7.13 Calculated results along the hypothetical BWR primary cooling lines

The effects of void rate on the concentrations of gaseous species, H_2 and O_2, are shown in **Figure 7.14**. The ratio of the concentration of H_2 and O_2 was not shifted to the H_2 rich value. The reason why the ratio was not consistent to the stoichiometric ratio was that most of oxidant existed as H_2O_2 but not O_2. H_2O_2 was not affected by carry over into the steam. But when the release rate of gaseous species was checked, the H_2/O_2 release ratio was as same as stoichiometric ratio of water. It was considered that there was some time delay for oxygen release after decomposition of H_2O_2 to O_2.

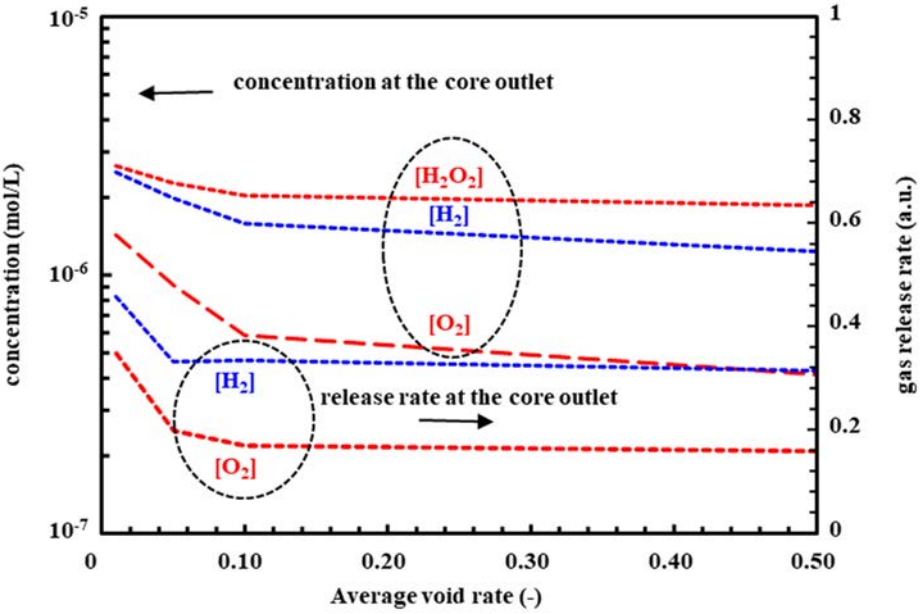

Figure 7.14 The effects of void rate on the concentrations and release rates of H_2O_2, O_2 and H_2

The void effects under neutral water were discussed in lots of literature related to BWR water radiolysis, but the effects on pH_T were not discussed in the previous document. The effects of void rate on $[H_2O_2]$ are shown in **Figure 7.15**. The concentration of hydrogen peroxide $[H_2O_2]$ at the core outlet decreased with pH_T as well as void rate.

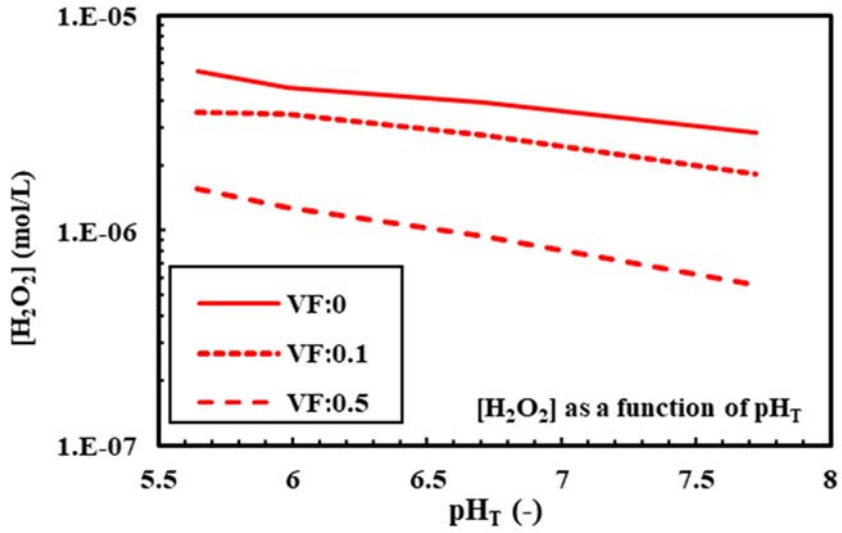

Figure 7.15 Effects of void rate on $[H_2O_2]$

As a result of H_2 injection into the downcomer region, $[H_2O_2]$ decreased and the decrease rate increased as pH_T (**Figure 7.16**). It suggested that elevated pH_T enhance hydrogen effects on $[H_2O_2]$ suppression and moderation of corrosive conditions. Much more precise calculation of the effects of pH_T and void rate on water radiolysis and ECP are required to understand the corrosive circumstance suppressions.

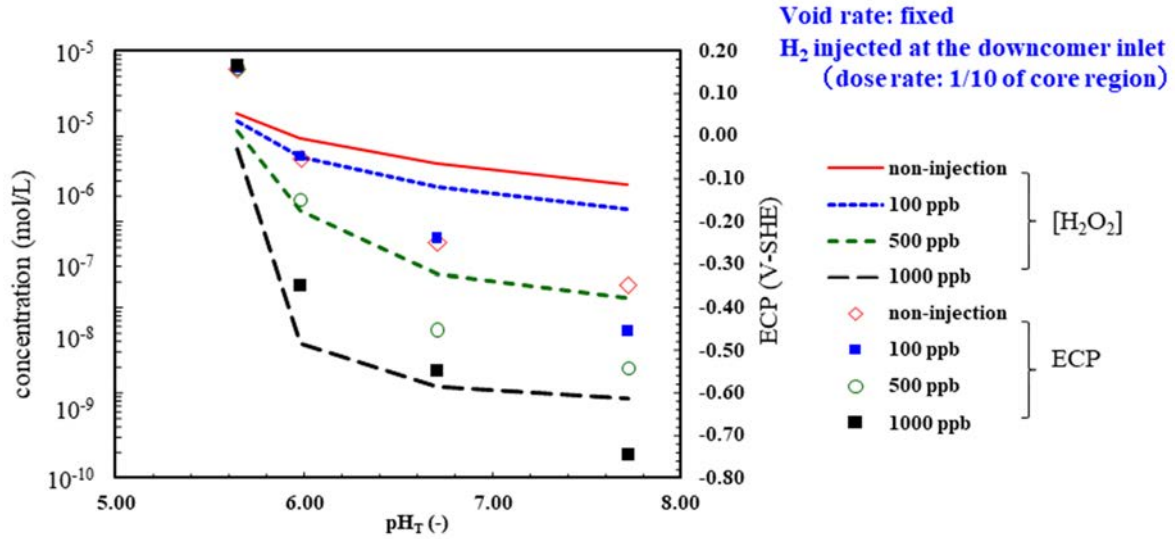

Figure 7.16 Effects of pH_T and injected $[H_2]$ on $[H_2O_2]$ and ECP

The $[H_2O_2]$ and ECP for a typical BWR plant were calculated with WRAC-JAEA and the results were illustrated in **Figure 7.17** [75]. At present situation, dose rate distribution of the core regions and downcomer regions were not sufficiently well tuned. Much more precise calculations were required, which might be one of the future subjects.

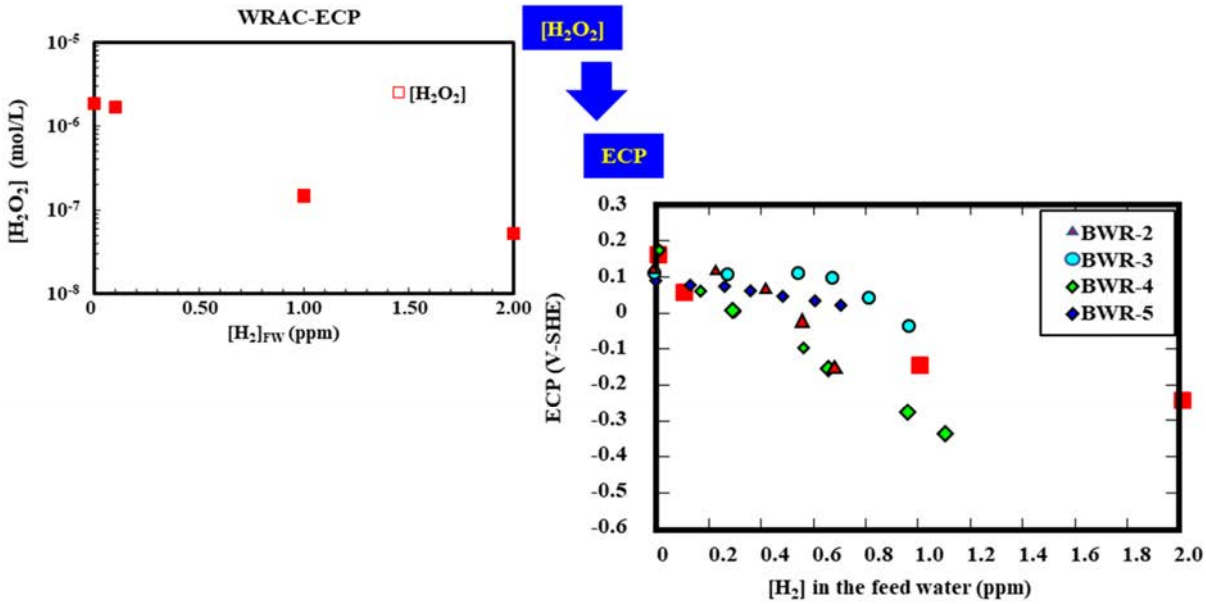

Figure 7.17 Relationship of ECP and injected $[H_2]$

7.2 Electrochemical Corrosion Potential

7.2.1 $[O_2]$ Dependent ECP

Lots of ECP data were available in publications. Major data were obtained as a function of $[O_2]$ under neutral water conditions [54), 60), 77)] The measured ECPs and calculated ones are shown in **Figure 7.18**. In the standard

calculation, the mass transfer coefficients for the surface boundary layers (MTBL coefficient) and the oxide layers (MTOL coefficient) were 1.0×10^{-5} and 1.0×10^{-6} m/s, respectively. The ECP dependence on the MTOL coefficient was much larger than on the MTBL coefficient. The deviations of the calculated results due to the MTOL coefficients for the oxide layers were shown in the figures. The calculated result depended on the thickness of the oxide layer as well as [O_2]. The increased thickness of the oxide layer resulted in a larger mass transfer of ferric ions through the layer and then smaller anodic current densities, which contributed toward increasing the calculated ECP. The effects of the mass transfer coefficient across the oxide layers (anodic current densities) are depicted in Figure 9.13. The preparation of test specimens, experimental procedures, and their histories all had a significant impact on the thickness of oxide layers. At the early stage of the ECP measurement with well mechanically polished test specimens, the thickness of the layers might be very thin, and their mass transfer coefficients were so small to reduce ECP while increasing experimental time resulted in a thicker oxide layer to increase ECP. For comparing observed and computed ECPs, the uncertainties displayed in the figures as a function of mass transfer coefficients were acceptable. Under the low [O_2] conditions the oxide layers developed much slower than those under the high [O_2] conditions. The thinner oxide layers resulted in the larger MTOL coefficients, which resulted in the gap between the calculated and measured ECPs.

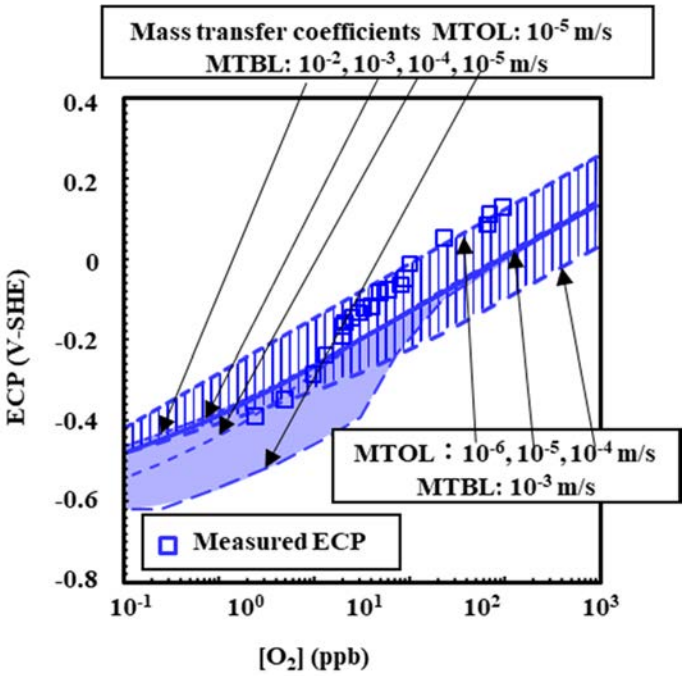

Figure 7.18 O_2 concentration dependent ECP

The calculated result depended on the thickness of the oxide layer as well as [O_2]. The increased thickness of the oxide layer resulted in a larger mass transfer of ferric ions through the layer and then smaller anodic current densities, which contributed toward increasing the calculated ECP. The effects of the mass transfer coefficient across the oxide layers (anodic current densities) are depicted in Figure 7.18. The preparation of test specimens, experimental procedures, and their histories all had a significant impact on the thickness of oxide layers. At the early stage of the ECP measurement with well mechanically polished test specimens, the thickness of the layers might be very thin, and their mass transfer coefficients were so small to reduce ECP while increasing experimental time resulted in a thicker oxide layer to increase ECP. For comparing observed and computed ECPs, the uncertainties displayed in the figures as a function of mass transfer coefficients were acceptable.

Under the low [O_2] conditions the oxide layers developed much slower than those under the high [O_2] conditions. The thinner oxide layers resulted in the larger MTOL coefficients, which resulted in the gap between the calculated and measured ECPs.

7.2.2 [H_2O_2] Dependent ECP

Some ECP data were obtained as a function of [H_2O_2] under neutral water conditions [54), 77)]. The measured ECPs as a function of [H_2O_2] and calculated ones were shown in **Figure 7.19**. The predicted result was also influenced by the thickness of the oxide layer and the concentration of [H_2O_2]. The MTBL coefficients for the surface boundary layers and the MTOL coefficient for the oxide layers in the standard computation were 1.0×10^{-5} and 1.0×10^{-6} m/s, respectively. The deviations of the calculated results due to the MTOL coefficients were shown in the figures.

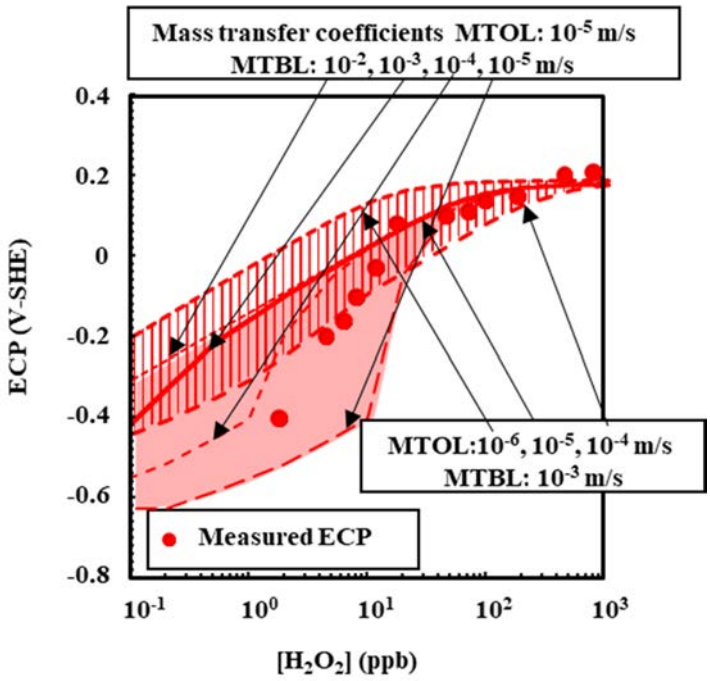

Figure 7.19 H_2O_2 concentration dependent ECP

7.2.3 pH Dependent ECP

The measured ECP data as a function of pH was shown only in a publication [78)], where ECP was measured with changing pH with Na^+ concentrations under neutral water conditions with adding 400 ppb of O_2. The calculated ECP was much affected by the concentration of [H^+] (**Figure 7.20**). In the standard calculation, the MTBL coefficients for the surface boundary layers and the MTOL coefficient for the oxide layers were 1.0×10^{-5} and 1.0×10^{-6} m/s, respectively. The figures depicted the differences in calculated findings due to the MTOL coefficients. The MTBL coefficients for the surface boundary had negligibly small effects on the surface boundary layers. And, the pH dependence was mainly from the pH dependent ferrous ion solubility.

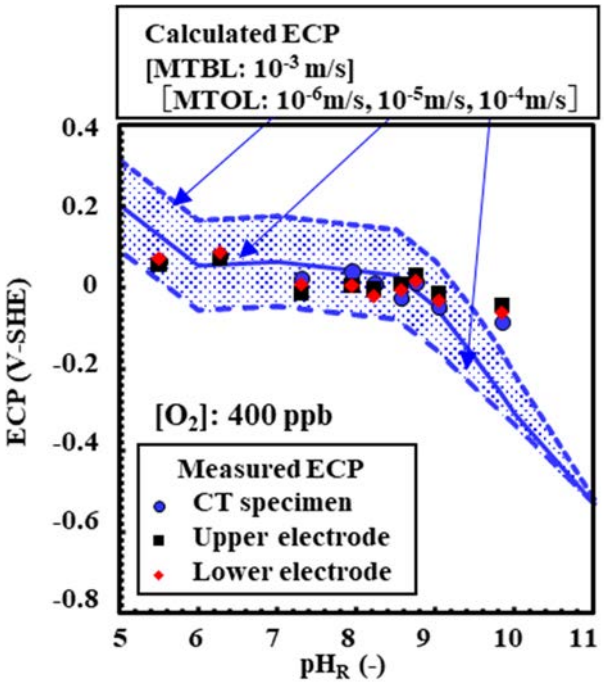

Figure 7.20 pH dependent ECP

(mass transfer coefficient, MTBL : 10^{-3} m/s)

7.2.4 Calculation for In-pile-loop Experiments

ECP was calculated with the WRAC-JAEA with applying the calculated [H_2O_2], [O_2] and [H_2] shown in Figure 7.11. The calculated results were shown in **Figure 7.21** with the measured ECP. The calculated results with neglecting the backward reaction are shown in Figure 7.15 a), while those with applying the AECL-proposed reaction rate, 1330 L/mol/s are shown in Figure 7.15b). In this paper, the AECL-proposed reaction rate was applied for ECP analysis due to only reason why the calculated ECP agreed with the results measured in INCA in-pile-loop.

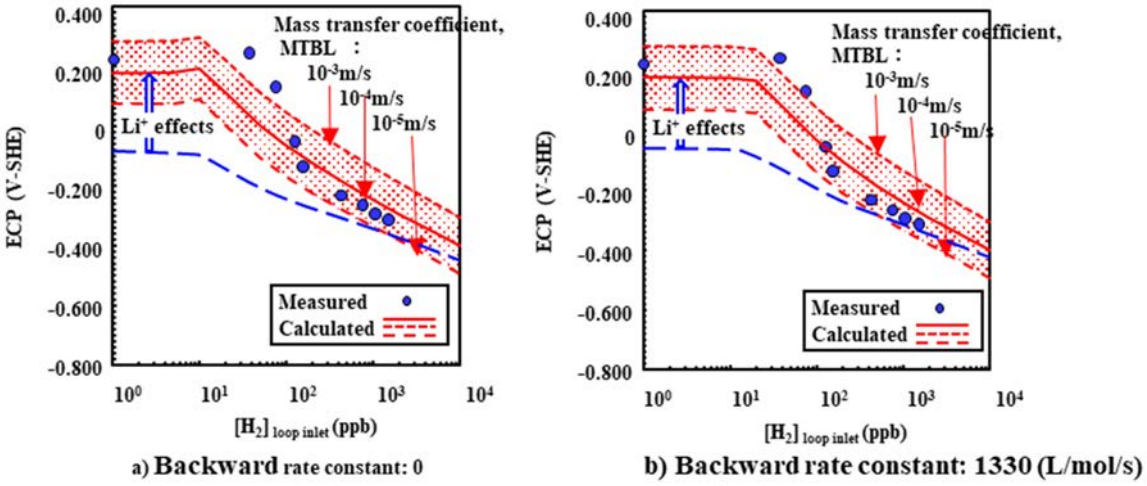

Figure 7.21 Inlet H_2 dependent ECP in the INCA loop (pH_T: 6.67)

under irradiation (MO coefficient: 10^{-6} m/s)

The calculated ECP was much affected by the [Li^+]. In the standard calculation, the mass transfer coefficients for the surface boundary layers and the oxide layers were 1.0×10^{-4} and 1.0×10^{-6} m/s, respectively. The deviations of the calculated results due to the mass transfer coefficients were shown in the figures. The anodic current densities were determined mainly by "$H_2 \Rightarrow 2H^+ + 2e^-$" but not by metal dissolution reaction. So, the effects of the mass transfer coefficients for the oxide layers were negligibly small. Without Li^+, ECP around low $[H_2]_{loop\ inlet}$, the calculated ECP was so low due to decreasing [H^+], while as a result of the Li^+ effects on the anodic current densities ECP was increased. Around 500 ppb of $[H_2]_{loop\ inlet}$ the $[H_2O_2]$ reached the constant level which was determined by pH, where the increased anodic current densities due to the reaction of "$H_2 \Leftrightarrow 2H^+ + 2e^-$" suppressed the ECP as a function of $[H_2]_{loop\ inlet}$. Then the calculated ECP agreed with the measured within a reasonable discrepancy [3]. Unfortunately, the effects of "$H_2O_2+2Li^+ +2e^- \Rightarrow 2LiOH$" as well as "$O_2+4Li^+ +4e^- \Rightarrow 2Li_2O$" on ECP were not well supported by the experimental data. The validation of their contribution on ECP is still one of future subjects.

7.3 Calculated Results of the Coupled Model of Water Radiolysis and ECP Analysis

To evaluate the dose rate dependence on $[H_2O_2]$ and then ECP, irradiated zones shown in **Table 7.8** were assumed for the coupled model [70].

Table 7.8 Irradiation conditions calculated for the downstream of the irradiation zone in the in-pile-loop (INCA)

Case	Dose rate	Other parameters
G F	Full dose rate as same as those in the core region (Table 4)	As same as those in the core region*
G 0.1	Gamma dose rate was 1/10 of G 1	Ditto
G 0.01	Gamma dose rate was 1/100 of G 1	Ditto
G 0.001	Gamma dose rate was 1/1000 of G 1	Ditto

* temperature: 290°C, pH_T:7.1

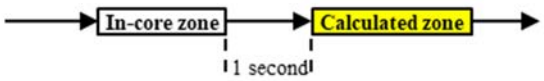

The concentrations of H_2O_2 in the downstream (assumed 1 second after In-core zone) of the irradiated segment in the INCA in-pile loop were calculated with WRAC-JAEA code as functions of the dose rate and the $[H_2]_{loop\ inlet}$, and then, ECP was calculated as a function of the calculated $[H_2O_2]$, which were shown in **Figure 7.22**. The $[H_2O_2]$ in the irradiated segment reached the constant value around 100 ppb of $[H_2]$, while ECP decreased monotonously with $[H_2]_{loop\ inlet}$ [Figure 7.22 a) and b)], while the $[H_2O_2]$ in the non-irradiation segment ECP sharply decreased with $[H_2]_{loop\ inlet}$ and reached the constant level determined by hydrogen generation-potential (~ −0.6 V-SHE) [Figure 7.22 b)]. Unfortunately, any measured ECP was not reported yet. The optimal region of injected $[H_2]$ could be designated as between the maximum $[H_2]$ for mitigating PWSCC crack growth rate to a half value of the peak one and the minimum $[H_2]$ for maintaining ECP lower than -0.2 V-SHE. The ECP target value, -0.2 V-SHE, was evaluated from the old data from the literature [79), 80)].

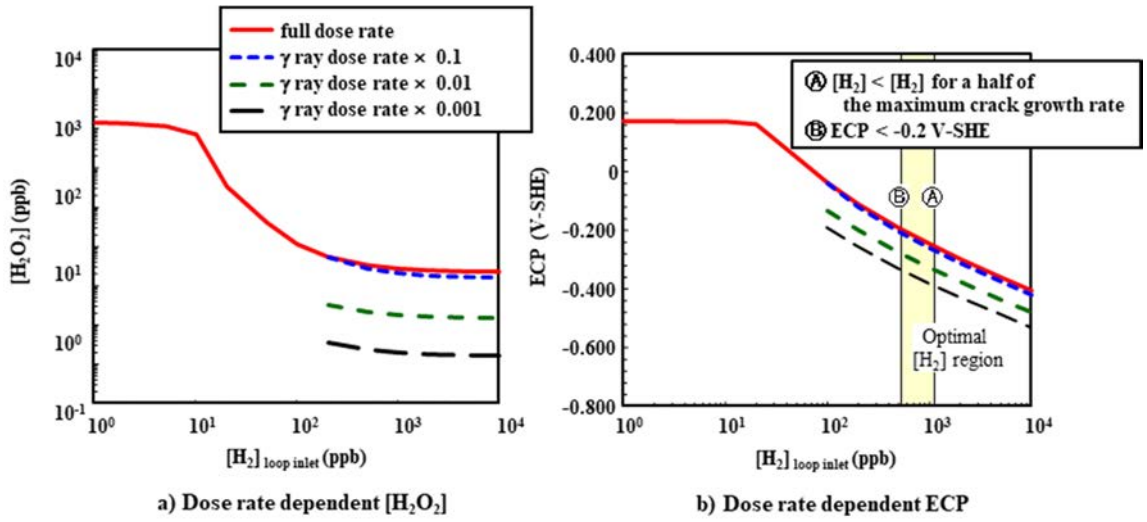

Figure 7.22 Dose rate-dependent ECP in the INCA loop (pH_T: 6.67)

(Backward rate constant: 1330 L/mol/s, MO coefficient: 10^{-6} m/s, MS coefficient: 10^{-4} m/s)

7.3.1 Effects of pH_T on ECP

The metal polarization curves might depend on not only the oxide thickness on the metal but also the pH of the water. So to apply the metal polarization curve determined for BWR coolant condition (neutral water) to PWR primary coolant conditions (pH_T > 6.9), the effects of pH, as well as oxide film, should be carefully considered. A method for self-determined anodic polarization curves can be used for this purpose, in which the potential dependent metal anodic polarization current is defined as indicated in Eq. (4-30). Furthermore, anodic current for each oxidant is added to the metal anodic polarization current to obtain the total anodic current, which is defined as stated in Eq (4-31). The dependence of pH_T on ECP is shown in **Figure 7.23**.

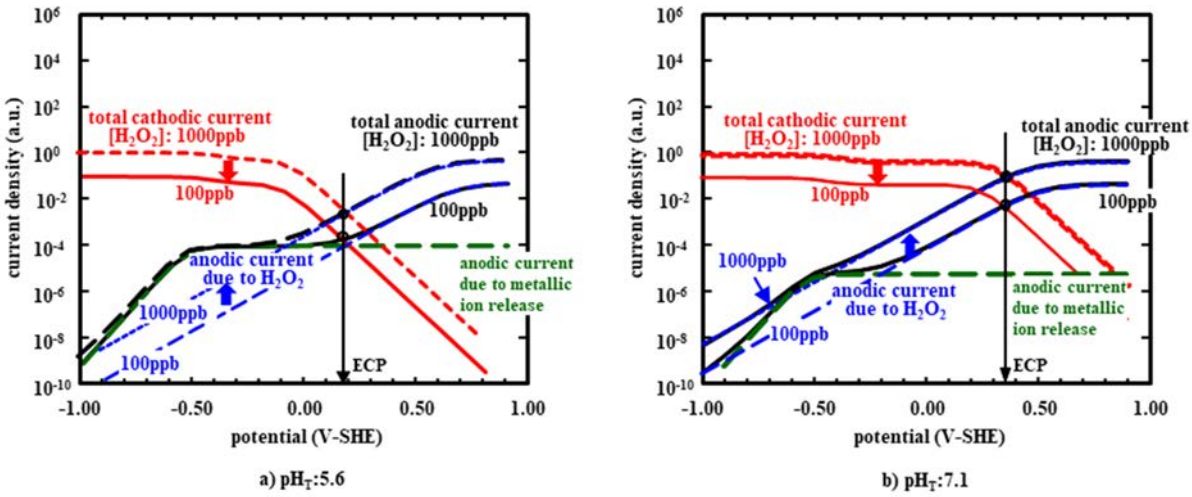

Figure 7.23 Balances of the anodic and cathodic current densities

([H_2O_2]: 100 and 1000 ppb)

As a result of increasing pH, the solubility of metallic ion was decreased to result in lower anodic current density, which increased ECP. The counter ion of the pH reagent (Li^+), on the other hand, increased anodic current density. Finally, total anodic and cathodic currents were balanced to determine the pH_T value. The effects of Li^+ on ECP are discussed in the section below.

7.3.2 Effects of Li^+ on ECP

The effect of [Li^+] on ECP was shown in Figure 7.21 b). The effects were mainly from the increased cathodic currents densities due to "$H_2O_2 + 2Li^+ + 2e^- \Rightarrow 2LiOH$", which were illustrated in **Figure 7.24** a). Under high pH_T conditions, decreasing [H^+] resulted in the lower ECP but as a result of "$H_2O_2 + 2Li^+ + 2e^- \Rightarrow 2LiOH$" reaction, the cathodic current densities were increased in a wide potential region, and then, resulted in higher ECP.

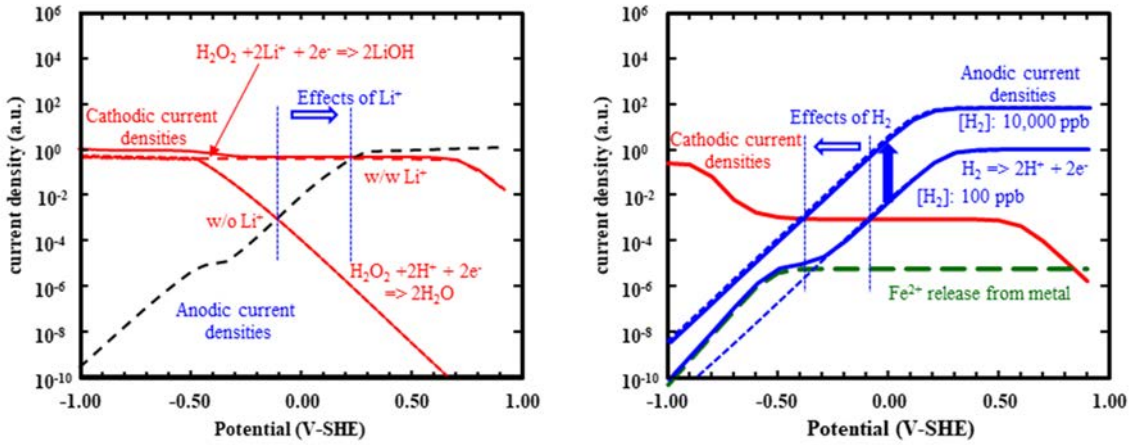

Figure 7.24 Balances of the anodic and cathodic current densities (pH_T: 7.1)

7.3.3 Effects of H^+ on ECP

The effect of [H_2] on ECP was also shown in Figure 7.24 b). The effects were mainly from the increased anodic currents densities due to "$H_2 \Rightarrow 2H^+ + 2e^-$," which were illustrated in Figure 7.24 b). H_2O_2 determined ECP was at a constant level due to the leveling out of [H_2O_2] under higher [H_2] addition circumstances, while ECP was reduced due to the direct impacts of increased hydrogen anodic current densities (Figure 7.24 b)).

7.3.4 Effects of Energy Deposition on ECP

The PWSCC occurred not in the core center but the peripheral zone of the core, which was defined as the low or medium irradiation zones. [H_2] dependent ECP shown in Figure 7.21 b) was the typical values under the fully irradiated zone, where even when [H_2] was controlled in the optimal [H_2] control region (less than 2 ppm) the ECP was kept under −0.2 V-SHE. Of course, too low [H_2] lower than 0.5 ppm might increase ECP larger than −0.2 V-SHE. So, [H_2] should be controlled between 0.5 and 2.0 ppm as the optimal [H_2] region.

The evaluation targets for PWSCC occurrences and their propagations might be out of the core, where the energy deposition rate might be sufficiently lower than in the core region. Figure 7.22 shows ECP as a function of dose rate and [H_2], indicating that ECP may be regulated with a safety margin of less than −0.2 V-SHE, especially in places with dose rates less than 1/10 of the reactor core irradiation conditions.

Here as one of the control targets of ECP for mitigating PWSCC, "−0.2 V-SHE" was indicated, which was one of the targets values for mitigating IACCC in BWR conditions. The ECP target value for mitigating IGSCC in BWR conditions was confirmed by applying a lot of experimental data and plant data.

Unfortunately, the relationship between the PWSCC occurrence and their propagation and ECP was not supported well.

Much more experiments on the relationship between ECP and PWSCC occurrence and propagation should be carried out to determine the suitable water chemistry control for multitargets, *e.g.*, PWSCC mitigation, radiation field control and fuel cladding corrosion mitigation.

7.3.5 Comparison of the Measured and Calculated ECP

In the article, procedures to determine the ECP in the PWR conditions were described and the calculated results were introducing. The comparison of the calculated and measured ECPs was shown in **Figure 7.25** [54), 61), 70), 71), 77), 81), 82)], where measured ECPs under miscellaneous water chemistry conditions were compared with the calculated ones. At this time, the target deviations between calculated and observed results were within ±100 mV, whereas the future target was within ±50 mV. Only a few computed outcomes were found outside of the target zone, but the majority of the results were spread within it.

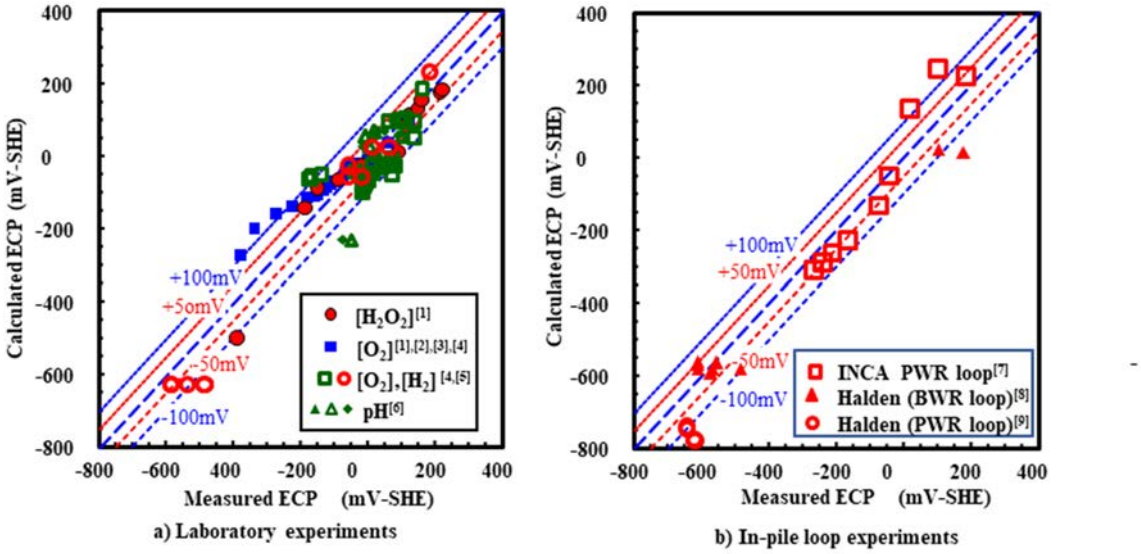

Figure 7.25 Laboratory experiments and in-pile loop experiments

References:

[1] Wada Y, et al. Effects of hydrogen peroxide on intergranular stress corrosion cracking of stainless steel in high temperature water, (III). J Nucl Sci Technol. 2000;37(10):901–912.

[2] Wada Y, Watanabe A, Tachibana M, et al. Mitigation effect of alkaline water chemistry upon intergranular stress corrosion cracking of sensitized 304 stainless steel. Journal of Nuclear Science and Technology. 2001;38(8):621–632.

[3] Kim Y.J. CRD data on ECP behavior of various alloys containing noble metals. GE CR&D; 1993. BWR-TR-93–02.

[4] Hanawa S, et al., Preliminary verification of water radiolysis and ECP calculation models by In-pile ECP measurements, Proc. International Conference on Water Chemistry of Nuclear Reactor Systems; NPC2018, 2018 Sept 9-14; San Francisco, USA. [USB memory].

[5] Kim Y.J, et al. Development of ECP models for BWR applications, Proceedings, Symp. Environmental Degradation of Materials in Nuclear Power Systems – Water reactors 7. 1998 Aug 13-15; Amelia Island: ANS.

[6] Macdonald D.D, Uriquidi-Macdonald M. Thin-layer mixed potential model for the corrosion of high level nuclear waste canisters. Corrosion. 1990;46: 380–390.

[7] Takiguchi H, Ullberg M, Uchida S. Optimization of dissolved hydrogen concentration for control of primary coolant radiolysis in pressurized water reactors. J Nucl Sci Technol. 2004;41:601–609.

[8] Bennett P, et. al. In-Core ECP measurements under LWR conditions in the halden reactor. Proc. 10th Int. Conf. Environmental Degradation of Materials in Nuclear Power Systems - Water Reactors-, 2001: Aug. 5-10, Lake Tahoe, Nevada, NACE (in CD-ROM).

[9] Bosch RW, et al., In-pile electrochemical measurements on AISI 304 and AISI 306 in PWR conditions- experimental results. J Nucl Mater. 2007;360:304–314.

7.3.6 Evaluation of the Corrosive Conditions in PWR Primary Coolant

The combined analysis of water radiolysis and ECP codes was applied to determine the corrosive conditions on BWR primary coolant. The combined analysis was well validated for experimental data but there were still some gaps between the analytical results and measured one for BWR plant data. The gaps were mainly from the complex plant situations, e.g., (a) cooling water flow patterns (flow velocity and flow mixing), (b)

radiation qualities and distributions and (c) steam generation and transfer of major radiolytic species from the liquid phase to gas phase [25]. Lots of efforts were made to collect plant data related to corrosive conditions in BWRs and to improve the combined analysis for BWRs based on the collected data [24), 75].

The combined analysis for PWRs has been just started. It is expected that the same problems and subjects to be gotten over for BWR primary coolant are supposed. As future subjects for improving and applying the corrosive condition evaluation procedures for PWR primary coolant, the following items should be prepared.

(1) The coupled procedures are going to be applied for operating PWR primary cooling systems to confirm their validity.

(2) Material tests under high temperature and higher pH conditions are strongly recommended to obtain the relationship between ECP and PWSCC and other material flaws.

(3) Plant data related to corrosive conditions and material performance in PWR primary coolant should be collected systematically to validate the combined analysis.

(4) Finally, the optimal hydrogen concentration for each plant is going to be confirmed along with evaluating its adverse effects.

In BWR the threshold ECP to prevent IGSCC was designated as -230 mV-SHE [2]. The threshold ECP for PWSCC was not clearly defined yet. There were few data to evaluate the relationship between PWSCC and ECP (**Figure 7.26**) [80]. In this report, the relationship between ECP and IGSCC occurrence was discussed based on low ECP data (ECP < -500 mV-SHE). These data showed IGSCC caused by the increase in hydrogen concentration was suppressed when ECP was higher than -800 mV. However, there was no data above ECP -500mV. The upper limit of ECP to prevent IGSCC caused by the oxidative environment is needed to be estimated. Thus, the extrapolation of the lowest ECP to prevent IGSCC in the oxidative environment was attempted.

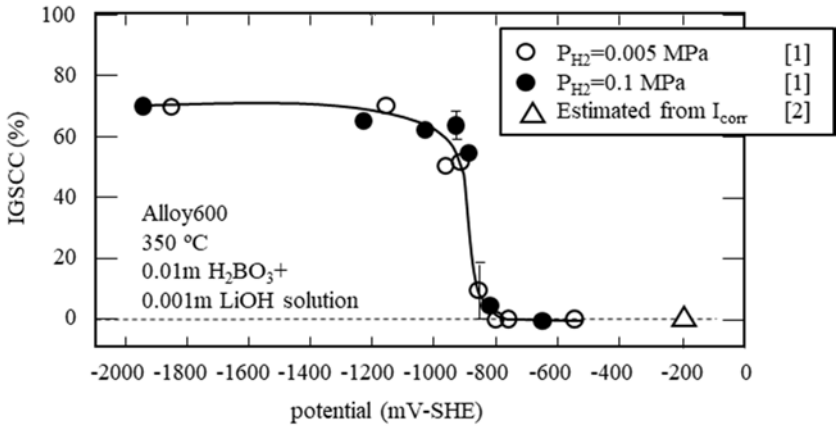

Figure 7.26 Percentage of IGSCC on the fracture surface

of Alloy 600 as a function of applied potential vs. SHE

References:

[1] Totsuka N, Szklarska-Smialowska Z, Hydrogen induced IGSCC of Ni containing FCC alloys in high temperature water, Proc. 3rd Int. symposium on Environmental Degradation of materials in nuclear power systems – water reactors, TMS, (1988).

[2] Macdonald D.D, Uriquidi-Macdonald M, Thin-layer mixed potential model for the corrosion of high level nuclear waste canisters, Corrosion, 46; 380-390 (1990).

IGSCC crack growth rate for BWR conditions was considered determined by I_{corr} but not E_{corr} [71]. In **Figure 7.27**, anodic polarization curve for nickel-based alloy 600 are shown as functions of ECP [28]. This figure showed that the current density did not significantly change with increasing ECP up to at least -200 mV,

which suggested that IGSCC crack growth rate below -200 mV-SHE were the same level and IGSCC occurrence below -200mV-SHE were almost the same. So, in Figure 7.21 at -200 mV-SHE, a triangle symbol was added to show IGSCC (%) =0. These were just speculation which should be confirmed with the measured data.

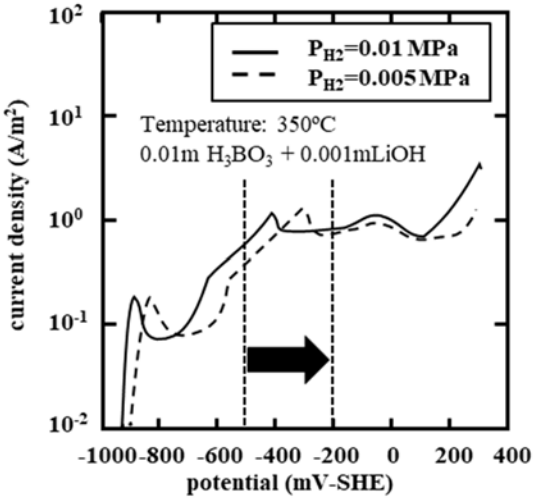

Figure 7.27 Anodic polarization curves of Alloy 600

ECP calculated as a function of $[H_2]_{inlet}$ was compared with the measured ECP at INCA loop. For PWR primary system ECP was calculated. For the calculation major data for energy deposition in the core were prepared as shown in Table 7.3. Radiation energy deposition in the core peripherals were assumed as about a half of that in the core and 1/5 of that. But there are only a few differences in the concentrations of radiolytic species were obtain in the core region and its peripherals even when there were 5 times differences in energy deposition rates.

In SG energy deposition was mainly from ^{16}N, whose value was calculated by assuming the source in the core due to ^{16}O (n,p)^{16}N reaction and accumulation of ^{16}N due to fast circulation of the cooling water from core to core through SG (**Figure 7.28**).

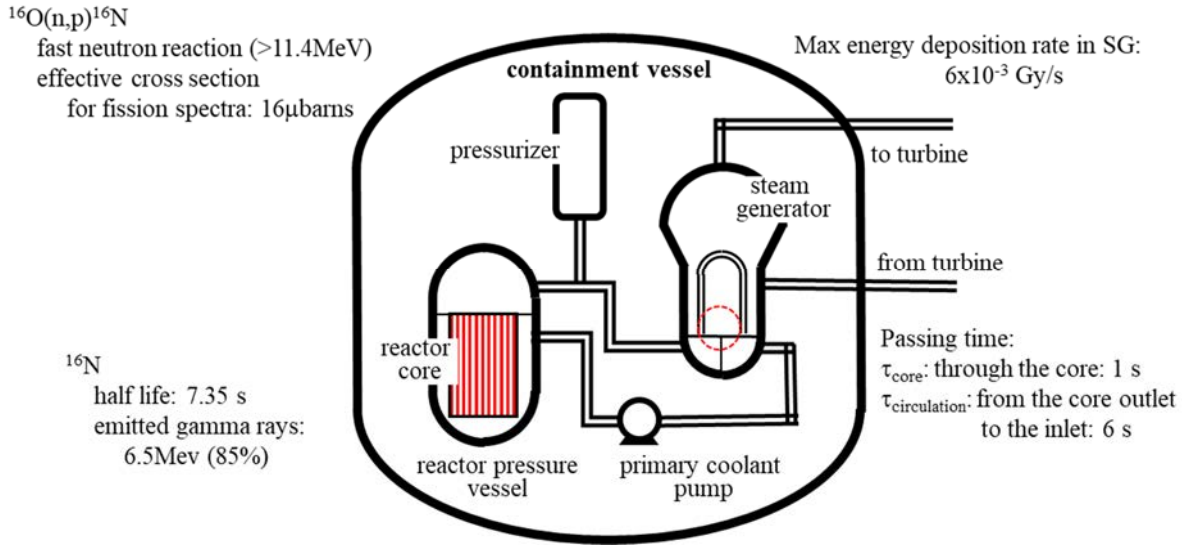

Figure 7.28 Major components of primary system

Based on the energy deposition shown in Table 7.3 for the core region and Figure 7.23 for SG, ECP as functions of $[H_2]$injected were calculated (**Figure 7.29**). The optimal hydrogen concentration $[H_2]_{optimal}$ should satisfy both lower ECP than PWSCC occurrence (-0.2 V-SHE) and lower $[H_2]$ than 1 ppm. The calculated results showed that the optimal hydrogen concentration could be determined even in core region (Figure 7.29).

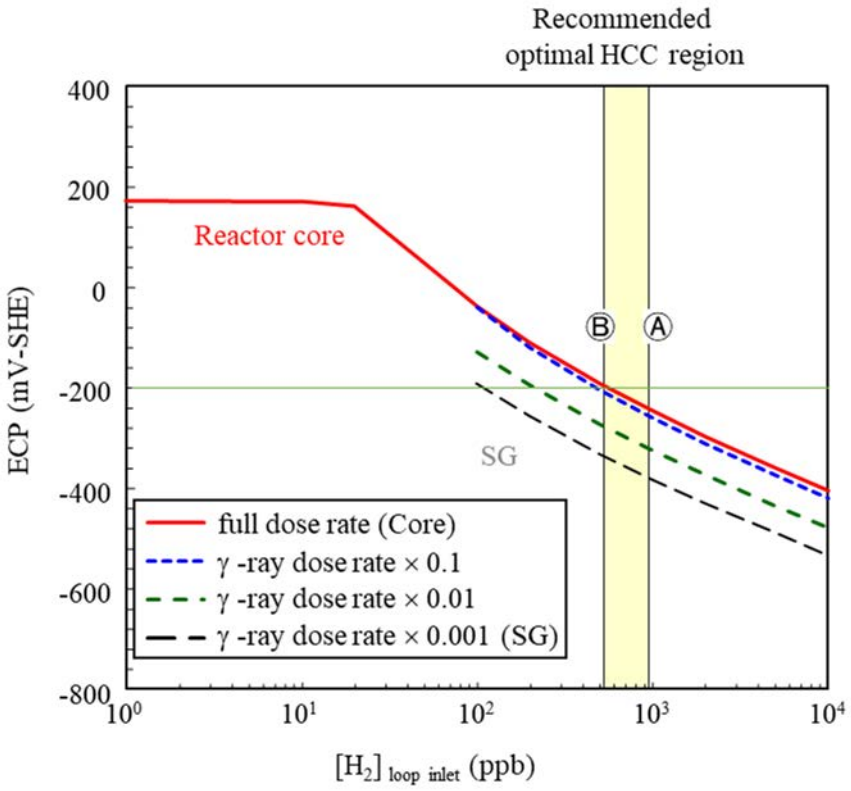

Figure 7.29 ECP of Alloy-182 at the downstream of the core in INCA loop

As a result of evaluation of water radiolysis and ECP, it was confirmed that the ECPs in the core region, core peripherals and SG region could be maintained under the PWSCC threshold level with injecting hydrogen with its concentration between 200-1000ppb. This calculation result was shown as an example. For the better estimation of the optimal H_2 injection, detailed input data of each plant should be used.

7.4 Verification and Validation of the Coupled Code

7.4.1 Key Parameter to Determine Corrosive Conditions

Schematic diagram of BWR primary cooling system is shown in Figure 2.6

Corrosive conditions in the BWR primary cooling system are determined mainly by radiolytic species, most of which are unstable in high temperature conditions and difficult to be determined in the sampled water. ECP can be measured directed under high temperature conditions if ECP sensors can in installed. From both sides of easy measurement under high temperature conditions and easy application for the JSME guideline, ECP can be applied as the major index for corrosive conditions in BWR primary cooling system.

However, the locations where ECP sensors can be installed are restricted for only clean-up water lines, vessel drain lines and some of in-core monitoring guide tubes. Major parts of the system are out of direct measurement region, where corrosive conditions should be determined by applying numerical simulation codes. One the most important purposes to determine corrosive conditions is to predict IGSCC occurrence of stainless steel piping and components. The IGSCC crack growth rate has been shown as the standard code of JSME (**Figure 7.30** [83]).

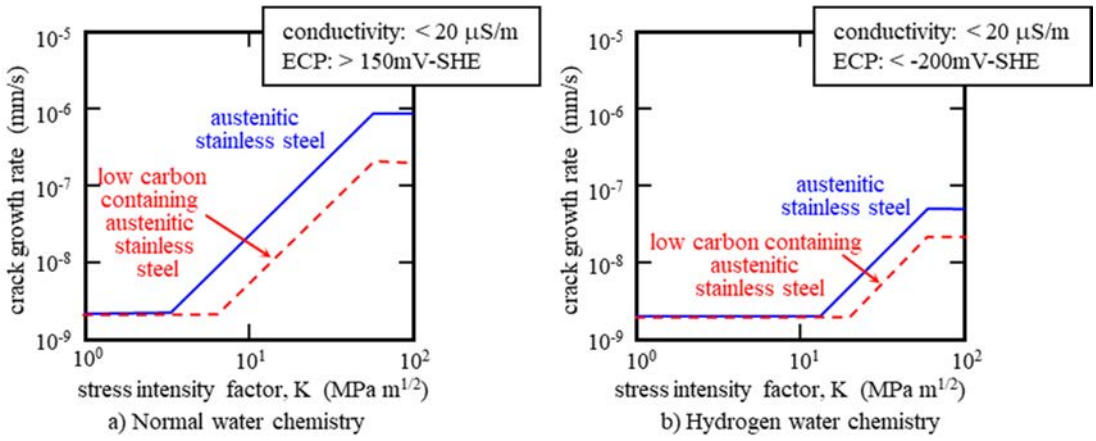

Figure 7.30 JSME guidelines for evaluation of crack growth rate [6)]

7.4.2 Standardization of Coupled Evaluation Procedures for Corrosive Conditions

There are three styles of standardizations for evaluation procedures of corrosive conditions in BWR primary cooling system (**Table 7.9**). The analytical procedures of the corrosive circumstances in BWR primary cooling system have been developed, while those in PWRs have not well developed yet. So, the procedures for V&V of the software for the corrosive circumstances for PWRs might follow the procedures for BWRs [24)]. The fundamental aspect of the V&V procedures might be the same both for BWRs and PWRs. The document shown in the section introduces the standard procedures for V&V for he software for the corrosive circumstances of PWRs as well as BWRs.

Even evaluation procedures of corrosive conditions in BWR primary cooling system have not been established yet, because the water radiolysis analysis faced at the difficulties to obtain the accurate plant data bases, e.g., dose rate distributions in the core and its peripheral regions and precise flow distributions especially in downcomer and jet pump regions. Uncertainties of those data resulted in large uncertainties of the water radiolysis calculation results. Those data should be collected not from the specialists of water chemistry but also from those of all engineering groups, e.g., nuclear design groups, thermal hydraulic design groups and plant operation groups.

Here, the latest situations of V&V of the software of coupled evaluation procedures for corrosive conditions are introduced and major targets for establishing the V&V of the software of coupled evaluation procedures are introduced.

Table 7.9 Styles of standards for evaluation procedures of corrosive conditions in BWR primary cooling system

Style	Proposed procedures	Basic evaluation tools	Evaluated and registered	Remarks
Only one standard code	(1) several codes developed different organizations should be unified into a standard code	V&V method for the standard code	independent organization, i.e., JAEA code center	peripheral codes, e.g., core and radiation shielding calculation and thermal hydraulic codes, should be included into the standard code
Parallel standard codes	(2) each code developed by an organization might be registered as one of the standard code	V&V method for each code	independent organization, i.e., JAEA code center	peripheral codes are recommended to be involved into the standard code or major out put of the peripheral code should be involved into the standard
	(3) each code developed by an organization should be registered as a code for an authorized evaluation procedure	V&V method for each procedure	independent organization, which applies the codes, based on the authorized evaluation procedures	peripheral codes are involved into a standard evaluation procedure

The most orthodox approach to authorize the corrosive condition determination procedures is to establish a standard code and a standard data set ((1) in Table 7.9). But even if the standard codes are authorized, it is still difficult to unify the plant specification data, e.g., radiation absorption in the water and hydrodynamics properties, which are from different design codes applied by the plant venders. For this, complete unification of plant design codes and procedures are required, which is not realistic solutions.

In order to authorize each set of the simulation codes possessed by some organizations or some groups as standard codes for determination of corrosive conditions, the codes should be evaluated as sufficiently reliable codes based on V&V procedures [84), 85)86)]. It is important to authorize more than two code systems as the standard ones for cross checking the evaluated corrosive conditions by the third parties, e.g., the government.

For authorize individual code systems as the standard one, there are two approaches, one is to evaluate the code systems by the independent organization, e.g., the code center of the JAEA, to be registered as the standard code systems there and to apply the registered standard code systems for corrosive condition evaluation ((2) in Table 7.9). In the case the independent organization should administer the code systems themselves and at the same time peripheral codes and their supporting data.

The other approach is firstly to determine the standard procedures based on self -operated V&V evaluation and to register the procedures at the AESJ Standard Committee and secondarily for the utilities of the evaluation procedures to evaluated them by the V&V procedures, to open the their V&V results and to apply them for corrosive conditions in the primary cooling system of BWRs ((3) in Table 7.9).

7.4.3 Verification Procedures

1) Water radiolysis codes

(i) Charge and mass balance for the first step of the verification

Numerical expressions of the codes should be shown exactly in the document. The major flames of the codes are also shown in the document. Major input data, *e.g.*, physical and chemical properties of radiolysis and electrochemistry analyses, are also listed in the document.

For the first step of the verification of the code, it should be confirmed that charge and mass were balanced through the entire system and the entire time mesh points. Positive and negative charges in any location along the flow path should be balanced, while mass of H and O should be balanced. The discrepancies of charges and mass at any location and time mesh should be less than 1 %.

(ii) Benchmark analysis for the second step verification

Benchmark problems shown in **Table 7.10** were prepared for verification of the water radiolysis codes.

Table 7.10 Conditions for benchmark calculation

1) geometry : infinite uniform solution

2) initial condition : ideal pure water without any additives

3) calculated cases :

Purpose	g-values	rate constants	temperature (°C)	energy deposition (W/g-water)	
				gamma rays	neutrons
Object 1	reference (Table 7.10)	reference (Table 7.11)	25	0	1
				1	0
				1	1
Object 2	own	own	285	0	1
				1	0
				1	1

Two kinds of the benchmark problems were prepared for verifying the codes themselves and code systems containing calculation constants. Both results should be evaluated and the evaluated results should be summarized in the document.

For Object 1 to verify that the model equations were compiled in the codes correctly, the calculation were carried out based on given G-values and rate constants (**Tables 7.11** and **7.12**).

Table 7.11 Reference g-value at 25 ˚C

Chemical species	$-H_2O$	H	e_{aq}	H^+	H_2	O_2	H_2O_2	HO_2	O_2^-	HO_2^-	OH	OH^-
Gamma	4.14	0.61	2.7	2.7	0.43	0	0.61	0.03	0	0	2.86	0
Neutron	3.15	0.50	0.93	0.93	0.88	0	0.99	0.04	0	0	1.09	0

Table 7.12 Reference reaction set at 25 ˚C

No.	Reaction	Rate constant	No.	Reaction	Rate constant
1	$e_{aq} + H_2O \Rightarrow H + OH^-$	1.6×10	17	$H_2O_2 + OH \Rightarrow HO_2 + H_2O$	2.7×10^7
2	$e_{aq} + H^+ \Rightarrow H$	2.4×10^{10}	18	$H + H_2O_2 \Rightarrow OH + H_2O$	9.0×10^7
3	$e_{aq} + OH \Rightarrow OH^-$	2.4×10^{10}	19	$H + O_2 \Rightarrow HO_2$	1.9×10^{10}
4	$e_{aq} + H_2O_2 \Rightarrow OH + OH^-$	1.3×10^{10}	20	$HO_2 \Rightarrow H^+ + O_2^-$	8.0×10^5
5	$2H \Rightarrow H_2$	1.0×10^{10}	21	$O_2^- + HO_2 \Rightarrow HO_2^- + O_2$	1.5×10^7
6	$e_{aq} + HO_2 \Rightarrow HO_2^-$	2.0×10^{10}	22	$2HO_2 \Rightarrow O_2 + H_2O_2$	2.7×10^6
7	$e_{aq} + O_2 \Rightarrow O_2^-$	1.9×10^{10}	23	$2O_2^- + 2H_2O \Rightarrow O_2 + H_2O_2 + 2OH^-$	5.6×10^3
8	$2\,e_{aq} + 2H_2O \Rightarrow H_2 + 2OH^-$	1.64×10^6	24	$H + HO_2 \Rightarrow H_2O_2$	2.0×10^{10}
9	$2OH \Rightarrow H_2O_2$	5.0×10^9	25	$H + O_2^- \Rightarrow HO_2^-$	2.0×10^{10}
10	$HO_2 + OH \Rightarrow O_2 + H_2O$	1.2×10^{10}	26	$O_2^- + e_{aq} + H_2O \Rightarrow HO_2^- + OH^-$	1.8×10^8
11	$O_2^- + OH \Rightarrow O_2 + OH^-$	1.2×10^{10}	27	$H_2O_2 + OH^- \Rightarrow HO_2^- + H_2O$	5.0×10^8
12	$H + OH^- \Rightarrow e_{aq} + H_2O$	2.0×10^7	28	$H_2O \Rightarrow H^+ + OH^-$	2.59×10^{-5}
13	$H + e_{aq} + H_2O \Rightarrow H_2 + OH^-$	4.5×10^8	29	$O_2^- + H^+ \Rightarrow HO_2$	5.0×10^{10}
14	$H^+ + OH^- \Rightarrow H_2O$	1.44×10^{11}	30	$HO_2^- + H_2O \Rightarrow H_2O_2 + OH^-$	1.02×10^4
15	$H + OH \Rightarrow H_2O$	2.0×10^{10}	31	$HO_2^- + e_{aq}^- + H_2O \Rightarrow OH + 2\,OH^-$	6.3×10^7
16	$H_2 + OH \Rightarrow H + H_2O$	3.4×10^7			

Four parties had joined for the Objective 1 benchmark analyses. The results for benchmark calculations for the Object 1 are shown in **Figure 7.31.** As a result of applying the common data bases, the results were distributed only in the range of 10% discrepancies. The calculated results of WRAC-JAEA were added to the Figure 7.31 to compare their accuracies. As a result of applying the common data sets, the results were distributed in the previous data distribution of 4 parties [24].

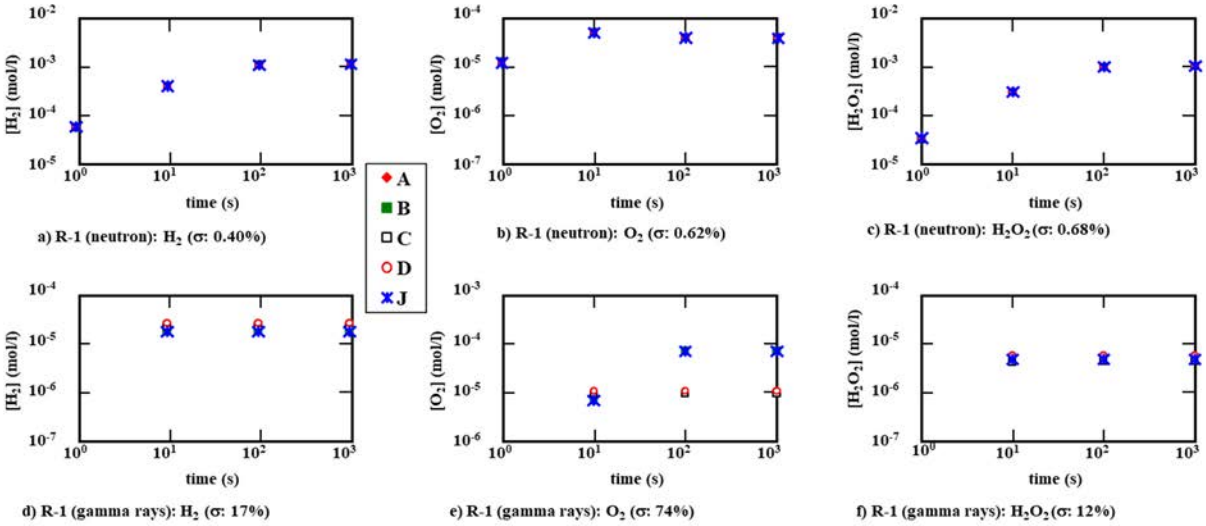

Figure 7.31 An example of benchmark calculations [Given G-values and rate constants]

The results for Objective 2 benchmark calculations are shown in **Figure 7.32.** The differences, which were from mainly from rate constants and G-values applied for each code, were within a factor of 10 (+1000%, -90%). The discrepancies could be compensated with plant data for the radiolysis calculation through the entire BWR primary cooling system. The calculated results based on WRAC-JAEA were distributed in the previous bench mark evaluation results for 4 parties.

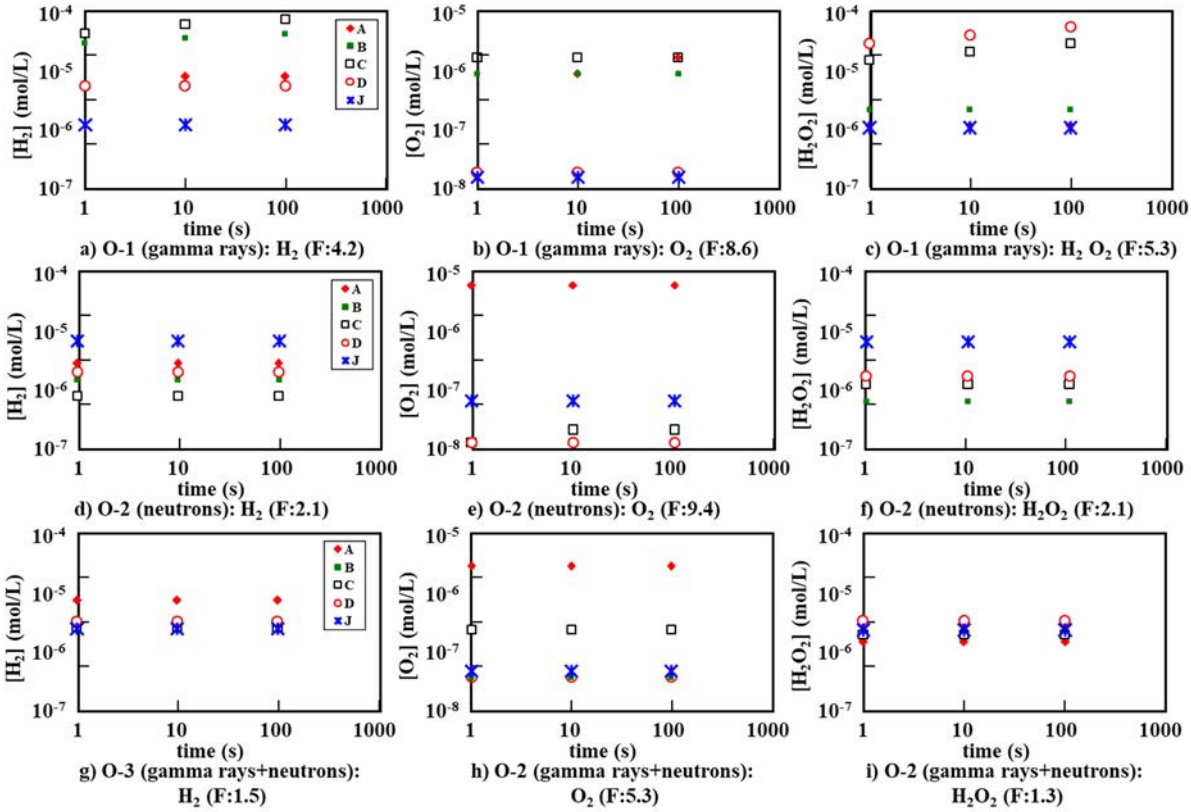

Figure 7.32 An example of benchmark calculations [Own G-values and rate constants]

One of the possible reasons why the calculated results for oxygen concentrations were scattered in the wild ranges was considered to be from the applied G-values and rate constants. Based on the latest surveys on G-values and rates constants, changes in G-values for gamma-rays were rather small, while those for neutrons were wildly distributed as shown in **Table 7.13**. Especially, those for neutrons were much different. Especially, the latest G-values generating H_2O_2 were 2 times larger than the old data, which might influence the data scattering. Not only G-values but also rate constants were reevaluated as Japan common data sets. Benchmark analysis of water radiolysis calculation codes was the first step not only for improving the codes themselves but also improving the calculation data sets, i.e., G-values and rate constants.

Table 7.13 G-values for high temperature water

a) Gamma rays

Species	Japan Common [1]	Elliot [2]	Sunaryo [3]	Christensen [4]	Lundgren [5]	Elliot & Bartels [6]	Sanguanmith [7]	JAEA
e^-_{aq}	3.41	3.53	3.54	3.5	3.5	3.475	2.57	3.5
$H^•$	0.87	0.9	0.94	0.9	0.9	1.43	1.25	0.9
H^+	3.41	3.53	3.54	3.5	3.5	3.475	2.57	3.5
H_2	0.6	0.625	0.56	0.6	0.6	0.61	0.57	0.67
H_2O_2	0.31	0.5	1.06	0.55	0.65	0.29	0.34	0.55
$HO_2^•$	0	0	0	0	0	0	0	0
$^•OH$	4.86	4.68	3.48	4.5	4.3	5.545	4.28	4.5

b) neutrons

Species	Japan Common [1]	Elliot [2]	Sunaryo [3]	Christensen [4]	Lundgren [5]	Elliot & Bartels [6]	Butarbuitar [8]	JAEA
e^-_{aq}	0.68	0.61	0.68	0.65	0.6	1.29	0.62	0.6
$H^•$	0.52	0.34	0.52	0.45	0.5	0.59	0.98	0.5
H^+	0.68	0.61	0.68	0.65	0.6	1.29	0.622	0.6
H_2	1.52	1.26	1.52	1.26	1.4	0.94	0.99	1.5
H_2O_2	1.22	0.65	1.29	0.85	1.04	0.4	0.57	1.14
$HO_2^•$	0	5	0	0.05	0.04	0.03	0.02	0.04
$^•OH$	1.8	2.02	1.66	1.77	1.7	2.87	2.33	1.7
OH^-	0	0	0	0	0	0	0	0

References:

[1] Division of Water Chemistry (DWC). Latest situation and major subjects on evaluation procedures of corrosive conditions in BWR primary coolant. 2022, DWC Report #2022-0001, Division of water chemistry, atomic energy society of Japan (in Japanese).

[2] Elliot A.J, Chenier P, Ouellette D.C, Temperature dependence of g values for H_2O and D_2O irradiated with low linear energy transfer radiation, J Chem Soc Faraday Trans. 89, 1193(1993); Elliot A.J, Rate constants and g-values for the simulation of the radiolysis of light water over the range 0-300 deg C, AECL-11073, COG-94-167 (1994).

[3] Sunaryo G.R, Katsumura Y, Ishigure K, Radiolysis of water at elevated temperatures—III. Simulation of radiolytic products at 25 and 250ºC under the irradiation with g-rays and fast neutrons, Radiation physics and chemistry, 45 (5), 1995, pp.703-714.

[4] Christensen H, Molander A, Lassing A, Tomani H, Experimental studies of radiolysis in an in-core loop in the Studsvik R2 reactor, Water chemistry of nuclear reactor systems 7, Bournemouth, UK 1996, Vol 1, 138.

[5] Lundgren K, Wijkström H and Wikmark G, Recent developments in the BwrChem Radiolysis Code, 4th Workshop on LWR Coolant Radiolysis and Electrochemistry, 2002, Apr, 26, Avignon, France SFEN 2002.

[6] Elliot AJ, Bartels DM, The Reaction Set, Rate Constants and g-Values for the Simulation of the Radiolysis of Light Water over the Range 20 to 350°C Based on Information Available in 2008, AECL Report 153-127160-450-001, 2009.

[7] Sanguanmith S, Muroya Y, Meesungnoen J, Lin M, Katsumura Y, Kohan L.M, Guzonas D.A, Stuart C.R, Jay-Gerin J.P, Low-linear energy transfer radiolysis of liquid water at elevated temperatures up to 350ºC: Monte-Carlo simulations, Chemical Physics Letters. 2011;508:224.

[8] Butarbutar S.L, Sanguanmith S, Meesungnoen J, Sunaryo G.R, Jay-Gerin J.P, Calculation of the yields for the primary species formed from the radiolysis of liquid water by fast neutrons at temperatures between 25–350ºC, Radiation research. 2014;181:659.

The other discrepancies of the results are summarized in **Table 7.14.**

Table 7.14 Previous evaluation for benchmark calculations of 4 parties

Objective 1 :verification and validation of numerical procedures	
• neutrons ;	good agreement for primary/secondary products
• γ-rays ;	separated into two groups
• neutrons + γ-rays ;	discrepancy caused by results for γ-rays
Objective 2 : characterization of current input set	
• differences in the results for primary products	
• much differences in the results for secondary products	

7.4.4 Validation Procedures

Corrosive condition evaluation codes consist of two independent codes. Validation processes are divided into three, *i.e.*, validation of water radiolysis code, ECP calculation code and the coupled code of water radiolysis and ECP.

1) Water Radiolysis code

Some data from operating power plant can be applied for evaluation of the code. A schematic diagram of the BWR primary cooling system and locations for water sampling and installing water chemistry sensors are shown in Figure 2.6.

Stable species of radiolytic ones, e.g., O_2 and H_2, can be measured in the water samples taken from the sampling lines. But unstable one, e.g., H_2O_2, is difficult to be measured, because most of them disappear along the sampling lines. Under low hydrogen concentrations, some amount of hydrogen peroxide can be detected in the sampled water, even if the concentration decreases due to thermal decomposition along the sampling line but the data can be extrapolated to the original concentration by applying the code. But it is difficult to extrapolate them from under detectable level.

An example of the measured [O_2] is shown as a function of injected [H_2] in **Figure 7.33**. The discrepancies between the calculated and the measured which were from not only calculation errors but also measured errors, especially [O_2] around the less than several ppb regions were within a factor of 2 for the larger than several.

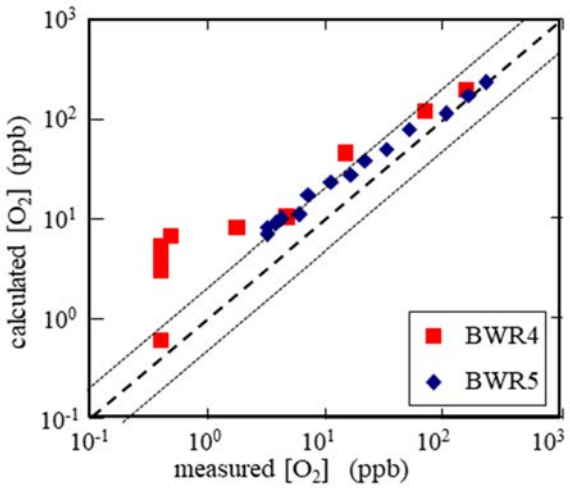

Figure 7.33 Relationship between the measured [O_2] and the calculated

2) Coupled code for evaluation of corrosive conditions

As a consequence of the coupling analysis, final corrosive condition by applying ECP as the index of corrosive conditions can be compared with the code results. An example of the relationship between the measured ECP at the plant and those calculated at the same plant is shown in **Figure 7.34** with the discrepancy of ±50 mV.

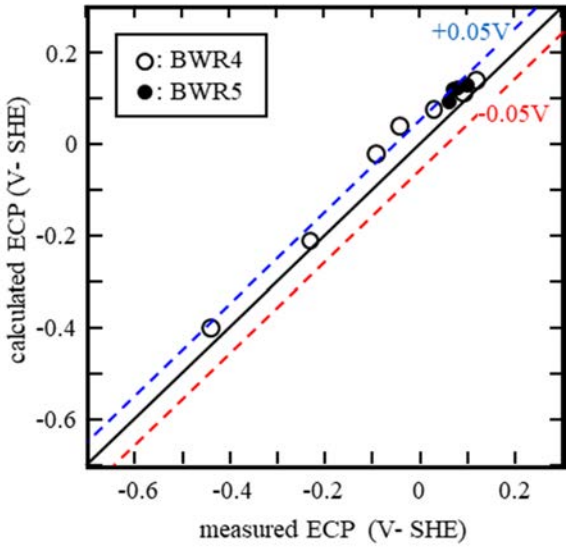

Figure 7.34 Relationship between ECP measured at the plant and the calculated

7.4.5 Discussions on V&V

The most important aspects for the V&V evaluation of the computer codes is the unity of the procedures, where each process has been defined and the manner for the document should be clearly described for external evaluation. In the paper, examples of the V&V evaluation of the computer codes related to determination of corrosive conditions in BWR primary cooling system are shown.

The accuracies of the water radiolysis code and then the coupled code to determine ECP were not high enough for their application for evaluating corrosive conditions in BWR primary cooling system. The causes of inaccuracies are from mainly evaluation of plant parameters. The inaccuracies might be improved by coupling of the plant data and calculation constants for water radiolysis code with comparing the calculated results with the measured ones at the operating plants. The evaluation accuracies of relative values of the concentrations of radiolytic species along the flowing path were reasonably high, where the absolute values of the concentrations of radiolytic species could be normalized by the measured ones to determine highly accurate absolute concentrations of radiolytic species at any location of the BWR primary cooling system and then to determine ECP distribution in the entire plant system. So, it is essential to confirm the calculated ECP by applying the measured ones and then to calibrate the calculated values with the measured ones.

In future large scale standardization including plant analysis code is required to avoid confirmation of the calculated results with the measured at each plant.

For better understanding the V&V evaluation of the computer codes relater corrosive conditions in BWR primary cooling system, the evaluation procedures are summarized as a check sheet (**Table 7.15**). Any person and any organization to apply their computer codes to evaluate the corrosive conditions in BWR primary cooling system should carry out V&V evaluation according to the check sheet and the evaluated results should be published in the suitable journal, e.g. J. Nucl. Sci. Technol., to authorize them for the public. The procedures mentioned above are essential for preparing for traceability of evaluation procedures.

Table 7.15 Check sheet for verification and validation of the codes

Evaluation	Water radiolysis code	ECP calculation code	Coupled code for evaluation of corrosive conditions
Verification	• Charge & mass balances [± 1%]*2	-	-
	• Benchmark calculation (Objective 1)	• Anodic & cathodic polarization curves	
	[Figure 7.31]* [± 10%]*2	Organization own data base [± 10mV]	
	• Benchmark calculation (Objective 2)	• Relationship between ECP and [H_2O_2]	
	[Figure 7.32] [Factor of 10]	Organization own data base [± 10mV]	
Validation	• Comparison with plant data	• ECP experimental results	• Comparison with plant data
	[Figure 7.33] [Factor of 10]	**[Figure 7.34]** [± 50mV]	**[Figure 7.34]** [± 50mV]

* Examples *2 Required accuracies for the evaluation step

8. Calculation Code Manual of WRAC-JAEA

The computer code, WRAC-JAEA, can be operated on PCs. The users' of WRAC-JAEA have to prepare several groups of input data. For calculating the corrosive circumstances of BWR and PWR primary cooling systems, 5 sets of INPUT DATA must be prepared.

8.1 TITLE-INPUT

In the input sheet, the title of the calculation case, number of calculation points, number of calculation cases and major water chemistry parameters, i.e., [B], [Li], [O_2], [H_2] and [H_2O_2] at the inlet as the initial guesses and [H_2] at hydrogen injection point, are defined. The description of TITLE-INPUT is shown in **Table 8.1**.

TITLE(I), I=1,12: The title of the calculation case is defined.

ICASEN: number of calculation cases

iitermax: Maximum number of iteration

BoronC: [B]inlet (ppm)

LiOHC: [Li]inlet {ppm}

O2C: $[O_2]_{inlet}$ (ppb)

IDH: $[H_2]_{inlet}$ (ppb)

H2O2C: $[H_2O_2]_{inlet}$ (ppb)

H2INJ: $[H_2]$ at the injection point (ppb)

Table 8.1 Examples of TITLE-INPUT

	Sheet 1	**TITLE(12): FORMAT(12A5)**					
	Sheet 2	**ICASEN**			**iitermax**		
		number of calculation cases			maximum number of iteration		
Sheet 3 - ICASEN	name	$[B]_{inlet}$	$[Li]_{inlet}$	$[O_2]_{inlet}$	$[H_2]_{inlet}$	$[H_2O_2]_{inlet}$	$[H_2]_{injection\ point}$
	unit	ppm	ppm	ppb	ppb	ppb	ppb
	cases	**BoronC**	**LiOHC**	**O2C**	**IDH**	**H2O2C**	**H2INJ**

a) PWR INCA in-pile loop calculation

PWR INCA in-pile loop calculation					
9			1		
1600.00	2.00	1.00	1.00	1.00	0.00
1600.00	2.00	1.00	10.00	1.00	0.00
1600.00	2.00	1.00	100.00	1.00	0.00
1600.00	2.00	1.00	1000.00	1.00	0.00
1600.00	2.00	1.00	10000.00	1.00	0.00
1600	2.00	1.00	10000	1.00	0.00
1600	0.5	1.00	10000	1.00	0.00
800	4	1.00	10000	1.00	0.00
1.00E-04	1.00E-04	1.00	10000	1.00	0.00

b) BWR primary loop calculation

BWR primary loop calculation					
3			2		
1.00E-04	1.00E-04	1.00	1.00	1.00	1.00
1.00E-04	1.00E-04	1.00	1.00	1.00	100.00
1.00E-04	1.00E-04	1.00	1.00	1.00	1000

As examples, two cases are prepared for PWR INCA loop analysis and BWR hydrogen injection analysis.

Example 1 was the calculation for PWR, where the INCA in-pile loop experiment was simulated. The loop was one-through type where water conditions were high pH with injected suitable amounts of boron and lithium, and hydrogen was added to suppress the corrosive conditions. In the calculation 2 cases were run, one was the calculation for confirming the effects of hydrogen concentration, which was varied from 1 ppb to 10,000 ppb at the lop inlet at the fixed pH_T, and the other was the calculation for confirming the effects of pH_T by varying boron and lithium concentrations at the fixed hydrogen concentration, 10,000 ppb. The details of the input data were shown in Table 8.1.

Example 2 was the calculation for BWR, where simple model of a BWR primary cooling system was simulated. The calculated system was divided into 10 regions, which consisted of core region with boiling and under radiation irradiation, down-comer regions without boiling. In one of the down-comer regions, some amounts of hydrogen was injected and the effects of injected hydrogen concentration on suppression of $[H_2O_2]$ evaluated. The details of the input data were shown in Table 8.1.

The calculated results for two cases are shown in **Section 8.7**.

8.2 RN-INPUT

The RN-INPUT prepares major flow parameters of flow along each region. First, the number of the region, REG, is input. Then the flow condition data of each region are input. The description of RN-INPUT is shown in **Table 8.2**.

RT(i01): residence time of water in region i01 (s)

TEM(i01): average temperature of water in region i01 (K)

G2(i01): flow velocity in region i01 (m/s)

SOV(i01): surface to volume ration of the region REG i01 (1/m)

Q3(i01): gamma-ray energy absorption (Gy/s)

QN3(i01) : neutron energy absorption (Gy/s)

QA3(i01) : alpha-ray energy absorption (Gy/s)

VAL(14, i01): temperature of region i01 for ECP calculation (K)

VAL(15, i01) : flow velocity of region i01 for ECP calculation (m/s)

VAL(16, i01) : equivalent diameter of region i01 for ECP calculation (m)

VAL(1,i01): temperature at each node (input data) (K)

VAL(2,i01): void fraction (input data) (-)

VAL(3,i01): gas release rate of H_2 (1/s)

VAL(4,i01): calibration constant for H_2 (-)

VAL(5,i01): gas release rate of O_2 (1/s)

VAL(6,i01): calibration constant for O_2 (-)

VAL(7,i01): cross section area of each boiling channel (m^2)

VAL(8,i01): steam flow area cross section of each boiling channel (m^2)

VAL(9,i01): flow velocity of liquid (m/s)

VAL(10,i01): flow velocity of gas (m/s)

As examples, two cases are prepared for PWR INCA loop analysis and BWR hydrogen injection analysis.

The calculated results for two cases are shown in **Section 8.7**.

Table 8.2 Examples of RT-INPUT

a) PWR INCA in-pile loop calculation

name	Radiolysis				Energy absorption			ECP calculation			Transfer between liquid and fas phases									
	residence time	temperature	flow velocity	surface /volume	gamma	neutron	alpha	temperature	flow velocity	equivalent diameter	temperature	void fraction	H_2		O_2		channel cross section		flow velocity	
													gas release rate	calibration coeff	gas release rate	calibration coeff	total	steam	liquid	gas
unit	s	K	m/s	1/m	Gy/s	Gy/s	Gy/s	K	m/s	m	K	-	1/s	-	1/s	-	m^2	m^2	m/s	m/s
Region#	RT(i01)	TEM(i01)	G2(i01)	SOV(i01)	Q3(i01)	QN3(i01)	QA3(i01)	VAL(14,i01)	VAL(15,i01)	VAL(16,i01)	VAL(1,i01)	VAL(2,i01)	VAL(3,i01)	VAL(4,i01)	VAL(5,i01)	VAL(6,i01)	VAL(7,i01)	VAL(8,i01)	VAL(9,i01)	VAL(10,i01)
1	1.0	563.2	0.1	300.0	1.0	0.0	0.0	563.2	0.1	0.0	563.2	0.0	50.0	0.0	50.0	1.0	0.0	0.0	1.5	1.5
1	1.0	563.2	0.1	300.0	4000.0	4300.0	0.0	563.2	0.1	0.0	563.2	0.0	50.0	0.0	50.0	1.0	0.0	0.0	1.5	1.5
1	1.0	563.2	0.1	300.0	4000.0	4300.0	0.0	563.2	0.1	0.0	563.2	0.0	50.0	0.0	50.0	1.0	0.0	0.0	1.5	1.5
1	1.0	563.2	0.1	300.0	100.0	100.0	0.0	563.2	0.1	0.0	563.2	0.0	50.0	0.0	50.0	1.0	0.0	0.0	1.5	1.5

b) BWR primary loop calculation

name	Radiolysis				Energy absorption			ECP calculation			Transfer between liquid and gas phases									
	residence time	temperature	flow velocity	surface /volume	gamma	neutron	alpha	temperature	flow velocity	equivalent diameter	temperature	void fraction	H_2		O_2		channel cross section		flow velocity	
													gas release rate	calibration coeff	gas release rate	calibration coeff	total	gas area	liquid	gas
unit	s	K	m/s	1/m	Gy/s	Gy/s	Gy/s	K	m/s	m	K	-	1/s	-	1/s	-	m^2	m^2	m/s	m/s
Region#	RT(i01)	TEM(i01)	G2(i01)	SOV(i01)	Q3(i01)	QN3(i01)	QA3(i01)	VAL(14,i01)	VAL(15,i01)	VAL(16,i01)	VAL(1,i01)	VAL(2,i01)	VAL(3,i01)	VAL(4,i01)	VAL(5,i01)	VAL(6,i01)	VAL(7,i01)	VAL(8,i01)	VAL(9,i01)	VAL(10,i01)
1	1.0	553.0	0.1	300.0	100.0	100.0	0.0	553.0	0.1	0.0	553.0	0.0	50.0	1.0	50.0	1.0	0.0	0.0	1.5	1.5
2	1.0	553.0	0.1	300.0	1500.0	1500.0	0.0	553.0	0.1	0.0	553.0	0.1	50.0	1.0	50.0	1.0	0.0	0.0	1.7	2.0
3	1.0	553.0	0.1	300.0	100.0	100.0	0.0	553.0	0.1	0.0	553.0	0.5	50.0	1.0	50.0	1.0	0.0	0.0	2.6	4.6
4	1.0	553.0	0.1	300.0	0.0	0.0	0.0	553.0	0.1	0.0	553.0	0.0	50.0	1.0	50.0	1.0	0.0	0.0	1.5	1.5
5	1.0	553.0	0.1	300.0	0.0	0.0	0.0	553.0	0.1	0.0	553.0	0.0	50.0	1.0	50.0	1.0	0.0	0.0	1.5	1.5
6	1.0	553.0	0.1	300.0	0.0	0.0	0.0	553.0	0.1	0.0	553.0	0.0	50.0	1.0	50.0	1.0	0.0	0.0	1.5	1.5
7	1.0	553.0	0.1	300.0	0.0	0.0	0.0	553.0	0.1	0.0	553.0	0.0	50.0	1.0	50.0	1.0	0.0	0.0	1.5	1.5
8	1.0	553.0	0.1	300.0	0.0	0.0	0.0	553.0	0.1	0.0	553.0	0.0	50.0	1.0	50.0	1.0	0.0	0.0	1.5	1.5
9	1.0	553.0	0.1	300.0	100.0	0.0	0.0	553.0	0.1	0.0	553.0	0.0	50.0	1.0	50.0	1.0	0.0	0.0	1.5	1.5
10	1.0	553.0	0.1	300.0	0.0	0.0	0.0	553.0	0.1	0.0	553.0	0.0	50.0	1.0	50.0	1.0	0.0	0.0	1.5	1.5

8.3 NodeConnect-k2

The NodeConnect-k2 prepares major flow connections shown in RT-INPUT, REG, is input. With two input data, RT-INPUT and NodeConnect-k2, can prepare the perfect flow diagram. The description of NodeConnect-k2 is shown in **Table 8.3**.

PNDN(i01): Inlet region #

NDN(i01): Outlet region #

RRMIX(i01): Blanching ratio

RRMIX(i01)<0

LNDN=1, GNDN=0 only liquid phase passes without gas species

LNDN=0, GNDN=1 only liquid phase passes without liquid species

LNDN=0, GNDN=0 hydrogen injected

LNDN(i01): Weight ratio of liquid

GNDN(i01): Weight ratio of gas

Table 8.3 Examples of NodeConnect-k2

a) PWR INCA in-pile loop calculation

name	inlet node	outlet node	blanching ratio	weight factor of liquid	weight factor of gas
Region	PNDN(i01)	NDN(i01)	RRMIX(i01)	LNDN(i01)	GNDN(i01)
1	1	2	1	0	0
2	2	3	1	0	0
3	3	4	1	0	0

b) BWR primary loop calculation

name	inlet region	outlet region	blanching ratio	weight factor of liquid	weight factor of gas
Region	PNDN(i01)	NDN(i01)	RRMIX(i01)	LNDN(i01)	GNDN(i01)
1	1	2	1	0	0
2	2	3	1	0	0
3	3	4	-1	0	1
4	3	5	-1	1	0
5	5	6	1	0	0
6	6	7	1	0	0
5	5	8	1	0	0
8	8	9	-1	0	0
7	7	10	0.5	0	0
9	9	10	0.5	0	0
10	10	1	1	0	0

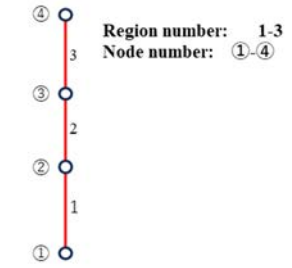

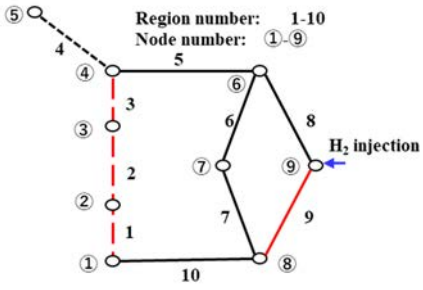

As examples, two cases are prepared for PWR INCA loop analysis and BWR hydrogen injection analysis.

The calculated results for two cases are shown in **Section 8.7**.

8.4 REACTIONk-A

The REACTIONk-A prepares major rate constants for water radiolysis calculation. The description of REACTIONk-A is shown in **Table 8.4**.

Usually, REACTIONk-A is applied any calculation cases. The calculations for BWR conditions are carried out with applying sufficiently lower values both for [B] and [Li] to keep neutral pH_T, while those for PWR conditions suitable values both for [B] and [Li] are applied to obtained suitable pH_T.

Reactants and products with the values of the order of reactions both for forward and backward reactions and easily translate the table to reaction forms. In order to prepare the source values of radiolytic species and their annihilation values, the reaction table are modified shown in Table 8.4. The rate constants both for bulk water and surfaces are also defined with their activation energy. Numbers of hydrogen and oxygen atoms and charge number are also applied for atom number and charge balances for validating the calculation steps.

Table 8.4 Example of REACTIONk-A

RN 43

Reactants			Products			Order of reaction						Rate constants		Surface rate constants		Activation energy		Number of H atoms						Number of O atoms						Charge numbers					
						forward			backward			forward	backward	forward	backward	forward	backward	forward			backward			forward			backward			forward			backward		
F1	F2	F3	R1	R2	R3	FN1	FN2	FN3	RN1	RN2	RN3	FK0	RK0	WFK0	WRK0	FAE	RAE	FHN1	FHN2	FHN3	RHN1	RHN2	RHN3	FON1	FON2	FON3	RON1	RON2	RON3	FCN1	FCN2	FCN3	RCN1	RCN2	RCN3
H+	OH-	NONE	H2O	NONE	NONE	1	1	0	1	0	0	1.54E+12	7.55E+00	1.54E+12	7.55E+00	1.26E+04	4.00E+04	1	1	0	2	0	0	0	1	0	1	0	0	1	-1	0	0	0	0
H2O2	NONE	NONE	OH	NONE	NONE	1	0	0	2	0	0	0.00E+00	0.00E+00	0.00E+00	0.00E+00	6.00E+04	0.00E+00	2	0	0	1	0	0	2	0	0	1	0	0	0	0	0	0	0	0
B0	OH-	NONE	B1-	NONE	NONE	1	1	0	1	0	0	6.19E+01	1.00E+00	6.19E+02	1.00E+01	0.00E+00	0.00E+00	0	1	0	1	0	0	0	1	0	1	0	0	0	-1	0	-1	0	0
B0	OH-	NONE	B2-	NONE	NONE	2	1	0	1	0	0	9.55E+01	1.00E+00	9.55E+02	1.00E+01	0.00E+00	0.00E+00	0	1	0	1	0	0	0	1	0	1	0	0	0	-1	0	-1	0	0
B0	OH-	NONE	B3-	NONE	NONE	3	1	0	1	0	0	1.97E+02	1.00E+00	1.97E+02	1.00E+01	0.00E+00	0.00E+00	0	1	0	1	0	0	0	1	0	1	0	0	0	-1	0	-1	0	0
B0	OH-	NONE	B4-	NONE	NONE	4	2	0	1	0	0	9.59E+03	1.00E+00	9.59E+03	1.00E+01	0.00E+00	0.00E+00	0	1	0	2	0	0	0	1	0	2	0	0	0	-1	0	-2	0	0
LiOH	NONE	NONE	Li+	OH-	NONE	1	0	0	1	1	0	1.00E+02	1.00E+01	0.00E+00	0.00E+00	0.00E+00	0.00E+00	1	0	0	0	1	0	1	0	0	0	1	0	0	0	0	1	-1	0
B1-	H+	NONE	B1H	NONE	NONE	1	1	0	1	0	0	1.00E+01	1.00E+01	0.00E+00	0.00E+00	0.00E+00	0.00E+00	1	1	0	2	0	0	1	0	0	1	0	0	-1	1	0	0	0	0
B2-	H+	NONE	B2H	NONE	NONE	1	1	0	1	0	0	1.00E+01	1.00E+01	0.00E+00	0.00E+00	0.00E+00	0.00E+00	1	1	0	2	0	0	1	0	0	1	0	0	-1	1	0	0	0	0
B3-	H+	NONE	B3H	NONE	NONE	1	1	0	1	0	0	1.00E+01	1.00E+01	0.00E+00	0.00E+00	0.00E+00	0.00E+00	1	1	0	2	0	0	1	0	0	1	0	0	-1	1	0	0	0	0
B4-	H+	NONE	B4H	NONE	NONE	1	2	0	1	0	0	1.00E+01	1.00E+01	0.00E+00	0.00E+00	0.00E+00	0.00E+00	2	1	0	4	0	0	2	0	0	2	0	0	-2	1	0	0	0	0
B1-	Li+	NONE	B1L	NONE	NONE	1	1	0	1	0	0	1.00E+01	1.00E+01	0.00E+00	0.00E+00	0.00E+00	0.00E+00	1	0	0	1	0	0	1	0	0	1	0	0	-1	1	0	0	0	0
B2-	Li+	NONE	B2L	NONE	NONE	1	1	0	1	0	0	1.00E+01	1.00E+01	0.00E+00	0.00E+00	0.00E+00	0.00E+00	1	0	0	1	0	0	1	0	0	1	0	0	-1	1	0	0	0	0
B3-	Li+	NONE	B3L	NONE	NONE	1	1	0	1	0	0	1.00E+01	1.00E+01	0.00E+00	0.00E+00	0.00E+00	0.00E+00	1	0	0	1	0	0	1	0	0	1	0	0	-1	1	0	0	0	0
B4-	Li+	NONE	B4L	NONE	NONE	1	2	0	1	0	0	1.00E+01	1.00E+01	0.00E+00	0.00E+00	0.00E+00	0.00E+00	2	0	0	2	0	0	2	0	0	2	0	0	-2	1	0	0	0	0
H	H	NONE	H2	NONE	NONE	1	1	0	1	0	0	9.00E+10	0.00E+00	9.00E+10	0.00E+00	1.26E+04	0.00E+00	1	1	0	2	0	0	0	0	0	0	0	0	0	0	0	0	0	0
E-	HO2	NONE	HO2-	NONE	NONE	1	1	0	1	0	0	3.00E+11	0.00E+00	3.00E+11	0.00E+00	1.26E+04	0.00E+00	0	1	0	1	0	0	0	2	0	2	0	0	-1	0	0	-1	0	0
E-	O2	NONE	O2-	NONE	NONE	1	1	0	1	0	0	2.60E+11	0.00E+00	2.60E+11	0.00E+00	1.26E+04	0.00E+00	0	0	0	0	0	0	0	2	0	2	0	0	-1	0	0	-1	0	0
E-	H2O	NONE	H2	OH-	NONE	2	2	0	1	2	0	1.75E+06	0.00E+00	1.75E+06	0.00E+00	1.26E+04	0.00E+00	0	2	0	2	1	0	0	1	0	0	1	0	-1	0	0	0	-1	0
OH	NONE	NONE	H2O2	NONE	NONE	2	0	0	1	0	0	2.50E+10	0.00E+00	2.50E+10	1.40E+00	8.40E+03	0.00E+00	1	0	0	2	0	0	1	0	0	2	0	0	0	0	0	0	0	0
OH-	H	NONE	E-	H2O	NONE	1	1	0	1	1	0	7.00E+08	0.00E+00	7.00E+08	0.00E+00	1.26E+04	0.00E+00	1	1	0	0	2	0	1	0	0	0	1	0	-1	0	0	-1	0	0
E-	H	H2O	OH-	H2	NONE	1	1	1	1	1	0	4.82E+09	0.00E+00	4.82E+09	0.00E+00	1.26E+04	0.00E+00	0	1	2	1	2	0	0	0	1	1	0	0	-1	0	0	-1	0	0
E-	HO2-	H2O	OH	OH-	NONE	1	1	1	1	2	0	5.35E+08	0.00E+00	5.35E+08	0.00E+00	1.26E+04	0.00E+00	0	1	2	1	1	0	0	2	1	1	1	0	-1	-1	0	0	-1	0
H	OH	NONE	H2O	NONE	NONE	1	1	0	1	0	0	2.30E+11	0.00E+00	2.30E+11	0.00E+00	1.26E+04	0.00E+00	1	1	0	2	0	0	0	1	0	1	0	0	0	0	0	0	0	0
OH	H2	NONE	H	H2O	NONE	1	1	0	1	1	0	1.40E+09	1.60E+04	1.40E+09	1.60E+04	1.93E+04	0.00E+00	1	2	0	1	2	0	1	0	0	0	1	0	0	0	0	0	0	0
H	O2	NONE	HO2	NONE	NONE	1	1	0	1	0	0	1.50E+11	0.00E+00	1.50E+11	0.00E+00	1.26E+04	0.00E+00	1	0	0	1	0	0	0	2	0	2	0	0	0	0	0	0	0	0
H	HO2	NONE	H2O2	NONE	NONE	1	1	0	1	0	0	3.00E+11	0.00E+00	3.00E+11	0.00E+00	1.26E+04	0.00E+00	1	1	0	2	0	0	0	2	0	2	0	0	0	0	0	0	0	0
H	O2-	NONE	HO2-	NONE	NONE	1	1	0	1	0	0	3.00E+11	0.00E+00	3.00E+11	0.00E+00	1.26E+04	0.00E+00	1	0	0	1	0	0	0	2	0	2	0	0	0	-1	0	-1	0	0
E-	O2-	H2O	HO2-	OH-	NONE	1	1	1	1	1	0	3.57E+09	0.00E+00	3.57E+09	0.00E+00	1.26E+04	0.00E+00	0	0	2	1	1	0	0	2	1	2	1	0	-1	-1	0	-1	-1	0
H	H2O2	NONE	OH	H2O	NONE	1	1	0	1	1	0	2.00E+09	0.00E+00	2.00E+09	0.00E+00	1.89E+04	0.00E+00	1	2	0	1	2	0	0	2	0	1	1	0	0	0	0	0	0	0
OH	H2O2	NONE	H2O	HO2	NONE	1	1	0	1	1	0	4.20E+08	0.00E+00	4.20E+08	0.00E+00	1.43E+04	0.00E+00	1	2	0	2	1	0	1	2	0	1	2	0	0	0	0	0	0	0
OH	HO2	NONE	H2O	O2	NONE	1	1	0	1	1	0	1.00E+11	0.00E+00	1.00E+11	0.00E+00	1.26E+04	0.00E+00	1	1	0	2	0	0	1	2	0	1	2	0	0	0	0	0	0	0
HO2	NONE	NONE	H2O2	O2	NONE	2	0	0	1	1	0	5.00E+07	0.00E+00	5.00E+07	0.00E+00	1.89E+04	0.00E+00	1	0	0	2	0	0	2	0	0	2	2	0	0	0	0	0	0	0
HO2	NONE	NONE	O2-	H+	NONE	1	0	0	1	1	0	3.90E+05	7.70E+11	3.90E+05	7.70E+11	1.26E+04	1.26E+04	1	0	0	0	1	0	2	0	0	2	0	0	0	0	0	-1	1	0
HO2	O2-	NONE	O2	HO2-	NONE	1	1	0	1	1	0	5.00E+08	0.00E+00	5.00E+08	0.00E+00	1.89E+04	0.00E+00	1	0	0	0	1	0	2	2	0	2	2	0	0	-1	0	0	-1	0
O2-	OH	NONE	OH-	O2	NONE	1	1	0	1	1	0	2.90E+11	0.00E+00	2.90E+11	0.00E+00	1.26E+04	0.00E+00	0	1	0	1	0	0	2	1	0	1	2	0	-1	0	0	-1	0	0
O2-	H2O	NONE	O2	H2O2	OH-	2	2	0	1	1	2	1.27E+05	0.00E+00	1.27E+05	0.00E+00	1.89E+04	0.00E+00	0	2	0	0	2	1	2	1	0	2	2	1	-1	0	0	0	0	-1
E-	H2O	NONE	H	OH-	NONE	1	1	0	1	1	0	2.90E+02	0.00E+00	2.90E+02	0.00E+00	1.26E+04	0.00E+00	0	2	0	1	1	0	0	1	0	0	1	0	-1	0	0	0	-1	0
E-	H+	NONE	H	NONE	NONE	1	1	0	1	0	0	2.60E+11	0.00E+00	2.60E+11	0.00E+00	1.26E+04	0.00E+00	0	1	0	1	0	0	0	0	0	0	0	0	-1	1	0	0	0	0
E-	OH	NONE	OH-	NONE	NONE	1	1	0	1	0	0	2.90E+11	0.00E+00	2.90E+11	0.00E+00	1.26E+04	0.00E+00	0	1	0	1	0	0	0	1	0	1	0	0	-1	0	0	-1	0	0
E-	H2O2	NONE	OH	OH-	NONE	1	1	0	1	1	0	2.40E+11	0.00E+00	2.40E+11	0.00E+00	1.26E+04	0.00E+00	0	2	0	1	1	0	0	2	0	1	1	0	-1	0	0	0	-1	0
H2O2	OH-	NONE	HO2-	H2O	NONE	1	1	0	1	1	0	1.00E+10	2.14E+05	0.00E+00	0.00E+00	1.26E+04	1.26E+04	2	1	0	1	2	0	2	1	0	2	1	0	0	-1	0	0	-1	0
H2O2	NONE	NONE	O2	H2O	NONE	1	0	0	0.5	1	0	1.40E-02	0.00E+00	1.40E-02	0.00E+00	6.00E+04	0.00E+00	2	0	0	0	2	0	2	0	0	2	1	0	0	0	0	0	0	0
H2O2	NONE	NONE	O2	H2O	NONE	1	0	0	0.5	1	0	1.40E-02	0.00E+00	1.40E-02	0.00E+00	6.00E+04	0.00E+00	2	0	0	0	2	0	2	0	0	2	1	0	0	0	0	0	0	0

8.5 G-VALUE

The G-VALUE prepares major G-values for water radiolysis calculation. The description of G-VALUE is shown in **Table 8.5**. Usually, G-VALUE is applied any calculation cases. The calculations for BWR conditions are carried out with applying zero value for energy absorption rate of alpha-rays, while those for PWR conditions suitable values for energy absorption rate of alpha-rays is applied.

Table 8.5 Example of G-VALUE

GVN＝7 **Unit: number / 100eV**

Specie	γ-rays	Neutrons	α-rays
H_2	0.6	1.5	1.65
H_2O_2	0.55	1.14	1.55
H	0.9	0.5	0.12
OH	4.5	1.7	0.45
HO_2	0	0.04	0
H^+	3.5	0.6	0.13
E^-	3.5	0.6	0.13

8.6 ECP-INPUT

The ECP-INPUT prepares major parameters for determining anodic and cathodic current densities for ECP calculation. In the input sheet, major data of empirical formula to determine the solubility of ferrous ions as functions of temperature and pH. The description of ECP-INPUT is shown in **Table 8.6**. The data also cover both for BWR and PWR.

IECPS: Option parameter

IECPS=0; ECP calculation is skipped.

IECPS=1; Proposed calculation.

IECPS=2; Applied the previous calculation based on the fixed anodic current densities.

IECPE: Number of species for anodic and cathodic current density calculations

IDECPS(i01), i01=1, IECPE: Name of species

IECPN: Number of data sets for cathodic and anodic current density calculation

IECPR1(i): reactant

IECPR2(i): other reactants

IECPP1(i): products

IECPP2(i): other products

IPWRR1(i): order of reaction; n1

IPWRR2(i): order of reaction; n2

IPWRP1(i): order of reaction; n3

IPWRP2(i): order of reaction; n4

RECPV1(i): rate constants

RECPV2(i): transfer coefficients

IECPV1(i): charge number, z

RECPV3(i): standard equivalent potential, Φ_0 (V-SHE)

Table 8.6 Example of ECP-INPUT

IECPS			=0 ECP calculation is skipped =1 Proposed calculation =2 Previuos calculation based on the fixed anodic current densities										1
IECPE			Number of species for cathodic and anodic current density calulation										1
IDECPS(i01), i01=1,IECPE			Name of species										1
IECPN			Number of data sets for cathodic and anodic current density calulation										1
IECPR1(i)	IECPR2(i)	IECPP1(i)	IECPP2(i)	IPWRR1(i)	IPWRR2(i)	IPWRP1(i)	IPWRP2(i)	RECPV1(i)	RECPV2(i)	IECPV1(i)	RECPV3(i)		
reactant	other reactant	products	other products	order of reaction				rate constants	transfer coefficients	z	Φ_0		i=1,IECPN
				n1	n2	n3	m4						
ISOLP, SOLPHH, SOLPHL, AAH0			Number of solbility sets, pH_{low} and pH_{high} for diving two temperature zones, and [H+]										
TISOL(i1)	FSOLF(i1,1)	FSOLF(i1,1)	FSOLF(i1,3)	FSOLF(i1,4)	FSOLF(i1,5)	FSOLF(i1,6)	FSOLF(i1,7)	FSOLF(i1,8)	FSOLF(i1,9)	FSOLF(i1,10)	FSOLF(i1,11)		FSOLF(i1,12)
temperature	FSOLF(i1,i2),i2=1,12; Constnats determing solubility shown in Table 4.2												
HHOXD1, HHBND1	Mass transfer coefficients both for oxid layers and sureface boundary												

EXAMPLE												
1												
8												
H2O2	O2	H2	H+	LiOH	Li+	H2O	Fe2+					
7												
1	4	-7	0	1	2	2	0	5.00E-06	0.5	2	1.58	
1	6	-5	0	1	2	2	0	1.00E-04	0.5	2	0.885	
2	4	-1	0	1	2	1	0	2.00E-04	0.7	2	0.48	
4	0	-3	0	1	4	2	0	5.00E-04	0.5	2		
-1	0	2	4	2	0	1	0	1.00E-10	0.3	2	0.48	
-3	0	4	0	1	0	2	1	1.00E-10	0.5	2		
0	0	8	0	1	0	0	0	1.00E-03	0.5	2	-0.44	
5	8.5	6.5 H+										
573	0.19	-10.4	2	-7.8	0.25	-7	2	-7	-0.1	-6.9	2	-6.9
523	0.29	-10.45	2	-8.05	0.2	-7	2	-6.5	-0.22	-6.9	2	-6.35
473	0.3	-11	2	-8.22	0.18	-7	2	-6	-0.1	-6.9	2	-5.9
423	0.35	-11.3	2	-8.6	0.18	-6.7	2	-5.7	-0.1	-7	2	-5.7
373	0.45	-11.4	2	-8.9	0.18	-6.7	2	-5.7	-0.1	-7	2	-5.7
1.00E-04	1.00E-04											

8.7 Results of the Example Calculations

8.7.1 PWR INCA in-pile Loop Calculation (Example 1)

The calculated results of example 1 (PWR INCA in-pile loop analysis) are shown in Appendix (**Table A-1.1 a)** and **b)** and their summaries are shown in **Figure 8.1** and **Table 8.7**.

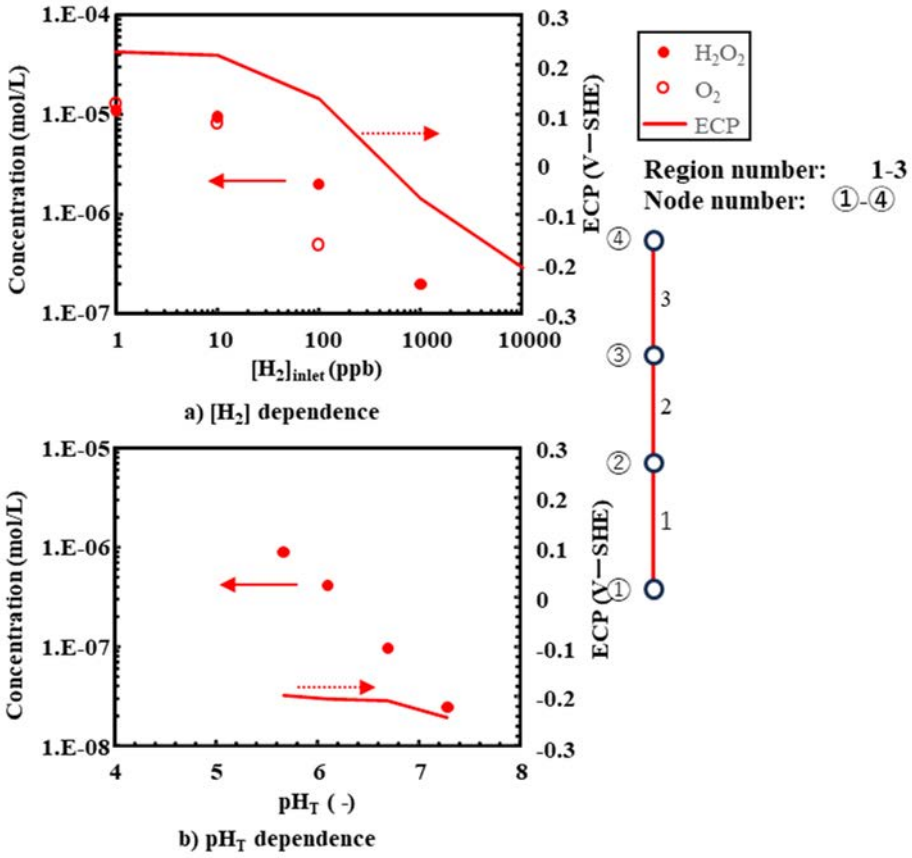

Figure 8.1 Calculated results of Example 1

Table 8.7 Example of output (PWR INCA in-pile loop)

Summary data for plotting

			[H2]			0								
B	L	H2	final	H+	H2O2	O2	H2	ECP	pHT	pHT	H2O2	ECP	H2	
1600	2	1	3	2.04E-07	1.12E-05	1.29E-05	3.81E-05	**2.26E-01**	6.69E+00					
1600	2	10	3	2.04E-07	9.52E-06	8.24E-06	3.55E-05	**2.20E-01**	6.69E+00					
1600	2	100	3	2.03E-07	2.00E-06	4.91E-07	3.97E-05	**1.32E-01**	6.69E+00					
1600	2	1000	3	2.03E-07	2.00E-07	1.37E-09	3.66E-04	**-6.94E-02**	6.69E+00					
1600	2	10000	3	2.03E-07	9.72E-08	5.81E-11	3.66E-03	**-2.08E-01**	6.69E+00					
800	4		3	5.20E-08	2.49E-08	2.30E-11	3.66E-03	**-2.42E-01**		7.28E+00				10000
1600	2		3	2.03E-07	9.72E-08	5.81E-11	3.66E-03	**-2.08E-01**		6.69E+00				10000
1600	0.5		3	8.02E-07	4.13E-07	6.40E-11	3.66E-03	**-2.04E-01**		6.10E+00				10000
1.00E-04	1.00E-04		3.00E+00	2.16E-06	8.91E-07	6.27E-11	3.66E-03	**-1.97E-01**		5.66E+00				10000

8.7.2 PWR Primary Coolant Calculation (Example 2)

Much more realistic calculation targets for PWR primary cooling system are shown in **Figure 8.2** (PWR example 2), which involve the reactor core and SG. The input data are shown in Appendix (**Table A-1.2)** and the summaries of the output are shown in **Figure 8.3**. When pH_T was larger 6.9, ECP in whole region was less than -0.30 V-SHE even when $[H_2]_{injected}$ was 1/5 of the standard concentration, 2 ppm. Unfortunately ECP was much affected by pH_T, and then when the pH_T decreased to lower than 6.3, ECP in the core region was much higher than the target value,-0.3 V-SHE.

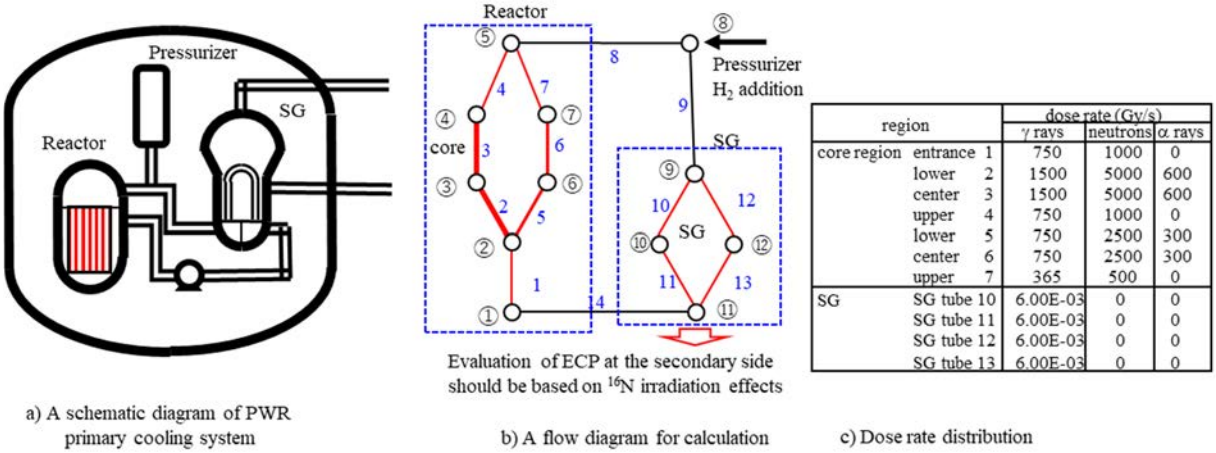

region			dose rate (Gy/s) γ rays	neutrons	α rays
core region	entrance	1	750	1000	0
	lower	2	1500	5000	600
	center	3	1500	5000	600
	upper	4	750	1000	0
	lower	5	750	2500	300
	center	6	750	2500	300
	upper	7	365	500	0
SG	SG tube	10	6.00E-03	0	0
	SG tube	11	6.00E-03	0	0
	SG tube	12	6.00E-03	0	0
	SG tube	13	6.00E-03	0	0

Figure 8.2 Example 2 for calculations of PWR primary loop

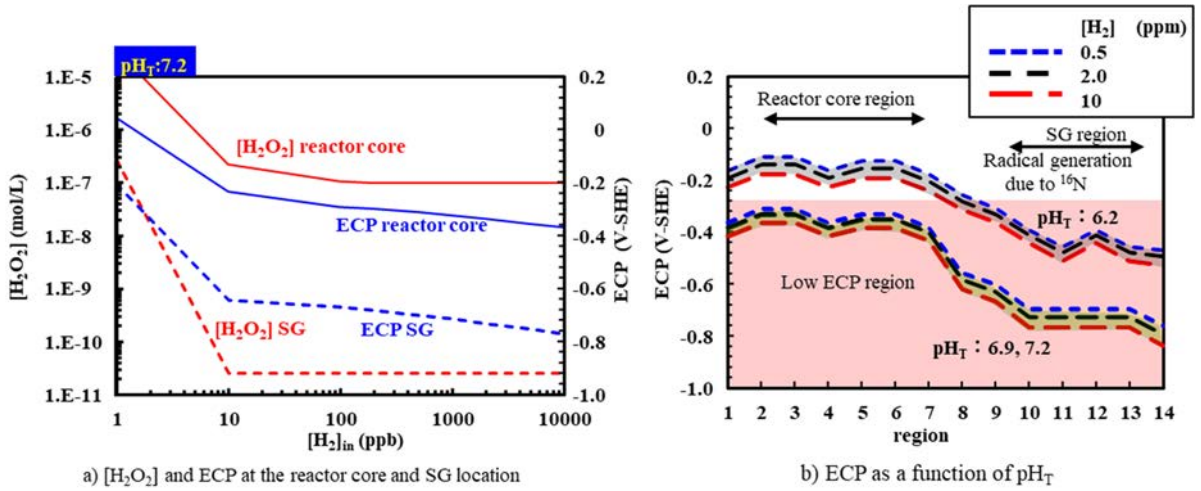

Figure 8.3 Calculated results for PWR primary cooling system (Example 2)

(Effects of $[H_2]$ and pH_T on $[H_2O_2]$ and ECP)

The calculated results were much affected by dose rate in the core region. So precise evaluation should be carried out based on the precise plant data to prepare for the suitable $[H_2]$ control to mitigate ECP without any serious $[H_2]$ for PWSCC.

8.7.3 BWR Primary Loop Calculation (Example 3)

The calculated results of example 3 (BWR primary loop analysis) are shown in Appendix (**Table A-2.1 a)** and **b)**) and their summaries are also shown in **Figure 8.4** and **Table 8.8**.

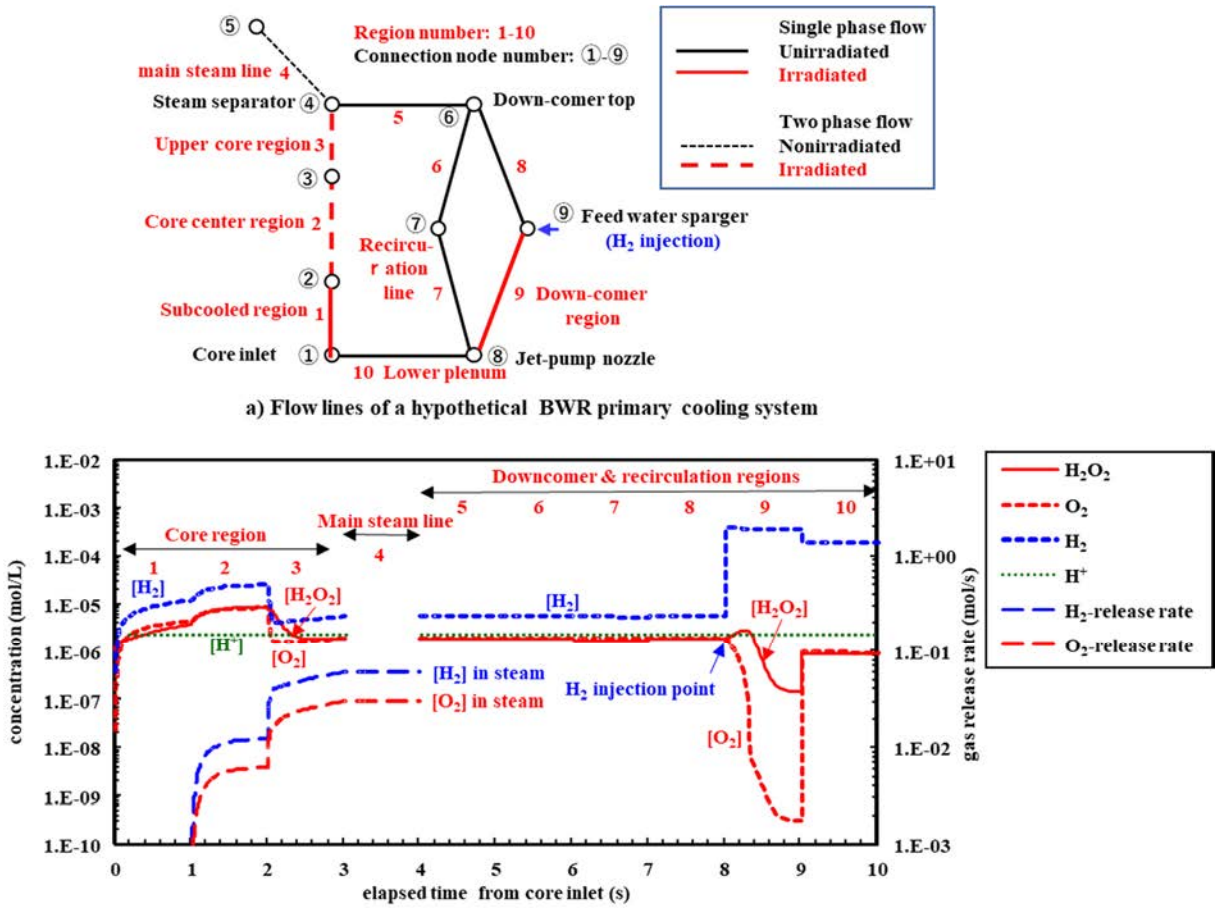

Figure 8.4 Calculated results of Example 3

Table 8.8 Example of output (BWR primary loop)

Summary data for plotting

[H2]		0					100					1000				
final		H+	H2O2	O2	H2	ECP	H+	H2O2	O2	H2	ECP	H+	H2O2	O2	H2	ECP
	1	2.33E-06	3.89E-06	4.56E-06	1.22E-05	**3.24E-02**	2.33E-06	3.88E-06	4.54E-06	1.22E-05	**3.22E-02**	2.33E-06	3.84E-06	4.45E-06	1.23E-05	**3.16E-02**
	2	2.35E-06	8.84E-06	8.47E-06	2.55E-05	**6.07E-02**	2.35E-06	8.82E-06	8.44E-06	2.55E-05	**6.06E-02**	2.35E-06	8.75E-06	8.35E-06	2.55E-05	**6.02E-02**
	3	2.32E-06	1.95E-06	1.91E-06	5.65E-06	**5.99E-03**	2.32E-06	1.95E-06	1.90E-06	5.65E-06	**5.96E-03**	2.32E-06	1.94E-06	1.89E-06	5.65E-06	**5.86E-03**
	4	2.32E-06	0.00E+00	0.00E+00	0.00E+00		2.32E-06	0.00E+00	0.00E+00	0.00E+00		2.32E-06	0.00E+00	0.00E+00	0.00E+00	
	5	2.31E-06	1.89E-06	1.94E-06	5.60E-06	**4.23E-03**	2.31E-06	1.88E-06	1.93E-06	5.60E-06	**4.20E-03**	2.31E-06	1.88E-06	1.92E-06	5.60E-06	**4.10E-03**
	6	2.31E-06	1.82E-06	1.95E-06	5.55E-06	**2.31E-03**	2.31E-06	1.81E-06	1.95E-06	5.55E-06	**2.28E-03**	2.31E-06	1.81E-06	1.94E-06	5.55E-06	**2.17E-03**
	7	2.31E-06	1.75E-06	1.96E-06	5.51E-06	**3.47E-04**	2.31E-06	1.75E-06	1.96E-06	5.51E-06	**3.13E-04**	2.31E-06	1.75E-06	1.95E-06	5.51E-06	**2.05E-04**
	8	2.31E-06	1.82E-06	1.95E-06	5.55E-06	**2.31E-03**	2.31E-06	1.81E-06	1.95E-06	5.55E-06	**2.28E-03**	2.31E-06	1.81E-06	1.94E-06	5.55E-06	**2.17E-03**
	9	2.32E-06	1.09E-06	2.84E-06	7.06E-06	**-3.22E-02**	2.31E-06	8.94E-07	1.68E-07	3.86E-05	**-6.98E-02**	2.31E-06	2.66E-07	5.69E-10	3.75E-04	**-1.89E-01**
	10	2.31E-06	1.38E-06	2.42E-06	6.24E-06	**-1.58E-02**	2.31E-06	1.29E-06	1.06E-06	2.20E-05	**-3.91E-02**	2.31E-06	9.91E-07	9.48E-07	1.90E-04	**-9.56E-02**

8.7.4 BWR Hydrogen Injection Demonstration Calculation (Example 4)

The calculated results of example 4 (BWR primary loop analysis) are shown in Appendix (**Table A-2.2 a)**) and their summaries are also shown in **Figures 8.5** and **8.6**. Region 17 (between node ⑬ and ⑮) is the recirculate line where cooling water went through the recirculation pipe and IGSCC should be strictly prevented. Even when sufficient amounts of hydrogen was injected into the feed water and mixed at the connection at ⑩, [H_2O_2] in the recirculation water was not sufficiently reduced due to lower water radiolysis effects at the vessel surface area at the down-comer region. In the example 4, the dose rate at the vessel wall surface area was varied to obtain the effects of the dose rate effects on the [H_2O_2] and ECP reductions under [H_2] injection.

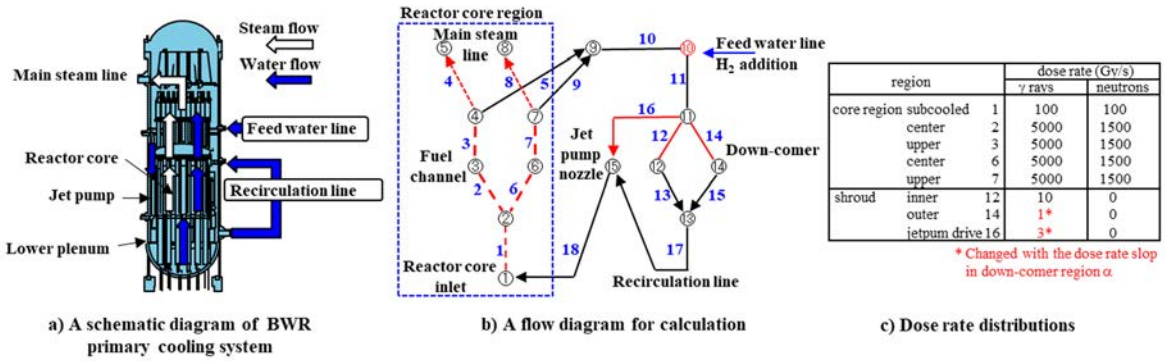

Figure 8.5 Example 4 for calculations of BWR primary loop

The calculated results for varied down-comer dose rate are shown in Figure 8.6. It was confirmed that the dose rate factor α, which designated as the ratio of the dose rate at the vessel surface area to that at the shroud surface area, resulted in a large differences in the [H_2O_2] reduction. It was confirmed that the measured results for BWR 2 through 5 [75] scattered in the region of [H_2O_2] for α=0.01 through 0.1. The dose rate distribution in the down-comer are much more affected by the reactor type and operational conditions. The more precise evaluation should be based on the precise plant and operational data.

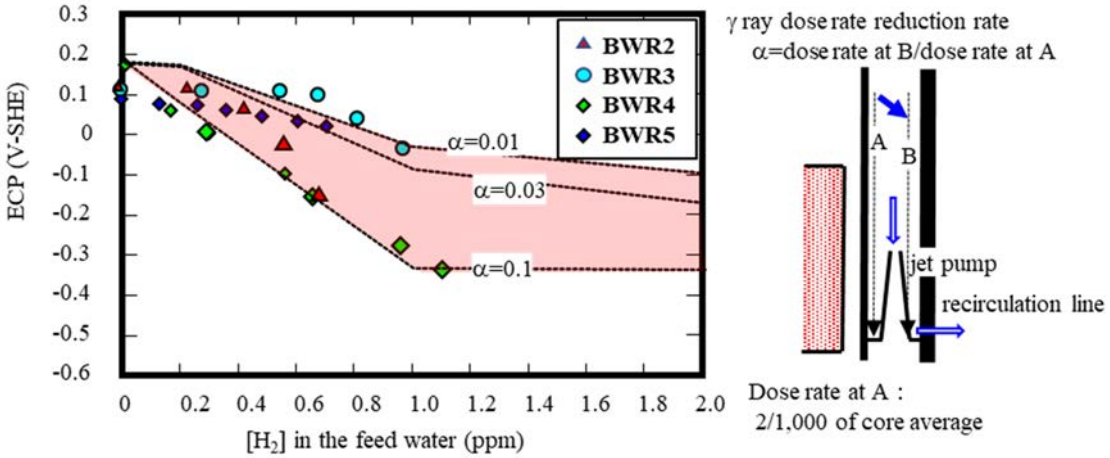

Figure 8.6 Comparison the calculated results with the measured (Example 4)

(H_2 injection effects)

The measured data are shown in the reference [1]

References:

[1] Division of Water Chemistry, Latest situation and major subjects on evaluation procedures of corrosive conditions in BWR primary coolant, 2022.

9. Summary

Analysis of corrosive circumstances in BWR and PWR primary cooling systems could be established by coupling water radiolysis analysis in the reactor core regions and ECP analysis based on the concentrations of radiolytic species obtained by water radiolysis analysis. Usually two kinds of analyses, water radiolysis and ECP analysis were developed separately. And their major targets were only for BWRs.

Recently demands of analyses of corrosive circumstances in PWR primary cooling systems are increasing to evaluate the optimal hydrogen injection for mitigation of PWSCC occurrence and their propagation. The coupled procedure code of water radiolysis and ECP analyses, WRAC-JAEA, has been developed to meet the latest requires.

Its water radiolysis analysis part involved the functions to analyse boiling effects on water radiolysis calculation. Both parts, water radiolysis and ECP analyses, were tightly coupled to transfer the calculated results of the water radiolysis analysis part to ECP analysis part. The tight coupling could increase the reliability of not only individual evaluation, i.e., water radiolysis and ECP analyses, but also total analysis results.

In the document, the background of the development of the coupled analysis code, their major targets, technical backgrounds and major feature of the analysis procedures. Furthermore, for users of the analysis code, users' manual of the WRAC-JAEA code and some examples of the code were attached.

By applying the WRAC-JAEA, traceability of the calculation might be improved, because all input data were involved in the output sheet. The verification of the code could be confirmed by checking the formulation and coding of WRAC-JAEA. Unfortunately, Validation of the WRAC-JAEA is still in the process of confirmation. For validation of the WRAC-JAEA code, much more data measured irradiation conditions. For instance, water radiolysis codes were supported by lots of BWR plant data. At the same time water radiolysis calculation for BWR plants needed lots of plant data, e.g., flow dynamics, thermal hydraulic, radiation distribution. And calculated results should be confirmed with the measured data, usually ECP data. Both kinds of data could be supplied by plant utilities and plant venders. Validation of the WRAC-JAEA for BWR plant analyses also need the same data bases. Its PWR application should be also supported by lots of plant data.

So, validation process of the WRAC-JAEA is still involved in future subjects. As a result of opening the WRAC-JAEA code, its users who try to analyse plant corrosive circumstances can evaluate the results with the plant data and improve the major constants based on the comparison of the analytical and measured results. The feed-back of results of comparisons might contribute its validation and increase its reliability.

Acknowledgement

The authors express their sincere thanks to Dr. Eishi Ibe for his pioneer work on water radiolysis calculation code, AQULY and SINFONY, and Dr. Yoichi Wada for his enthusiastic work on ECP analysis, especially anodic polarization curves. The WRAC-JAEA did not apply their achievements directly, but it was affected by their jobs. The authors showed their articles as references, but their discussions could not be shown in the reference.

The authors also express their thanks to Dr. Ryufuku of Visible Information Center, Inc. for his contribution to development of the original form of WRAC-J, Mr. Yuichiro Mori of Kawasaki Heavy Industries Ltd. for improving the original code and Dr. Hosoyamada for his contribution of adding boiling effects on the original code.

References

1) Uchida, S., Katsumura, Y., Water chemistry technology – one of the key technologies for safe and reliable nuclear power plant operation, J. Nucl. Sci. Technol., 50 (4), 2013, pp. 346-362.

2) Cowan, R.L., Mitigation of IGSCC of BWR internals with hydrogen water chemistry, Proceedings of the International Conference on Water Chemistry Nuclear Reactor Systems, Water Chemistry 7, 1996, Oct. 13-17, Bournemouth. UK, British Nuclear Energy Society. pp. 196-206.

3) Hata, K., Hanawa, S., Chimi, Y., Uchida, S., Optimization of dissolved hydrogen concentration for mitigating corrosive conditions of pressurized water reactor primary coolant under irradiation (1) Evaluation of water radiolysis, J. Nucl. Sci. Technol., 61 (4), 2024, pp. 448-458.

4) Hata, K., Hanawa, S., Chimi, Y., Uchida, S., Optimization of dissolved hydrogen concentration for mitigating corrosive conditions of pressurized water reactor primary coolant under irradiation (2) Evaluation of electrochemical corrosion potential, J. Nucl. Sci. Technol., 60 (8), 2022, pp. 867-880.

5) Japan Society of Mechanical Engineers, Codes for Nuclear Power Generation Facilities - Rules on Fitness - for Service for Nuclear Power Plants - JSME S NA1-2004, Japan, Maruzen Co. Ltd, 2004.

6) American Society of Mechanical Engineers, Boiler and Pressure Vessel Code, Section XI, Rules for In-service Inspection of Nuclear Power Plant Components, Division 1, USA, ASME, 2001.

7) Uchida, S., Satoh, T., Sugama, J., Yamashiro, N., Morishima, Y., Hirose, T., Miyazawa, T., Satoh, Y., Iinuma, K., Wada, Y., Tachibana, M., Effects of hydrogen peroxide on corrosion of stainless steel (III) - Evaluation of electric resistance of oxide film by equivalent circuit analysis for frequency dependent complex impedances., J. Nucl. Sci. Technol., 42 (1), 2005, pp. 66-74.

8) Ibe, E., Karasawa, H., Uchida, S., Radiation chemistry of radioactive nitrogen species in BWR Reactor Cores, J. Nucl. Sci. Technol., 28 (4), 1991, pp. 347-355.

9) de Curieres, I., The Evolution of Chemistry in PWR Nuclear Power Plants: Overview and Safety Perspectives. Proceedings. Water Chemistry of Nuclear Reactor Systems, NPC2014, 2014, Oct. 26-31, Sapporo (Japan), AESJ. (in CD-ROM).

10) Hanawa, S., Satoh, T., Mori, Y., Oogiyanagi, J., Kaji, Y., Uchida, S., A Water Radiolysis Code for the Irradiation Loop System, J. Power Energy Syst., 1 (2), 2007, pp. 123-133.

11) Division of Water Chemistry, Atomic Energy Society of Japan, Handbook of Water Chemistry of Nuclear Reactor System (Second Edition), Corona Publishing Co., Inc., Tokyo, Japan (2022 ISBN 978-4-339-06662-3 C3043. (in Japanese).

12) Takiguchi, H., Takamatsu, H., Uchida, S., Ishigure, K., Nakagami, M., Matsui, M., Water Chemistry Data Acquisition, Processing, Evaluation and Diagnosis Systems in Light Water Reactors, J. Nucl. Sci. Technol., 41 (2) , 2004, pp. 214-225.

13) Lister, D.H., Uchida, S., Determining water chemistry condition in nuclear reactor coolant, J. Nucl. Sci. Technol., 52 (4), 2014, pp. 451-466.

14) Uchida, S., Corrosion of Structural Materials and Electrochemistry in High Temperature Water of Nuclear Power Systems, Nuclear Safety and Simulation, 5 (1), 2014, pp.11-22.

15) Uchida, S., Latest Experience with Water Chemistry in Nuclear Power Plants in Japan, Power Plant Chemistry, 8 (5), 2006, pp. 282-292.

16) Uchida, S., Otoha, K., Ishigure, K., Water Chemistry – One of the key technologies for safety and reliable nuclear power plant operation, Proc.15th Pacific Basin Nuclear Conference, Sydney, Australia, 2006, Oct. 15-20, Australian Nuclear Association. (in CD-ROM).

17) Uchida, S., Takiguch, H., Lister, D.H., Instrumentation for monitoring and control of water chemistry for light water-cooled nuclear power plants. Power Plant. Chem., 12 (5), 2010, pp. 278-295.

18) Ibe, E., Uchida, S., Radiolytic Aspects in Boiling Water Reactor Primary Systems: Results from Numerical Simulation and Statistical Regression Analyses. Nucl. Sci. Eng., 89, 1985, pp. 330-350.

19) Ichikawa, N., Hemmi, H., Takagi, J., Precise Evaluation of Corrosion Environments of Structural Materials under Complex Water Flow Condition, (I) Estimation of Corrosion Potentials in Reactor Pressure Vessel Bottom of BWRs, Nucl. Sci. Tecchnol., 40 (8), 2003, pp. 583-590.

20) Ruiz, C.P., Lin, C.C., Robinson, R., Burns, R.W., Henshaw, J., Pathania, R., Model calculation of water radiolysis and electrochemical potentials in BWR primary coolant, II. Proc. Water Chemistry of Nuclear Reactor Systems 6, 1986, Oct. 13-17, Bournemouth (UK).

21) Ruiz, C.P., Lin, C.C., Robinson, R., Burns, R.W., Curtis, A.R., Model calculation of water radiolysis in BWR primary coolant. Proc. Water Chemistry of Nuclear Reactor Systems 7, 1996, Oct. 13-17, Bournemouth (UK).

22) Lundgren, K., Christensen, H., Model calculation of water radiolysis in the primary coolant circuit of Barseback-1 BWR. Proc. Water Chemistry of Nuclear Reactor Systems 7, 1996, Oct. 13-17, Bournemouth (UK).

23) Yeh, T.K., Chu, F., Electrochemical Corrosion Potential Modeling in the Primary Heat Transport Circuit of the Chinshan Boiling Water Reactor under the Condition of Hydrogen Water Chemistry with Noble Metal Coating, J. Nucl. Sci. Technol., 37 (12), 2000, pp. 1063-1074.

24) Uchida, S., Wada, Y., Takagi, J., Yamamoto, S., Hisamune, K., Verification and validation procedures of calculation codes for determining corrosive conditions in BWR primary cooling system based on water radiolysis and mixed potential models, J. Nucl. Sci. Technol., 51 (1), 2014, pp. 24-36.

25) Macdonald, D.D., Urquidi-Macdonald, M., Thin-layer mixed-potential model for the corrosion of high-level nuclear waste canisters, Corrosion, 46 (5), 1990, pp. 380-390.

26) Uchida, S., Shigenaka, N., Tachibana, M.,Wada, Y., Saakai, M., Akamani, K., Ohsumi, K., Effects of Hydrogen Peroxide on Intergranular Stress Corrosion Cracking of Stainless Steel in High Temperature Water, (I) Effects of Hydrogen Peroxide on Electrochemical Corrosion Potential of Stainless Steel, J. Nucl. Sci. Tecchnol., 35 (4), 1998, pp. 301-308.

27) Andresen. P., Hickling, J., Ahluwalia, A., et al., Effect of dissolved H_2 in primary water on the SCC growth rate of Ni alloys, Proc. International Conference on Water Chemistry of Nuclear Reactor Systems, NPC2008, 2008, Sept 15-18, Berlin (Germany), VGB Power Tech. (in CD-ROM).

28) Molander, A., Jenssen, A., Norring, K., et al., Comparison of PWSCC initiation and crack growth data for Alloy 600, Proc. International Conference on Water Chemistry of Nuclear Reactor Systems, NPC2008, 2008, Sep 15-18, Berlin (Germany) VGB Power Tech. (in CD-ROM).

29) König, M., Norring, K., Gott, K., et al., The influence of hydrogen concentration on the PWSCC susceptibility in alloy 600 in simulated primary water at 300°C, Proc International Symposium on Contribution of Materials Investigations and Operating Experience to LWRs' Safety, Performance and Reliability, Fontevraud IV. 1998 Sep 14-18, Paris (France), Société française d'énergie nucléaire (SFEN). 13a-A703.

30) Uchida, S., Naitoh, M., Okada, H., Suzuku, H., Water chemistry guidance in nuclear power plants in Japan. Power Plant Chem., 14 (1), 2012, pp. 278-295.

31) Yamashiro, N., Uchida, S., Satoh, Y., Morishima, Y., Yokoyama, H., Satoh, T., Sugama, J., Yamada, R., Determination of hydrogen peroxide in water by chemiluminescence detection, (1) Flow injection type hydrogen peroxide detection system. J. Nucl. Sci. Technol., 41 (9), 2004. pp. 890-897.

32) Standards Committee, Chemical analysis for primary coolant of PWR - boron, AESJ-SC-S002, 2010, Atomic Energy Society of Japan, Tokyo. (in Japanese).

33) Gjerde, D.T., Fritz, J.S., Ion chromatography, Weinheim, Wiley-VC, 2000.

34) Welz, B., Sperling, M., Atomic absorption spectrometry, Weinheim, Wiley-VC, 1999.

35) Vajda, N., Larosa, J., Pinter, T., Keomley, G., Bodizs, D., Molnar, Z.S., Analysis of actinides in the primary coolant of a WWER-440 type reactor, J. Radioanal. Nucl. Chem., 170 (2), 2005, pp. 399-409.

36) Bolz, M., Hoffman, W., Ruehle, W., Becker. F., Characterization of colloids in primary coolant, International Conference on Water Chemistry of Nuclear Reactor Systems 7; 1996 Oct 13-17, Bournemouth (British Nuclear Energy Society).

37) Knoll, G.F., Radiation detection and measurement, 3rd ed., Weinheim, Wiley, 1999.

38) IAEA, Coolant technology of water cooled reactors, Vienna, International Atomic Energy Agency, 1992. (IAEA-TECDOC-667).

39) IAEA, Data processing technologies and diagnostics for water chemistry and corrosion in nuclear power plants, Vienna, International Atomic Energy Agency, 2006. (IAEA-TECDOC-1505).

40) IAEA, High temperature on-line monitoring of water chemistry and corrosion control in water cooled power reactors, Vienna, International Atomic Energy Agency, 2002. (IAEA-TECDOC-1303).

41) Uchida, S., Ishigure, K., Takamatsu, H., Takiguchi, H., Nakagami, M., Matsui, M., Water chemistry data acquisition, processing, evaluation and diagnosis systems for nuclear power reactors, 14th International Conference on the Properties of Water and Steam, 2004, Aug. 31-Sep 3, pp. 551-558, Kyoto (Japan), International Association for Properties of Water and Steam.

42) Uchida, S., Corrosion monitoring applications in nuclear power plants. In: Ritter S, Molander A, editors. Corrosion monitoring in nuclear systems, European Federation of Corrosion Publications, Number 56, Maney Publishing, 2010. ISBN-13: 978-1-906540-98-2.

43) Ishida, K., Lister, D.H., In-situ measurement of corrosion of type 316 stainless steel in 280 ºC pure water via the electrical resistance of a thin wire, J. Nucl. Sci. Technol., 49 (11), 2012, pp. 1078-1091.

44) Turner, C., Guzonas, D., Improving chemistry performance in CANDU plants, International Conference on Water Chemistry of Nuclear Reactor Systems, NPC 2010, 2010 Oct 3-7, Quebec (Canada), Canadian Nuclear Society. (in CD-ROM).

45) Lu, Y.C., Define optimum conditions for steam generator tube integrity and an extended service life, 15th International Conference on Nuclear Engineering, ICONE-15-10854, 2007 Apr 22-26, Nagoya, Japan Society of Mechanical Engineer.

46) Ibe, E., Nagase, M., Sakagami, M., Uchida, S., Radiolytic environments in boiling water reactor cores, J. Nucl. Sci. Technol., 24 (3), 1987, pp. 220-226.

47) Ichikawa, N., Takagi, J., Precise evaluation of corrosion environments of structural materials under complex water flow condition (II), J. Nucl. Sci. Technol., 40 (11), 2003, pp. 941-950.

48) Yeh, T.K., McDonald, D.D., The efficiency of noble metals in reducing the corrosion potential in the primary coolant circuits of boiling water reactors operating under hydrogen water chemistry operation, J. Nucl. Sci. Technol., 43 (10), 2006, pp. 1228-1236.

49) Marshall, W.L., Franck, E.U., Ion product of water Substance, 0-1000ºC, 1-10,000 Bars, New international formulation and its background, J. Phys, Chem, Ref Data, 10 (2), 1981, pp. 295-304.

50) EPRI, PWR Advanced All-Volatile Treatment Additives, By-Products, and Boric Acid, EPRI TR100755 ,1992.

51) Ibe, E., Uchida, S., A Water Radiolysis Model in A Circulating Flow System with A Boiling Region and Its Application to Hydrogen Alternate Water Chemistry of Boiling Water Reactors, Nucl. Sci. Eng., **90**, 1985, pp. 140-157.

52) Uchida, S., Satoh, T., Tsukada, T., Miyazawa, T., Satoh, Y., Ishii, K., Evaluation of the Effects of Oxide Film on Electrochemical Corrosion Potential of Stainless Steel in High Temperature Water, Proc. 14th Int Conf. Environmental Degradation of Materials in Nuclear Power Systems - Water Reactors, Virginia Beach, VA, 2009, Aug. 22-27 ANS. (in CD-ROM).

53) Uchida, S., Naitoh, M., Okada, H., Hanawa, S., Lister, D.H., An empirical model for the corrosion of stainless steel in BWR primary coolant, Corrosion Engineering, Science and Technology, 58 (2), 2017, pp. 587-595.

54) Wada, Y., Watanabe, A., Tachibana, M., Uetake, N., Uchida, S., Ishigure, K., Effects of Hydrogen Peroxide on Intergranular Stress Corrosion Cracking of Stainless Steel in High Temperature Water, (III) - Crack Growth Rates in Corrosive Environment Determined by Hydrogen Peroxide, J. Nucl. Sci. Technol., 37 (10), 2000, pp. 901-912.

55) Uchida, S., Naitoh, M., Uehara, Y., Okada, H., Hiranuma, N., Sugino, W., Koshizuka, S., Lister, D.H., Evaluation of Flow Accelerated Corrosion of PWR Secondary Components by Corrosion Analysis Coupled Flow Dynamics Analysis (III), Evaluation of Pipe Wall Thinning Rate with the Coupled Model of Static Electrochemical Analysis and Dynamic Double Oxide Layer Analysis, J. Nucl. Sci. Technol., 46 (1), 2009, pp. 31-40.

56) Uchida, S., Satoh, T., Morishima, Y., Hirose, T., Miyazawa, T., Kakinuma, N., Satoh, Y., Usui, N., Wada, Y., Effects of Hydrogen Peroxide and Oxygen on Corrosion of Stainless Steel in High temperature water, Proc. 12th Int. Conf. Environmental Degradation of Materials in Nuclear Power Systems – Water Reactors, Snowbird, UT, 2005, Aug. 15-18, 2005, TMS. (in CD-ROM).

57) Uchida, S., Naitoh, M., Uehara, Y., Okada, H., Hiranuma, N., Sugino, W., Koshizuka, S., Evaluation of Flow Accelerated Corrosion of PWR Secondary Components by Corrosion Analysis Coupled Flow Dynamics Analysis (II), Evaluation of corrosive conditions in PWR secondary cooling system, J. Nucl. Sci. Technol., 45 (12), 2008, pp. 1275-1286.

58) Uchida S, Satoh T, Tsukada T, Miyazawa T, Satoh Y and Ishii K, Evaluation of the Effects of Oxide Film on Electrochemical Corrosion Potential of Stainless Steel in High Temperature Water, Proc. 14th Int Conf. Environmental Degradation of Materials in Nuclear Power Systems – Water Reactors, Virginia Beach, VA, Aug. 22-27, 2009, ANS, 2009 (in CD-ROM).

59) Hishida, M., Takabayashi, J., Kawakubo, T., Yamashina, Y., Polarization Curve Measurement in High Purity Water at Elevated Temperatures, Corrosion, 41 (10), 1985, pp. 570-574.

60) Kim, Y.J., Niedrach, L.W., Lin, C.C., Lamp, K.S., Development of ECP models for BWR applications, Proc. Symp. Environmental Degradation of Materials in Nuclear Power Systems – Water reactors 7. 1998, Aug. 13-15, Amelia Island (USA), ANS. (in CD-ROM).

61) Hanawa, S., Hata, K., Chimi, Y., Kasahara S., Preliminary Verification of Water Radiolysis and ECP Calculation Models by In-pile ECP Measurements, Proc. International Conference on Water Chemistry of Nuclear Reactor Systems; NPC2018, 2018, Sept 9-14; San Francisco, USA. (USB memory).

62) Tremaine, P.R., LeBlanc, J.C., The solubility of magnetite and hydrolysis and oxidation of Fe^{2+} in water to 300 °C, J. Solution Chemistry, 9(6), 1980, pp. 415-417.

63) Park, Y.J., Choi, K-C., Na, Y.K., Solubility study of nickel ferrite in boric acid using a flow-through autoclave system under high temperature and high pressure, Nucl. Eng. Technol., 48, 2016, pp. 554-558.

64) Macdonald, D.D., Uriquidi-Macdonald, M., Thin-layer mixed potential model for the corrosion of high level nuclear waste canisters, Corrosion, 46, 1990, pp. 380-390.

65) Wada, Y., Watanabe, A., Tachibana, M., Uetake, N., Nakamura, M., Akamine, K., Uchida, S., Mitigation Effect of Alkaline Water Chemistry upon Intergranular Stress Corrosion Cracking of Sensitized 304 Stainless Steel, J. Nucl. Sci. Technol., 38 (8), 2001, pp. 621-632.

66) Marichev, V.A., A Contact Electric Resistance Method for in-situ Investigation of Metal Surface in Electrolytes and Some New Possibilities in Corrosion and Electrochemical Studies, Corrosion Science, 38, 1996, pp. 531-558.

67) Uchida, S., Satoh, T., Tsukada, T., Satoh, Y., Miyazawa, T., Terach,i T., Wada, Y., Hosokawa, H., Properties of Oxide Films on Stainless Steel Exposed to Hydrogen Peroxide and Oxygen in High Temperature Water, Proc. Int. Conf. Water Chemistry of Nuclear reactor Systems, 2006, Oct. 23-26, Jeju (Korea), Korean Atomic Energy Research Institute. (in CD-ROM).

68) Abramowitz, M., Stegun, I.A., (Eds.). Handbook of Mathematical Functions with Formulas, Graphs, and Mathematical Tables, 9th printing, 1972, New York (US), Dover, p. 18.

69) Gear, C.E., The Numerical Integration of Ordinary Differential Equations, Mathematics of Computation, 21 (98), 1967, pp. 146-156.

70) Takiguchi, H., Ullberg, M., Uchida, S., Optimization of dissolved hydrogen concentration for control of primary coolant radiolysis in pressurized water reactors, J. Nucl. Sci. Technol., 41(5), 2004, pp. 601-609.

71) Urquidi-Macdonald, M., Pitt, J., Macdonald, D.D., The impact of radiolytic yield on the calculated ECP in PWR primary coolant circuits, J. Nucl. Mat., 362 (1), 2007, pp. 1-13.

72) Burns, W.G., Moor, M.E., Radiation enhancement of zircaloy corrosion in boiling water system: a study of simulated radiation chemical kinetics, Proceedings of First International Conference on Water Chemistry of Nuclear Reactor Systems, Water Chemistry 1. 1978, Oct 14-17, Bournemouth (UK). British Nuclear Energy Society (BNES), p. 78.

73) Christensen, H., Molander, A., Lassing, A., et al., Experimental studies of radiolysis in an in-core loop in the Studsvik R2 reactor, Proceedings of Water Chemistry of Nuclear Reactor Systems, Water Chemistry 7, 1996 Oct. 13–17, Bournemouth (UK), British Nuclear Energy Society (BNES). pp.138-140.

74) Elliot, A., Bartels, D.M., The Reaction set, rate constants and g-values for the simulation of radiolysis of light water over the range 20 to 350°C based on information available in 2008, AECL Report 153-127160-450-001, 2009.

75) Division of Water Chemistry (DWC), Latest situation and major subjects on evaluation procedures of corrosive conditions in BWR primary coolant, DWC Report #2022-0001, 2022, Division of Water Chemistry, Atomic Energy Society of Japan (in Japanese).

76) Muroya, Y., Yamashita, S., Lertnaisat, P., et al., Rate constant for the $H^{\cdot} + H_2O \rightarrow OH + H_2$ reaction at elevated temperatures measured by pulse radiolysis, Phys. Chem. Chem. Phys., 19 (45), 2017, pp. 30834-30841.

77) Kim, Y.J., Niedrach, L.W., Andresen, P.L., CRD data on ECP behavior of various alloys containing noble metals, BWR-TR-93-02, 1993, GE CR&D.

78) Indig, M.E., Nelson, J.L., Electrochemical measurements and modelling predictions in boiling water reactors under various operating conditions, Corrosion, 47 (3), 1991, pp. 202-209.

79) Hata, K., Uchida, S., Hanawa, S., Chimi, Y., Development of an analysis method for electrochemical corrosion potential in PWR primary coolant under irradiation, Proceedings International Symposium Contribution of Materials Investigations and Operating Experience to LWRs Safety, Performance and Reliability, FONTEVRAUD 10, 2022, Sep. 19-22, Avignon (France), Paper 86.

80) Totsuka, N., Szklarska-Smialowska, Z., Hydrogen induced IGSCC of Ni containing FCC alloys in high temperature water. Proceedings 3rd Int. Symposium on Environmental Degradation of Materials in Nuclear Power Systems – Water Reactors, 1988, Warrendale (PA), TMS, pp. 691-696.

81) Bennett, P., Hogberg, N., Karlsen, T., Thoresen, H., In-Core ECP Measurements under LWR Conditions

in the Halden Reactor, Proc. 10th Int. Conf. Environmental Degradation of Materials in Nuclear Power Systems - Water Reactors-, 2001, Aug. 5-10, Lake Tahoe (Nevada), NACE (in CD-ROM).

82) Bosch, R.W., Weber, M., Vankerberghen, M., In-pile electrochemical measurements on AISI 304 and AISI 306 in PWR conditions- Experimental results, J. Nucl. Mat., 360, 2007, pp. 304-314.

83) Uchida, S., Naitoh, M., Uewhara, Y., Okada, H., Hotta, K., Ichikjawa, R., Koshizuka, S., Evaluation Method of Corrosion Conditions in Cooling Systems of Nuclear Power Plants by Combined Analyses, Power Plant Chemistry, 9 (3), 2007, pp. 143-156.

84) Uchida, S., Hanawa, S., Nishiyama, Y., Nakamura, T., Satoh, T., Tsukada, T., Kysela, J., Determination of Electrochemical Corrosion Potential along the JMTR In-pile Loop (I) Evaluation of ECP of Stainless Steel in High Temperature Water as a Function of Oxidant Concentrations and Exposure Time, Nucl. Technol., 183 (1), 2013, pp. 119-135.

85) Uchida, S., Naitoh, M., Okada, H., Ohira, T., Koshizuka, S., Lister, D.H., Verification and Validation of Evaluation Procedures for Local Wall Thinning due to Flow Accelerated Corrosion and Liquid Droplet Impingement, Nucl. Technol. 178 (6), 2012, pp. 280-297.

86) Suzuki, H., Uchida, S., Naitoh, M., Okada, H., Koikari, S., Nagaya, Y., Nakamura, A., Koshizuka, S., Lister, D.H., Verification and Validation of One-Dimensional Flow-Accelerated Corrosion Evaluation Code, Nucl. Technol., 183 (1), 2013, pp. 62-74.

Abbreviations

AAS: Atomic Absorption Spectroscopy
AISI: American Iron and Steel Institute (US Civilian standards for iron and metals)
ASME: American Society of Mechanical Engineers
BWR: Boiling Water Reactor
CANDU: Canada Deuterium Uranium Reactor
CD: Compact Disk
CRD: Control Rod Drive
DAWAC: IAEA Coordinated Research Project, “Data Processing Technologies and Diagnostics for Water Chemistry and Corrosion Control in Nuclear Power Plants (2001-2005)”
ECP: Electrochemical Corrosion Potential
FAC: Flow Accelerated Corrosion
FDCI: Frequency-dependent Complex Impedance
FOLTM: Feeder Online Thickness Measurement
FORTRAN: Formula Translation
HEPro: Hydrogen Effusion Probe
HP heater, LP heater: High Pressure Heater and Low Pressure Heater
HWC: Hydrogen Water Chemistry
ICP-AES: Inductively Coupled Plasma with Atomic Emission Spectrometry
ICP-MS: Inductively Coupled Plasma with Mass Spectrometric Analysis
IGSCC: Intergranular Stress Corrosion Cracking
INCA: In-core Assembly. An In-pile Loop iInstalled in the Studsvik R2 reactor
JSME: Japan Society of Mechanical Engineers
LWR: Light Water-cooled Reactor
MTBL, MTOL: Mass Transfer Coefficients for the Surface Boundary Layers, Oxide Layers
NWC: Normal Water Chemistry
PAD: Program Analysis Diagram
pH_T, pH_R: pH at the Elevated Temperature and pH at the Room Temperature
PWR: Pressurized Water Reactor
PWSCC: Primary Water Stress Corrosion Cracking
RPV: Reactor Pressure Vessel
RWCS: Reactor Water Clean-up System
SG: Steam Generator

SHE: Standard Hydrogen Electrode
WACOL: IAEA Coordinated Research Project, “High Temperature On-line Monitoring of Water Chemistry and Corrosion Control in Water Cooled Power Reactors (1992-2001)”
WACOLIN: IAEA Coordinated Research Project, “Water Chemistry Control and Coolant Interactions with Fuel and Primary Circuit Materials in Water Cooled Power Reactors (1987–1991)”
WRAC-J: the Previous Version of WRAC-JAEA for BWR Water Chemistry Analysis Code
WRAC-JAEA: Water Radiolysis Analysis Code of JAEA. A Calculation Code for Determining Corrosive Conditions in the Primary Cooling Systems of BWRs and PWRs
XFS: X-ray Fluorescence Spectroscopy

Appendix

Appendix-A Examples of Output

A-1. PWR INCA in-pile Loop Analysis

Table A-1.1 a) Example of output (PWR INCA in-pile loop analysis): confirmation of input data

	Summary	of	the	INPUT	data	PWR	INCA	in-	pile	loop	calculation	test	cases2023	Nov
Case:	9iitermax:	1												
	IPREGN:													
	1.60E+03	2.00E+00	1.00E+00	1.00E+00	1.00E+00	0.00E+00								
	1.60E+03	2.00E+00	1.00E+00	1.00E+01	1.00E+00	0.00E+00								
	1.60E+03	2.00E+00	1.00E+00	1.00E+02	1.00E+00	0.00E+00								
	1.60E+03	2.00E+00	1.00E+00	1.00E+03	1.00E+00	0.00E+00								
	1.60E+03	2.00E+00	1.00E+00	1.00E+04	1.00E+00	0.00E+00								
	1.60E+03	2.00E+00	1.00E+00	1.00E+04	1.00E+00	0.00E+00								
	1.60E+03	5.00E-01	1.00E+00	1.00E+04	1.00E+00	0.00E+00								
	8.00E+02	4.00E+00	1.00E+00	1.00E+04	1.00E+00	0.00E+00								
	1.00E-04	1.00E-04	1.00E+00	1.00E+04	1.00E+00	0.00E+00								

	RT-INPUT	DATA	FILE	REG:	4.00E+00															
#	RT	TEM	G2	SOV	QG3	QN3	QA3	VAL(14)	VAL(15)	VAL(16)	VAL(1)	VAL(2)	VAL(3)	VAL(4)	VAL(5)	VAL(6)	VAL(7)	VAL(8)	VAL(9)	VAL(10)
	1.00E+00	5.63E+02	1.00E-01	3.00E+02	1.00E+00	0.00E+00	0.00E+00	5.63E+02	1.00E-01	1.33E-02	5.63E+02	0.00E+00	5.00E+01	1.00E-05	5.00E+01	1.00E+00	1.00E-03	1.00E-05	1.50E+00	1.50E+00
	1.00E+00	5.63E+02	1.00E-01	3.00E+02	4.00E+03	4.30E+03	0.00E+00	5.63E+02	1.00E-01	1.33E-02	5.63E+02	0.00E+00	5.00E+01	1.00E-05	5.00E+01	1.00E+00	1.00E-03	1.00E-05	1.50E+00	1.50E+00
	1.00E+00	5.63E+02	1.00E-01	3.00E+02	4.00E+03	4.30E+03	0.00E+00	5.63E+02	1.00E-01	1.33E-02	5.63E+02	0.00E+00	5.00E+01	1.00E-05	5.00E+01	1.00E+00	1.00E-03	1.00E-05	1.50E+00	1.50E+00
	1.00E+00	5.63E+02	1.00E-01	3.00E+02	1.00E+02	1.00E+02	0.00E+00	5.63E+02	1.00E-01	1.33E-02	5.63E+02	0.00E+00	5.00E+01	1.00E-05	5.00E+01	1.00E+00	1.00E-03	1.00E-05	1.50E+00	1.50E+00

	NodeConne	Data	FILE	NCN:	3
	PNDN	NDN	RRMIX	LNDN	GNDN
	1	2	1.00E+00	0	0
	2	3	1.00E+00	0	0
	3	4	1.00E+00	0	0

	REACTIO	DATA	FILE	RN:	43																															
	F1	F2	F3	R1	R2	R3	FN1	FN2	FN3	RN1	RN2	RN3	FK0	RK0	WFK0	WRK0	FAE)	RAE	FHN1	FHN2	FHN3	RHN1	RHN2	RHN3	FON1	FON2	FON3	RON1	RON2	RON3	FCH1	FCH2	FCH3	RCH1	RCH2	RCH3
H+	OH-	NONE	H2O	NONE	NONE	1.00E+00	1.00E+00	0.00E+00	1.00E+00	0.00E+00	0.00E+00	1.50E+12	7.50E+00	1.50E+12	7.50E+00	1.30E+04	4.00E+04	1	1	0	2	0	0	0	1	0	1	0	0	1	-1	0	0	0	0	
H2O2	NONE	NONE	OH	NONE	NONE	1.00E+00	0.00E+00	0.00E+00	2.00E+00	0.00E+00	0.00E+00	0.00E+00	0.00E+00	0.00E+00	0.00E+00	6.00E+04	0.00E+00	2	0	0	1	0	0	2	0	0	1	0	0	0	0	0	0	0	0	
B0	OH-	NONE	B1-	NONE	NONE	1.00E+00	1.00E+00	0.00E+00	1.00E+00	0.00E+00	0.00E+00	6.20E+01	1.00E+00	6.20E+02	1.00E+01	0.00E+00	0.00E+00	0	1	0	1	0	0	0	1	0	1	0	0	0	-1	0	-1	0	0	
B0	OH-	NONE	B2-	NONE	NONE	2.00E+00	1.00E+00	0.00E+00	1.00E+00	0.00E+00	0.00E+00	9.60E+01	1.00E+00	9.60E+02	1.00E+01	0.00E+00	0.00E+00	0	1	0	1	0	0	0	1	0	1	0	0	0	-1	0	-1	0	0	
B0	OH-	NONE	B3-	NONE	NONE	3.00E+00	1.00E+00	0.00E+00	1.00E+00	0.00E+00	0.00E+00	2.00E+02	1.00E+00	2.00E+02	1.00E+01	0.00E+00	0.00E+00	0	1	0	1	0	0	0	1	0	1	0	0	0	-1	0	-1	0	0	
B0	OH-	NONE	B4-	NONE	NONE	4.00E+00	2.00E+00	0.00E+00	1.00E+00	0.00E+00	0.00E+00	9.60E+03	1.00E+00	9.60E+03	1.00E+01	0.00E+00	0.00E+00	0	1	0	2	0	0	0	1	0	2	0	0	0	-1	0	-2	0	0	
LiOH	NONE	NONE	Li+	OH-	NONE	1.00E+00	0.00E+00	0.00E+00	1.00E+00	1.00E+00	0.00E+00	1.00E+02	1.00E+01	0.00E+00	0.00E+00	0.00E+00	0.00E+00	1	0	0	0	1	0	1	0	0	0	1	0	0	0	0	1	-1	0	
B1-	H+	NONE	B1H	NONE	NONE	1.00E+00	1.00E+00	0.00E+00	1.00E+00	0.00E+00	0.00E+00	1.00E+01	1.00E+01	0.00E+00	0.00E+00	0.00E+00	0.00E+00	1	1	0	2	0	0	1	0	0	1	0	0	-1	1	0	0	0	0	
B2-	H+	NONE	B2H	NONE	NONE	1.00E+00	1.00E+00	0.00E+00	1.00E+00	0.00E+00	0.00E+00	1.00E+01	1.00E+01	0.00E+00	0.00E+00	0.00E+00	0.00E+00	1	1	0	2	0	0	1	0	0	1	0	0	-1	1	0	0	0	0	
B3-	H+	NONE	B3H	NONE	NONE	1.00E+00	1.00E+00	0.00E+00	1.00E+00	0.00E+00	0.00E+00	1.00E+01	1.00E+01	0.00E+00	0.00E+00	0.00E+00	0.00E+00	1	1	0	2	0	0	1	0	0	1	0	0	-1	1	0	0	0	0	
B4-	H+	NONE	B4H	NONE	NONE	1.00E+00	2.00E+00	0.00E+00	1.00E+00	0.00E+00	0.00E+00	1.00E+01	1.00E+01	0.00E+00	0.00E+00	0.00E+00	0.00E+00	2	1	0	4	0	0	2	0	0	2	0	0	-2	1	0	0	0	0	
B1-	Li+	NONE	B1L	NONE	NONE	1.00E+00	1.00E+00	0.00E+00	1.00E+00	0.00E+00	0.00E+00	1.00E+01	1.00E+01	0.00E+00	0.00E+00	0.00E+00	0.00E+00	1	0	0	1	0	0	1	0	0	1	0	0	-1	1	0	0	0	0	
B2-	Li+	NONE	B2L	NONE	NONE	1.00E+00	1.00E+00	0.00E+00	1.00E+00	0.00E+00	0.00E+00	1.00E+01	1.00E+01	0.00E+00	0.00E+00	0.00E+00	0.00E+00	1	0	0	1	0	0	1	0	0	1	0	0	-1	1	0	0	0	0	
B3-	Li+	NONE	B3L	NONE	NONE	1.00E+00	1.00E+00	0.00E+00	1.00E+00	0.00E+00	0.00E+00	1.00E+01	1.00E+01	0.00E+00	0.00E+00	0.00E+00	0.00E+00	1	0	0	1	0	0	1	0	0	1	0	0	-1	1	0	0	0	0	
B4-	Li+	NONE	B4L	NONE	NONE	1.00E+00	2.00E+00	0.00E+00	1.00E+00	0.00E+00	0.00E+00	1.00E+01	1.00E+01	0.00E+00	0.00E+00	0.00E+00	0.00E+00	2	0	0	2	0	0	2	0	0	2	0	0	-2	1	0	0	0	0	
H	H	NONE	H2	NONE	NONE	1.00E+00	1.00E+00	0.00E+00	1.00E+00	0.00E+00	0.00E+00	9.00E+10	0.00E+00	9.00E+10	0.00E+00	1.30E+04	0.00E+00	1	1	0	2	0	0	0	0	0	0	0	0	0	0	0	0	0	0	
E-	HO2	NONE	HO2-	NONE	NONE	1.00E+00	1.00E+00	0.00E+00	1.00E+00	0.00E+00	0.00E+00	3.00E+11	0.00E+00	3.00E+11	0.00E+00	1.30E+04	0.00E+00	0	1	0	1	0	0	0	2	0	2	0	0	-1	0	0	-1	0	0	
E-	O2	NONE	O2-	NONE	NONE	1.00E+00	1.00E+00	0.00E+00	1.00E+00	0.00E+00	0.00E+00	2.60E+11	0.00E+00	2.60E+11	0.00E+00	1.30E+04	0.00E+00	0	0	0	0	0	0	0	2	0	2	0	0	-1	0	0	-1	0	0	
E-	H2O	NONE	H2	OH-	NONE	2.00E+00	2.00E+00	0.00E+00	1.00E+00	2.00E+00	0.00E+00	1.80E+06	0.00E+00	1.80E+06	0.00E+00	1.30E+04	0.00E+00	0	2	0	2	1	0	0	1	0	0	1	0	-1	0	0	0	-1	0	
OH	NONE	NONE	H2O2	NONE	NONE	2.00E+00	0.00E+00	0.00E+00	1.00E+00	0.00E+00	0.00E+00	2.50E+10	0.00E+00	2.50E+10	1.40E+00	8.40E+03	0.00E+00	1	0	0	2	0	0	1	0	0	2	0	0	0	0	0	0	0	0	
OH-	H	NONE	E-	H2O	NONE	1.00E+00	1.00E+00	0.00E+00	1.00E+00	1.00E+00	0.00E+00	7.00E+08	0.00E+00	7.00E+08	0.00E+00	1.30E+04	0.00E+00	1	1	0	0	2	0	1	0	0	0	1	0	-1	0	0	-1	0	0	
E-	H	H2O	OH-	H2	NONE	1.00E+00	1.00E+00	1.00E+00	1.00E+00	1.00E+00	0.00E+00	4.80E+09	0.00E+00	4.80E+09	0.00E+00	1.30E+04	0.00E+00	0	1	2	1	2	0	0	0	1	1	0	0	-1	0	0	-1	0	0	
E-	HO2-	H2O	OH	OH-	NONE	1.00E+00	1.00E+00	1.00E+00	1.00E+00	2.00E+00	0.00E+00	5.40E+08	0.00E+00	5.40E+08	0.00E+00	1.30E+04	0.00E+00	0	1	2	1	1	0	0	2	1	1	1	0	-1	-1	0	0	-1	0	
H	OH	NONE	H2O	NONE	NONE	1.00E+00	1.00E+00	0.00E+00	1.00E+00	0.00E+00	0.00E+00	2.30E+11	0.00E+00	2.30E+11	0.00E+00	1.30E+04	0.00E+00	1	1	0	2	0	0	0	1	0	1	0	0	0	0	0	0	0	0	
OH	H2	NONE	H	H2O	NONE	1.00E+00	1.00E+00	0.00E+00	1.00E+00	1.00E+00	0.00E+00	1.40E+09	1.60E+04	1.40E+09	1.60E+04	1.90E+04	0.00E+00	1	2	0	1	2	0	1	0	0	0	1	0	0	0	0	0	0	0	
H	O2	NONE	HO2	NONE	NONE	1.00E+00	1.00E+00	0.00E+00	1.00E+00	0.00E+00	0.00E+00	1.50E+11	0.00E+00	1.50E+11	0.00E+00	1.30E+04	0.00E+00	1	0	0	1	0	0	0	2	0	2	0	0	0	0	0	0	0	0	
H	HO2	NONE	H2O2	NONE	NONE	1.00E+00	1.00E+00	0.00E+00	1.00E+00	0.00E+00	0.00E+00	3.00E+11	0.00E+00	3.00E+11	0.00E+00	1.30E+04	0.00E+00	1	1	0	2	0	0	0	2	0	2	0	0	0	0	0	0	0	0	
H	O2-	NONE	HO2-	NONE	NONE	1.00E+00	1.00E+00	0.00E+00	1.00E+00	0.00E+00	0.00E+00	3.00E+11	0.00E+00	3.00E+11	0.00E+00	1.30E+04	0.00E+00	1	0	0	1	0	0	0	2	0	2	0	0	0	-1	0	-1	0	0	
E-	O2-	H2O	HO2-	OH-	NONE	1.00E+00	1.00E+00	1.00E+00	1.00E+00	1.00E+00	0.00E+00	3.60E+09	0.00E+00	3.60E+09	0.00E+00	1.30E+04	0.00E+00	0	0	2	1	1	0	0	2	1	2	1	0	-1	-1	0	-1	-1	0	
H	H2O2	NONE	OH	H2O	NONE	1.00E+00	1.00E+00	0.00E+00	1.00E+00	1.00E+00	0.00E+00	2.00E+09	0.00E+00	2.00E+09	0.00E+00	1.90E+04	0.00E+00	1	2	0	1	2	0	0	2	0	1	1	0	0	0	0	0	0	0	
OH	H2O2	NONE	H2O	HO2	NONE	1.00E+00	1.00E+00	0.00E+00	1.00E+00	1.00E+00	0.00E+00	4.20E+08	0.00E+00	4.20E+08	0.00E+00	1.40E+04	0.00E+00	1	2	0	2	1	0	1	2	0	1	2	0	0	0	0	0	0	0	
OH	HO2	NONE	H2O	O2	NONE	1.00E+00	1.00E+00	0.00E+00	1.00E+00	1.00E+00	0.00E+00	1.00E+11	0.00E+00	1.00E+11	0.00E+00	1.30E+04	0.00E+00	1	1	0	2	0	0	1	2	0	1	2	0	0	0	0	0	0	0	
HO2	NONE	NONE	H2O2	O2	NONE	2.00E+00	0.00E+00	0.00E+00	1.00E+00	1.00E+00	0.00E+00	5.00E+07	0.00E+00	5.00E+07	0.00E+00	1.90E+04	0.00E+00	1	0	0	2	0	0	2	0	0	2	2	0	0	0	0	0	0	0	
HO2	NONE	NONE	O2-	H+	NONE	1.00E+00	0.00E+00	0.00E+00	1.00E+00	1.00E+00	0.00E+00	3.90E+05	7.70E+11	3.90E+05	7.70E+11	1.30E+04	1.30E+04	1	0	0	0	1	0	2	0	0	2	0	0	0	0	0	-1	1	0	
HO2	O2-	NONE	O2	HO2-	NONE	1.00E+00	1.00E+00	0.00E+00	1.00E+00	1.00E+00	0.00E+00	5.00E+08	0.00E+00	5.00E+08	0.00E+00	1.90E+04	0.00E+00	1	0	0	0	1	0	2	2	0	2	2	0	0	-1	0	0	-1	0	
O2-	OH	NONE	OH-	O2	NONE	1.00E+00	1.00E+00	0.00E+00	1.00E+00	1.00E+00	0.00E+00	2.90E+11	0.00E+00	2.90E+11	0.00E+00	1.30E+04	0.00E+00	0	1	0	1	0	0	2	1	0	1	2	0	-1	0	0	-1	0	0	
O2-	H2O	NONE	O2	H2O2	OH-	2.00E+00	2.00E+00	0.00E+00	1.00E+00	1.00E+00	2.00E+00	1.30E+05	0.00E+00	1.30E+05	0.00E+00	1.90E+04	0.00E+00	0	2	0	0	2	1	2	1	0	2	2	1	-1	0	0	0	0	-1	
E-	H2O	NONE	H	OH-	NONE	1.00E+00	1.00E+00	0.00E+00	1.00E+00	1.00E+00	0.00E+00	2.90E+02	0.00E+00	2.90E+02	0.00E+00	1.30E+04	0.00E+00	0	2	0	1	1	0	0	1	0	0	1	0	-1	0	0	0	-1	0	
E-	H+	NONE	H	NONE	NONE	1.00E+00	1.00E+00	0.00E+00	1.00E+00	0.00E+00	0.00E+00	2.60E+11	0.00E+00	2.60E+11	0.00E+00	1.30E+04	0.00E+00	0	1	0	1	0	0	0	0	0	0	0	0	-1	1	0	0	0	0	
E-	OH	NONE	OH-	NONE	NONE	1.00E+00	1.00E+00	0.00E+00	1.00E+00	0.00E+00	0.00E+00	2.90E+11	0.00E+00	2.90E+11	0.00E+00	1.30E+04	0.00E+00	0	1	0	1	0	0	0	1	0	1	0	0	-1	0	0	-1	0	0	
E-	H2O2	NONE	OH	OH-	NONE	1.00E+00	1.00E+00	0.00E+00	1.00E+00	1.00E+00	0.00E+00	2.40E+11	0.00E+00	2.40E+11	0.00E+00	1.30E+04	0.00E+00	0	2	0	1	1	0	0	2	0	1	1	0	-1	0	0	0	-1	0	
H2O2	OH-	NONE	HO2-	H2O	NONE	1.00E+00	1.00E+00	0.00E+00	1.00E+00	1.00E+00	0.00E+00	1.00E+10	2.10E+05	0.00E+00	0.00E+00	1.30E+04	1.30E+04	2	1	0	1	2	0	2	1	0	2	1	0	0	-1	0	0	-1	0	
H2O2	NONE	NONE	O2	H2O	NONE	1.00E+00	0.00E+00	0.00E+00	5.00E-01	1.00E+00	0.00E+00	1.40E-02	0.00E+00	1.40E-02	0.00E+00	6.00E+04	0.00E+00	2	0	0	0	2	0	2	0	0	2	1	0	0	0	0	0	0	0	

	GVALUE	DATA	FILE	GVN:	7
	GID	data1	data2	data3	
H2	6.00E-01	1.50E+00	1.65E+00		
H2O2	5.50E-01	1.14E+00	1.55E+00		
H	9.00E-01	5.00E-01	1.20E-01		
OH	4.50E+00	1.70E+00	4.50E-01		
HO2	0.00E+00	4.00E-02	0.00E+00		
H+	3.50E+00	6.00E-01	1.30E-01		
E-	3.50E+00	6.00E-01	1.30E-01		

	ECP-INPU	DATA	FILE										
	CURRENT	DENSITY	DATA	IECPE	8H2O2	O2	H2	H+	LiOH	Li+	H2O	Fe2+	
	IECPN	IECPR1	IECPR2	IECPP1	IECPP2	IPWRR1	IPWRR2	IPWRP1	IPWRP2	RECPV1	RECPV2	IECPV1	RECPV3
	1	1	4.00E+00	-7.00E+00	0	1	2	2	0	5.00E-06	4.50E-01	2	1.58E+00
	2	1	6	-5	0	1	2	2	0	5.00E-10	3.00E-01	2	8.85E-01
	3	2	4	-1	0	1.00E+00	2.00E+00	1	0	2.00E-04	7.00E-01	2	4.80E-01
	4	4	0	-3	0	2.00E+00	0.00E+00	1	0	5.00E-04	5.00E-01	2	0.00E+00
	5.00E+00	-1.00E+00	0.00E+00	2.00E+00	4.00E+00	1.00E+00	0.00E+00	1.00E+00	2.00E+00	1.00E-01	5.00E-01	2.00E+00	4.80E-01
	6.00E+00	-3.00E+00	0.00E+00	4.00E+00	0.00E+00	1.00E+00	0.00E+00	2.00E+00	0.00E+00	5.00E-05	3.00E-01	2.00E+00	0.00E+00
	7.00E+00	0.00E+00	0.00E+00	8.00E+00	0.00E+00	0.00E+00	0.00E+00	1.00E+00	0.00E+00	1.00E-03	5.00E-01	2.00E+00	-4.40E-01
	ISOLP	SOLPHH	SOLPHL	AAH0:	5.00E+00	8.50E+00	6.50E+00	H+					
	TISOL	(FSOLF(1)	FSOLF(2)	FSOLF(3)	FSOLF(4)	FSOLF(5)	FSOLF(6)	FSOLF(7)	FSOLF(8)	FSOLF(9)	FSOLF(10)	FSOLF(11)	FSOLF(12)
	5.70E+02	1.90E-01	-1.00E+01	2.00E+00	-7.80E+00	2.50E-01	-7.00E+00	2.00E+00	-7.00E+00	-1.00E-01	-6.90E+00	2.00E+00	-6.90E+00
	5.20E+02	2.90E-01	-1.00E+01	2.00E+00	-8.10E+00	2.00E-01	-7.00E+00	2.00E+00	-6.50E+00	-2.20E-01	-6.90E+00	2.00E+00	-6.30E+00
	4.70E+02	3.00E-01	-1.10E+01	2.00E+00	-8.20E+00	1.80E-01	-7.00E+00	2.00E+00	-6.00E+00	-1.00E-01	-6.90E+00	2.00E+00	-5.90E+00
	4.20E+02	3.50E-01	-1.10E+01	2.00E+00	-8.60E+00	1.80E-01	-6.70E+00	2.00E+00	-5.70E+00	-1.00E-01	-7.00E+00	2.00E+00	-5.70E+00
	3.70E+02	4.50E-01	-1.10E+01	2.00E+00	-8.90E+00	1.80E-01	-6.70E+00	2.00E+00	-5.70E+00	-1.00E-01	-7.00E+00	2.00E+00	-5.70E+00
	HHOXD1	HHBND1	1.00E-05	1.00E-04									
	<<<<<<<<<	Iteration	no.->	1Case	#	1.00E+00							

Table A-1.1 b) Example of output (PWR INCA in-pile loop analysis): list of output data

| | Summary | of | the | INPUT | data | PWR | INCA | in- | pile | loop | calculation | test | case s2023 | Nov | | |

Table A-1.2 Input data of Example 2 for calculation of PWR primary loop: confirmation of input data

	Summary	of	the	INPUT	data	PWR	primaloop	calcutest	case	for	hydroinjecanalyprepaby
Case:	9iitermax:	5									
	IPREGN:										
	1.60E+03	2.00E+00	1.00E+00	1.00E+00	1.00E+00	1.00E+00					
	1.60E+03	2.00E+00	1.00E+00	1.00E+00	1.00E+00	1.00E+01					
	1.60E+03	2.00E+00	1.00E+00	1.00E+00	1.00E+00	1.00E+02					
	1.60E+03	2.00E+00	1.00E+00	1.00E+00	1.00E+00	2.00E+02					
	1.60E+03	2.00E+00	1.00E+00	1.00E+00	1.00E+00	5.00E+02					
	1.60E+03	2.00E+00	1.00E+00	1.00E+00	1.00E+00	1.00E+03					
	1.60E+03	2.00E+00	1.00E+00	1.00E+00	1.00E+00	2.00E+03					
	1.60E+03	2.00E+00	1.00E+00	1.00E+00	1.00E+00	5.00E+03					
	1.60E+03	2.00E+00	1.00E+00	1.00E+00	1.00E+00	1.00E+04					

	RT-INPUT	DATA	FILE	REG:	1.40E+01															
#	RT	TEM	G2	SOV	QG3	QN3	QA3	VAL(14)	VAL(15)	VAL(16)	VAL(1)	VAL(2)	VAL(3)	VAL(4)	VAL(5)	VAL(6)	VAL(7)	VAL(8)	VAL(9)	VAL(10)
	2.00E+00	5.83E+02	4.50E+00	3.00E+02	7.50E+02	1.00E+03	0.00E+00	5.53E+02	1.00E-01	1.33E-02	5.53E+02	0.00E+00	5.00E+01	1.00E+00	5.00E+01	1.00E+00	1.00E-03	1.00E-05	1.50E+00	1.50E+00
	2.00E+00	5.83E+02	4.50E+00	3.00E+02	1.50E+03	5.00E+03	6.00E+02	5.53E+02	1.00E-01	1.33E-02	5.53E+02	0.00E+00	5.00E+01	1.00E+00	5.00E+01	1.00E+00	5.00E-04	1.00E-05	1.50E+00	1.50E+00
	1.00E+00	5.83E+02	4.50E+00	3.00E+02	1.50E+03	5.00E+03	6.00E+02	5.53E+02	1.00E-01	1.33E-02	5.53E+02	0.00E+00	5.00E+01	1.00E+00	5.00E+01	1.00E+00	5.00E-04	1.00E-05	1.50E+00	1.50E+00
	2.00E+00	5.83E+02	4.50E+00	3.00E+02	7.50E+02	1.00E+03	0.00E+00	5.53E+02	1.00E-01	1.33E-02	5.53E+02	0.00E+00	5.00E+01	1.00E+00	5.00E+01	1.00E+00	5.00E-04	1.00E-05	1.50E+00	1.50E+00
	2.00E+00	5.83E+02	4.50E+00	3.00E+02	7.50E+02	2.50E+03	3.00E+02	5.53E+02	1.00E-01	1.33E-02	5.53E+02	0.00E+00	5.00E+01	1.00E+00	5.00E+01	1.00E+00	5.00E-04	1.00E-05	1.50E+00	1.50E+00
	1.00E+00	5.83E+02	4.50E+00	3.00E+02	7.50E+02	2.50E+03	3.00E+02	5.53E+02	1.00E-01	1.33E-02	5.53E+02	0.00E+00	5.00E+01	1.00E+00	5.00E+01	1.00E+00	5.00E-04	1.00E-05	1.50E+00	1.50E+00
	1.00E+00	5.83E+02	1.00E+00	3.00E+02	3.75E+02	5.00E+02	0.00E+00	5.53E+02	1.00E-01	1.33E-02	5.53E+02	0.00E+00	5.00E+01	1.00E+00	5.00E+01	1.00E+00	5.00E-04	1.00E-05	1.50E+00	1.50E+00
	1.00E+00	5.83E+02	1.00E+00	3.00E+02	0.00E+00	0.00E+00	0.00E+00	5.53E+02	1.00E-01	1.33E-02	5.53E+02	0.00E+00	5.00E+01	1.00E+00	5.00E+01	1.00E+00	1.00E-03	1.00E-05	1.50E+00	1.50E+00
	1.00E+00	5.83E+02	1.00E+00	3.00E+02	0.00E+00	0.00E+00	0.00E+00	5.53E+02	1.00E-01	1.33E-02	5.53E+02	0.00E+00	5.00E+01	1.00E+00	5.00E+01	1.00E+00	1.00E-03	1.00E-05	1.50E+00	1.50E+00
	1.00E+00	5.83E+02	1.00E-01	3.00E+02	6.00E-03	0.00E+00	0.00E+00	5.53E+02	1.00E-01	1.33E-02	5.53E+02	0.00E+00	5.00E+01	1.00E+00	5.00E+01	1.00E+00	5.00E-04	1.00E-05	1.50E+00	1.50E+00
	1.00E+00	5.83E+02	1.00E-01	3.00E+02	6.00E-03	0.00E+00	0.00E+00	5.53E+02	1.00E-01	1.33E-02	5.53E+02	0.00E+00	5.00E+01	1.00E+00	5.00E+01	1.00E+00	5.00E-04	1.00E-05	1.50E+00	1.50E+00
	1.00E+00	5.83E+02	1.00E-01	3.00E+02	6.00E-03	0.00E+00	0.00E+00	5.53E+02	1.00E-01	1.33E-02	5.53E+02	0.00E+00	5.00E+01	1.00E+00	5.00E+01	1.00E+00	5.00E-04	1.00E-05	1.50E+00	1.50E+00
	1.00E+00	5.83E+02	1.00E-01	3.00E+02	6.00E-03	0.00E+00	0.00E+00	5.53E+02	1.00E-01	1.33E-02	5.53E+02	0.00E+00	5.00E+01	1.00E+00	5.00E+01	1.00E+00	5.00E-04	1.00E-05	1.50E+00	1.50E+00
	1.00E+00	5.83E+02	1.00E+00	3.00E+02	0.00E+00	0.00E+00	0.00E+00	5.53E+02	1.00E-01	1.33E-02	5.53E+02	0.00E+00	5.00E+01	1.00E+00	5.00E+01	1.00E+00	1.00E-03	1.00E-05	1.50E+00	1.50E+00

	NodeConn	Data	FILE	NCN:	16
	PNDN	NDN	RRMIX	LNDN	GNDN
	1	2	1.00E+00	0	0
	2	3	1.00E+00	0	0
	3	4	1.00E+00	0	0
	4	8	5.00E-01	0	0
	1	5	1.00E+00	0	0
	5	6	1.00E+00	0	0
	6	7	1.00E+00	0	0
	7	8	5.00E-01	0	0
	8	9	-1.00E+00	0	0
	9	10	1.00E+00	0	0
	10	11	1.00E+00	0	0
	11	14	5.00E-01	0	0
	9	12	1.00E+00	0	0
	12	13	1.00E+00	0	0
	13	14	5.00E-01	0	0
	14	1	1.00E+00	0	0

	REACTION	DATA	FILE	RN:	43								
	F1	F2	F3	R1	R2	R3	FN1	FN2	FN3	RN1	RN2	RN3	FK0
H+	OH-	NONE	H2O	NONE	NONE	1.00E+00	1.00E+00	0.00E+00	1.00E+00	0.00E+00	0.00E+00	1.50E+12	7.50E+00
H2O2	NONE	NONE	OH	NONE	NONE	1.00E+00	0.00E+00	0.00E+00	2.00E+00	0.00E+00	0.00E+00	0.00E+00	0.00E+00
B0	OH-	NONE	B1-	NONE	NONE	1.00E+00	1.00E+00	0.00E+00	1.00E+00	0.00E+00	0.00E+00	6.20E+01	1.00E+00
B0	OH-	NONE	B2-	NONE	NONE	2.00E+00	1.00E+00	0.00E+00	1.00E+00	0.00E+00	0.00E+00	9.60E+01	1.00E+00
B0	OH-	NONE	B3-	NONE	NONE	3.00E+00	1.00E+00	0.00E+00	1.00E+00	0.00E+00	0.00E+00	2.00E+02	1.00E+00
B0	OH-	NONE	B4-	NONE	NONE	4.00E+00	2.00E+00	0.00E+00	1.00E+00	0.00E+00	0.00E+00	9.60E+03	1.00E+00
LiOH	NONE	NONE	Li+	OH-	NONE	1.00E+00	0.00E+00	0.00E+00	1.00E+00	1.00E+00	0.00E+00	1.00E+02	1.00E+01
B1-	H+	NONE	B1H	NONE	NONE	1.00E+00	1.00E+00	0.00E+00	1.00E+00	0.00E+00	0.00E+00	1.00E+01	1.00E+01
B2-	H+	NONE	B2H	NONE	NONE	1.00E+00	1.00E+00	0.00E+00	1.00E+00	0.00E+00	0.00E+00	1.00E+01	1.00E+01
B3-	H+	NONE	B3H	NONE	NONE	1.00E+00	1.00E+00	0.00E+00	1.00E+00	0.00E+00	0.00E+00	1.00E+01	1.00E+01
B4-	H+	NONE	B4H	NONE	NONE	1.00E+00	2.00E+00	0.00E+00	1.00E+00	0.00E+00	0.00E+00	1.00E+01	1.00E+01
B1-	Li+	NONE	B1L	NONE	NONE	1.00E+00	1.00E+00	0.00E+00	1.00E+00	0.00E+00	0.00E+00	1.00E+01	1.00E+01
B2-	Li+	NONE	B2L	NONE	NONE	1.00E+00	1.00E+00	0.00E+00	1.00E+00	0.00E+00	0.00E+00	1.00E+01	1.00E+01
B3-	Li+	NONE	B3L	NONE	NONE	1.00E+00	1.00E+00	0.00E+00	1.00E+00	0.00E+00	0.00E+00	1.00E+01	1.00E+01
B4-	Li+	NONE	B4L	NONE	NONE	1.00E+00	2.00E+00	0.00E+00	1.00E+00	0.00E+00	0.00E+00	1.00E+01	1.00E+01
H	H	NONE	H2	NONE	NONE	1.00E+00	1.00E+00	0.00E+00	1.00E+00	0.00E+00	0.00E+00	9.00E+10	0.00E+00
E-	HO2	NONE	HO2-	NONE	NONE	1.00E+00	1.00E+00	0.00E+00	1.00E+00	0.00E+00	0.00E+00	3.00E+11	0.00E+00
E-	O2	NONE	O2-	NONE	NONE	1.00E+00	1.00E+00	0.00E+00	1.00E+00	0.00E+00	0.00E+00	2.60E+11	0.00E+00
E-	H2O	NONE	H2	OH-	NONE	2.00E+00	2.00E+00	0.00E+00	1.00E+00	2.00E+00	0.00E+00	1.80E+06	0.00E+00
OH	NONE	NONE	H2O2	NONE	NONE	2.00E+00	0.00E+00	0.00E+00	1.00E+00	0.00E+00	0.00E+00	2.50E+10	0.00E+00
OH-	H	NONE	E-	H2O	NONE	1.00E+00	1.00E+00	0.00E+00	1.00E+00	1.00E+00	0.00E+00	7.00E+08	0.00E+00
E-	H	H2O	OH-	H2	NONE	1.00E+00	1.00E+00	1.00E+00	1.00E+00	1.00E+00	0.00E+00	4.80E+09	0.00E+00
E-	HO2-	H2O	OH	OH-	NONE	1.00E+00	1.00E+00	1.00E+00	1.00E+00	2.00E+00	0.00E+00	5.40E+08	0.00E+00
H	OH	NONE	H2O	NONE	NONE	1.00E+00	1.00E+00	0.00E+00	1.00E+00	0.00E+00	0.00E+00	2.30E+11	0.00E+00
OH	H2	NONE	H	H2O	NONE	1.00E+00	1.00E+00	0.00E+00	1.00E+00	1.00E+00	0.00E+00	1.40E+09	0.00E+00
H	O2	NONE	HO2	NONE	NONE	1.00E+00	1.00E+00	0.00E+00	1.00E+00	0.00E+00	0.00E+00	1.50E+11	0.00E+00
H	HO2	NONE	H2O2	NONE	NONE	1.00E+00	1.00E+00	0.00E+00	1.00E+00	0.00E+00	0.00E+00	3.00E+11	0.00E+00
H	O2-	NONE	HO2-	NONE	NONE	1.00E+00	1.00E+00	0.00E+00	1.00E+00	0.00E+00	0.00E+00	3.00E+11	0.00E+00
E-	O2-	H2O	HO2-	OH-	NONE	1.00E+00	1.00E+00	1.00E+00	1.00E+00	1.00E+00	0.00E+00	3.60E+09	0.00E+00
H	H2O2	NONE	OH	H2O	NONE	1.00E+00	1.00E+00	0.00E+00	1.00E+00	1.00E+00	0.00E+00	2.00E+09	0.00E+00
OH	H2O2	NONE	H2O	HO2	NONE	1.00E+00	1.00E+00	0.00E+00	1.00E+00	1.00E+00	0.00E+00	4.20E+08	0.00E+00
OH	HO2	NONE	H2O	O2	NONE	1.00E+00	1.00E+00	0.00E+00	1.00E+00	1.00E+00	0.00E+00	1.00E+11	0.00E+00
HO2	NONE	NONE	H2O2	O2	NONE	2.00E+00	0.00E+00	0.00E+00	1.00E+00	1.00E+00	0.00E+00	5.00E+07	0.00E+00
HO2	NONE	NONE	O2-	H+	NONE	1.00E+00	0.00E+00	0.00E+00	1.00E+00	1.00E+00	0.00E+00	3.90E+05	7.70E+11
HO2	O2-	NONE	O2	HO2-	NONE	1.00E+00	1.00E+00	0.00E+00	1.00E+00	1.00E+00	0.00E+00	5.00E+08	0.00E+00
O2-	OH	NONE	OH-	O2	NONE	1.00E+00	1.00E+00	0.00E+00	1.00E+00	1.00E+00	0.00E+00	2.90E+11	0.00E+00
O2-	H2O	NONE	O2	H2O2	OH-	2.00E+00	2.00E+00	0.00E+00	1.00E+00	1.00E+00	2.00E+00	1.30E+05	0.00E+00
E-	H2O	NONE	H	OH-	NONE	1.00E+00	1.00E+00	0.00E+00	1.00E+00	1.00E+00	0.00E+00	2.90E+02	0.00E+00
E-	H+	NONE	H	NONE	NONE	1.00E+00	1.00E+00	0.00E+00	1.00E+00	0.00E+00	0.00E+00	2.60E+11	0.00E+00
E-	OH	NONE	OH-	NONE	NONE	1.00E+00	1.00E+00	0.00E+00	1.00E+00	0.00E+00	0.00E+00	2.90E+11	0.00E+00
E-	H2O2	NONE	OH	OH-	NONE	1.00E+00	1.00E+00	0.00E+00	1.00E+00	1.00E+00	0.00E+00	2.40E+11	0.00E+00
H2O2	OH-	NONE	HO2-	H2O	NONE	1.00E+00	1.00E+00	0.00E+00	1.00E+00	1.00E+00	0.00E+00	1.00E+10	2.10E+05
H2O2	NONE	NONE	O2	H2O	NONE	1.00E+00	0.00E+00	0.00E+00	5.00E-01	1.00E+00	0.00E+00	1.40E-02	0.00E+00

	RK0	WFK0	WRK0	FAE)	RAE	FHN1	FHN2	FHN3	RHN1	RHN2	RHN3	FON1	FON2	FON3	RON1	RON2	RON3	FCH1	FCH2	FCH3	RCH1
H+	1.50E+12	7.50E+00	1.30E+04	4.00E+04	1	1	0	2	0	0	0	1	0	1	0	0	1	-1	0	0	0
H2O2	0.00E+00	0.00E+00	6.00E+04	0.00E+00	2	0	0	1	0	0	2	0	0	1	0	0	0	0	0	0	0
B0	6.20E+02	1.00E+01	0.00E+00	0.00E+00	0	1	0	1	0	0	0	1	0	1	0	0	0	-1	0	-1	0
B0	9.60E+02	1.00E+01	0.00E+00	0.00E+00	0	1	0	1	0	0	0	1	0	1	0	0	0	-1	0	-1	0
B0	2.00E+02	1.00E+01	0.00E+00	0.00E+00	0	1	0	1	0	0	0	1	0	1	0	0	0	-1	0	-1	0
B0	9.60E+03	1.00E+01	0.00E+00	0.00E+00	0	1	0	2	0	0	0	1	0	2	0	0	0	-1	0	-2	0
LiOH	0.00E+00	0.00E+00	0.00E+00	0.00E+00	1	0	0	0	1	0	1	0	0	0	1	0	0	0	0	1	-1
B1-	0.00E+00	0.00E+00	0.00E+00	0.00E+00	1	1	0	2	0	0	1	0	0	1	0	0	-1	1	0	0	0
B2-	0.00E+00	0.00E+00	0.00E+00	0.00E+00	1	1	0	2	0	0	1	0	0	1	0	0	-1	1	0	0	0
B3-	0.00E+00	0.00E+00	0.00E+00	0.00E+00	1	1	0	2	0	0	1	0	0	1	0	0	-1	1	0	0	0
B4-	0.00E+00	0.00E+00	0.00E+00	0.00E+00	2	1	0	4	0	0	2	0	0	2	0	0	-2	1	0	0	0
B1-	0.00E+00	0.00E+00	0.00E+00	0.00E+00	1	0	0	1	0	0	1	0	0	1	0	0	-1	1	0	0	0
B2-	0.00E+00	0.00E+00	0.00E+00	0.00E+00	1	0	0	1	0	0	1	0	0	1	0	0	-1	1	0	0	0
B3-	0.00E+00	0.00E+00	0.00E+00	0.00E+00	1	0	0	1	0	0	1	0	0	1	0	0	-1	1	0	0	0
B4-	0.00E+00	0.00E+00	0.00E+00	0.00E+00	2	0	0	2	0	0	2	0	0	2	0	0	-2	1	0	0	0
H	9.00E+10	0.00E+00	1.30E+04	0.00E+00	1	1	0	2	0	0	0	0	0	0	0	0	0	0	0	0	0
E-	3.00E+11	0.00E+00	1.30E+04	0.00E+00	0	1	0	1	0	0	0	2	0	2	0	0	-1	0	0	-1	0
E-	2.60E+11	0.00E+00	1.30E+04	0.00E+00	0	0	0	0	0	0	0	2	0	2	0	0	-1	0	0	-1	0
E-	1.80E+06	0.00E+00	1.30E+04	0.00E+00	0	2	0	2	1	0	0	1	0	0	1	0	-1	0	0	0	-1
OH	2.50E+10	1.40E+00	8.40E+03	0.00E+00	1	0	0	2	0	0	1	0	0	2	0	0	0	0	0	0	0
OH-	7.00E+08	0.00E+00	1.30E+04	0.00E+00	1	1	0	0	2	0	1	0	0	0	1	0	-1	0	0	-1	0
E-	4.80E+09	0.00E+00	1.30E+04	0.00E+00	0	1	2	1	2	0	0	0	1	1	0	0	-1	0	0	-1	0
E-	5.40E+08	0.00E+00	1.30E+04	0.00E+00	0	1	2	1	1	0	0	2	1	1	1	0	-1	-1	0	0	-1
H	2.30E+11	0.00E+00	1.30E+04	0.00E+00	1	1	0	2	0	0	0	1	0	1	0	0	0	0	0	0	0
OH	1.40E+09	0.00E+00	1.90E+04	0.00E+00	1	2	0	1	2	0	1	0	0	0	1	0	0	0	0	0	0
H	1.50E+11	0.00E+00	1.30E+04	0.00E+00	1	0	0	1	0	0	0	2	0	2	0	0	0	0	0	0	0
H	3.00E+11	0.00E+00	1.30E+04	0.00E+00	1	1	0	2	0	0	0	2	0	2	0	0	0	0	0	0	0
H	3.00E+11	0.00E+00	1.30E+04	0.00E+00	1	0	0	1	0	0	0	2	0	2	0	0	0	-1	0	-1	0
E-	3.60E+09	0.00E+00	1.30E+04	0.00E+00	0	0	2	1	1	0	0	2	1	2	1	0	-1	-1	0	-1	-1
H	2.00E+09	0.00E+00	1.90E+04	0.00E+00	1	2	0	1	2	0	0	2	0	1	1	0	0	0	0	0	0
OH	4.20E+08	0.00E+00	1.40E+04	0.00E+00	1	2	0	2	1	0	1	2	0	1	2	0	0	0	0	0	0
OH	1.00E+11	0.00E+00	1.30E+04	0.00E+00	1	1	0	2	0	0	1	2	0	1	2	0	0	0	0	0	0
HO2	5.00E+07	0.00E+00	1.90E+04	0.00E+00	1	0	0	2	0	0	2	0	0	2	2	0	0	0	0	0	0
HO2	3.90E+05	7.70E+11	1.30E+04	1.30E+04	1	0	0	0	1	0	2	0	0	2	0	0	0	0	0	-1	1
HO2	5.00E+08	0.00E+00	1.90E+04	0.00E+00	1	0	0	0	1	0	2	2	0	2	2	0	0	-1	0	0	-1
O2-	2.90E+11	0.00E+00	1.30E+04	0.00E+00	0	1	0	1	0	0	2	1	0	1	2	0	-1	0	0	-1	0
O2-	1.30E+05	0.00E+00	1.90E+04	0.00E+00	0	2	0	0	2	1	2	1	0	2	2	1	-1	0	0	0	0
E-	2.90E+02	0.00E+00	1.30E+04	0.00E+00	0	2	0	1	1	0	0	1	0	0	1	0	-1	0	0	0	-1
E-	2.60E+11	0.00E+00	1.30E+04	0.00E+00	0	1	0	1	0	0	0	0	0	0	0	0	-1	1	0	0	0
E-	2.90E+11	0.00E+00	1.30E+04	0.00E+00	0	1	0	1	0	0	0	1	0	1	0	0	-1	0	0	-1	0
E-	2.40E+11	0.00E+00	1.30E+04	0.00E+00	0	2	0	1	1	0	0	2	0	1	1	0	-1	0	0	0	-1
H2O2	0.00E+00	0.00E+00	1.30E+04	1.30E+04	2	1	0	1	2	0	2	1	0	2	1	0	0	-1	0	0	-1
H2O2	1.40E-02	0.00E+00	6.00E+04	0.00E+00	2	0	0	0	2	0	2	0	0	2	1	0	0	0	0	0	0

	GVALUE	DATA	FILE	GVN:	7
	GID	data1	data2	data3	
H2	6.00E-01	1.50E+00	1.65E+00		
H2O2	5.50E-01	1.14E+00	1.55E+00		
H	9.00E-01	5.00E-01	1.20E-01		
OH	4.50E+00	1.70E+00	4.50E-01		
HO2	0.00E+00	4.00E-02	0.00E+00		
H+	3.50E+00	6.00E-01	1.30E-01		
E-	3.50E+00	6.00E-01	1.30E-01		

	ECP-INPU	DATA	FILE										
	CURRENT	DENSITY	DATA	IECPE	8H2O2	O2	H2	H+	LiOH	Li+	H2O	Fe2+	
	IECPN	IECPR1	IECPR2	IECPP1	IECPP2	IPWRR1	IPWRR2	IPWRP1	IPWRP2	RECPV1	RECPV2	IECPV1	RECPV3
	1.00E+00	1.00E+00	4.00E+00	-7.00E+00	0.00E+00	1.00E+00	2.00E+00	2.00E+00	0.00E+00	5.00E-05	4.50E-01	2.00E+00	1.58E+00
	2.00E+00	2.00E+00	4.00E+00	-1.00E+00	0.00E+00	1.00E+00	2.00E+00	1.00E+00	0.00E+00	5.00E-03	5.00E-01	2.00E+00	4.80E-01
	3.00E+00	4.00E+00	0.00E+00	-3.00E+00	0.00E+00	2.00E+00	0.00E+00	1.00E+00	0.00E+00	1.00E-08	5.00E-01	2.00E+00	0.00E+00
	4.00E+00	-1.00E+00	4.00E+00	2.00E+00	4.00E+00	1.00E+00	2.00E+00	1.00E+00	2.00E+00	5.00E-06	5.00E-01	2.00E+00	4.80E-01
	5.00E+00	-3.00E+00	0.00E+00	4.00E+00	0.00E+00	1.00E+00	0.00E+00	2.00E+00	0.00E+00	1.00E-06	3.00E-01	2.00E+00	0.00E+00
	6.00E+00	0.00E+00	0.00E+00	8.00E+00	0.00E+00	0.00E+00	0.00E+00	1.00E+00	0.00E+00	1.00E-03	5.00E-01	2.00E+00	-4.40E-01
	ISOLP	SOLPHH	SOLPHL	AAH0:	5.00E+00	8.50E+00	6.50E+00	H+					
	TISOL	(FSOLF(1)	FSOLF(2)	FSOLF(3)	FSOLF(4)	FSOLF(5)	FSOLF(6)	FSOLF(7)	FSOLF(8)	FSOLF(9)	FSOLF(10)	FSOLF(11)	FSOLF(12)
	5.70E+02	1.90E-01	-1.00E+01	2.00E+00	-7.80E+00	2.50E-01	-7.00E+00	2.00E+00	-7.00E+00	-1.00E-01	-6.90E+00	2.00E+00	-6.90E+00
	5.20E+02	2.90E-01	-1.00E+01	2.00E+00	-8.10E+00	2.00E-01	-7.00E+00	2.00E+00	-6.50E+00	-2.20E-01	-6.90E+00	2.00E+00	-6.30E+00
	4.70E+02	3.00E-01	-1.10E+01	2.00E+00	-8.20E+00	1.80E-01	-7.00E+00	2.00E+00	-6.00E+00	-1.00E-01	-6.90E+00	2.00E+00	-5.90E+00
	4.20E+02	3.50E-01	-1.10E+01	2.00E+00	-8.60E+00	1.80E-01	-6.70E+00	2.00E+00	-5.70E+00	-1.00E-01	-7.00E+00	2.00E+00	-5.70E+00
	3.70E+02	4.50E-01	-1.10E+01	2.00E+00	-8.90E+00	1.80E-01	-6.70E+00	2.00E+00	-5.70E+00	-1.00E-01	-7.00E+00	2.00E+00	-5.70E+00
	HHOXD1	HHBND1	1.00E-06	1.00E-04									

A-2. BWR Primary Loop Analysis

Table A-2.1 a) Output data of Example 3 for BWR primary loop analysis: confirmation of input data

	Summary	of	the	INPUT	data	BWR	pri	mary	loop	calculation	test	case	study2023	NOV						
Case:	3iitermax:	2																		
	IPREGN:																			
	1.00E-04	1.00E-04	1.00E+00	1.00E+00	1.00E+00	1.00E+00														
	1.00E-04	1.00E-04	1.00E+00	1.00E+00	1.00E+00	1.00E+02														
	1.00E-04	1.00E-04	1.00E+00	1.00E+00	1.00E+00	1.00E+03														
	RT-INPUT	DATA	FILE	REG:	10															
#	RT	TEM	G2	SOV	QG3	QN3	QA3	VAL(14)	VAL(15)	VAL(16)	VAL(1)	VAL(2)	VAL(3)	VAL(4)	VAL(5)	VAL(6)	VAL(7)	VAL(8)	VAL(9)	VAL(10)
	1.00E+00	5.53E+02	1.00E-01	3.00E+02	1.00E+02	1.00E+02	0.00E+00	5.53E+02	1.00E-01	1.33E-02	5.53E+02	0.00E+00	5.00E+01	1.00E+00	5.00E+01	1.00E+00	1.00E-03	1.00E-05	1.50E+00	1.50E+00
	1.00E+00	5.53E+02	1.00E-01	3.00E+02	1.50E+03	1.50E+03	0.00E+00	5.53E+02	1.00E-01	1.33E-02	5.53E+02	1.00E-01	5.00E+01	1.00E+00	5.00E+01	1.00E+00	1.00E-03	5.00E-05	1.66E+00	1.97E+00
	1.00E+00	5.53E+02	1.00E-01	3.00E+02	1.00E+02	1.00E+02	0.00E+00	5.53E+02	1.00E-01	1.33E-02	5.53E+02	5.00E-01	5.00E+01	1.00E+00	5.00E+01	1.00E+00	1.00E-03	5.00E-04	2.55E+00	4.55E+00
	1.00E+00	5.53E+02	1.00E-01	3.00E+02	0.00E+00	0.00E+00	0.00E+00	5.53E+02	1.00E-01	1.33E-02	5.53E+02	0.00E+00	5.00E+01	1.00E+00	5.00E+01	1.00E+00	1.00E-03	1.00E-05	1.50E+00	1.50E+00
	1.00E+00	5.53E+02	1.00E-01	3.00E+02	0.00E+00	0.00E+00	0.00E+00	5.53E+02	1.00E-01	1.33E-02	5.53E+02	0.00E+00	5.00E+01	1.00E+00	5.00E+01	1.00E+00	1.00E-03	1.00E-05	1.50E+00	1.50E+00
	1.00E+00	5.53E+02	1.00E-01	3.00E+02	0.00E+00	0.00E+00	0.00E+00	5.53E+02	1.00E-01	1.33E-02	5.53E+02	0.00E+00	5.00E+01	1.00E+00	5.00E+01	1.00E+00	5.00E-04	1.00E-05	1.50E+00	1.50E+00
	1.00E+00	5.53E+02	1.00E-01	3.00E+02	0.00E+00	0.00E+00	0.00E+00	5.53E+02	1.00E-01	1.33E-02	5.53E+02	0.00E+00	5.00E+01	1.00E+00	5.00E+01	1.00E+00	5.00E-04	1.00E-05	1.50E+00	1.50E+00
	1.00E+00	5.53E+02	1.00E-01	3.00E+02	0.00E+00	0.00E+00	0.00E+00	5.53E+02	1.00E-01	1.33E-02	5.53E+02	0.00E+00	5.00E+01	1.00E+00	5.00E+01	1.00E+00	5.00E-04	1.00E-05	1.50E+00	1.50E+00
	1.00E+00	5.53E+02	1.00E-01	3.00E+02	1.00E+02	0.00E+00	0.00E+00	5.53E+02	1.00E-01	1.33E-02	5.53E+02	0.00E+00	5.00E+01	1.00E+00	5.00E+01	1.00E+00	5.00E-04	1.00E-05	1.50E+00	1.50E+00
	1.00E+00	5.53E+02	1.00E-01	3.00E+02	0.00E+00	0.00E+00	0.00E+00	5.53E+02	1.00E-01	1.33E-02	5.53E+02	0.00E+00	5.00E+01	1.00E+00	5.00E+01	1.00E+00	1.00E-03	1.00E-05	1.50E+00	1.50E+00

	NodeConne	Data	FILE	NCN:	11
	PNDN	NDN	RRMIX	LNDN	GNDN
	1	2	1.00E+00	0	0
	2	3	1.00E+00	0	0
	3	4	-1.00E+00	0	1
	3	5	-1.00E+00	1	0
	5	6	1.00E+00	0	0
	6	7	1.00E+00	0	0
	5	8	1.00E+00	0	0
	8	9	-1.00E+00	0	0
	7	10	5.00E-01	0	0
	9	10	5.00E-01	0	0
	10	1	1.00E+00	0	0

	REACTIO	DATA	FILE	RN:	43																															
	F1	F2	F3	R1	R2	R3	FN1	FN2	FN3	RN1	RN2	RN3	FK0	RK0	WFK0	WRK0	FAE)	RAE	FHN1	FHN2	FHN3	RHN1	RHN2	RHN3	FON1	FON2	FON3	RON1	RON2	RON3	FCH1	FCH2	FCH3	RCH1	RCH2	RCH3
H+	OH-	NONE	H2O	NONE	NONE	1.00E+00	1.00E+00	0.00E+00	1.00E+00	0.00E+00	0.00E+00	1.50E+12	7.50E+00	1.50E+12	7.50E+00	1.30E+04	4.00E+04	1	1	0	2	0	0	0	1	0	1	0	0	1	-1	0	0	0	0	
H2O2	NONE	NONE	OH	NONE	NONE	1.00E+00	0.00E+00	0.00E+00	2.00E+00	0.00E+00	0.00E+00	0.00E+00	0.00E+00	0.00E+00	0.00E+00	6.00E+04	0.00E+00	2	0	0	1	0	0	2	0	0	1	0	0	0	0	0	0	0	0	
B0	OH-	NONE	B1-	NONE	NONE	1.00E+00	1.00E+00	0.00E+00	1.00E+00	0.00E+00	0.00E+00	6.20E+01	1.00E+00	6.20E+02	1.00E+01	0.00E+00	0.00E+00	0	1	0	1	0	0	0	1	0	1	0	0	0	-1	0	-1	0	0	
B0	OH-	NONE	B2-	NONE	NONE	2.00E+00	1.00E+00	0.00E+00	1.00E+00	0.00E+00	0.00E+00	9.60E+01	1.00E+00	9.60E+02	1.00E+01	0.00E+00	0.00E+00	0	1	0	1	0	0	0	1	0	1	0	0	0	-1	0	-1	0	0	
B0	OH-	NONE	B3-	NONE	NONE	3.00E+00	1.00E+00	0.00E+00	1.00E+00	0.00E+00	0.00E+00	2.00E+02	1.00E+00	2.00E+02	1.00E+01	0.00E+00	0.00E+00	0	1	0	1	0	0	0	1	0	1	0	0	0	-1	0	-1	0	0	
B0	OH-	NONE	B4-	NONE	NONE	4.00E+00	2.00E+00	0.00E+00	1.00E+00	0.00E+00	0.00E+00	9.60E+03	1.00E+00	9.60E+03	1.00E+01	0.00E+00	0.00E+00	0	1	0	2	0	0	0	1	0	2	0	0	0	-1	0	-2	0	0	
LiOH	NONE	NONE	Li+	OH-	NONE	1.00E+00	0.00E+00	0.00E+00	1.00E+00	1.00E+00	0.00E+00	1.00E+02	1.00E+01	0.00E+00	0.00E+00	0.00E+00	0.00E+00	1	0	0	0	1	0	1	0	0	0	1	0	0	0	0	1	-1	0	
B1-	H+	NONE	B1H	NONE	NONE	1.00E+00	1.00E+00	0.00E+00	1.00E+00	0.00E+00	0.00E+00	1.00E+01	1.00E+01	0.00E+00	0.00E+00	0.00E+00	0.00E+00	1	1	0	2	0	0	1	0	0	1	0	0	-1	1	0	0	0	0	
B2-	H+	NONE	B2H	NONE	NONE	1.00E+00	1.00E+00	0.00E+00	1.00E+00	0.00E+00	0.00E+00	1.00E+01	1.00E+01	0.00E+00	0.00E+00	0.00E+00	0.00E+00	1	1	0	2	0	0	1	0	0	1	0	0	-1	1	0	0	0	0	
B3-	H+	NONE	B3H	NONE	NONE	1.00E+00	1.00E+00	0.00E+00	1.00E+00	0.00E+00	0.00E+00	1.00E+01	1.00E+01	0.00E+00	0.00E+00	0.00E+00	0.00E+00	1	1	0	2	0	0	1	0	0	1	0	0	-1	1	0	0	0	0	
B4-	H+	NONE	B4H	NONE	NONE	1.00E+00	2.00E+00	0.00E+00	1.00E+00	0.00E+00	0.00E+00	1.00E+01	1.00E+01	0.00E+00	0.00E+00	0.00E+00	0.00E+00	2	1	0	4	0	0	2	0	0	2	0	0	-2	1	0	0	0	0	
B1-	Li+	NONE	B1L	NONE	NONE	1.00E+00	1.00E+00	0.00E+00	1.00E+00	0.00E+00	0.00E+00	1.00E+01	1.00E+01	0.00E+00	0.00E+00	0.00E+00	0.00E+00	1	0	0	1	0	0	1	0	0	1	0	0	-1	1	0	0	0	0	
B2-	Li+	NONE	B2L	NONE	NONE	1.00E+00	1.00E+00	0.00E+00	1.00E+00	0.00E+00	0.00E+00	1.00E+01	1.00E+01	0.00E+00	0.00E+00	0.00E+00	0.00E+00	1	0	0	1	0	0	1	0	0	1	0	0	-1	1	0	0	0	0	
B3-	Li+	NONE	B3L	NONE	NONE	1.00E+00	1.00E+00	0.00E+00	1.00E+00	0.00E+00	0.00E+00	1.00E+01	1.00E+01	0.00E+00	0.00E+00	0.00E+00	0.00E+00	1	0	0	1	0	0	1	0	0	1	0	0	-1	1	0	0	0	0	
B4-	Li+	NONE	B4L	NONE	NONE	1.00E+00	2.00E+00	0.00E+00	1.00E+00	0.00E+00	0.00E+00	1.00E+01	1.00E+01	0.00E+00	0.00E+00	0.00E+00	0.00E+00	2	0	0	2	0	0	2	0	0	2	0	0	-2	1	0	0	0	0	
H	H	NONE	H2	NONE	NONE	1.00E+00	1.00E+00	0.00E+00	1.00E+00	0.00E+00	0.00E+00	9.00E+10	0.00E+00	9.00E+10	0.00E+00	1.30E+04	0.00E+00	1	1	0	2	0	0	0	0	0	0	0	0	0	0	0	0	0	0	
E-	HO2	NONE	HO2-	NONE	NONE	1.00E+00	1.00E+00	0.00E+00	1.00E+00	0.00E+00	0.00E+00	3.00E+11	0.00E+00	3.00E+11	0.00E+00	1.30E+04	0.00E+00	0	1	0	1	0	0	0	2	0	2	0	0	-1	0	0	-1	0	0	
E-	O2	NONE	O2-	NONE	NONE	1.00E+00	1.00E+00	0.00E+00	1.00E+00	0.00E+00	0.00E+00	2.60E+11	0.00E+00	2.60E+11	0.00E+00	1.30E+04	0.00E+00	0	0	0	0	0	0	0	2	0	2	0	0	-1	0	0	-1	0	0	
E-	H2O	NONE	H2	OH-	NONE	2.00E+00	2.00E+00	0.00E+00	1.00E+00	2.00E+00	0.00E+00	1.80E+06	0.00E+00	1.80E+06	0.00E+00	1.30E+04	0.00E+00	0	2	0	2	1	0	0	1	0	0	1	0	-1	0	0	0	-1	0	
OH	NONE	NONE	H2O2	NONE	NONE	2.00E+00	0.00E+00	0.00E+00	1.00E+00	0.00E+00	0.00E+00	2.50E+10	0.00E+00	2.50E+10	1.40E+00	8.40E+03	0.00E+00	1	0	0	2	0	0	1	0	0	2	0	0	0	0	0	0	0	0	
OH-	H	NONE	E-	H2O	NONE	1.00E+00	1.00E+00	0.00E+00	1.00E+00	1.00E+00	0.00E+00	7.00E+08	0.00E+00	7.00E+08	0.00E+00	1.30E+04	0.00E+00	1	1	0	0	2	0	1	0	0	0	1	0	-1	0	0	-1	0	0	
E-	H	H2O	OH-	H2	NONE	1.00E+00	1.00E+00	1.00E+00	1.00E+00	1.00E+00	0.00E+00	4.80E+09	0.00E+00	4.80E+09	0.00E+00	1.30E+04	0.00E+00	0	1	2	1	2	0	0	0	1	1	0	0	-1	0	0	-1	0	0	
E-	HO2-	H2O	OH	OH-	NONE	1.00E+00	1.00E+00	1.00E+00	1.00E+00	2.00E+00	0.00E+00	5.40E+08	0.00E+00	5.40E+08	0.00E+00	1.30E+04	0.00E+00	0	1	2	1	1	0	0	2	1	1	1	0	-1	-1	0	0	-1	0	
H	OH	NONE	H2O	NONE	NONE	1.00E+00	1.00E+00	0.00E+00	1.00E+00	0.00E+00	0.00E+00	2.30E+11	0.00E+00	2.30E+11	0.00E+00	1.30E+04	0.00E+00	1	1	0	2	0	0	0	1	0	1	0	0	0	0	0	0	0	0	
OH	H2	NONE	H	H2O	NONE	1.00E+00	1.00E+00	0.00E+00	1.00E+00	1.00E+00	0.00E+00	1.40E+09	1.60E+04	1.40E+09	1.60E+04	1.90E+04	0.00E+00	1	2	0	1	2	0	1	0	0	0	1	0	0	0	0	0	0	0	
H	O2	NONE	HO2	NONE	NONE	1.00E+00	1.00E+00	0.00E+00	1.00E+00	0.00E+00	0.00E+00	1.50E+11	0.00E+00	1.50E+11	0.00E+00	1.30E+04	0.00E+00	1	0	0	1	0	0	0	2	0	2	0	0	0	0	0	0	0	0	
H	HO2	NONE	H2O2	NONE	NONE	1.00E+00	1.00E+00	0.00E+00	1.00E+00	0.00E+00	0.00E+00	3.00E+11	0.00E+00	3.00E+11	0.00E+00	1.30E+04	0.00E+00	1	1	0	2	0	0	0	2	0	2	0	0	0	0	0	0	0	0	
H	O2-	NONE	HO2-	NONE	NONE	1.00E+00	1.00E+00	0.00E+00	1.00E+00	0.00E+00	0.00E+00	3.00E+11	0.00E+00	3.00E+11	0.00E+00	1.30E+04	0.00E+00	1	0	0	1	0	0	0	2	0	2	0	0	0	-1	0	-1	0	0	
E-	O2-	H2O	HO2-	OH-	NONE	1.00E+00	1.00E+00	1.00E+00	1.00E+00	1.00E+00	0.00E+00	3.60E+09	0.00E+00	3.60E+09	0.00E+00	1.30E+04	0.00E+00	0	0	2	1	1	0	0	2	1	2	1	0	-1	-1	0	-1	-1	0	
H	H2O2	NONE	OH	H2O	NONE	1.00E+00	1.00E+00	0.00E+00	1.00E+00	1.00E+00	0.00E+00	2.00E+09	0.00E+00	2.00E+09	0.00E+00	1.90E+04	0.00E+00	1	2	0	1	2	0	0	2	0	1	1	0	0	0	0	0	0	0	
OH	H2O2	NONE	H2O	HO2	NONE	1.00E+00	1.00E+00	0.00E+00	1.00E+00	1.00E+00	0.00E+00	4.20E+08	0.00E+00	4.20E+08	0.00E+00	1.40E+04	0.00E+00	1	2	0	2	1	0	1	2	0	1	2	0	0	0	0	0	0	0	
OH	HO2	NONE	H2O	O2	NONE	1.00E+00	1.00E+00	0.00E+00	1.00E+00	1.00E+00	0.00E+00	1.00E+11	0.00E+00	1.00E+11	0.00E+00	1.30E+04	0.00E+00	1	1	0	2	0	0	1	2	0	1	2	0	0	0	0	0	0	0	
HO2	NONE	NONE	H2O2	O2	NONE	2.00E+00	0.00E+00	0.00E+00	1.00E+00	1.00E+00	0.00E+00	5.00E+07	0.00E+00	5.00E+07	0.00E+00	1.90E+04	0.00E+00	1	0	0	2	0	0	2	0	0	2	2	0	0	0	0	0	0	0	
HO2	NONE	NONE	O2-	H+	NONE	1.00E+00	0.00E+00	0.00E+00	1.00E+00	1.00E+00	0.00E+00	3.90E+05	7.70E+11	3.90E+05	7.70E+11	1.30E+04	1.30E+04	1	0	0	0	1	0	2	0	0	2	0	0	0	0	0	-1	1	0	
HO2	O2-	NONE	O2	HO2-	NONE	1.00E+00	1.00E+00	0.00E+00	1.00E+00	1.00E+00	0.00E+00	5.00E+08	0.00E+00	5.00E+08	0.00E+00	1.90E+04	0.00E+00	1	0	0	0	1	0	2	2	0	2	2	0	0	-1	0	0	-1	0	
O2-	OH	NONE	OH-	O2	NONE	1.00E+00	1.00E+00	0.00E+00	1.00E+00	1.00E+00	0.00E+00	2.90E+11	0.00E+00	2.90E+11	0.00E+00	1.30E+04	0.00E+00	0	1	0	1	0	0	2	1	0	1	2	0	-1	0	0	-1	0	0	
O2-	H2O	NONE	O2	H2O2	OH-	2.00E+00	2.00E+00	0.00E+00	1.00E+00	1.00E+00	2.00E+00	1.30E+05	0.00E+00	1.30E+05	0.00E+00	1.90E+04	0.00E+00	0	2	0	0	2	1	2	1	0	2	2	1	-1	0	0	0	0	-1	
E-	H2O	NONE	H	OH-	NONE	1.00E+00	1.00E+00	0.00E+00	1.00E+00	1.00E+00	0.00E+00	2.90E+02	0.00E+00	2.90E+02	0.00E+00	1.30E+04	0.00E+00	0	2	0	1	1	0	0	1	0	0	1	0	-1	0	0	0	-1	0	
E-	H+	NONE	H	NONE	NONE	1.00E+00	1.00E+00	0.00E+00	1.00E+00	0.00E+00	0.00E+00	2.60E+11	0.00E+00	2.60E+11	0.00E+00	1.30E+04	0.00E+00	0	1	0	1	0	0	0	0	0	0	0	0	-1	1	0	0	0	0	
E-	OH	NONE	OH-	NONE	NONE	1.00E+00	1.00E+00	0.00E+00	1.00E+00	0.00E+00	0.00E+00	2.90E+11	0.00E+00	2.90E+11	0.00E+00	1.30E+04	0.00E+00	0	1	0	1	0	0	0	1	0	1	0	0	-1	0	0	-1	0	0	
E-	H2O2	NONE	OH	OH-	NONE	1.00E+00	1.00E+00	0.00E+00	1.00E+00	1.00E+00	0.00E+00	2.40E+11	0.00E+00	2.40E+11	0.00E+00	1.30E+04	0.00E+00	0	2	0	1	1	0	0	2	0	1	1	0	-1	0	0	0	-1	0	
H2O2	OH-	NONE	HO2-	H2O	NONE	1.00E+00	1.00E+00	0.00E+00	1.00E+00	1.00E+00	0.00E+00	1.00E+10	2.10E+05	0.00E+00	0.00E+00	1.30E+04	1.30E+04	2	1	0	1	2	0	2	1	0	2	1	0	0	-1	0	0	-1	0	
H2O2	NONE	NONE	O2	H2O	NONE	1.00E+00	0.00E+00	0.00E+00	5.00E-01	1.00E+00	0.00E+00	1.40E-02	0.00E+00	1.40E-02	0.00E+00	6.00E+04	0.00E+00	2	0	0	0	2	0	2	0	0	2	1	0	0	0	0	0	0	0	

	GVALUE	DATA	FILE	GVN:	7
	GID	data1	data2	data3	
H2	6.00E-01	1.50E+00	1.65E+00		
H2O2	5.50E-01	1.14E+00	1.55E+00		
H	9.00E-01	5.00E-01	1.20E-01		
OH	4.50E+00	1.70E+00	4.50E-01		
HO2	0.00E+00	4.00E-02	0.00E+00		
H+	3.50E+00	6.00E-01	1.30E-01		
E-	3.50E+00	6.00E-01	1.30E-01		

	ECP-INPU	DATA	FILE										
	CURRENT	DENSITY	DATA	IECPE	8H2O2	O2	H2	H+	LiOH	Li+	H2O	Fe2+	
	IECPN	IECPR1	IECPR2	IECPP1	IECPP2	IPWRR1	IPWRR2	IPWRP1	IPWRP2	RECPV1	RECPV2	IECPV1	RECPV3
	1	1	4	-7	0	1	2	2	0	5.00E-06	4.50E-01	2	1.58E+00
	2	1	6	-5	0	1	2	2	0	5.00E-10	3.00E-01	2	8.85E-01
	3	2	4	-1	0	1	2	1	0	2.00E-04	7.00E-01	2	4.80E-01
	4	4	0	-3	0	2	0	1	0	5.00E-04	5.00E-01	2	0.00E+00
	5	-1	0	2	4	1	0	1	2	1.00E-01	5.00E-01	2	4.80E-01
	6	-3	0	4	0	1	0	2	0	5.00E-05	3.00E-01	2	0.00E+00
	7	0	0	8	0	0	0	1	0	1.00E-03	5.00E-01	2	-4.40E-01
	ISOLP	SOLPHH	SOLPHL	AAH0:	5	8.50E+00	6.50E+00	H+					
	TISOL	(FSOLF(1)	FSOLF(2)	FSOLF(3)	FSOLF(4)	FSOLF(5)	FSOLF(6)	FSOLF(7)	FSOLF(8)	FSOLF(9)	FSOLF(10)	FSOLF(11)	FSOLF(12)
	5.70E+02	1.90E-01	-1.00E+01	2.00E+00	-7.80E+00	2.50E-01	-7.00E+00	2.00E+00	-7.00E+00	-1.00E-01	-6.90E+00	2.00E+00	-6.90E+00
	5.20E+02	2.90E-01	-1.00E+01	2.00E+00	-8.10E+00	2.00E-01	-7.00E+00	2.00E+00	-6.50E+00	-2.20E-01	-6.90E+00	2.00E+00	-6.30E+00
	4.70E+02	3.00E-01	-1.10E+01	2.00E+00	-8.20E+00	1.80E-01	-7.00E+00	2.00E+00	-6.00E+00	-1.00E-01	-6.90E+00	2.00E+00	-5.90E+00
	4.20E+02	3.50E-01	-1.10E+01	2.00E+00	-8.60E+00	1.80E-01	-6.70E+00	2.00E+00	-5.70E+00	-1.00E-01	-7.00E+00	2.00E+00	-5.70E+00
	3.70E+02	4.50E-01	-1.10E+01	2.00E+00	-8.90E+00	1.80E-01	-6.70E+00	2.00E+00	-5.70E+00	-1.00E-01	-7.00E+00	2.00E+00	-5.70E+00
	HHOXD1	HHBND1	1.00E-05	1.00E-04									
	<<<<<<<<<	Iteration	no.->	1Case	#	1							

Table A-2.1 b) Output data of Example 3 for BWR primary loop analysis: example of output data

| | Summary | of | the | INPUT | data | BWR | pri | mary | loop | calculation | test | case | study2023 | NOV | | |

Table A-2.2 Input data of Example 4 for calculation of BWR hydrogen injection effects: confirmation of input data

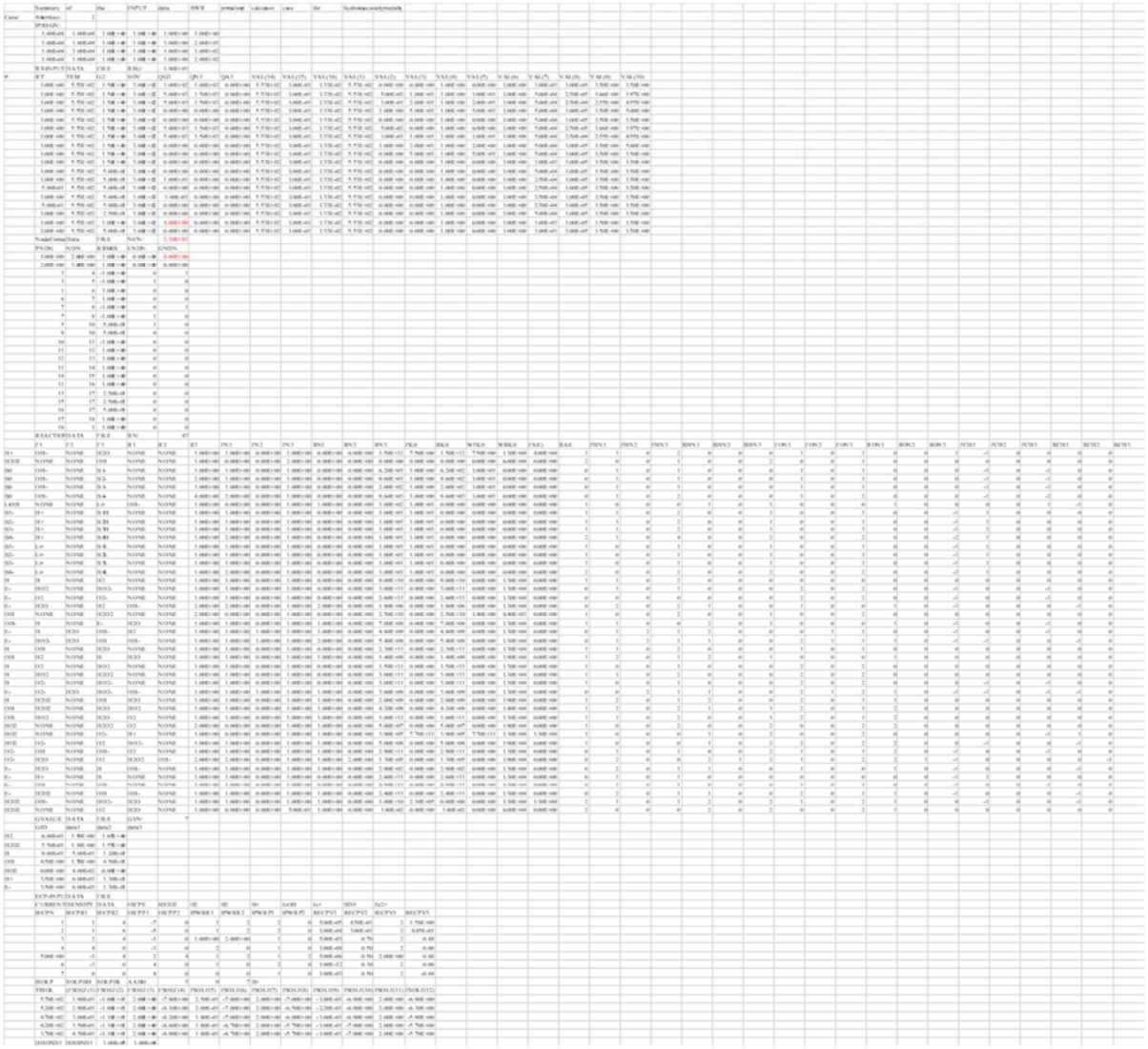

Appendix-B PAD of Major Sub-codes and Subroutines for Water Radiolysis (INPUT)

Table B.1 Fine PAD of Subroutine INPUT (1)

Fine PAD for Subroutine INPUT

```
99      call INPUT(Q,Q3,QN,QN3,QA,QA3,HWC,&
              &RN,F1,F2,F3,R1,R2,R3,FN1,FN2,FN3,RN1,RN2,RN3,FK0, &
              &RK0,WFK0,WRK0,FK,RK,WFK,WRK,FAE,RAE,REG,ID,C,CAQ2,N, &
              &GG,GN,GA,HN,ON,CH,TEM0,TEM,DIO,O2C,O2C2,RT,G2,WDE,NCN, &
              &PNDN,NDN,RMIX, H2O2C2,IDH2,VAL,CONV2, ACC1)
347     Subroutine INPUT(Q,Q3,QN,QN3,QA,QA3,HWC, &
              &RN,F1,F2,F3,R1,R2,R3,FN1,FN2,FN3,RN1,RN2,RN3,FK0, &
              &RK0,WFK0,WRK0,FK,RK,WFK,WRK,FAE,RAE,REG,ID,C,CAQ2,N, &
              &GG,GN,GA, HN,ON,CH,TEM0,TEM,DIO,O2C,O2C2,RT,G2,WDE,NCN,&
              & PNDN,NDN,RMIX, H2O2C2,IDH2,VAL,CONV2,ACC1)
```

Integer（11）	HWC:	1 for Fist call and 0 for second calculation (Usually 0)
	DIO:	as same as above
	RN:	number of reactions
	N:	total number of species
	REG:	total region number.
	NCN:	total node connection number
	HN(40):	Number of O for each specie for calculation
	ON(40):	Number of H for each specie for calculation
	CN(40):	Number of charges for each specie for calculation
	PNDN(999):	inlet node number
	NDN(999):	outlet node number
Real（40）	VAL(16,998):	
	CONV2:	conversion condition
	ACC1:	acceleration factor
	O2C:	[O2] at inlet (ppb) (input)
	O2C2:	[O2] at inlet (mol/m3)
	H2O2C2:	[H2O2] at inlet (mol/m3)
	Q3(998):	gamma ray energy deposition rate in each region Gy/s)
	QN3(998):	neutron energy deposition rate in each region Gy/s)
	QA3(998):	alpha ray energy deposition rate in each region Gy/s)
	FN1(RN):	reaction order of forward reaction for column 1 (input)
	FN2(RN):	reaction order of forward reaction for column 2 (input)
	FN3(RN):	reaction order of forward reaction for column 3 (input)
	RN1(RN):	reaction order of backward reaction for column 1 (input)
	RN2(RN):	reaction order of backward reaction for column 2 (input)
	RN3(RN):	reaction order of backward reaction for column 3 (input)

Table B.2 Fine PAD of Subroutine INPUT (2)

	FK(998,40):	rate constant for each forward reaction for each region
	RK(998,40):	rate constant for each backward reaction for each region
	WFK(998,40):	surface rate constant for each forward reaction for each region
	WRK(998,40):	surface rate constant for each forward reaction for each region
	FK0(40)	rate constant for each forward reaction for SC
	RK0(40):	rate constant for each backward reaction for SC
	WFK0(40):	surface rate constant for each forward reaction for SC
	WRK0(40):	surface rate constant for each backward reaction for SC
	FAE(40):	activation energy for each forward reaction
	RAE(40):	activation energy for each backward reaction
	GG(40):	G-value due to gamma rays for each specie
	GN(40):	G-value due to neutrons for each specie
	GA(40):	G-value due to alpha rays for each specie
		Those were killed for boiling version
	C(998,40):	initial concentration of each specie (mol/m3)
	CAQ2(998):	density of H2O in each region (mol/m3)
	TEM0:	standard temperature (558K)
	TEM(998):	temperature at each region (K)
	RT(998):	residence time for each region (s)
	WDE(998):	water density at each region
	G2(998):	velocity at each region (m/s)
	IDH2:	[H2] at inlet (mol/m3)
	RMIX(999):	mixing rate at node inlet
Character（7）	F1(40):	name of each specie in 1st column of reaction table
	F2(40):	name of each specie in 2nd column of reaction table
	F3(40):	name of each specie in 3rd column of reaction table
	R1(40):	name of each specie in 4th column of reaction table
	R2(40):	name of each specie in 5th column of reaction table
	R3(40):	name of each specie in 6th column of reaction table
	ID(40):	series name of species

Calculation:

Read major input data.

Transfer the calculation constant for regional image.

SPECIES(R3,FS,NUL,RN,FSN,FHN,FON,FCH,FHN1,FON1,FCH1)

Data rearranging of rate constants

INTCONC(N,ID,IC,FS,FSN,RS,RSN,1,CAQ,FHN,FON,FCH,
RHN,RON,RCH,HN,ON,CH,1,O2C2,IDH2,H2O2C2)

Setting initial values for calculation matrix (Region#1)

INTCONC(N,ID,IC,FS,FSN,RS,RSN,1,CAQ,FHN,FON,FCH,
RHN,RON,RCH,HN,ON,CH,1,O2C2,IDH2,H2O2C2)

Setting initial values for calculation matrix (Region#>2)

GVALUE(N,ID,GID,GVN,GG,GN,GA,data1,data2,data3)

Calculation of energy deposition rate based on G-value and energy absorption

Appendix-C PAD of Major Sub-codes and Subroutines for Water Radiolysis (WRAC)

Table C.1 Fine PAD of Subroutine WRAC (1)

Fine PAD for Subroutine WRAC

```
235     call WRAC(i02,RN,N,Q2,QN2,QA2, F1,F2,F3,R1,R2,R3, &
                & ID,GG,GN,GA,C1,CAQ, FK1,RK1,WFK1,WRK1, &
                & FN1,FN2,FN3,RN1,RN2,RN3,HWC,DIO, G,HN,ON,CH,RT2, &
                & T0,Lo0,WDEN,RWDEN,O2C2,H2O2C2,IDH2,CONV2,ACC1)
585     Subroutine WRAC (REG,RN,N,Q2,QN2,QA2,F1,F2,F3, &
                & R1,R2,R3,ID,GG,GN,GA,C1,CAQ,FK1,RK1,WFK1,WRK1, &
                & FN1,FN2,FN3,RN1,RN2,RN3,HWC,DIO, G,HN,ON,CH,RT,&
                & T0,Lo0,WDEN,RWDEN,O2C2,H2O2C2,IDH2,CONV2,ACC1)
```

Integer（8）	REG:	total region number.
	RN:	number of reactions
	N:	total number of species
	HWC:	1 for Fist call and 0 for second calculation (Usually 0)
	DIO:	as same as above
	HN(N):	Number of O for each specie for calculation
	ON(N):	Number of H for each specie for calculation
	CH(N):	Number of charges for each specie for calculation
Rea（25）：	Q2:	energy deposition due to gamma rays at the region
	QN2:	energy deposition due to neutrons at the region
	QA2:	energy deposition due to alpha rays at the region
	T0:	initially=0, then =T0+T at BDFNEWTON
	Lo0:	initially=0, then =Lo at BDFNEWTON
	GG(N):	G-value due to gamma rays for each specie
	GN(N):	G-value due to neutrons for each specie
	GA(N):	G-value due to alpha rays for each specie
	C1(N):	concentration of each specie at the region
	CAQ:	density of H2O at the region
	FN1(RN):	rate constants of forward reaction for column 1 (input)
	FN2(RN):	rate constants of forward reaction for column 2 (input)
	FN3(RN):	rate constants of forward reaction for column 3 (input)
	RN1(RN):	rate constants of backward reaction for column 1 (input)
	RN2(RN):	rate constants of backward reaction for column 2 (input)
	RN3(RN):	rate constants of backward reaction for column 3 (input)
	G:	velocity at the region (m/s)
	RT:	residence time at the region (s)
	WDEN:	density of H2O at the region
	RWDEN:	relative density of H2O vs that at the inlet
	O2C:	[O2] at inlet (ppb) (input)
	O2C2:	[O2] at inlet (mol/m3)
	H2O2C2:	[H2O2] at inlet (mol/m3)
	CONV2:	conversion condition
	ACC1:	acceleration factor
Character（7）：	F1(N):	name of each specie in 1st column of reaction table
	F2(N):	name of each specie in 2nd column of reaction table
	F3(N):	name of each specie in 3rd column of reaction table
	R1(N):	name of each specie in 4th column of reaction table
	R2(N):	name of each specie in 5th column of reaction table
	R3(N):	name of each specie in 6th column of reaction table
	ID(N):	series name of species

Table C.2 Fine PAD of Subroutine WRAC (2)

Calculation:

Calculation of the concentration of radiolytic species for each region

INITCALC

Setting initial values for mass balance calculation

EULER

Prepare for the differential equations (fn(t)=dCn(t)/dtt)

GREACTION(FN1,FN2,FN3,RN1,RN2,RN3,FK1,RK1,RN, N,Y2,GENX)

DREACTION(FN1,FN2,FN3,RN1,RN2,RN3,FK1,RK1,RN, N,Y2,DISX)

Calculation of annihilation terms of secondary reactions of species

gasset('CALC_DY:',N,Y2,XGAS)

Determination of gas emission and adsorption coeff.

gascon('INITCALC: ',N,DT,C1)

Calculation of concentrations in gas phase

BALANCE(REG,N,C1,HN,ON,CH,HOR,CHR,ID,RWDEN,O2C2,H2O2C2,IDH2)

Calculation of H/O and charge balance to validate the radiolytic calculation

SUB5(REG,N,CNT,dtCNT,BDFY1,BDFY2,BDFY3, BDFY4,BDFY5,BDFY6, BDFf1,BDFf2,BDFf3,BDFf4,BDFf5,BDFf6, PRC2,PRDC2,C1,DC)

Replacing the calculated concentration for time steps for giving the guess value for BDF calculations

BDFINIT(BDFY6, BDFf6,C1,DC,N)

Setting the initial values for BDF calculation (6th)

BDFINIT(BDFY5,BDFf5,C1,DC,N)

Setting the initial values for BDF calculation (5th)

BDFINIT(BDFY4,BDFf4,C1,DC,N)

Setting the initial values for BDF calculation (4th)

BDFINIT(BDFY3,BDFf3,C1,DC,N)

Setting the initial values for BDF calculation (3rd)

BDFINIT(BDFY2,BDFf2,C1,DC,N)

Setting the initial values for BDF calculation (2nd)

BDFINIT(BDFY1,BDFf1,C1,DC,N)

Setting the initial values for BDF calculation (1st)

BDFNEWTON

Control of BDF calculation

INIT_BDF

Setting the initial values for BDF calculation

NEWTON

Integration calculation based on Newton method

MATRIX(NEW, N, Ym,PY,BE0,h,FN1,FN2,FN3,RN1,RN2,RN3,FK1,RK1, RN)

Calculation of matrix for calculating radiolytic specie concentrations without boiling

DGREACTION(FN1,FN2,FN3,RN1,RN2,RN3,FK1,RK1,RN, N,Ym,DFGEN)

Prepare for the differential form (dfn(t)/dt) of the original differential equations

DDREACTION(FN1,FN2,FN3,RN1,RN2,RN3,FK1,RK1,RN, N,Ym,DFDIS)

Prepare for the differential form (dfn(t)/dt) of the original differential equations

FF3CAL

Control of function and mass transfer from liquid to gas phase

GREACTION(FN1,FN2,FN3,RN1,RN2,RN3,FK1,RK1,RN, N,Y2,GENX)

Calculation of source terms (Secondary generations) of radiolysis calculation.

DREACTION(FN1,FN2,FN3,RN1,RN2,RN3,FK1,RK1,RN, N,Y2,DISX)

Calculation of annihilation terms of secondary reactions of species

Table C.3 Fine PAD of Subroutine WRAC (3)

gasset('CALC_DY:',N,Y2,XGAS)

Determination of gas emission and adsorption coeff.

RENRITU(NEW,ff3,DX,N,N+1)

Determination of calculation matrix in a time mesh

SQMEAN(N,Ym,ID,DX,PY,CONV)

Determination of convergence

gascon('BDFNEWTON:',N,BDT,C1)

Calculation of gaseous specie concentrations

BALANCE(REG,N,C1,HN,ON,CH,HOR,CHR,ID,RWDEN,O2C2,H2O2C2,IDH2)

Calculation of H/O and charge balance to validate the radiolytic calculation

CALC_DY(REG,N,FN1,FN2,FN3,RN1,RN2,RN3,FK1,RK1,WFK1,WRK1,RN, GG,GN,GA, Q2,QN2,QA2, Y2,fY2,DC)

Setting calculation matrix and mass transfer from liquid to gas phase (gasset)

GREACTION(FN1,FN2,FN3,RN1,RN2,RN3,FK1,RK1,RN, N,Y2,GENX)

Calculation of source terms (Secondary generations) of radiolysis calculation.

DREACTION(FN1,FN2,FN3,RN1,RN2,RN3,FK1,RK1,RN, N,Y2,DISX)

Calculation of annihilation terms of secondary reactions of species

gasset('CALC_DY :',N,Y2,XGAS)

Determination of gas emission and adsorption coeff.

SUB3(BDFY1,BDFY2,BDFY3,BDFY4,BDFY5,BDFY6,BDFf1,BDFf2,BDFf3, BDFf4,BDFf5,BDFf6,C1,DC,N,REG)

Reading calculation variables for regions

SUB4(REG,N,C1,DC,PRC2,PRDC2)

Reading component variables for species

SUB6(REG,N,BDFY1,BDFY2,BDFY3,BDFY4,BDFY5,BDFY6, BDFf1,BDFf2,BDFf3,BDFf4,BDFf5,BDFf6,PRC2,PRDC2)

Replacing calculation variables for regions

Appendix-D PAD of Major Sub-codes and Subroutines for ECP Calculations (ECPCAL)

Table D.1 Fine PAD of Subroutine ECPCAL

Fine PAD for Subroutine ECPCAL

241 call CALECP(ECP,CATHOD,VAL(14,i02),VAL(15,i02),VAL(16,i02),&
& C1(INH2),C1(INO2),C1(INH2O2))

2734 SUBROUTINE CALECP(ECP,CATHOD,T,U,d,ACH2,ACO2,ACHO)

Integer（0）

Real（8）

ECP:	ECP (V-SHE)
CATHOD:	Cathodic current density (A/m2)
T:	temperature (°C)
U:	flow velocity (m/s)
d:	equivalent diameter (m)
ACH2:	[H2] (mol/dm3)
ACO2:	[O2] (mol/dm3)
ACHO:	[H2O2] (mol/dm3)

Character（0）

Calculation: ECP calculation based on the standard anodic current density

The calculation are going to be replaced new model based on the coupled mode of oxide layer growth and electrochemistry.

ECP calculation for each region as a result of the intersection of total cathodic and anodic current densities

SOLUBILITY

Calculation of ferrous ion as a function of t and pH (interpolation of the empirical formula)

CURRENTDNS

Calculation of cathodic and anodic current densities

This is a blank page.